TECHNICAL REPORT STANDARD PAGE

1. Title and Subtitle
Development of a Design Methodology for Geosynthetic Reinforced Pavement Using Finite Element Numerical Modeling

2. Author(s)
Murad Y. Abu-Farsakh, Ph.D., P.E.;
Mehdi Zadehmohamad, Ph.D.

3. Performing Organization Name and Address
Louisiana Transportation Research Center
4101 Gourrier Avenue
Baton Rouge, LA 70808

4. Sponsoring Agency Name and Address
Louisiana Department of Transportation and Development
P.O. Box 94245
Baton Rouge, LA 70804-9245

5. Report No.
FHWA/LA.25/718

6. Report Date
November 2025

7. Performing Organization Code
LTRC Project Number: 20-3GT
SIO Number: DOTLT1000346

8. Type of Report and Period Covered
Final Report
June 2020 - June 2025

9. No. of Pages
220

10. Supplementary Notes
Conducted in Cooperation with the U.S. Department of Transportation, Federal Highway Administration.

11. Distribution Statement
Unrestricted. This document is available through the National Technical Information Service, Springfield, VA 21161.

12. Key Words
Geosynthetic reinforced pavement; benefit index; modifying coefficients; prediction model

13. Abstract

This study was completed using finite element (FE) analysis to assess the benefits of using geosynthetic reinforcement in flexible pavements. A comprehensive parametric study was performed to determine the effect of different variables like asphalt layer thickness, base thickness, geosynthetic type and stiffness, and subgrade stiffness for low, medium, and high volume traffic roads. The FE simulations were run for 100 load cycles, and the resulting permanent deformation (PD) was used to calibrate the ME rutting equation parameters for each layer. The PD data was extrapolated to determine the pavement's service life. The comparison of the PD curves of the unreinforced and reinforced sections was used to calculate the Traffic Benefit Ratios (TBR) at different rutting targets. By establishing the ratio between the calibrated rutting curves of the base and subgrade layers, the reduction coefficients for the PD equations α_b and α_s were derived, which can be used directly in the design of geosynthetic reinforced pavements. The calculated TBR values were then used as input parameters in AASHTOWare software to quantify

geosynthetic benefits in terms of effective resilient modulus ($M_{R\text{-}eff}$) and Equivalent Base Thickness (EBT).

The results of the study showed that incorporating one layer of geogrid or geotextile at the base-subgrade interface significantly reduces pavement rutting. The study found that using geogrid is more effective than using geotextile in reducing rutting due to an interlocking mechanism with the base aggregates. The TBR values increased with deeper rutting and higher geosynthetic stiffness. The optimal combination of TBR, $M_{R\text{-}eff}$, and EBT for low volume roads with asphalt thickness of 3.5 in. was found to be at a base thickness of 10 in. For medium volume roads (6.5 in. asphalt thickness) and high volume roads (10 in. asphalt thickness), the benefits are reduced with an increase in base thickness.

Several prediction models were developed to estimate the benefits of using geosynthetics in flexible pavements based on the influential parameters of TBR, $M_{R\text{-}eff}$, EBT, and α_b and α_s PD reduction coefficients. These prediction models include regression models and machine learning (ML) models, including Multiple Linear Regression (MLR), Multivariate Exponential Regression (MER), Decision Tree (DT), Support Vector Machine (SVM), Random Forest (RF), and Gradient Boosting (GB). The accuracy of these models was evaluated using different metrics criteria, including the coefficient of determination (R^2), Mean Square Error (MSE), and Mean Absolute Error (MAE). The results showed that the RF and GB models for a given combination of unseen parameters of pavement structure can accurately estimate the benefits of using geosynthetics in pavement structure in terms of TBR, $M_{R\text{-}eff}$, EBT, and α_b and α_s PD reduction coefficients in rut models.

Further, FE-ME results were used to propose a new rutting model for base and subgrade layers. The proposed rutting model can capture the reinforcing effect of geosynthetics and changes in different variables of pavement structure by changing the calibration coefficient, α*.

Project Review Committee

Each research project will have an advisory committee appointed by the LTRC Director. The Project Review Committee is responsible for assisting the LTRC Administrator or Manager in the development of acceptable research problem statements, requests for proposals, review of research proposals, oversight of approved research projects, and implementation of findings.

LTRC appreciates the dedication of the following Project Review Committee Members in guiding this research study to fruition.

LTRC Administrator/Manager

Gavin P. Gautreau, P.E.
Pavement and Geotechnical Research Administrator

Members

Xingwei Chen, Francisco Gudiel, Christophe Fillastre, Philip Graves, Mark Ordogne, Jeff Lambert, James Ball, Qiming Chen

Directorate Implementation Sponsor

Chad Winchester, P.E.
DOTD Chief Engineer

Development of a Design Methodology for Geosynthetic Reinforced Pavement Using Finite Element Numerical Modeling

by
Murad Y. Abu-Farsakh, Ph.D., P.E.
Mehdi Zadehmohamad, Ph.D.

Louisiana Transportation Research Center
4101 Gourrier Avenue
Baton Rouge, LA 70808

LTRC Project No. 20-3GT
SIO No. DOTLT1000346

conducted for
Louisiana Department of Transportation and Development
Louisiana Transportation Research Center

November 2025

Abstract

This study was completed using finite element (FE) analysis to assess the benefits of using geosynthetic reinforcement in flexible pavements. A comprehensive parametric study was performed to determine the effect of different variables like asphalt layer thickness, base thickness, geosynthetic type and stiffness, and subgrade stiffness for low, medium, and high volume traffic roads. The FE simulations were run for 100 load cycles, and the resulting permanent deformation (PD) was used to calibrate the ME rutting equation parameters for each layer. The PD data was extrapolated to determine the pavement's service life. The comparison of the PD curves of the unreinforced and reinforced sections was used to calculate the Traffic Benefit Ratios (TBR) at different rutting targets. By establishing the ratio between the calibrated rutting curves of the base and subgrade layers, the reduction coefficients for the PD equations α_b and α_s were derived, which can be used directly in the design of geosynthetic reinforced pavements. The calculated TBR values were then used as input parameters in AASHTOWare software to quantify geosynthetic benefits in terms of effective resilient modulus ($M_{R\text{-}eff}$) and Equivalent Base Thickness (EBT).

The results of the study showed that incorporating one layer of geogrid or geotextile at the base-subgrade interface significantly reduces pavement rutting. The study found that using geogrid is more effective than using geotextile in reducing rutting due to an interlocking mechanism with the base aggregates. The TBR values increased with deeper rutting and higher geosynthetic stiffness. The optimal combination of TBR, $M_{R\text{-}eff}$, and EBT for low volume roads with asphalt thickness of 3.5 in. was found to be at a base thickness of 10 in. For medium volume roads (6.5 in. asphalt thickness) and high volume roads (10 in. asphalt thickness), the benefits are reduced with an increase in base thickness.

Several prediction models were developed to estimate the benefits of using geosynthetics in flexible pavements based on the influential parameters of TBR, $M_{R\text{-}eff}$, EBT, and α_b and α_s PD reduction coefficients. These prediction models include regression models and machine learning (ML) models, including Multiple Linear Regression (MLR), Multivariate Exponential Regression (MER), Decision Tree (DT), Support Vector Machine (SVM), Random Forest (RF), and Gradient Boosting (GB). The accuracy of these models was evaluated using different metrics criteria, including the coefficient of determination (R^2), Mean Square Error (MSE), and Mean Absolute Error (MAE). The results showed that the RF and GB models for a given combination of unseen parameters of pavement structure can

accurately estimate the benefits of using geosynthetics in pavement structure in terms of TBR, $M_{R\text{-}eff}$, EBT, and α_b and α_s PD reduction coefficients in rut models.

Further, FE-ME results were used to propose a new rutting model for base and subgrade layers. The proposed rutting model can capture the reinforcing effect of geosynthetics and changes in different variables of pavement structure by changing the calibration coefficient, α*.

Acknowledgements

This research project was funded by the Louisiana Department of Transportation and Development (DOTD) and the Louisiana Transportation Research Center (LTRC). The help and support of Dr. Zhongjie Zhang, former LTRC Pavement and Geotechnical Administrator, and Gavin P. Gautreau, current LTRC Pavement and Geotechnical Administrator, are gratefully acknowledged.

Implementation Statement

The use of geosynthetics has long been known to significantly improve the performance of both the paved and unpaved roads constructed over weak to medium stiff subgrade soils. A comprehensive finite element (FE) parametric study was conducted in this study to evaluate the effect of different variables and parameters contributing to the benefits of using geosynthetic reinforcement in flexible pavements for low, medium, and high volume traffic roads. These variables included the thickness of asphalt layer, thickness of base course layer, type and stiffness of geosynthetics, and subgrade stiffness. The results of this study clearly demonstrated the potential benefits of using geosynthetic reinforcement (e.g., geogrids and geotextiles) in flexible pavements by improving the strength and stiffness of the base aggregate layer, stabilizing the subgrade layer, and reducing the pavement's permanent deformation (i.e., rutting) under cyclic "traffic" loading.

The benefits of geosynthetic reinforcement in flexible pavements were quantified in terms of Traffic Benefit Ratios (TBR) for different rutting targets, effective resilient modulus ($M_{R\text{-}eff}$) of base course layer, equivalent base thickness (EBT), and the permanent deformation (i.e., rutting) reduction factors for base and subgrade (α_b and α_s) for use in rut models. Several regression and machine learning (ML) models, figures, and tables were developed to evaluate the TBR, $M_{R\text{-}eff}$, EBT, and α_b and $\alpha_s$coefficients for use in the design of flexible pavements as a function of different variables and configurations within the context of the AASHTO Mechanistic-Empirical Pavement Design Guide (MEPDG).

The findings of this research can be effectively implemented in the design of geosynthetic reinforced flexible pavements, especially in conditions where it is difficult to stabilize or treat weak subgrade soils with cement or lime, as well as for widening highways and constructing highway exits or entrances over weak to medium stiffness subgrade soils. The benefits of geosynthetic reinforcement are more evident in pavement sections with small asphalt/base thicknesses, high geosynthetic stiffness, and low subgrade strength and stiffness (with resilient modulus $M_R < 4500$ psi or CBR < 3).

This report provides guidelines and a methodology for implementing the benefits of geosynthetic reinforcement in the design of flexible pavements within the MEPDG framework. This was accomplished by developing regression equations and ML models and providing figures/tables to quantify and incorporate the benefits of geosynthetic reinforcement in flexible pavement design. It is anticipated that the findings of this research

will promote the use of geosynthetic reinforcement technology for the improved design and construction of flexible pavements in Louisiana.

Table of Contents

List of Tables

List of Figures

Introduction

The United States has more than 4.2 million miles of public roads to transport people and goods on a daily basis. These roads face an increasing traffic volume annually, with vehicle miles driven surpassing 3.28 trillion in 2024, a rise of approximately 25% from 2000. Unfortunately, the percentage of public roadways in poor or fair condition (~43%) has remained unchanged in recent years due to the increasing degradation of U.S. roads [1]. It is noteworthy that while highways are usually well-kept, a large proportion of roads in poor or fair condition can be found in urban and rural collector roads and non-interstate systems. This leads to an increased cost for U.S. drivers, who must spend approximately $130 billion annually on extra vehicle repairs and operating costs due to the worsening condition of roads. Additionally, the share of vehicle miles driven on roads rated as "poor" has increased from 15% to approximately 17% in the past ten years [2].

According to an American Society of Civil Engineers (ASCE) report, more than 62% of funds invested in roadways were allocated to preservation, marking a 3% rise compared to the previous reporting period of the Federal Highway Administration [1]. This is due to the aging and deterioration of roadways [3]. As a result, it is anticipated that $41 billion will be spent in the next 20 years. Nevertheless, to address the current and anticipated backlogs, it will require an average annual expenditure of $53 billion for repairing and building new pavements and other operational issues. Spending levels must increase by 29% to address this problem [1].

The inadequacy of many existing roads due to the rapid growth in traffic volume and the escalating costs of materials and energy provide motivation for exploring cost-effective alternatives to existing methods of building and rehabilitating roads. Reinforcing and stabilizing paved and unpaved roads with geosynthetics offers one such alternative solution. In recent years, many geosynthetics (e.g., geogrids and geotextiles) were developed and used to improve the performance of pavements. The concept of using geosynthetics in roadway construction started in the 1970s. Since that time, many experimental, analytical, and numerical studies have been conducted to evaluate the benefits of using geosynthetics in pavements. The geosynthetic type, geometry and interlocking of geogrids, location and layers of geosynthetics, base thickness, and subgrade strength have a significant effect on the performance of geosynthetic reinforced flexible pavement [4] [5] [6] [7] [8]. It was reported in the literature that the use of geosynthetics in pavement structures can contribute to the following benefits: (1) extending the pavement’s projected service life; (2) reducing the

thickness of base layer for a given service life; and (3) helping construct pavements over weak subgrades. Although the benefits of the inclusion of geosynthetics within pavement as base reinforcement and/or subgrade stabilization have been widely recognized, the mechanism of reinforcement is still not fully understood in these applications.

The literature reveals considerable research aimed at developing design guidelines, empirical relationships, and/or design methods for certain reinforcement-pavement conditions and design requirements. The current primary flexible pavement design method that accounts for geosynthetic reinforcement uses a modified 1993 AASHTO flexible pavement design guide [9]. This approach involves quantifying the structural contribution of geosynthetic reinforcement by adding the increase in the structural layer coefficient of the base course and/or the reduction in the thickness of the base course [8] [10] [11] [12]. No method or specification for the design of flexible pavements with geosynthetic reinforcement is nationally or universally accepted, and the design and analysis of such structures are still being investigated. Further, the new AASHTO Mechanistic-Empirical Pavement Design Guide (MEPDG) does not include the pavement sections with geosynthetic reinforcement due to the lack of a proper understanding of the geosynthetic reinforcement mechanisms in pavements, especially the quantification of the geosynthetic benefit. These restrictions seriously inhibit the further development of reinforcement technology. Therefore, these limitations provide motivation for continual research on geosynthetic reinforced pavements to better understand their benefits and incorporate their effects into pavement design involving mechanistic-empirical pavement design methods.

Over the last decade, the Louisiana Transportation Research Center (LTRC) conducted several research studies on the application of geosynthetics in flexible pavements [4] [13] [14]. Various experimental techniques have been used in these studies. These include laboratory repeated load triaxial tests on reinforced specimens, laboratory cyclic plate load tests, field cyclic plate load tests, and full-scale field lanes tested using the Accelerated Load Facility (ALF) at the Pavement Research Facility (PRF) site. The experimental studies confirmed the benefits of geosynthetics in improving the performance of the pavement sections in terms of reducing the surface permanent deformation and extending the service life of pavement sections. The experimental studies, especially the full-scale field studies, are often costly and time consuming; therefore, only a limited number of variables were investigated in these studies. However, the experimental data from previous studies provides tremendously useful information and unique opportunities to verify, validate, and calibrate the finite element (FE) numerical models. The calibrated FE numerical model can then be used to conduct comprehensive FE parametric studies to evaluate the effect of different

variables and parameters contributing to the benefits and performance of geosynthetic reinforced/stabilized flexible pavements.

This study focused on evaluating the benefits of using geosynthetic reinforcement in flexible pavements through conducting extensive FE numerical analyses of the geosynthetic reinforced pavement systems. Several FE models were first developed to simulate the performance of geosynthetic reinforced pavements on different traffic sections built over subgrade soils of different strength conditions. The experimental data obtained from the previous studies (e.g., laboratory cyclic plate load tests and full-scale accelerated load tests) were used to calibrate and validate these models. The developed FE models were then used to conduct extensive parametric study to examine the effect of different variables and parameters (e.g., base thickness; type, location and stiffness of geosynthetics; and subgrade strength condition) for the performance of pavement cross sections of low, medium, and high volume traffic roads in Louisiana. This focused on the effects of geosynthetic reinforcement on permanent surface deformation (i.e., rutting) behavior of flexible pavements. Design methodology and guidelines were proposed for the geosynthetic-reinforced pavements that fall within the context of Mechanistic-Empirical Pavement Design Guideline (MEPDG).

Objectives

The primary objectives of this research project were to:

1. Develop finite element (FE) models to simulate the performance of geosynthetic reinforced pavements built over subgrade soils of different strengths under various traffic conditions.
2. Calibrate and validate and the FE models with the results of the laboratory box cyclic plate load tests and full-scale accelerated load tests on geosynthetic reinforced test lanes constructed at the PRF site.
3. Conduct an FE parametric study to evaluate the effect of different variables and parameters contributing to the benefits and improved performance of geosynthetic reinforced pavements for different traffic loads and different subgrade soil strengths
4. Conduct a sensitivity analysis to examine the effect of reinforcement properties for a range of pavement cross sections of low, medium, and high volume roads in Louisiana. This study focused on the effects of reinforcement on permanent surface deformation (i.e., rutting).
5. Develop a design procedure for geosynthetic reinforced pavements that generally falls within the context of the Mechanistic-Empirical Pavement Design Guideline (MEPDG) and is compatible with procedures developed under the NCHRP 1-37A Design Guide.

Scope

The project's research scope was to study the benefits and improved performance of flexible pavements reinforced with geosynthetics and to develop a design methodology and guidelines for geosynthetic reinforced pavements aligned within the context of mechanistic-empirical pavement design guidelines. The research objectives included developing finite element (FE) models, calibrating and validating the models, conducting a comprehensive FE parametric study to evaluate the effects of different variables, conducting a sensitivity analysis, and developing a design methodology for geosynthetic reinforced pavements.

Over the past decade, the Louisiana Transportation Research Center (LTRC) has conducted several research studies on the use of geosynthetics to reinforce flexible pavements [4] [14]. These studies have employed various experimental methods such as laboratory repeated load triaxial tests, laboratory cyclic plate load tests, field cyclic plate load tests, and full-scale field accelerated load tests. The results of these studies confirmed the significant benefits of using geosynthetic reinforcement in terms of reducing permanent deformation and increasing the service life of flexible pavements. However, these studies are costly and time-consuming, and therefore have a limited number of tests and variables investigated. In the meantime, the result data from these large field experiments provide valuable information and an opportunity to verify and validate the FE numerical models that are developed in this research.

After the developed FE numerical models were calibrated, they were utilized to conduct a comprehensive parametric study to determine the effect of different variables and parameters contributing to the effectiveness and performance of geosynthetic reinforced/stabilized pavements. This study explored the influence of factors such as the type and stiffness of geosynthetics, number and placement of geosynthetic layers, thickness of the base course layer, strength and stiffness of subgrade soil, and traffic volume (low, medium, and heavy). Based on the results from the FE parametric study, several regression equations, ML models, and figures/charts were developed to help the Louisiana Department of Transportation and Development (DOTD) pavement and geotechnical engineers incorporate the geosynthetic benefits into a design methodology compatible with the framework of the Mechanistic-Empirical Pavement Design Guide (MEPDG).

Literature Review

Introduction

Pavement types refer to the various materials and construction methods used to create a road surface or a paved area. The type of pavement used depends on factors such as the expected traffic volume, subgrade condition, climate, cost, and durability requirements. Common pavement types include asphalt concrete, which is a mixture of asphalt binder and aggregates; cementitious concrete, which a mixture of cement binder, water and aggregate, and is known for its durability and strength; brick and cobblestone, which are popular for pedestrian areas and historic districts; gravel and pavers, which are commonly used in rural areas and low traffic driveways, sidewalks, patios, and driveways; and chip seal, which is a pavement surface treatment commonly used for low traffic roads and rural highways. Each pavement type has its own unique advantages and disadvantages and is chosen based on the specific needs of the project.

Flexible Pavement

Flexible pavement is a type of road surface made up of multiple layers of geomaterials that are designed to be flexible under traffic loading. These pavements are commonly used in areas where the subgrade is relatively weak or unstable because they can bridge over weaker soil spots. The layers of flexible pavement typically include a subgrade layer, a subbase layer, a base layer, and an asphalt concrete surface layer.

The subgrade layer is the natural or treated ground below the pavement, and the subbase layer is a layer of compacted aggregates (e.g., crushed stone) or treated soil that are placed on top of the subgrade to improve its strength and stability. The base layer is another layer of compacted aggregates, untreated or treated with cement/asphalt, that serves to distribute the load of traffic evenly and provide further support for the surface layer. The surface layer is the final layer, typically made of asphalt concrete, which provides the driving surface and protects the underlying layers from weather and wear.

Flexible pavements are designed to distribute the traffic load over a wide area, reducing the stresses transferred to subgrade soil and allowing the pavement to be flexible under traffic loading. This helps reduce cracking and other types of pavement distress and can lead to a longer pavement lifespan.

Flexible Pavement Structure

A traditional flexible pavement system is composed of multiple layers, including the top layer of asphalt concrete (AC), granular base course, and subgrade layer; see Figure 1. The amount of stress transmitted to a specific point within each layer is influenced by the thickness and stiffness of the layers above it. The primary purpose of pavement layers is to reduce stress so that each point within the system can withstand acceptable stresses and deformations over its designated service life.

Figure 1. Flexible pavement sublayers [15]

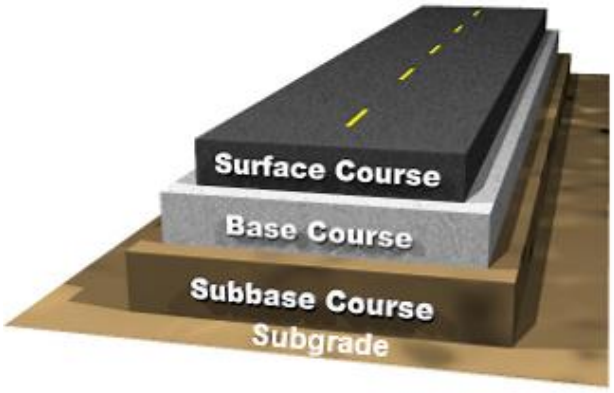

Asphalt concrete surface layer(s). The asphalt concrete surface layer is typically divided into two parts: a binder course and a surface course, which are constructed independently and joined together with a tack coat at the interface. The surface course, which is the topmost layer, is thinner and contains smaller aggregates and more bitumen compared to the binder course, which is situated directly above the prime-coated base layer. In some cases, flexible pavements are constructed using only a single uniform bituminous course layer placed on top of the base course layer.

Base course layer. The base course layer is situated immediately beneath the asphalt concrete layer. The base course layer can be constructed using various materials, including stone fragments, slag, soil-aggregate mixtures, cement-treated granular materials, reclaimed asphalt pavement (RAP), or bituminous-aggregate mixtures. The base layer offers additional stiffness and resistance to fatigue, while also reducing the amount of stress that is transmitted to subbase or subgrade. It can also serve as a drainage layer and provide resistance against frost. The grading, size, soundness, and permeability of the materials used are all critical factors for evaluating the suitability of the base layer.

Subbase layer. In certain cases, another layer, which is composed of a different material than the base layer, is placed between the base layer and the subgrade, which is called subbase layer. The subbase layer can be constructed using materials similar to base materials but with lower strength, which include stone fragments, slag, soil-aggregate mixtures, cement-treated granular materials, reclaimed asphalt pavement (RAP), or bituminous-aggregate mixtures. The subbase layer can serve as a transition load transfer layer between the base and subgrade layers.

Subgrade. The subgrade can be untreated natural ground or an improved/treated soil layer that lies directly beneath the pavement layers. Below the subgrade lies the natural ground or embankment. It provides a foundation for the pavement layers and distributes the load from the traffic loads to the natural soil underneath. The subgrade layer of a pavement system should possess certain characteristics, such as strength, stiffness, and ease of compaction. To assess subgrade strength, the following parameters have traditionally been used as design criteria: California Bearing Ratio (CBR), shear strength, and resilient modulus (M_R).

According to one AASHTO report, subgrade strength is defined based on the above parameters in the context of normal highway truck traffic or typical highway construction equipment [16]:

- Firm subgrade: CBR > 8; shear strength > 240 kPa; M_R > 80MPa
- Moderate strength subgrade: 3 < CBR < 8; 90kPa < shear strength < 240KPa; 30 MPa < M_R < 80 MPa
- Low strength subgrade: CBR < 3; shear strength < 90 kPa; M_R < 30 MPa.

The resilient modulus method is considered to provide more conservative results by requiring the soil to operate within the elastic range of stress.

Causes for Flexible Pavement Deterioration

Flexible pavements are not immune to the challenges of deterioration that can compromise their structural integrity and longevity. These pavements, consisting of layers of asphalt and aggregates, can experience several factors contributing to their degradation. Among the key culprits are heavy traffic loads, which can subject the pavement to fatigue damage, resulting in cracks, rutting, and deformation. Additionally, the natural aging of asphalt binders, often accelerated by exposure to sunlight, oxygen, and temperature fluctuations, leads to increased brittleness and susceptibility to cracking. Moisture infiltration, either from precipitation or

poor drainage, can weaken the pavement structure or cause issues like freeze-thaw damage and pothole formation. Environmental factors, subgrade weaknesses, inadequate maintenance, and the effects of aging infrastructure further compound the challenges faced by flexible pavements. Addressing these deteriorating factors through proper design, construction, and maintenance practices is crucial for the durability and safety of road networks.

Overloading. Traffic overloading, a pressing concern in transportation infrastructure, occurs when vehicles exceed the designed weight limits for a given roadway. This excess load, often driven by heavy trucks and freight carriers, can have detrimental effects on roadways, therefore accelerating their deterioration and reducing their service life. Overloaded vehicles exert higher stress on pavement surfaces, leading to premature wear and fatigue, manifesting as ruts, cracks, and potholes. Traffic overloading not only endangers the integrity of the transportation infrastructure but also poses a safety hazard for all road users.

Aging. Over time, the binder in asphalt undergoes a natural aging process that significantly affects the performance and longevity of road surfaces. Binder aging is a complex phenomenon influenced by various environmental, thermal, and mechanical factors, and understanding it is crucial for maintaining safe and sustainable transportation infrastructure. Binder aging primarily occurs due to the exposure of asphalt pavements to environmental stressors such as sunlight (i.e., UV radiation), oxygen, moisture, and temperature fluctuations. These factors collectively lead to the degradation of the binder, which is typically a bituminous material derived from crude oil.

Environmental conditions. The surrounding environmental conditions also play a pivotal role in the deterioration of pavement infrastructure. Extreme weather fluctuations, such as the freeze-thaw cycles in colder climates and prolonged exposure to UV radiation in sunnier regions, have a profound impact on pavement materials. Freeze-thaw cycles cause the water trapped within pavement layers to expand and contract, creating internal stress that can lead to cracks and potholes. UV radiation, on the other hand, accelerates the aging of asphalt binders, making them more brittle and less flexible over time. Moisture, in the form of rain or snow, can infiltrate the pavement structure, weakening its layers and promoting distress. Further, environmental factors like heavy rainfall can exacerbate drainage issues, leading to water accumulation beneath the pavement, which weakens the base and subbase layers.

Inadequate design and construction. The practices of inadequate design and construction serve as a major factor in pavement deterioration. When pavement structures are not designed to accommodate the anticipated traffic loads or environmental conditions,

premature distress becomes inevitable. Insufficient pavement thickness, inadequate compaction during construction, and poor material selection can all contribute to reduced pavement durability. Likewise, improper drainage design or the absence of effective stormwater management can lead to water infiltration and weakened pavement layers. Suboptimal construction practices can result in weak joints and improper compaction, causing uneven surfaces and susceptibility to distress, such as rutting and cracking. Inadequate design and construction not only shorten the service life of pavements but also increase maintenance and rehabilitation costs.

Types of Flexible Pavement Failures

The primary purpose of constructing pavement structures is to withstand the weight of vehicles and safely distribute the loads to the underlying subgrade soil. The pavement design process aims to identify the most cost-effective combination of asphalt concrete (AC) and base layer thickness and material type, considering the subgrade properties and the expected traffic loads over the pavement's lifetime.

Unfortunately, flexible pavements are prone to multiple types of failure due to a variety of factors such as excessive traffic volume, ambient conditions, and quality of pavement materials. Fatigue cracking, thermal cracking, and rutting are among the most common forms of flexible pavement failures. Rutting is a permanent deformation of the pavement surface induced by repetitive traffic loads, resulting in depressions in the wheel path. Pavement failures sometimes require whole pavement repair, not only remedial treatment of the visible pavement surface. To compensate for building a pavement structure on a poor subgrade soil layer, it may be necessary to thicken pavement layers or employ high quality base course material. However, there is a lack of stone in Louisiana, and depletion of high quality aggregates across the U.S. is accelerating due to increased demands on transportation networks.

Fatigue cracking. Fatigue cracking develops as a result of recurrent loading on the pavement, resulting in a network of linked fractures in the wheel path; see Figure 2. Fatigue cracking is defined as the phenomenon of fracture under repeated or fluctuating stress having a maximum value generally less than the tensile strength of the material [17]. Although the base course layer is an intermediary element of the pavement structure, its correct functioning in the road pavement layers is vitally important.

Figure 2. Fatigue cracking in flexible pavement [17]

Thermal cracking. Low temperature cracking and thermal fatigue cracking are examples of this sort of suffering. Low temperature cracking is commonly linked with flexible pavements in northern areas of the U.S. and parts of Canada where winter temperatures can drop below -10°F (-23°C). Thermal fatigue cracking can develop in considerably milder climates if an overly hard asphalt is employed, or if the asphalt hardens with age. If the mix stiffness and fracture-strength characteristics as a function of temperature and duration of loading are known and the temperature data on the site are available, the possibility for low temperature cracking for a specific pavement may be determined. When the estimated thermal stress exceeds the fracture strength, the pavement will break. Thermal fatigue cracking is analogous to repetitive load fatigue cracking. The tensile strain in the asphalt layer induced by the daily temperature cycle is to blame. Miner's hypothesis can be used to calculate cumulative harm [18].

Rutting. Rutting is a type of permanent deformation that occurs on the surface of flexible pavements due to repeated traffic loads. It is characterized by the formation of longitudinal or transverse depressions or channels in the wheel path, which can negatively impact the pavement's ride quality and safety; see Figure 3. Rutting is typically caused by a combination of factors, including insufficient thickness or strength of the pavement layers, inadequate compaction of asphalt mix during construction, and high traffic volume and axle loads. Rutting can also occur due to environmental factors such as high temperatures and moisture contents, which can soften the asphalt binder and reduce the pavement's ability to resist deformation. Proper design, construction, and maintenance practices, including adequate pavement thickness, proper mix design and compaction, and timely repairs, can help prevent rutting and prolong the pavement's service life.

Figure 3. Rutting failure in flexible pavements

Flexible Pavement Design Methods

The concept behind flexible pavement systems, which aim to provide a protective layer over the subgrade to ensure the pavement's durability under specific traffic and environmental conditions, dates to the Roman era, which served as the foundation for modern flexible pavement design. An illustration in Figure 4 demonstrates the evolution of road design techniques from the 1930s to the present day [19].

Figure 4. Evolution of pavement design methods [19]

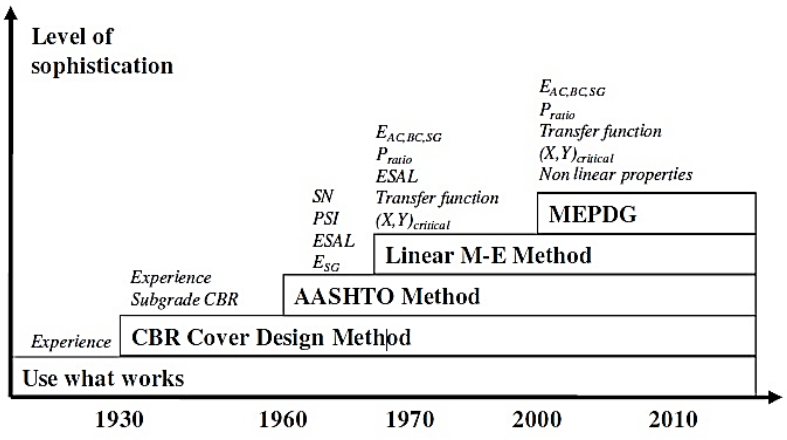

During the 1930s Great Depression, the Cover Based Design Process evolved, which used a single input of the California Bearing Ratio (CBR) but still depended primarily on engineering judgment. When the American Association of State Highway and Transportation

Officials (AASHTO) Road Test became increasingly prominent in the 1960s, new pavement design methods had been developed. In 1993, the American Association of State Highway and Transportation Officials (AASHTO) introduced an empirically-based pavement design guide [9]. In 2004, the National Cooperative Highway Research Program (NCHRP) created a guide for designing new and rehabilitated pavement structures using mechanistic-empirical (ME) principles [20]. Many attempts have been made to incorporate geosynthetic reinforcement into the AASHTO and ME design procedures. This paper analyzes the advantages and disadvantages of various techniques for developing geosynthetic reinforced flexible pavements [19].

1993 AASHTO Guide

One of the methods for designing flexible pavements in North America is the guide for the design of pavement structures published in 1993 by AASHTO [9]. Empirical equations which were developed from the AASHTO road tests conducted in the late 1950s are used by the AASHTO guide. The guide treats the pavement as a multi-layer elastic system with an overall structural number (SN) that reflects the total thickness of the pavement and its ability to resist repeated traffic loading. To ensure the pavement can support expected traffic loads and experience an acceptable loss in serviceability over time, the required SN is selected based on the pavement's specifications. Design factors fall into four broad categories, which include traffic loading, environment, materials, and failure criteria.

Traffic loading. Traffic loading is an important design factor in the AASHTO 1993 guide for flexible pavement design. The guide uses the concept of equivalent single axle loads (ESALs) to determine the pavement design. An ESAL is a hypothetical load applied to the pavement surface, which represents the effect of all the loads that are expected to be carried by the pavement over its design life. To design for traffic loading, the guide requires the estimation of the traffic volume and composition, including the number and weight of commercial vehicles, passenger vehicles, and other vehicles. The traffic loading is expressed in terms of ESALs and is determined based on the expected traffic volume and axle load distribution. The guide also considers the number of load repetitions expected during the pavement’s design life, which can be affected by factors such as traffic growth and seasonal variation. The pavement design is based on the number of ESALs that the pavement is expected to carry over its design life, and this is used to determine the required structural number (SN) for the pavement. The SN is a dimensionless parameter that represents the ability of the pavement structure to resist deformation under traffic loading.

Number of repetitions. A common and simplified approach in pavement design is to use equivalent factors to convert each load group into an 18-kip (80-kN) single-axle load, instead of analyzing the stresses and strains caused by each axle-load group separately. However, it is noted that the equivalency between different loads can vary depending on the failure criterion being used. For example, equivalent factors based on fatigue cracking may differ from those based on permanent deformation. Therefore, the use of a single equivalent factor to analyze different types of distress is based on experience and may not be completely accurate.

Environment. The AASHTO Guide for the design of pavement structures considers several environmental factors that can affect the pavement design. These factors include temperature, precipitation, and freeze-thaw cycles, which can impact the performance and durability of pavement structures. Temperature can have a significant impact on the properties of pavement materials, such as the strength and stiffness of asphalt. The method provides guidelines for selecting appropriate material properties based on the expected temperature range during the pavement's design life. The amount and frequency of precipitation can also affect pavement performance, as water infiltration can lead to a loss of support under the pavement layers and promote damage due to freeze-thaw cycles. The AASHTO 1993 design provides guidance on selecting appropriate drainage systems and pavement layers to manage water infiltration and promote pavement longevity.

Serviceability. In the AASHTO 1993 pavement design guide, the loss in serviceability is referred to as the Pavement Condition Index (PCI). PCI is a measure of the overall condition of a pavement section based on the type, extent, and severity of surface distresses observed on the pavement surface. The AASHTO 1993 guide provides guidance on the PCI values that can be used as a measure to determine when pavement rehabilitation or reconstruction is necessary. AASHTO 1993 recommends that pavement rehabilitation or reconstruction be considered when the PCI value falls below a certain threshold. For example, for flexible pavements, rehabilitation or reconstruction should be considered when the PCI value falls below 60. The AASHTO 1993 guide also provides guidance on how to estimate the PCI value based on the type and severity of surface distress observed on the pavement surface. The distresses considered in PCI calculation include cracking, rutting, faulting, roughness, and patching.

Mechanistic-Empirical Pavement Design Guide (MEPDG)

The mechanistic-empirical method of pavement design uses the principles of material mechanics to relate an input, such as a wheel load, to an output, such as pavement stress or strain. These response values are then used to predict pavement distress based on field

performance and laboratory tests. Relying on observed performance is crucial because theoretical calculations alone have not been enough to design pavements that perform well in practice. Kerkhoven and Dormon proposed using the vertical compressive strain on the subgrade surface as a failure criterion to minimize permanent deformation [21]. Saal and Pell recommended utilizing horizontal tensile strain at the bottom of the asphalt layer to minimize fatigue cracking [22]. The concept of using these strain measures for pavement design was first introduced in the U.S. by Dormon and Metcalf [23]. The approach of limiting permanent deformation by using vertical compressive strain is based on the relationship between plastic and elastic strains in paving materials. By restricting elastic strains on the subgrade, elastic strains in other pavement components above the subgrade are also controlled, thereby limiting the amount of permanent deformation on the pavement surface. Utilizing mechanistic approaches has several benefits, such as improving the reliability of design, enabling the prediction of various types of distress, and making it possible to extrapolate from limited laboratory and field data.

In 2004, NCHRP created a guide for designing new and rehabilitated pavement structures using mechanistic-empirical (ME) principles [20]. This method relies on detailed data input and mechanistic principles to minimize the dependence on empirical observations and correlations, which may not be applicable in every situation. The ME approach strives to enhance design reliability, reduce life-cycle expenses, better assess the impact of seasonal moisture and drainage variations, and anticipate potential failure modes to prevent untimely failures. The ME Design Method is a road performance prediction technique consisting of two interrelated components, mechanistic and empirical. Calculation models for this method rely on input parameters such as pavement layers, traffic, and climatic conditions, as well as the materials used. The obtained output is then compared to the initial design hypothesis, and if it falls short, the design undergoes an iterative process of modification and re-evaluation. The design method's flowchart depicting its various components is illustrated in Figure 5.

Figure 5. Flowchart for ME Design [20]

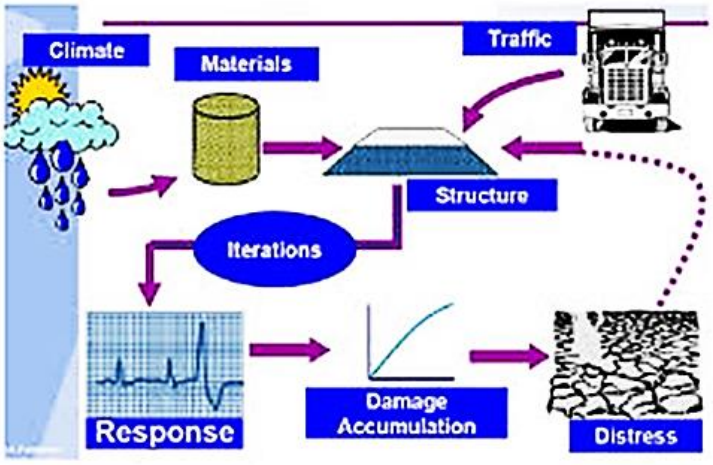

NCHRP's design guide offers three levels of input depending on various factors like the project's importance, pavement performance sensitivity to a particular input, resources available to the designer, and input information available during the design phase [20].

The first level, which has the highest accuracy, requires physical testing of hot mix asphalt, including dynamic modulus, creep compliance, and indirect tensile strength, as well as unbound materials, including resilient modulus actual site testing. The second level, which is considered to have intermediate accuracy, utilizes established correlations to determine the required inputs. For instance, dynamic modulus can be estimated based on tests conducted on binders, aggregate gradation, and mix properties. Finally, the third level has the lowest accuracy, with inputs typically based on national or regional default values, such as the physical properties and binder type used to characterize asphalt concrete mixes.

Traffic and loading. For the structural design and analysis of pavement structures, truck traffic plays a crucial role. In contrast to the previous version of the AASHTO 1993 Guide for pavement design, the MEPDG approach does not require using the ESAL approach for traffic characterization. Instead, the MEPDG uses complete axle-load spectrum data for each axle type for both new pavement and rehabilitation design procedures. The full axle-load spectra data is obtained by processing weighing-in-motion (WIM) data. To estimate the normalized axle-load distributions and truck-volume distribution. The FHWA Traffic Monitoring Guide and NCHRP Report 547 give guidance on collecting and analyzing truck weight data [24] [25]. The processing of axle-weight and truck-volume data requires a detailed and extensive analysis to determine the numerous truck traffic related inputs to the MEPDG design method.

Environment. To predict pavement distress using the MEPDG, it is necessary to have detailed climatic data, which includes hourly temperature, precipitation, wind speed, relative humidity, and cloud cover. This data is used to forecast the temperature and moisture content in each pavement layer and are utilized as inputs for the site factor parameter for the smoothness prediction models. To obtain this information, weather stations located in various regions of the U.S. are used. The MEPDG software has many embedded weather stations to make it easier for the user to implement. The user needs to know the project's longitude and latitude, and the software will automatically select the six weather stations closest to the location. The user can view the weather stations' longitude, latitude, elevation, and available months of data and select the appropriate stations to create a virtual weather station at the project location for distress predictions. Multiple weather stations can be selected to generate the climatic data required by the MEPDG. It is advisable to choose weather stations with comparable elevations, although temperatures are adjusted for elevation differences.

Performance criteria. The performance criteria, also known as analysis parameters in MEPDG software, are utilized to ensure that the design of a pavement will perform satisfactorily throughout its anticipated service life. To assess the adequacy of a design, the designer selects critical limits or threshold values. These values might indicate agency policies concerning pavement conditions that initiate major rehabilitation or reconstruction activities, or they may represent average values along a project. The criteria values are similar to those used in the AASHTO 1993 guide, in which initial and terminal serviceability index levels are established. For instance, criteria for distress and international roughness index (IRI) could be selected based on the pavement's condition and its impact on safety, maintenance requirements, possibility of pavement rehabilitation, and design reliability (~90%). If a project surpasses a performance criterion, it could result in maintenance or rehabilitation needs sooner than anticipated.

Geosynthetics

The use of reinforcing inclusions to improve the mechanical properties of soils dates to ancient times. However, only within the last 30 years or so, analytical and experimental studies have led to contemporary soil reinforcement techniques; one of these techniques is the use of geosynthetic materials in roadways. The most commonly used types of geosynthetics in pavement applications are geogrids and geotextiles.

Geosynthetics refers to planer products made of polymer material, utilized alongside geomaterials in many geotechnical engineering and pavement projects. These products are

produced in controlled environments. Geosynthetics possess various material properties that are crucial during their production, quality control, and design use. Index properties relate to the manufacture and quality control of geosynthetics, while performance properties are associated with design. Different geosynthetic products can perform diverse functions, and thus they must be designed to meet the minimum criteria required to perform such functions. Some of the primary functions of geosynthetics used in soil reinforcement include separation, filtration, stabilization, reinforcement, drainage, infiltration barrier, and protection. The most commonly used geosynthetics for reinforcement purposes are geotextiles and geogrids, which have found widespread application in pavement reinforcement and are the subject of this study; see Figure 6.

Figure 6. Geosynthetics used as reinforcement:
(a) woven geotextile (b) non-woven geotextile (c) geogrid (d) geocells

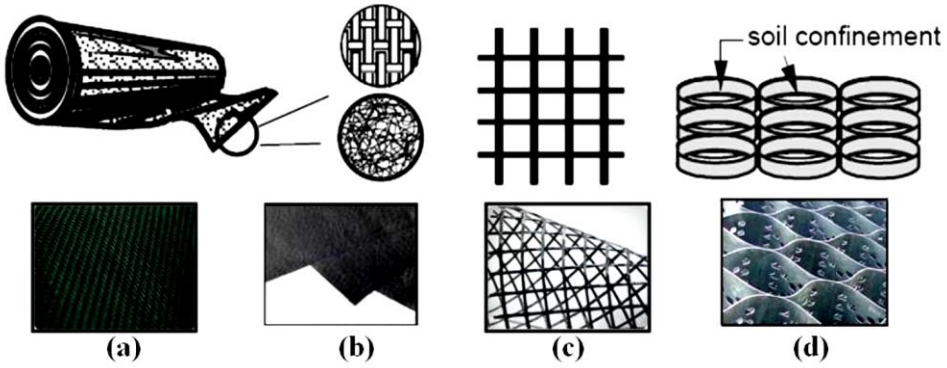

Geogrids

Geogrids are a type of geosynthetic product primarily designed to serve a reinforcement function in transportation projects. They feature uniformly spaced aperture openings between their longitudinal and transverse elements, which facilitates interlocking between the soil/granular particles on both sides of the installed sheet, leading to increased interaction between the geogrid and geomaterials. Geogrids are manufactured using materials such as polypropylene, polyethylene, polyester, or coated polyester. Flexible polyester and coated polyester geogrids feature junctions that are typically woven, knitted, or laser bonded. They are coated with materials like PVC or acrylics to protect filaments from construction damage. Rigid polypropylene and polyethylene geogrids are either extruded or punched sheet drawn and have in-plane ribs with integral junctions. Geogrids are classified based on their resistance to in-plane loads in one direction (uniaxial), two directions (biaxial), or any

direction (triaxial); see Figure 7. Uniaxial geogrids are suitable for walls and slopes, while biaxial and triaxial geogrids are preferred for base reinforcement in pavements.

Figure 7. Geogrid reinforcements

Field and laboratory tests have shown that geogrid reinforced roads exhibit improved performance. In the past, biaxial geogrids were commonly employed for unpaved roads. A new type of geogrid, known as the triangular aperture geogrid, has recently been introduced to the market. This geogrid is expected to have uniform tensile strength and stiffness in all directions. Geogrids placed at the interface between the base and subgrade offer several benefits, including confinement of granular particles, increased base stiffness, reduction of shear stress at the interface, improved stress distribution, and enhanced tensioned membrane effect.

Geotextiles

Geotextile is a permeable layer of geosynthetic material composed entirely of textiles. They are available in woven or non-woven varieties and have a heavy fabric-like appearance that is both flexible and porous. The use of textiles in pavement structures dates back to ancient Persian times, where natural fibers were employed to stabilize weak soils. However, it was not until the 1920s that the United States began using cotton textiles for road construction. With the introduction of synthetic fibers, road construction became more practical and advantageous. Various samples of geotextiles can be seen in Figure 8.

Figure 8. Different types of geotextiles

Geotextiles can be produced in three different ways: knitted, woven, and non-woven. Woven geotextiles are created by weaving warp and weft yarns together, which can be made from spun, multi-filament, fibrillated, or slit film materials. On the other hand, non-woven geotextiles are made by thermally bonding or mechanically interlocking fibers or filaments, with needle-punching being the most common method for civil engineering applications [26]. Geotextiles are commonly used in road projects to reinforce, stabilize, separate, and filter materials, both for paved and unpaved roads [27] [8].

Geosynthetic Applications in Pavement Engineering

Geosynthetics can generally be utilized to perform a variety of functions, including reinforcement, separation, filtration, and drainage. The primary mechanism functions of geosynthetics in pavements are discussed in the following sections.

Geosynthetics Reinforcement Mechanism in Pavements

Depending on the type of interaction, the properties of the soil and reinforcement, and the desired types and levels of improvement (e.g., design service, reducing rutting, or reducing layer thickness), four improvement mechanisms (i.e., reinforcement functions) can be distinguished: (1) confinement effect (i.e., lateral restraint effect), (2) improved bearing capacity, (3) tensioned membrane, and (4) stabilization function. These functions are illustrated below:

Confinement effect (i.e., lateral restraint effect). Both geogrids and geotextiles can be used for reinforcement applications via interface friction between geosynthetics and geomaterials and interlocking between geogrid apertures and granular materials, causing lateral confinement (i.e., restrain) effect; see Figure 9. The aperture size and geometry, rib shape, and junction shape of geogrids all contribute to the interlock behavior and the interface load transfer. The effectiveness of interlocking is influenced by the in-plane stiffness of the geogrid and the stability of its ribs and junctions. When the base aggregate layer is subjected to traffic loading, the aggregate tends to move laterally. Due to relative displacement between aggregate and reinforcement, interface friction force is induced at the base aggregate-reinforcement interface. The developed interface shear resistance between the base aggregate and the geosynthetic transfers shear load from the base layer to a tensile load in the geosynthetic. Consequently, lateral deformation or potential tensile strain in the base layer is restrained. As a result, vertical deformation of the pavement surface is reduced. Since base aggregates are stress-dependent materials, improved lateral confinement can also increase the modulus/compressive strength of base course aggregates.

Figure 9. Interlocking between geogrid and granular particles and lateral restraint [5]

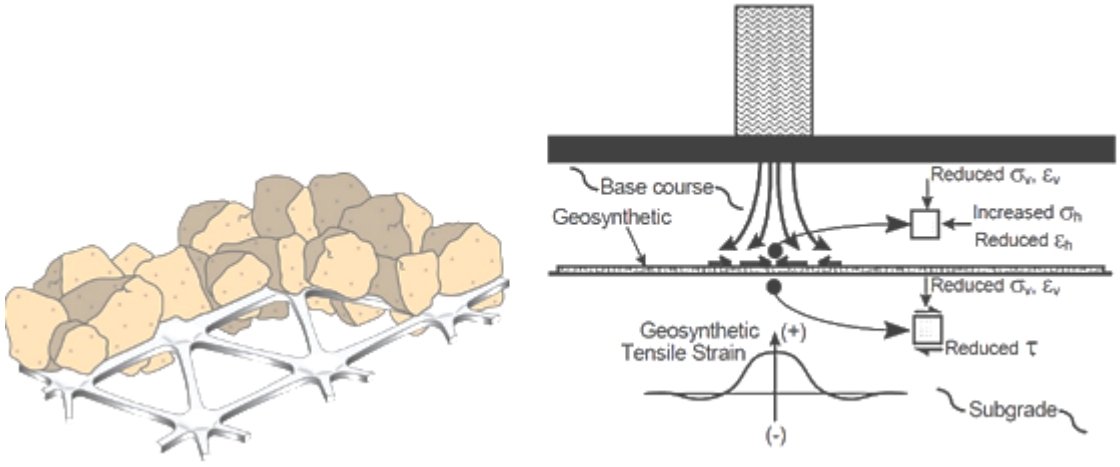

Maxwell et al. outlined the benefits of using geosynthetic reinforcement in pavement structures [28]. Recently, Tutumluer et al. presented a state-of-the-practice article on the transportation applications of geosynthetics, design methods, and recent findings on geosynthetics used in road and airfield pavements and ballasted railway tracks [8]. Without geogrids, traffic loads would cause the granular base to move downward and outward, resulting in shear stresses at the interface between the base and the subgrade. However, by interlocking with the aggregate particles, the stiffer geosynthetic can absorb these shear

stresses, which in turn reduces lateral strain in the granular layer. Geogrids can provide lateral confinement to the aggregate base course through shear resistance and friction between the geogrid and the surrounding aggregate, provided that there is an appropriate ratio between the geogrid aperture size and the aggregate grain size. The confinement offered by the geogrid enhances the modulus of the aggregate, leading to better vertical stress distribution over the subgrade and ultimately reducing the vertical subgrade deformation.

Improved bearing capacity. The inclusion of geosynthetics within the base layer, or at the base-subgrade interface, will result in improving the bearing capacity by changing the geometry of the potential failure envelop to be within the base layer; see Figure 10. This process prevents the most adverse mechanisms from occurring. The figure also demonstrates how the stiffer geosynthetic layer can absorb a significant amount of shear stress and reduce the amount transferred to the subgrade layer. This results in the subgrade being subjected to lower levels of vertical and shear stresses and eventually reduces the pavement's deformation.

Figure 10. Improved bearing capacity effect of using geosynthetics in flexible pavements [29]

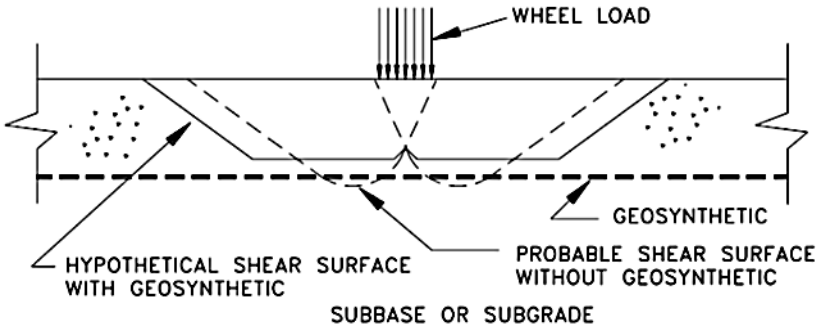

Tensioned membrane effect. The geosynthetic layer is a thin, flexible material that can stretch and form a curved concave shape, known as a tensioned membrane, when subjected to a perpendicular load, provided there is no slack or folds; see Figure 11. Due to its stiffness, the curved reinforcement develops an upward force to support the wheel load and reduce the vertical stress acting on the subgrade. When a wheel passes over the geosynthetic layer, the tension in the layer reduces the pressure applied on the subgrade beneath the wheel. Beyond the wheel, the tensioned membrane effect counteracts the heaving of the subgrade caused by the wheel loading, leading to an increase in pressure applied on the subgrade beyond the wheel. As a result, the subgrade is stabilized, and its heave is reduced. However, the tensioned membrane effect is only significant when traffic is channelized, and the rut depth is

substantial, typically exceeding 4 in. (100 mm). The reinforcement should have enough width and stiffness to prevent it from failing by pull-out and tension.

Stabilization function. This is the process whereby the particles interlocking with the geogrid are confined within the geogrid apertures and/or interface friction (geogrids and geotextiles), resulting in reduced particle movement and rotation. When the particles restrained in this way, they influence particles adjacent to them and confer a degree of confinement to them, resulting in a stabilized granular layer.

Figure 11. Tensioned membrane effect of geosynthetics in flexible pavements [30]

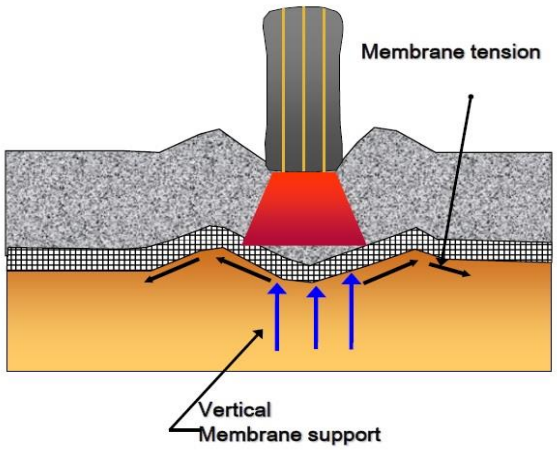

Separation

Separation between layers is very important in the design of flexible pavements when a weak subgrade and subgrade with fine content is encountered. It is a time-dependent process, in which the base course layer thickness decreases with time due to the intrusion of granular base aggregate into weak fine subgrades, and/or the movement/pumping of subgrade fines into the granular base layer; see Figure 12. When the fines from the subgrade migrate into the overlying granular base due to repeated traffic loads, the properties of the base will be negatively impacted. This results in an intermixed or contaminated layer at the interface between the base course and subgrade that can reduce the base thickness, permeability, and strength/stiffness of the base course layer, therefore increasing the risk of structural failure in the pavement system. Factors influencing the particle migration are the size and gradation of the base course layer, thickness of the pavement layers above the subgrade, subgrade strength, fines content and their plasticity, and the traffic load and intensity.

Figure 12. Separation effect of geosynthetics in flexible pavements [31]

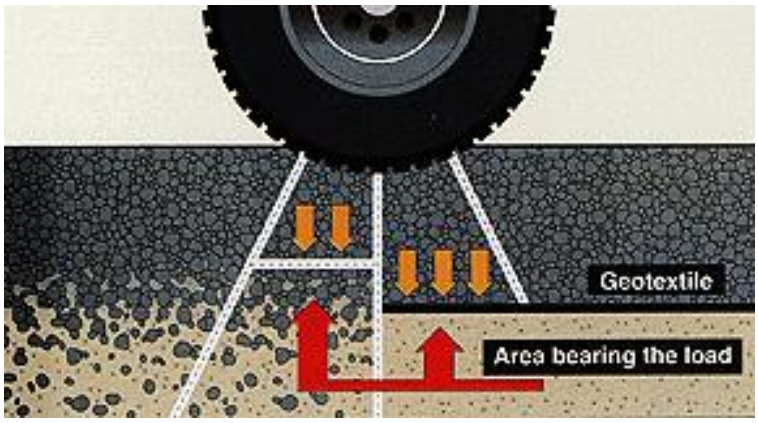

Factors Affecting the Benefits of Geosynthetics in Pavements

The benefits of using geosynthetics in flexible pavements has been addressed by many researchers in the literature, including reducing the base course layer and extending the service life of pavement. The base course thickness for a given flexible pavement can be reduced when geosynthetic reinforcement is included in the design. This reduction is usually defined by the Base Course Reduction (BCR) factor, which is defined as the ratio of the thickness of the reinforced base course layer to that of the unreinforced base course that will have the same service life under the same traffic level. Many studies have indicated that geogrids and geotextiles have successfully been used to provide a platform for construction over soft subgrades. The literature also reported extended service lives for pavement sections with the inclusion of geosynthetics when compared to similar pavement sections without geosynthetics. The influence of geosynthetic reinforcement on rutting behavior or the service life of the flexible pavement is defined by the Traffic Benefit Ratio (TBR). TBR is defined as the ratio of the number of cycles needed to achieve a particular rut depth in a reinforced section to that of an unreinforced section with identical layer thicknesses, material properties, and loading characteristics.

The amount of improvement in pavement performance with the inclusion of geosynthetics depends on many factors, including the strength and stiffness of subgrade, thickness of base layer, type and stiffness of geosynthetic material, location of reinforcement in pavement, etc. Previous studies have shown that the weaker the subgrade, the greater the improvement geosynthetics provided, and that there was little improvement obtained for subgrades with high California Bearing Ratio (CBR). Another factor that plays an important role in the performance of geosynthetic reinforcement in pavements is the thickness of the base course

layer. The benefit of geosynthetics generally decreases as the thickness of the base course layer increases.

The improved performance of geosynthetic reinforced pavement also depends on the properties of geosynthetics, such as the type and tensile modulus, flexural stiffness of geogrid, aperture stability modulus of geogrid, junction strength of geogrid, aperture size of geogrid, frictional capacity with fill materials, and filtration capabilities for geotextiles. While the overall geosynthetic benefits are realized, the effect of each of these parameters in isolation on the pavement performance is not quantified. The appropriate selection of geosynthetics is therefore compromised by the difficulty in associating their relevant properties to pavement performance. Some of the properties currently used in specifications may be unnecessary, resulting in increased costs of application. The properties needed to meet the reinforcement requirements should be evaluated. The majority of the work in the literature indicated better performance for higher tensile modulus geosynthetics (e.g., geogrids and geotextiles) than lower tensile modulus geosynthetics. Given that there are no nationally accepted specifications for properties of geosynthetics under confined conditions (i.e., within pavement), this needs to be further investigated.

The location of a geosynthetic layer or layers relative to the base course layer may be distinguished as an important factor contributing to the success of the design of flexible pavements with reinforced bases. Many studies suggested that geogrid reinforcement benefits are dependent upon the location of the reinforcement layer. Generally, the location of geogrid layers depends on the subgrade strength, the thickness of the base course layer, and the magnitude of applied load. Moghaddas-Nejad and Small suggested that for small loads and a thin base course layer thickness of less than 10 in., a geogrid's optimal location will be in the middle of the base layer [7] [32]. For moderate loads, studies indicated that the placing a geogrid in the middle position of an 8 in. thick base layer resulted in better rutting performance than one placed at the bottom [14] [33]. In the case of heavier loads, Haas et al. suggested that the optimal location of geogrids was at the bottom of base layers up to 10 in. in thickness [34]. However, Perkins and Haas et al. indicated that, for heavy loads and bases thicker than 10 in, the optimal location was at the middle of the base layer [34] [35]. For very heavy loads, Perkins and Ismeik indicated that the bottom of a 12 in. thick base was better than the middle [33]. Haas et al. showed that in the case of a weak subgrade underlying a thick base course layer, optimal results were obtained when the geogrid reinforcement was placed within the subgrade [34]. They also suggested that for optimal effects, the geogrid reinforcement of flexible pavement should be placed in the zone of moderate elastic tensile strain of 0.05 to 0.2 percent beneath the center of the load application. Al-Qadi et al.

concluded from their accelerated testing on full-scale pavement sections with base thicknesses of 8, 12, and 18 in. that for a thin base course layer, placing geogrid at the subgrade/base course interface resulted in the best performance. Additionally, the geogrid should be placed at the upper third of the base course layer for a thicker base course layer of greater than 12 in. [6]. Abu-Farsakh and Chen conducted a series of cyclic plate load testing on pavement sections with 12 in. thick base [14] [36]. In their study, better performance was observed when the geogrid layer was placed at the upper third of base layer than when the geogrid was placed at the base-subgrade interface or at the middle of the base layer [14] [36].

Review of Previous Experimental Studies

Cyclic Plate Load Tests

Previous investigations on the behavior of geosynthetic reinforced pavement sections involved the use of either monotonic or cyclic loading in small-scale test sections. Laboratory-scale studies are necessary to evaluate the benefits of geosynthetic inclusion in pavement construction and to conduct large-scale testing. By utilizing a controlled testing environment, lab-scale testing provides a more cost-effective and simpler alternative to expensive field investigations.

Abdelhalim et al. conducted tests on several pavement sections using a plate loading system to examine the effect of geogrid reinforcement placed at the subgrade-base interface under poor and strong subgrades [37]. The results showed that geogrid reinforced sections exhibited greater resistance to rutting, requiring more loading cycles before reaching a failure rutting depth of 0.79 in. (20 mm) when compared to unreinforced sections. The study also found that the pre-tensioning of the geogrids during installation did not provide significant advantages when compared to ordinary installation methods [37]. Based on these findings, Carrol et al. proposed a design method that involved converting the thicknesses of unreinforced aggregate base layers to equivalent thicknesses for geogrid reinforced sections [38]. This method is presented in Figure 13, which was developed based on the experimental results of a single type of geogrid. The point of inflection in Figure 13 represents the minimum required thickness.

Figure 13. Proposed design criteria for base course thickness [38]

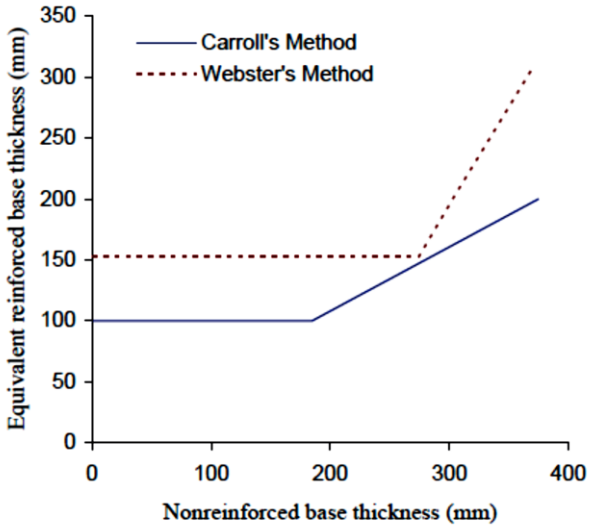

Haas et al. conducted a comprehensive study to assess the advantages of including geogrids in flexible pavements. They subjected pavement sections with varying characteristics to cyclic loading via a steel plate [34]. Rutting depth, subgrade-base interface vertical stress, and geogrid rib tensile strains were measured. The results showed that geogrids tripled the loading cycle capacity and reduced base course thickness by 25-50%. For thin base layers, the optimal geogrid placement was at the subgrade-base interface, while for thick base layers, the midpoint of the base layer was recommended.

Al-Qadi et al. examined road sections in Virginia with poor subgrade conditions, using various geotextiles, geogrids, base course thicknesses, and subgrade strengths. Dynamic loading with a steel plate measured the asphalt rutting depth using LVDTs [39]. The study found that both geotextiles and geogrids improved the poor subgrade soil road performance, but with different mechanisms. Geotextiles separated soil from granular base materials, while geogrids did not offer this benefit.

Montanelli et al. conducted a lab-scale testing program in 1997 to assess the impact of geogrid reinforcement on roadways [10]. They tested sections constructed on a subgrade soil with CBRs ranging from 1-18% using a cyclic plate system. To align with the AASHTO design method, the authors introduced the Base Course Reduction (BCR) coefficient, which is the ratio of geogrid reinforced to unreinforced aggregate base material coefficients. The experimental results showed that the BCR ratio ranged from 1.5 to 2, depending on the subgrade strength (i.e., CBR value). This ratio can be used to determine the structural number

(SN) of the reinforced paved road in the AASHTO design method using the following equation:

$$SN = a_1 D_1 + a_2 D_2 G \quad (1)$$

Equation (1) defines the thickness of the HMA and base course layers (in inches) as D_1 and D_2, respectively. The structural coefficients a_1 and a_2 are assigned to the asphalt and aggregate base layers, respectively, to quantify the strength and structural capacity of pavement layers in unreinforced pavement sections. Additionally, "G" signifies the base layer reinforcing coefficient (BCR). To determine the thickness of the geogrid reinforced base layer, the following equation can be used:

$$D_2 = \frac{SN - a_1 D_1}{a_2 D_2} \quad (2)$$

In 1999, Perkins et al. conducted an extensive laboratory study on pavement systems, using a 6.6×6.6×4.9 ft. (2×2×1.5 m) reinforced concrete box and 9 kips (40 kN) cyclic load applied through a 12 in. (304 mm) diameter steel plate [35]. They tested 20 sections with varying subgrade conditions, geosynthetic placements, two geogrid types, one geotextile type, and base layer thicknesses, as well as measuring geosynthetic strains, rutting depth, subgrade stress, moisture content, and pavement temperature. Geogrid reinforcement significantly improved the sections with poor subgrade soil (i.e., CBR of 1.5%) but had minor benefits on stiff subgrade soil (i.e., CBR of 20%). Heavy-duty geogrids outperformed light-duty ones, with both surpassing geotextile reinforced sections. Optimal geogrid placement at mid-depth in the aggregate base layer was critical for improved performance. In 2004, Perkins et al. conducted cyclic triaxial tests on granular base materials on reinforced and unreinforced sections with geogrids [40]. The cylindrical test sections, 2 ft. (60 cm) in height and 1 ft. (30 cm) in diameter, used four types of geosynthetics, including two geogrids, one geotextile, and one geocomposite, all placed at mid-depth. Their results showed that geosynthetic reinforcement did not significantly affect unbound aggregate resilience but substantially reduced the rutting depth.

Leng et al. conducted 14 laboratory tests at North Carolina State University to assess biaxial geogrid reinforced aggregates over a poor subgrade [41]. Cyclic loading with a 1 ft. diameter plate was applied, and the rutting depth and bottom base layer stress were recorded. Geogrid inclusion reduced rutting depth and improved subgrade-base stress distribution. Moghaddas-Nejad and Small performed drained triaxial tests on geogrid reinforced fine gravel and sand

[42]. The results showed that rutting depth improved with increasing deviator stress, though not the resilient deformation.

Chen et al. investigated the geogrid reinforced aggregate base layers on a weak subgrade by conducting cyclic plate load testing [43]. They used various sensors for instrumentation and found that geogrid improved the pavement performance on CBR 0.5% subgrade, increasing the Traffic Benefit Ratio (TBR) to 3.5 for 1 in. rutting. Geogrid also enhanced stress distribution and reduced subgrade deformation. However, the foil strain gauges were unsuitable for long-term monitoring due to high cyclic loading.

Abu-Farsakh and Chen conducted a cyclic plate load testing program to investigate the effects of geogrid reinforcement in flexible pavements [36]. The pavement test sections were prepared using a test box with dimensions of 6.5×6.5×5.5 ft. (2×2×1.7 m), and cyclic loading was applied through a 1 in. (2.5 cm) thick circular plate with a diameter of 1 ft. (305 mm). The hydraulic actuator provided a sinusoidal vertical loading of 9 kips (40 kN), which applied a pressure of 80 psi (550 kPa) on the surface of the asphalt layer. These conditions simulated the standard single-axle dual tires force of 18,000 lbs. (80 kN). The subgrade soil was silty clay with a liquid limit (LL) of 31 and plasticity index (PI) of 15, while the base course layer was crushed limestone aggregates with D_{10} of 0.015 in. (0.382 mm) and D_{50} of 0.123 in. (3.126 mm). Design level 2 superpave asphalt mixture with a thickness of 7.5 in. (19 cm) was used as the HMA material in their study, and four different types of geogrids were used to reinforce the aggregate base layer. The number of cyclic loadings applied to reach a rutting depth of 3/4 in. (19.1 mm) was recorded. According to the experimental results of this investigation, the use of geogrid reinforcement in the base course layer led to a significant reduction in pavement surface rutting depth. Moreover, greater improvements in rutting depth were observed in test sections that were reinforced, with geogrids having higher tensile strength. The optimal location for geogrid reinforcement was found to be the upper third of the base course layer.

Qian et al. compared unreinforced and triaxial geogrid reinforced base course layers on poor subgrade in a large testing box at the University of Kansas [44]. They found out that the triaxial geogrids significantly reduced the rutting depth and vertical stress at the subgrade-base interface, with heavier-duty geogrids showing greater improvement. Back calculations revealed that as the number of cycles increased, the modulus ratio and stress distribution angle decreased, and this reduction was faster for unreinforced bases than reinforced ones. Sharbaf and Ghafoori assessed the impact of two types of geogrids in flexible pavements to reduce the base course thickness [45]. They conducted six laboratory tests, measuring pressure and vertical stresses with pressure cells and a linear variable differential transformer

(LVDT). Their results showed that geogrids reduced the rutting and vertical stresses, increasing load applications by 1.5 to 7.5 times, and reducing base course thickness by approximately 7% in strong soil. Geogrid B (triaxial) outperformed geogrid A (biaxial), resulting in lower pressures and higher Traffic Benefit Ratios, making it more effective in reducing base layer thickness.

Perkins et al. investigated whether geotextile materials used as separators in flexible pavements offer reinforcement benefits for typical Montana Department of Transportation (MDT) pavements [12]. They constructed test sections targeting a CBR value of 2.5 and measured subgrade properties during and after construction. Results indicated that the unreinforced section and the two sections with geotextiles performed similarly in rutting performance. The study did not quantify the separation benefit of geotextiles, a recognized advantage on most state roadways. However, geotextiles for separation may reduce rehabilitation needs, extend maintenance intervals, and prolong pavement service life. While the primary cost of geotextiles is separation, they may also reinforce during wet seasons. Overall, the study suggests geotextiles as separators in flexible pavements may offer added benefits in reducing pavement deterioration and enhancing rehabilitation decisions.

Luo et al. performed large-scale testing on geosynthetic reinforced pavements built inside an 8 ft. diameter by 6 ft. high circular steel tank [7]. They used two geosynthetics, one geogrid and one geotextile. The pavement sections consist of 6 in. of HMA and 6 and 10 in. of base aggregate layers. The geosynthetic layer was placed at the bottom of the 6 in. sections and in the middle of the 10 in. sections. The pavement sections were loaded using static and dynamic loadings. The dynamic loading included applying 9, 12, and 16 kips load levels for 80, 100 and 150 cycles, respectively. Their study also included laboratory repeated loading triaxial testing, 2-D axisymmetric finite element (FE), and ANN modeling. They found that geogrids are more effective when placed at the center of thick aggregate base layers exceeding 10 in. (254 mm) in depth, and at the bottom (i.e., interface of subgrade and base course) for thinner base course layers 6 to 10 in. (152 to 254 mm) in depth. Based on their study, they developed a Composite Geosynthetic–Base Course Model subroutine for use in AASHTOWare pavement ME design software [7]. The results of their study suggest that placement of geogrid at the interlayer of the subgrade and base course will influence the pressure reduction below the geosynthetic [7].

Abu-Farsakh et al. conducted cyclic plate load tests on seven full-scale test sections that were constructed over soft subgrades to investigate the performance of geosynthetic reinforced pavements [14]. Cyclic load at a frequency of 0.77 Hz was applied through a 305 mm diameter steel plate. The test results clearly show the benefits of geosynthetics in

significantly reducing pavement rutting. The test section with double geosynthetic layers performed better than the other six sections studied. After eliminating the effect of variations in construction, the benefits of geosynthetic reinforcement are quantified within the context of the AASHTOWare Pavement ME Design Guide. The developed design procedure can quantify the contribution of geosynthetics in pavements to base reinforcement as well as subgrade stabilization. A design methodology is proposed that falls within the context of MEPDG.

Nazeri et al. conducted an experimental study inside a steel test box using static plate load tests to evaluate the efficiency of a multi-task geosynthetic comprised of a geogrid and a nonwoven geotextile layer in decreasing the required thickness of base course constructed over different soft subgrades [46]. The geosynthetics were placed at the base-subgrade interface for both reinforcing and separation functions. The results demonstrated that in case of composite-geosynthetic inclusion, the required thickness of base course could be reduced by 17-23%, depending on the strength of underlying subgrade layer. The use of geosynthetic end-fixation led to better functionalities of all reinforcements in fixed-end models compared to free-end ones. The results also demonstrated that the efficiency of the geocomposite is contingent on the thickness of the base course such that the efficiency of the reinforcement reduces as the base course thickness increases.

Marelli et al. conducted laboratory tests to evaluate the performance of 3-D biaxial geogrid for base stabilization of pavements through interaction with the granular aggregate [47]. The tests included pullout, composite stiffness, cyclic plate load, and full-scale rolling wheel load tests. The results clearly demonstrated the advantage of using the 3-D biaxial geogrids over the traditional planar geogrids on enhancing the pavement performance.

Divakar et al. conducted a series of cyclic plate load tests to examine the potential utilization of marginal materials reinforced with geosynthetics for sustainability in the pavement sector [48]. The various geosynthetics used in the research include geogrid, geocell, double geogrid, and geocell combined with geogrid. Several unreinforced and geosynthetic reinforced pavement sections were built in the lab using landslide debris as the base material supported by a black cotton soil subgrade. The effectiveness of geosynthetic reinforcement was measured in relation to permanent deformation, resilient deformation, reduction in rut depth, traffic improvement ratio, decrease in vertical stresses applied to the subgrade, and reduction in base layer thickness. The test findings show that geogrid reinforcement notably decreased rut depth and enhanced the traffic capacity. Further, across all types of geosynthetic reinforcements, the pairing of geogrid and geocell excelled in reducing permanent deformation and rut depth.

Jayalath et al. performed small-scale cyclic load tests to investigate the rutting behavior of unreinforced and geogrid-reinforced unpaved pavements utilizing a circular mold with a diameter of 12 in. and a height of 20.5 in. [49]. Cyclic load tests were performed on a granular base with different thicknesses using the selected types of geogrids (composite or biaxial) placed within the granular layer and/or at the base-subgrade interface. The test results indicated that placing a geogrid at the base-subgrade interface can significantly decrease the permanent deformation when the thickness of the granular base is relatively thin. The results also showed that a biaxial geogrid placed at the middle of the granular base is more effective in minimizing the rut depth compared to composite or biaxial geogrids located at the base-subgrade junction. The advantages of geogrid reinforcement appear to decrease with an increasing base thickness. Enhanced rut resistance in unpaved granular pavements was first observed with double reinforcement, followed by biaxial geogrid placed in the middle of granular base, composite geogrid in the middle of the granular base, composite geogrid at the base-subgrade interface, and biaxial geogrid at the base-subgrade interface.

Srivastava and Balunaini performed a laboratory experiment inside a test chamber (1.5 m × 1.5 m × 1.1 m) to assess how geogrid and geotextile reinforced expansive subgrades influence the behavior of pavements under varying swell pressure caused by expansive subgrades [50]. Three scenarios were examined: one featuring a 400 mm wet mix macadam layer placed directly on the subgrade; another with a 400 mm wet mix macadam layer on a 250 mm prepared subgrade; and the third with a 400 mm wet mix macadam layer on a 500 mm prepared subgrade. A 250 mm diameter plate was used to simulate the differential swell pressure, leading to a potential vertical rise of 12.5 mm in the unreinforced area of the subgrade. Identical pressure was exerted on reinforced scenarios, where geotextile and geogrid reinforcements were located at the subgrade level to alleviate heave caused by swelling. Geotextile reinforcement decreased potential vertical rise by 85%, 78%, and 58% at swell pressures of 150 kPa, 225 kPa, and 425 kPa, respectively, whereas geogrid reinforcement led to reductions of 77%, 68%, and 36% under identical pressures.

Badiger et al. carried out an experimental investigation to assess the efficacy of geosynthetic reinforced recycled concrete aggregate (RCA) in granular subbase applications under repeated loading conditions [51]. Several sections were constructed under various conditions: unreinforced, geogrid reinforced, geocell reinforced, and a combination of geocell and basal geogrid reinforced. The findings indicated that the geosynthetic reinforced RCA performed similarly to conventional aggregates. Geosynthetic reinforced pavements demonstrated a reduction in permanent deformation ranging from 0.13 to 0.41 when compared to

unreinforced sections. The combination of geocell and basal geogrid reinforced sections achieved the highest Traffic Benefit Ratio (TBR), recording 4.55 for conventional aggregates and 7.25 for RCA. Further, geosynthetic reinforced sections exhibited a decrease in residual pressure by a factor of 0.14 to 0.39 when compared to unreinforced sections. Strain analysis revealed that geocell and basal geogrid reinforced sections provided superior load distribution compared to sections reinforced solely with geogrid.

Field Investigations

Accelerated Pavement Testing (APT) has been utilized by several agencies in the U.S. for the past 30 years. This testing involves constructing and instrumenting test lane sections to examine various materials and configurations by applying a load and tire pressure equivalent to what pavement experiences in the field, with variables including load and tire pressures and tire wheel speed. The accelerated loading facility continues to apply loading until the pavement lane section fails or reaches a specified rut depth, while pressure cells, environmental sensors, and strain gauges collect data for analysis. The APT system features test tracks in a facility that can be indoor or outdoor, as shown in Figure 14, and utilizes an automated single wheel load with one or two axles that repeatedly runs over the test track, providing a good simulation of in-service pavement performance and offering a rapid indication of pavement performance under more severe conditions.

Figure 14. Louisiana Accelerated Loading Facility (ALF)

Cancelli and Montanelli compared the performance of geogrid and geotextile inclusion in pavement lane sections [52]. They found that the geogrid inclusion reduced the base layer thickness, especially with higher tensile modulus. High strength geotextile was better for base-subgrade separation. Geogrids increased the load applications at 0.197 in. (5 mm) rutting depth by a factor of 200, with a suggested TBR of 10. Greater improvements occurred with geogrids on poor subgrade soil. Including geogrids raised the structural layer coefficient

of the base course to 1.5-2.0. Perkins and Edens studied the performance of geogrid and geotextile reinforced pavements [11]. All geosynthetics reduced rutting depth and stresses, with no significant differences between geogrid and geotextile performance.

Tingle and Webster tested four geosynthetic reinforced pavement lane sections [53]. The unreinforced section had a 20 in. (50.8 cm) thick base layer. The woven and nonwoven geotextile reinforced sections had 15 in. (38.1 cm) base layers. Another section had a 10 in. (25.4 cm) base with geocomposite reinforcement. Subgrade soil intruded 5 in. (12.7 cm) and punched 1.5 in. (3.8 cm) in the unreinforced section. No subgrade rutting was recorded. Woven geotextile caused a 3 in. (7.6 cm) rutting depth. Nonwoven geotextile resulted in 3 in. (7.6 cm) rutting and 7.5 in. (190 mm) intrusion. Geocomposite caused 2 in. (5.1 cm) subgrade rutting. Recommended base course reduction factors were 0.75 for geotextile-reinforced sections and 0.5 for geocomposite reinforced sections.

Aran conducted a long-term study on geogrid reinforced test lane pavements [54]. Two sections were built in 1986 and 1990. In 1986, geogrid was placed at the subgrade-base interface with a 10 in. (25.4 cm) base layer. The unreinforced section had a 2 in. (5 cm) thicker HMA layer. In 1990, geogrid was placed in a 4 in. (10 cm) base layer, while the unreinforced section had 6 in. (15 cm) lime-stabilized subgrade. Their performance was evaluated in 1991, 2004, and 2005. The results showed that the geogrid reinforced sections matched the unreinforced section with a 2 in. (5 cm) thicker HMA layer. Geogrid inclusion improved thinner pavement sections more effectively.

Helstrom et al. studied the benefits of geosynthetic reinforcement in flexible pavements. They created two test lane series over subgrade soil with a standard penetration number of 7 [55]. Series 1 had a 12 in. (300 mm) base layer, while Series 2 had a 24 in. (600 mm) base layer. Each series had four reinforced sections. The first two sections used geogrids placed at the subgrade-base and mid-base depths, while the third section had a geogrid placed in the middle of the base with a drainage geocomposite at the subgrade-base. The fourth section had the drainage geocomposite at the subgrade-base. All sections had a 6 in. (150 mm) HMA layer. Their results showed that geogrid and drainage composite in 12 in. (300 mm) base layers increased the structural coefficient by 5% and 17%, respectively. No notable results were observed for the 24 in. (600 mm) base layers. The drainage geocomposite did not affect the subgrade pore water pressure. The long-term force in the geogrid ranged from 18-83%, which is equivalent to a 1-3 in. (25-75 mm) thicker base layer thickness.

Al-Qadi et al. investigated the geogrid benefits in low volume flexible pavements [6]. They built nine test sections with subgrade soils (CBR = 4%) and different aggregate base layer

thicknesses of 8 in. (202 mm), 12 in. (304 mm), and 18 in. (458 mm). The HMA layers varied from 3 in. (75 mm) to 5 in. (128 mm). Two types of geogrid were used in their test sections. Their results showed that the inclusion of geogrid resulted in reducing rutting depth, especially in thin base layers and the upper third of thick base layers.

Duncan et al. conducted an experimental study to investigate the effect of geogrid reinforcement on the strength characteristics of aggregate base materials [56]. The study involved preparing specimens with various soil materials both with and without geogrid reinforcement placed at the mid-depth of the samples. Their results showed that the CBR value of the soil was improved by the inclusion of geogrid reinforcement.

Henry et al. studied the performance of geogrid reinforced flexible pavements with thick HMA and base course layers [57]. They constructed eight test lane sections with varying HMA and base course thicknesses. The subgrade was silt, and the reinforcement layer was placed between the subgrade and base course. Water was added to the subgrade to reach a target modulus. They measured the elastic deformation and rutting depth on the HMA and subgrade-base interface using coils, recorded stresses with pressure cells, and measured strains on geogrid ribs with foil strain gauges. A heavy vehicle simulator applied dynamic loads. The inclusion of geogrid increased the cyclic loadings by 1.3 to 1.4 times but did not notably improve sections with thick HMA and base course layers. The elastic vertical strains did not decrease in any layer.

Cox et al. carried out a field study to investigate the effect of geogrid reinforcement on the rutting depth of flexible pavements [58]. The researchers used a Vibroseis (shaker) to apply cyclic loading to the surface of geosynthetic reinforced pavement sections. They installed a line of LVDTs on the surface of the test sections to measure the elastic deformation and permanent rutting depth. The results of their experiment showed that thicker base course layer pavements had lower rutting depths. However, the researchers did not observe any significant improvements in pavement performance due to geogrid reinforcement. This could be because there was not enough strain in the pavement section to activate the reinforcement layer.

McCartney et al. studied the benefits of geogrid reinforcement on full-scale flexible pavements under static surface loading [59]. Their research focused on an Arkansas frontage road with sixteen 50 ft. (15 m) long sections, various geosynthetic types, control sections, and two base course thicknesses. They conducted static plate load tests applying a maximum static surface stress of 78 psi (540 kPa) to each section. The maximum deflections under this stress ranged from 0.10 to 0.16 in. (2.5 to 4 mm). To account for asphalt layer effects, they

used multiple unload-reload curves and calculated tangent stiffness. The stiffness in reinforced sections decreased less from wet to dry seasons. The study used Poisson's ratios of base course layers, considering geosynthetic reinforcement, to assess the lateral confinement. The static plate load tests were reliable for evaluating the geosynthetic reinforced pavement sections, showing rational trends with reinforcement type and base course thickness.

Al-Qadi et al. conducted a field full-scale test program on low volume flexible roadways to study geogrid reinforcement's effectiveness in base course layers [60]. They used pavement sections with varying HMA and base course thicknesses built on a subgrade with CBR = 4%. Over 170 gauges monitored responses such as rutting depth, temperature, strains, moisture, pore-water pressure, and stresses during cyclic loading via an accelerated transportation loading system. Their results demonstrated that the geogrid reduced rutting and delayed cracking, and that the vertical deflection and stress decreased with lower loading speeds. The key finding was the geogrid's reduction in the horizontal displacement of granular materials, especially in loading directions. The optimal location of geogrid placement was found to be at the upper third of a thick base course layer, especially for sections built over poor subgrade soils.

Jersey et al. conducted a field study on geogrid reinforced base course in a thin flexible pavement section subjected to accelerated traffic loading [61]. They compared it with two unreinforced control sections. Periodic measurements of pavement stiffness and permanent deformations showed superior performance for the geogrid reinforced pavement section. The researchers developed Traffic Benefit Ratios and base course structural coefficients based on these results to compare different pavement structures.

Greene et al. studied the effect of geosynthetic reinforcement on pavement performance in Florida's organic soil-rich regions [62]. They conducted the research on a realigned section of State Road 15 near Lake Okeechobee. Four 500 ft. sections with different combinations of geogrids and geotextiles, placed both below the base and above the organic material, were compared to a control section with no geosynthetic reinforcement. The results of their study revealed that surcharging alone greatly improved pavement performance. Geosynthetic reinforcement doubled the ESALs allowed on the unreinforced section. Rigid extruded geogrids or woven geotextiles placed below the base provided a slightly stiffer and better-performing pavement than flexible geogrids. The study recommended using rigid extruded geogrid or woven geotextile at the bottom of the base layer combined with a woven geotextile above the organic material layer for new roadways over thick organic deposits or for reconstruction when feasible.

Abu-Farsakh et al. conducted full-scale tests on six geosynthetic reinforced test lane sections 80 ft. long and 13 ft. wide, using moving wheel accelerated load tests [14]. In their study, two lanes were reinforced by one or two layers of triaxial geogrids, two sections were reinforced by one layer of high strength woven geotextile with different base layer thickness, and the remaining two sections were control sections. The test lanes were instrumented with a variety of sensors to measure the load- and environment-associated pavement response and performance. The results of their study demonstrate the benefits of using geosynthetics in reducing the permanent deformation in the pavement structure. They developed four empirical models through nonlinear regression to quantify the benefits of geosynthetics in pavements over weak subgrade soil. The models included the Traffic Benefit Ratio (TBR), Base Course Reduction (BCR), an increase in resilient modulus due to geosynthetics in the base layer, and an increase in resilient modulus due to geosynthetics in subgrade stabilization. The experimental data verified these models, showing that geosynthetic reinforcement redistributes applied load, reducing stress concentration and improving vertical stress distribution on the subgrade layer. Their results showed less accumulated permanent deformation, lower maximum vertical stress on the subgrade, and reduced rutting, base, and subgrade permanent deformations. The double geosynthetic reinforcement lanes showed the best performance but involve higher initial cost of geosynthetics.

Imjai et al. conducted full-scale trial test sections in Thailand to assess geosynthetics' performance as pavement reinforcement [63]. They embedded geosynthetics at various depths in four test sections and monitored the structural responses using various sensors. Their results showed that all configurations reduced the vertical static stresses by up to 66% and the dynamic stresses by up to 72%. Geosynthetics improved the rut resistance, with a maximum Traffic Benefit Ratio (TBR) of 13.70, an effectiveness stiffness ratio of 12.70, and a minimum rutting reduction ratio of 0.74. The most effective configuration included a geotextile within the asphalt layer and a geogrid under the base layer. Non-linear finite element analyses validated these findings, suggesting that geosynthetics can extend the lifetimes and maintenance periods of pavements.

Perkins and Cuelho conducted an indoor full-scale accelerated load testing to evaluate the performance of two geotextile reinforced pavement sections as (woven and non-woven) compared to an unreinforced section to assess the benefit geotextiles in terms of extending the service life of pavements [12]. The constructed test sections had a nominal section of 3.4 in. of HMA and 13.3 in. of base course aggregate on a clay subgrade with a CBR of 3.5. The test sections were loaded with 1 million traffic passes. The test results showed that the three test sections performed similarly in terms of rutting performance. This demonstrated

moderate reinforcement benefit of geotextiles for weaker subgrade conditions during seasonally wetter periods. The study did not quantify the separation benefits of geotextiles, which are applicable to most roadways. The benefit lies in the geotextile's function as a separator, which may reduce the cost of rehabilitation and reconstruction operations and ensure the structural performance of the pavement during seasonal periods in which the subgrade may become wet and weak.

Singh et al. carried out an experimental investigation in a test pit of 9 m long and 2.7 m wide to evaluate the effectiveness of geosynthetic reinforced unpaved roads under moving wheel load tests in terms of permanent surface deformation of the pavement [64]. Geogrid and geotextile were utilized for reinforcing the unpaved road test sections. The rut depth was assessed across the wheel path's transverse direction following a specific number of wheel passes. Traffic Benefit Ratio (TBR) and performance index were utilized to assess the efficiency of geosynthetic reinforcement in unpaved roads. Following 350 vehicle passes, the test sections reinforced with geotextile and geogrid experience a reduction in rutting of 44.89% and 28.57%, respectively. Their test results demonstrated that the inclusion of geosynthetic reinforcement significantly reduces rutting and increases the stability of the reinforced test sections when compared to the unreinforced sections.

Shahkolahi et al. conducted full-scale field pavement tests to assess the benefits of using geogrids to stabilize pavements constructed on soft and expansive subgrade soil in terms of their impact on the initial composite stiffness and long-term pavement performance [65]. Sections with different geogrid arrangements were constructed and monitored for a period of three years. The results indicated that incorporating geogrids enhances the bearing capacity of the pavement section by diminishing the vertical pressures from traffic on the underlying materials. The results also reveal that having two geogrid layers, one placed at the subgrade-subbase interface and another at the subbase-base interface, provides greater improvement of the bearing capacity compared to installing just one geogrid at the subgrade-subbase interface.

Previous Numerical Studies

To evaluate the impact of geosynthetics on pavement structures, parametric studies and finite element (FE) numerical modeling were utilized in many research studies in the literature to study the effect of different variables and parameters contributing to the benefits of geosynthetic reinforcement in pavements. These models were designed to compute the pavement responses, such as stresses, strains, and deformations, of pavements with and without inclusion of geosynthetic layers under various loading configurations. These

responses can then be analyzed to determine the effectiveness of using geosynthetics as base reinforcement. The FE models included several elements, such as geometric characteristics of geosynthetics, traffic loading, constitutive models of materials, and interface conditions. Table 1 summarizes the characteristics of the FE models developed in the literature for geosynthetic reinforced pavements and the corresponding modeling techniques employed. It is noted that all of the pavement models in Table 1 were flexible pavements, as no models were identified for rigid pavements involving geosynthetic reinforcement.

Table 1. Summary of finite element (FE) model studies on geosynthetic reinforced pavements

Authors	Model	AC	Base	Subgrade	Geosynth
Leng & Gabr [66]	3-D	Linear elastic	Extended Drucker-Prager with hyperbolic yield criterion	Extended Drucker-Prager with hyperbolic yield criterion	Linear elastic
Abu-Farsakh & Nazzal [4]	2-D	Elastic- perfectly plastic	Two critical surface plasticity model	Modified Cam Clay	Linear elastic
Kown et al. [67]	2-D	Linear elastic	Linear isotropic	Anisotropic elastic	Linear elastic
Perkins et al. [68]	2-D	Isotropic linear elastic	Isotropic linear elastic	Isotropic linear elastic	Linear elastic
Gu [13]	2-D	Elastic-perfectly plastic	Elastoplastic bounding surface model	Modified Cam Clay	Linear elastic
Kim & Lee [69]	3-D	Linear elastic	Extended Drucker-Prager with hyperbolic yield criterion	Extended Drucker-Prager with hyperbolic yield criterion	Linear elastic
Gu et al. [70]	2-D	Viscoelastic material using Prony series	Non-linear cross anisotropic	Linear elastic	Linear elastic
Zhi et al. [71]	3-D	Nonlinear visco-elastic	Linear elastic	Linear elastic	-
Sun et al. [72]	2-D	Bilinear cohesive zone model	Linear elastic	Linear elastic	-

Barksdale et al. conducted FE numerical modeling to evaluate the structural performance of geosynthetic reinforced and unreinforced pavements under laboratory cycling load testing [73]. Their results showed that the placement of geogrid at the interface between base and subgrade layers led to a reduction in vertical strain when compared to unreinforced

pavement. According to Al-Qadi et al., the appropriate utilization of geogrid can prevent sudden failures and collapse during the construction of pavements and help to avoid potential structural issues [39]. They stated that the actual impact of geogrids on flexible pavements is not fully understood.

Wathugala et al. aimed to investigate the impact of geosynthetic stiffness on the behavior of pavement by developing a two-dimensional axisymmetric finite element model; see Figure 15 [74]. They compared the results of six different analyses: Case 1, which involved linear elastic models with geosynthetics (subdivided into Case 1a with a stiffness of E = 145 ksi [1 GPa] and Case 1b with a stiffness of E = 14,500 ksi [100 GPa]; Case 2, which involved linear elastic models without geosynthetics; Case 3, which involved elastic-plastic models with geosynthetics (subdivided into Case 3a with a stiffness of E = 145 ksi and Case 3b with a stiffness of E = 14,500 ksi); and Case 4, which involved elastic-plastic models without geosynthetics. The subgrade's non-linear behavior under cyclic loads was modeled using the constitutive model. The base course layer was modeled using the same approach used to model the subgrade layer. The geogrid layer's thickness was 0.1 in. (2.5 mm), and the bonding between the soil and geogrid was assumed not to be full. They concluded that the inclusion of geosynthetics reduced the permanent rut depth by almost 20% for a single load cycle, with the geosynthetic's flexural rigidity being the primary contributing factor to this reduction.

Figure 15. 2-D finite element (FE) model of reinforced pavement [74]

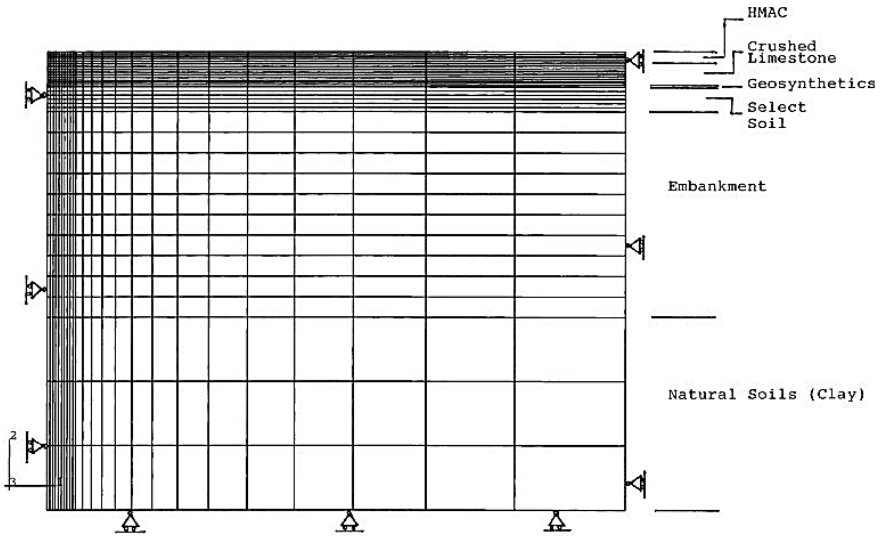

In 2001, Perkins conducted a study using a two-dimensional axisymmetric FE simulation model to evaluate the effects of high modulus geogrid reinforcement on pavement

performance under static and dynamic loading conditions [75]. He used a mechanistic model consisting of a 3-D FE model that matched the nominal conditions of a pavement test facility previously described by Perkins in 1999 [5]. The facility was 6.6 ft. x 6.6 ft. x 5 ft. deep reinforced concrete box in which the roadway cross section was constructed and loaded cyclically with a 9 kips (40 kN) load applied at a period of 1.5 sec. to a 1 ft. (30.4 cm) diameter steel plate resting on a waffled rubber pad on the asphalt concrete surface. The 3-D model was used to account for the potential influence of the box's square corners and for the geosynthetic inclusion with direction-dependent material properties; see Figure 16. An FE model for one-quarter of the box was created due to the symmetry of the box. The study varied the layer thickness for the parametric study performed. They used elasto-plastic constitutive models for the majority of the pavement layers. The bounding surface plasticity model described by Dafalias and Hermann was used to account for the positive effect of aggregate confinement on the increase in stiffness and strength of the base aggregate [76]. An orthotropic linear-elastic model was used for geosynthetics, which accounted for anisotropy by specifying the in-plane shear modulus and in-plane Poisson's ratio to account for differences in elastic modulus between machine and cross-machine directions. The study extracted principal response parameters from the FE model, including vertical strain in the top of the subgrade and bulk stress in the unbound base aggregate layer. These response parameters were used in empirical damage models to predict the long-term pavement performance and define reinforcement benefit. Reinforcement benefit was defined in terms of an extension of service life of the pavement, a reduction in aggregate thickness for equivalent service life, or a combination of both. The damage models were calibrated from reinforced and unreinforced pavement test sections, and the model was shown to provide general descriptions of reinforcement mechanisms that were consistent with those previously observed in instrumented pavement test sections.

Figure 16. Finite element (FE) model of unreinforced pavement test sections [75]

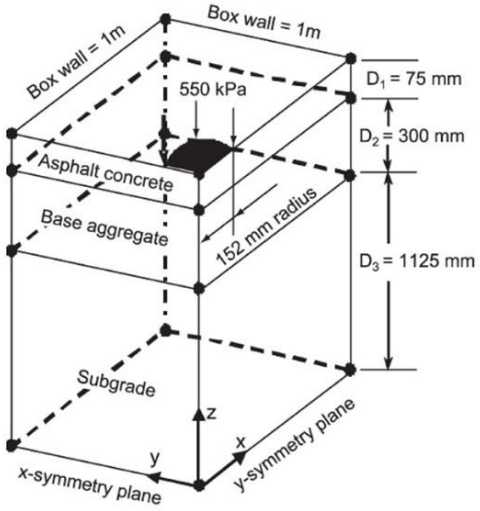

Ling and Liu utilized PLAXIS software to develop a 2-D plane strain FE model for examining the behavior of geogrid reinforced asphalt pavement under monotonic loading [77]. They explored the impact of using associated and non-associated flow rules for soil and asphalt materials, as well as the design parameters such as geosynthetic stiffness, asphalt layer thickness, and subgrade foundation strength on pavement behavior. The sand and asphalt layers were modeled using simple elastic-plastic model utilizing the Mohr-Coulomb criteria to model the soil. Linear elastic properties were used to simulate geosynthetics. Three types of analysis were conducted to simulate loading effects: (1) sand subgrade foundation alone, (2) pavement over sand foundation or “unreinforced pavement,” and (3) geosynthetic reinforced pavement. Ling and Liu found that using the associated and non-associated flow rules produced similar results for the pavement system, although the failure load was higher when an associated flow rule was used. Moreover, non-associated flow rule results were more suitable for the simple elastic-plastic analysis of asphalt pavements than for reinforced pavements. Increasing the stiffness of the geogrid improved the load-settlement relationship, with no upper limit for this improvement. The effect of geosynthetic reinforcement was more significant for weaker subgrades than stiffer subgrades.

Perkins et al. created a response model for flexible pavements reinforced with geosynthetics using FE analysis [40]. The model used an isotropic linear elastic model for the asphalt concrete and geosynthetic layers, while the base and subgrade layers were modeled using an isotropic nonlinear elastic model. Additionally, a Coulomb friction model was employed to describe the shear interaction along each of the geosynthetic contact surfaces. The model consisted of four modules: one for describing reinforcement during compaction and three that

were used iteratively to depict the effects of reinforcement during traffic loading. When combined with an empirical model that accounts for the growth of permanent interface shear stress with traffic passes on a reinforced pavement, the response model provided a rational method for evaluating the performance of reinforced pavements and demonstrating the benefits of geosynthetics.

Leng and Gabr performed FE numerical analysis using ABAQUS to study the effectiveness of geosynthetic reinforced unpaved pavement sections [77]. They verified their model of geosynthetic reinforced pavements using their earlier experimental work. The researchers found that decreasing the modulus ratio of the aggregate layer to the subgrade layer improved the performance of the geosynthetic reinforced section. Further, a higher geogrid modulus or better soil/aggregate-geogrid interface property led to a significant reduction in critical pavement responses.

Kwon et al. employed FE analyses to investigate the behavior of geosynthetic reinforced flexible pavements [67]. They used nonlinear isotropic and anisotropic elastic models to describe the behavior of granular base and subgrade materials, respectively. According to the findings, the critical pavement responses due to traffic loading were generally reduced when high stiffness geosynthetic reinforcement was used. They also employed cross-anisotropic base characterization that resulted in higher percentage reductions in critical pavement responses, indicating increased benefits of geosynthetic reinforcement.

Howard and Warren created an axisymmetric FE model to analyze data collected from seventeen heavily monitored geosynthetic reinforced test sections [78]. Geosynthetics were modeled using 1-D tension elements. The behavior of the asphalt was represented by a linear elastic model, while a hyperbolic model was used to describe the non-linear stress-dependent behavior of the granular materials, including compacted subgrade. The Mohr-Coulomb model was used to simulate the properties of natural soil, and the same model was also used to represent its non-linear properties.

Saad et al. utilized 3-D FE analyses to investigate the impacts of geosynthetic reinforcement on the performance of pavement structures; see Figure 17 [79]. The AC and geosynthetic reinforcement layers were modeled using a linear elastic model, while the base course and subgrade layers were modeled using Drucker-Prager and Modified Cam-Clay (MCC) models, respectively. The findings demonstrated that the placement of geosynthetic reinforcement at the base-AC interface resulted in the most significant reduction, up to 46-48%, in lateral fatigue strain at the bottom of the AC layer. They concluded that placing

geosynthetics in thin bases was especially effective in decreasing vertical strain at the top of the subgrade layer.

Figure 17. 3-D finite element (FE) model geometry [79]

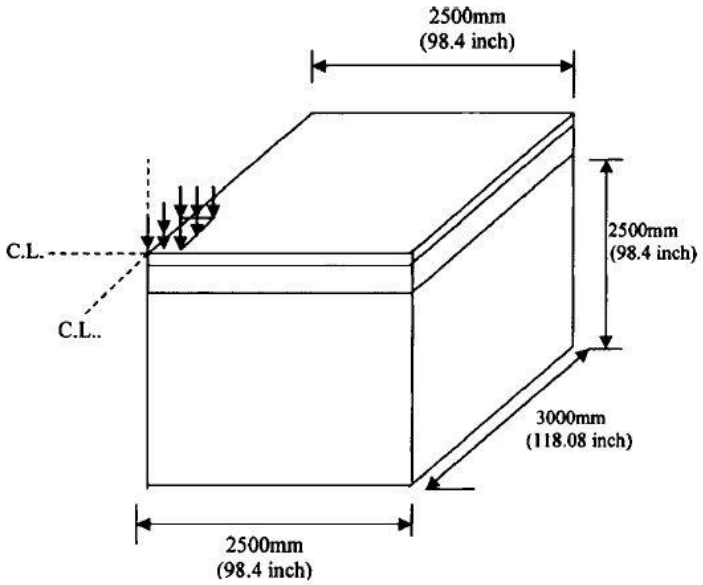

Abu-Farsakh and Nazzal developed a 2-D axisymmetric FE model to evaluate the effect of reinforcing the base course layer with geogrids in a flexible pavement structure; see Figure 18 [4]. They investigated the influence of various factors, such as the thickness of the base course layer, the strength of the subgrade soil, and the stiffness of the geogrid layer, on the performance of flexible pavements. To quantify the degree of improvement achieved by geogrids, they used the rut depth after two million load cycles to develop regression models. The study utilized five different reinforced base course thicknesses and three subgrade types: weak, moderate, and stiff. Four biaxial geogrids were used and placed at the bottom of the base layer. The FE model used eight-node bi-quadratic axisymmetric quadrilateral elements for the subgrade, base, and asphalt concrete layer, while three-node quadratic membrane elements with a thickness of 0.079 in. (2 mm) were used for geosynthetic reinforcement. The Drucker-Prager elastic-plastic model was used to simulate the behavior of base course and subgrade, while an elastic-perfectly plastic model was used to model the AC layer. Additionally, the geosynthetic material behavior was modeled using a linear elastic model. They found that the use of geosynthetic reinforcement reduced the permanent deformation (i.e., rutting) of pavement sections. The degree of reduction was dependent on the stiffness of the subgrade, the geogrid stiffness, and the thickness of the base layer. Moreover, the effect was more significant for weaker subgrades than stiffer ones. They also discovered that the

effect of geogrid reinforcement decreased as the thickness of the base layer increased, while it improved as the stiffness of the subgrade layer increased.

Figure 18. Axisymmetric finite element (FE) model [4]

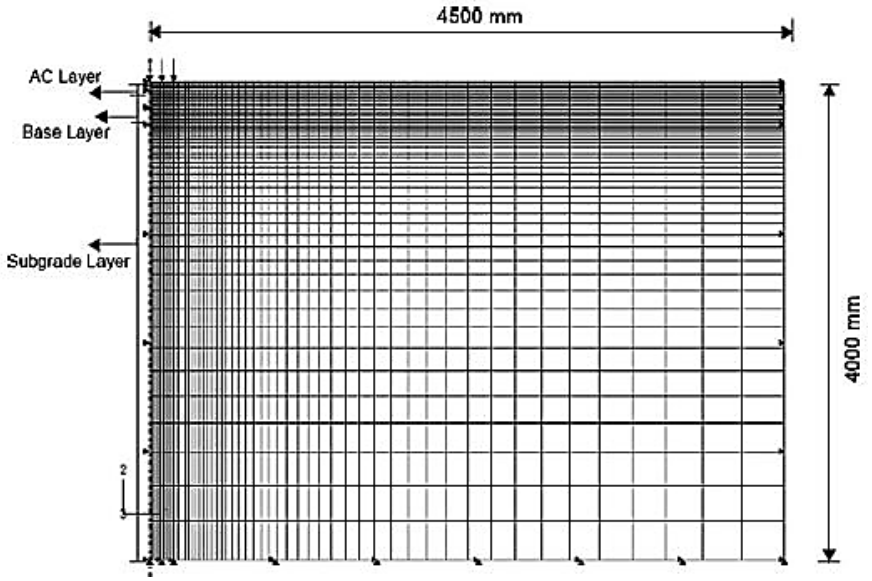

Perkins et al. have developed a mechanistic-empirical model for geosynthetic base reinforced flexible pavements based on FE analysis [80]. The FE model incorporated traditional components of an existing unreinforced mechanistic-empirical model developed through NCHRP Project 1-37A, including FE response modeling, material models for asphalt concrete, unbound aggregate base and subgrade, and damage models for asphalt concrete fatigue cracking. The model also included components for geosynthetics, such as structural elements, material models, and geosynthetic-aggregate interaction. The model accounted for the influence of geosynthetics on the lateral confinement of base aggregate during construction and subsequent traffic loading. The model also adopted a modified permanent deformation damage model for aggregate within the influence zone of reinforcement. The results showed favorable agreement with existing unreinforced mechanistic-empirical models, indicating a significant improvement over other models for reinforced pavements.

Kwon et al. developed an FE model for analyzing flexible pavements reinforced with geogrids that are intended for use in low to moderate traffic volumes and have a relatively thin HMA surface layer [81]. The model used linear isotropic and anisotropic elastic constitutive models to represent the behavior of base and subgrade materials, respectively, and took into account compaction and pre-loading induced base course residual stresses. To validate the model, data was collected from instrumented full-scale pavements constructed

with both geogrid reinforced and control test sections. The model's predictions, which used nonlinear anisotropic characterizations of the granular base layer moduli, were found to better capture the magnitudes and trends in the measured response data. Further, the predictions made by the mechanistic model at different locations in the test sections were reasonably consistent with many field-measured responses under varying load levels.

Gu conducted an FE parametric study to evaluate the performance of geogrid reinforced bases in flexible pavement systems [13]. She used FE models to analyze the effect of different design parameters on the performance of geogrid reinforced pavements, and multiple regression models were developed to estimate the benefits of reinforced geomaterials under different combinations of the design parameters. The results showed that geogrid reinforcement of the base course layer reduced lateral strains within the base course and subgrade layers, with more appreciable benefits observed in sections with weak subgrades compared to those with moderate or stiff subgrades. The increase in geogrid tensile modulus resulted in a significant reduction of permanent deformation, although the effect decreased with an increase in the thickness of the reinforced base course layer and subgrade strength. The results also showed that geogrids can extend the service life of pavements, with Traffic Benefit Ratios (TBR) of up to 3.4 obtained for pavement sections over weak subgrades. Regression models were developed to predict the benefits of reinforcing the base course layers in terms of TBR, which indicated that the geogrid improvement increased with increasing the geogrid stiffness and decreasing in base course layer thickness and subgrade strength.

Kim and Lee conducted a study on geogrid reinforced flexible pavement in low volume roads through a 3-D FE analysis; see Figure 19 [69]. The goal of their study was to investigate the structural benefits of geogrid reinforcement in flexible pavements and analyze the behavior of pavement foundation under traffic loading. The authors developed a mechanistic model for geogrid reinforced flexible pavement and employed stress-dependent resilient modulus models in both base and subgrade layers to characterize the resilient response of geomaterials under wheel loading. The model also incorporated the geogrid characteristics and residual stress resulting from aggregate and geogrid interaction. The authors analyzed four different pavement configurations to measure the differences in pavement responses before and after the installation of geogrid. They found that geogrid reinforcement improved the stress distribution within the pavement layer and reduced the critical pavement responses, such as vertical surface deflection, tensile strain in asphalt concrete, and compressive strain in subgrade. The study found up to 18% reduction in vertical strain at the top of subgrade and 68% reduction in tensile strain at the bottom of asphalt concrete in the geogrid reinforced

pavement sections. The placement of geogrid on top of weak subgrade was found to be particularly effective compared to that on strong subgrade. Kim and Lee's study found that the surface deflections in geogrid reinforced pavement sections were smaller than those in unreinforced pavement sections, and the reduction in surface deflection was greater when the asphalt concrete layer was thinner. The predicted vertical strains at the top of subgrade layer were significantly affected by geogrid reinforcement, and the stiffening effect around the geogrid layer reduced vertical strains at the top of subgrade. The placement of geogrid reinforcement tended to reduce the vertical subgrade responses due to the tensioned membrane effect. The residual stress resulting from the confinement between the aggregate base and geogrid significantly influenced the reduction of tensile strains at the bottom of asphalt concrete, which is related to the fatigue life of pavements.

Figure 19. 3-D finite element (FE) meshes used in geogrid reinforced flexible pavement [69]

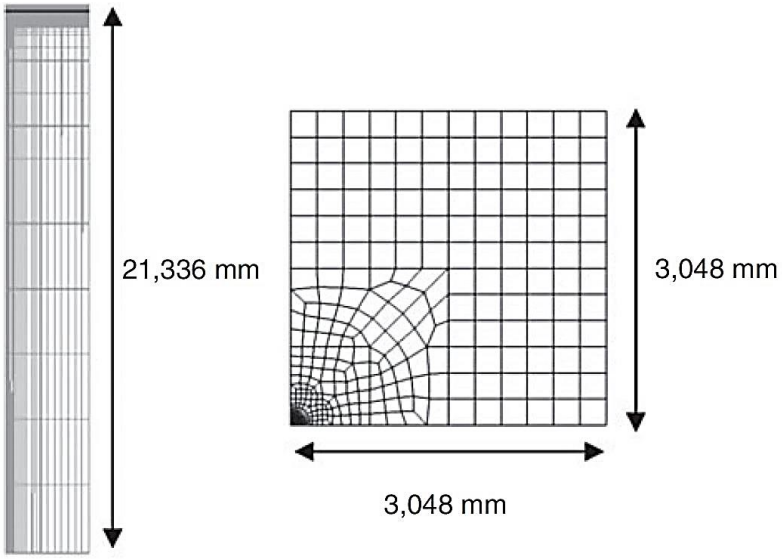

Taherkhani and Jalali used ABAQUS software to assess the efficacy of geosynthetics in decreasing the critical strains in geogrid reinforced flexible pavements under a range of dynamic axle load levels and different geogrid stiffness values [82]. Geogrids, which were installed at the bottom of the asphaltic layer, were shown to be effective in reducing the tensile strains in asphalt but had no impact on the compressive strains in subgrade. Additionally, the use of geogrids resulted in reducing tensile and compressive strains in the subgrade [64].

Luo et al. and Gu et al. used FE analysis to develop a methodology to quantify the influence of geogrid reinforcement on the performance of flexible pavement structures [7] [70]. To achieve their objective, the researchers used an FE technique to develop geogrid reinforced flexible pavement structure models that focused on characterizing the lateral confinement and vertical membrane effect of geogrid; see Figure 20. They also conducted a full-scale soil tank test to assess the validity of the developed models by comparing the FE predicted pavement responses to those measured in the tank test. The study found that the placement of geogrid increased the stiffness of the base course and reduced the vertical stresses around the geogrid layer, but could not effectively reduce the tensile strain at the bottom of asphalt concrete. This suggests that geogrid reinforcement is beneficial for reducing the rutting damage in the base course and subgrade, but not effective in prolonging the fatigue life of flexible pavement. To quantify the influence of geogrid, the geogrid reinforced flexible pavement structure was equivalent to an unreinforced flexible pavement structure with modified material properties. The modified material properties were then input into the pavement ME design software to predict the performance of geogrid reinforced flexible pavements. Two case studies were conducted to predict the performance of two geogrid reinforced pavement sections that were identified from the long-term pavement performance (LTPP) database. The predicted performance was found to be consistent with field measurements, which validated the accuracy of the proposed approach.

Figure 20. Schematic view of finite element (FE) model [70]

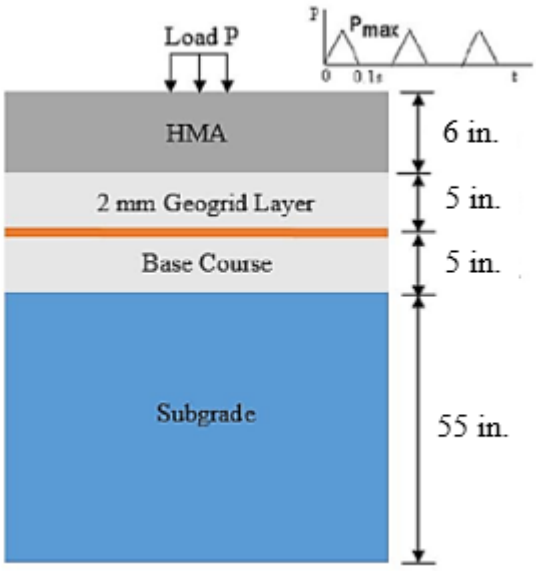

Zihong et al. conducted an FE analysis utilizing ABAQUS software on low volume flexible pavements enhanced with geotextile under static loading to assess the reinforcement's effect on rutting performance, geosynthetic location, and reduction of base course thickness [83]. The findings indicated a notable reduction in rutting of up to 25.2% for the unreinforced pavement system from geotextile reinforcement at the base-subgrade and AC-base interfaces. The deflection response characteristics of the pavement system were influenced by the elastic modulus of the geosynthetic material, its placement location, and the number of reinforcement layers. A reduction in base course thickness up to 30% was accomplished without compromising the structural integrity of the pavement.

Chhetri and Deb developed a 3-D FE model to evaluate the effectiveness of using geogrid reinforcement in flexible pavements over soft subgrade soils of varying strengths based on California bearing ratio (CBR) [84]. The findings reveal that the geogrid layer effectively reduced the vertical compressive strain by approximately 40%. With increasing CBR values, there is a reduction in vertical strain. The influence zone extends up to a depth of 12 in. within the subgrade layer. At the surface of the subgrade, vertical strain decreases by approximately 17%, 39%, and 49% as the CBR values increase from 1% to 3%, 5%, and 8%, respectively.

Methodology

Introduction

In order to evaluate, quantify, and incorporate geosynthetic benefits in MEPDG design of flexible pavements, several previous research studies adopted the results of finite element (FE) models and incorporated the resilient vertical strain of reinforced pavements into the MEPDG rutting equations [11]. However, these studies are usually based on a static FE model, which did not consider the benefit of geosynthetics under cyclic loading. Further, linear elastic constitutive models were often used in these studies, which were not able to capture the plastic (i.e., permanent) deformation of the pavement sections. Consequently, in these studies, the effect of geosynthetics on pavements is not fully accounted for. It is important to note that the geosynthetic layer usually shows a greater effect when certain plastic deformation in the soil occurs.

Proposed Approach

In this study, a new approach was adopted to evaluate and incorporate geosynthetic benefits, in which both the resilient vertical strain and rutting of each pavement sublayer from 100 loading cycles in quasi-static FE models were incorporated into MEPDG rut equations to extend the long-term loading cycles and hence to derive the Traffic Benefit Ratio (TBR) for the various geosynthetic reinforced pavement sections. Sophisticated constitutive models were used to simulate material behavior. Figure 21 presents the workflow of this study using the proposed FE numerical modeling coupled with a Mechanistic-Empirical (ME) approach to quantify the long-term benefits of geosynthetics in flexible pavements, which is summarized below:

1. Parametric studies based on FE analysis:

a) 2-D axisymmetric quasi-static FE models were first developed to simulate the pavement response of geosynthetics, both for geogrids and geotextiles, under repeated loads in low, medium, and high volume traffic. A total of 100 FE load cycles were first applied for each case. The developed FE model considered the confining effect on the base course aggregates caused by the geosynthetic reinforcement. A new modeling approach was proposed to simulate the interlocking mechanism between aggregates and geogrids, which differentiated the reinforcement effect in geogrids from geotextiles.

b) A series of FE simulations were conducted considering unreinforced and geosynthetic reinforced conditions, various base course thicknesses, different subgrade conditions, and different material properties. For each analysis, the resilient vertical strain of each sublayer is derived, which is an important input parameter for the subsequent ME analysis. Additionally, the rutting curves from the 100 load cycles for each pavement sublayer were also obtained.

2. Calibration of MEPDG factors:

   For each pavement layer, the corresponding calibration factor (β_{s1}) in the ME rutting equations was calibrated to fit the rutting curves obtained from the 100 load cycles of FE results using regression analysis based on the least square of error criterion.

3. Estimation of pavement service life:

a) The rutting curve for each pavement layer was extrapolated for long-term service loads using the calibrated rut factors and ME rutting equation to establish the long-term rutting versus the number of load cycle curves.

b) Estimate the total load cycles to achieve 0.5 in., 0.75 in., and 1 in. total rutting targets.

4. (4-1) The Traffic Benefit Ratio (TBR) for each scenario involving the reinforcement of geogrids or geotextiles was determined by calculating the total number of load cycles required to achieve the specified rutting target. This metric provides a quantitative assessment of the effectiveness of these reinforcement methods in enhancing the pavement's performance under traffic loads.

   (4-2) The modifying α coefficients for base and subgrade layers (α_b and α_s) were calculated by comparing the calibrated rutting curves of each layer for the reinforced models with the corresponding unreinforced model.

5. The calculated TBRs from Step 4-1 were used as an input in the AASHTOWare software to derive other benefit metrics based on the calculated TBR benefits, each providing valuable insights into the performance and cost-effectiveness of the pavement reinforcement scenarios. In this step, the objective was to determine the number of traffic loading cycles required for an unreinforced pavement section to reach a specific rutting target, such as 0.5, 0.75, or 1 in. This value was then multiplied by the Traffic Benefit Ratio (TBR) to reflect the improved performance achieved through reinforcement. By increasing the number of traffic loading cycles in this manner, the new rutting value surpasses the initially selected rutting target. To address this situation, adjustments were

made to the base course input values in subsequent steps, namely S6-1 and 6-2. These adjustments involved either increasing the thickness of the base course or enhancing its stiffness.

6. (6-1) The Equivalent Base Thickness (EBT) values were derived, which represent the additional thickness of the base layer that would achieve the same performance benefits as the geosynthetic reinforcement in the pavement structure. In other words, EBT quantifies how much the base layer's thickness would need to be increased to achieve the same structural integrity and performance enhancements that the geosynthetic reinforcement provide.

   (6-2) In this step, the structural benefits of reinforcement were calculated in terms of increased effective resilient modulus ($M_{R\text{-}eff}$) of base layer. By calculating the increase in this modulus due to the presence of geosynthetic reinforcement, design engineers gain valuable insights into how the pavement structure's mechanical properties are improved.

7. In this step, the focus was on the development of prediction models designed to calculate various benefit metrics associated with the use of geosynthetics in pavement structures. These benefit metrics include the Traffic Benefit Ratio (TBR), Equivalent Base Thickness (EBT), all of which have been calculated in preceding steps. The prediction models used input parameters from parametric study to calculate each benefit metric, using regression and machine learning (ML) algorithms. To establish these models, regression and ML algorithms were employed to establish relationships between the input parameters and the benefit metrics.

8. In this step, the focus was on the development of new rutting models specifically for the base course and subgrade layers within the pavement structure. These rutting models were designed to account for the effects of geosynthetic reinforcement and leverage input parameters derived from the analysis. Key factors considered in these models include the calculated elastic and plastic strains experienced by these layers. The goal of proposing these new rutting models was to create predictive tools that can more accurately estimate the rutting behavior of the base course and subgrade materials when geosynthetics are integrated into the pavement.

Figure 21. Workflow to quantify the benefits of geosynthetic reinforcement in pavement structure

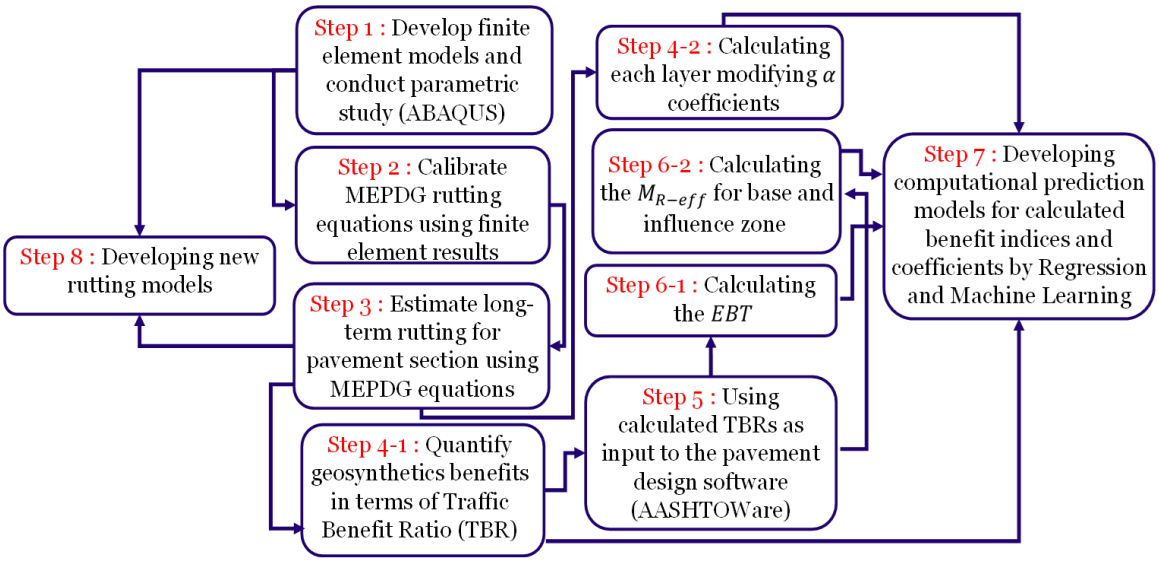

Develop Finite Element (FE) Models

In this study, the commercial FE program ABAQUS was used to develop models to simulate the behavior of unreinforced and geosynthtic reinforced pavements under cyclic loading. 2-D axisymmetric FE models were developed to simulate the different geosynthetic reinforced pavement sections. The pavement layers were modeled using eight-node biquadratic axisymmetric quadrilateral elements (CAX8R). The geosynthetic reinforcement was simulated using three-node membrane elements. Sensitivity analyses were initially conducted on the FE models to identify the dimensions and degree of refinement of the FE mesh for use to simulate the unreinforced and geosynthetic reinforced pavement sections in this study.

Model Geometry

Several FE models were first conducted using different mesh dimensions to select the model dimension that ensures no boundary effect occurs (i.e., less than 1% change in stresses). Consequently, the 2-D axisymmetric model with a radius of 200 in. and depth of 250 in. were selected. Additionally, a series of FE models were then created with a different number of mesh elements to assess the mesh sensitivity and identify the degree of mesh refinement needed to optimize the number of elements that give accurate results. Mesh sensitivity analysis is a critical step in numerical simulations, particularly in FE analysis. It involves varying the mesh density or element size to evaluate its impact on simulation results. This

process is of paramount importance because it helps ensure the accuracy and reliability of simulation outcomes.

A mesh that is too coarse may overlook fine details and yield inaccurate results, while an excessively fine mesh can lead to computationally intensive simulations. By systematically assessing mesh sensitivity, engineers and researchers can strike a balance between computational efficiency and precision, thereby enabling them to make informed decisions and predictions. Figure 22 shows the pavement responses (e.g., vertical strain at the middle of base course layer and at the top of subgrade layer) to the vehicular loading for an unreinforced section model.

Figure 22. Comparison of vertical strain at top of subgrade layer and middle of base course stiffness with 10 in. base thickness and weak subgrade for different number of elements

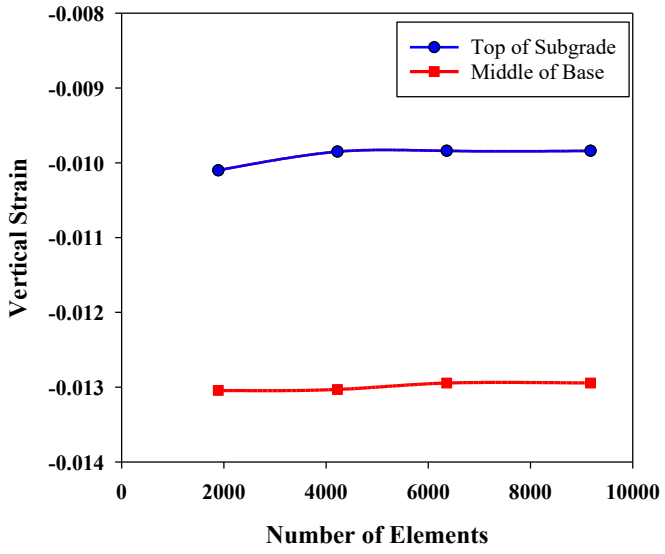

Based on the mesh sensitivity analysis, an FE model with a total of 9,176 elements was selected (i.e., 744 elements for HMA, 1,860 elements for the base, and 6,572 elements for the subgrade). Figure 23 depicts the dimensions and mesh size of the FE models adopted in this study. The right and left boundaries are restrained horizontally, and the bottom is restrained both in horizontal and vertical directions.

Figure 23. Dimension and mesh for the finite element (FE) model

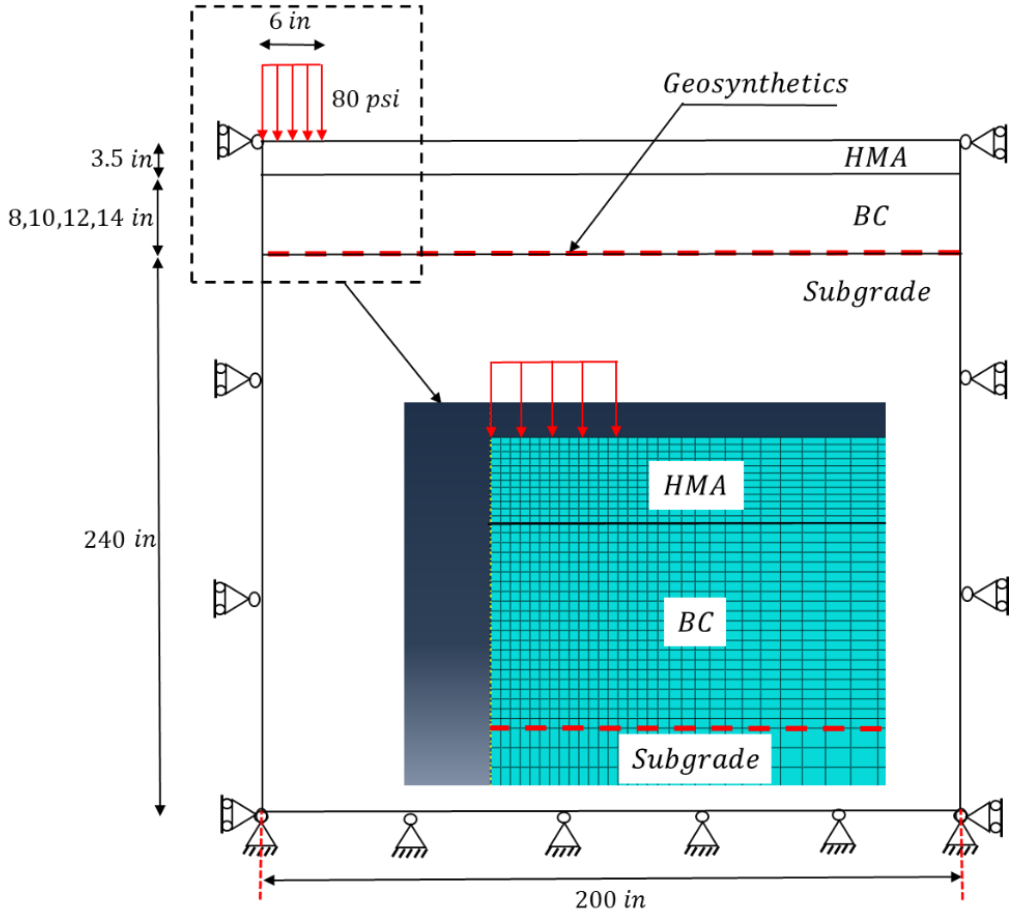

Loading Model

The characteristics (e.g., magnitude, shape, and duration) of the vehicular load differ with respect to the wheel parameters such as wheel type, load, and speed. Ideally, the vehicular load should be applied as a moving load on a 3-D FE model. However, simulating such a loading condition is time-consuming and requires massive computational resources. This is not feasible, especially when a large number of parametric studies are needed to understand the behavior of geosynthetic reinforcement under different conditions and scenarios. In 2-D simulations, it is practical to use static loads instead of moving loads [85]. The applied stress model is often assumed to have a triangular or sinusoidal shape with duration and magnitude related to the type and speed of the vehicle [79]. The pressure and contact area for the wheel adopted in this study are similar to the specification in the MEPDG design guideline, i.e., a uniform distributed pressure of 80 psi and a circular contact area of 113.1 in^2 (a circular area

with a radius of 6 in.). A haversine distribution was adopted for simulating wheel loading in this study, in which the load F at the time t is calculated from the following equation:

$$F = \frac{P(1-\cos(\frac{2\pi t}{T}))}{2} \quad (3)$$

where the peak pressure is assumed to be 80 psi (P = 80 psi), and one load cycle total time is 0.1 seconds (T = 0.1 seconds) with the rest time of 0.9 sec., which produces a moving wheel load with the frequency of 1 Hz and contact duration of 0.1 sec.; see Figure 24. The haversine shape loading is not readily available in ABAQUS software. Hence, a Fortran subroutine was written to implement the haversine wheel loading into ABAQUS software using the user subroutine (DLOAD). A total of 100 load cycles were simulated for each unreinforced and geosynthetic reinforced pavement section.

Figure 24. Haversine distribution of the vehicular loading

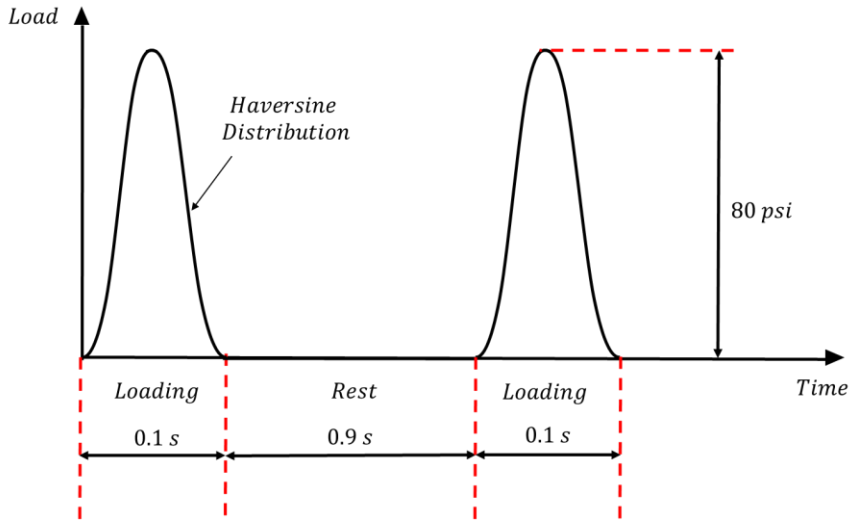

Material Characteristics and Constitutive Models

The selection of material characteristics and constitutive models constitutes a critical foundation in the realm of numerical modeling, particularly in the field of civil engineering. This decision influences the accuracy, reliability, and predictive power of numerical simulations, making it a critical aspect of any modeling study. The intricate interplay of material properties, such as elasticity, plasticity, viscosity, and thermal behavior, coupled with the choice of appropriate constitutive models, dictates how a material or structure responds to external forces, loads, and environmental conditions. Accurate representation of these

characteristics not only ensures the fidelity of simulations but also plays an integral role in guiding engineering designs, optimizing material selection, and solving complex real-world problems.

Hot Mix Asphalt (HMA)

The HMA material typically experiences time-dependent (i.e., viscoelastic) behavior under vehicle loading. To study the viscoelastic behavior of HMA and simulate it using a numerical model, the bulk and shear moduli of asphalt material need to be characterized. The Prony series can be used to numerically simulate the viscoelastic characteristics of HMA material, which are described as follows:

$$G(t) = G_0\left(1 - \sum_{i=1}^{n} G_i\,(1 - e^{-t/\tau})\right) \tag{4}$$

$$K(t) = K_0\left(1 - \sum_{i=1}^{n} K_i\,(1 - e^{-t/\tau})\right) \tag{5}$$

where, $G(t)$ is relaxation shear modulus;
$K(t)$ is relaxation bulk modulus;
G_0 is instantaneous shear modulus;
K_0 is the instantaneous bulk modulus; and
G_i, K_i and τ are the input coefficients.

In order to calculate the relevant Prony series parameters (τ, G, and k) for use in the FE simulations, the master curve of dynamic modulus is fitted with the Prony series for at least five steps [25]. Table 2 summarizes the Prony series parameters used for HMA properties in this study adopted from Al-Qadi et al. [6].

Table 2. Prony series parameters for HMA

Elastic Properties	**Poisson's ratio**				0.35		
	Instantaneous Modulus (ksi)				500		
Viscoelastic Properties	g_i, k_i	0.452	0.278	0.148	0.108	0.00746	0.00436
	τ_i	0.000113	0.00314	0.013	0.184	2.29	25.7

Base Course Layer

Crushed limestone is a very common unbound granular base course material in flexible pavements in Louisiana. In this research, the Modified Drucker-Prager with cap plasticity model was used to simulate the behavior of the granular base material. This constitutive model has been broadly used in numerical modeling of different geotechnical engineering applications. This model considers the effect of intermediate principal stress, stress path, dilatancy, and stress history. The Modified Drucker-Prager with cap plasticity model yield surface, consists of three primary parts: (1) Drucker-Prager shear failure surface, (2) elliptical cap, with a right-angle intersection to the mean effective stress axis, and (3) transition region, which connects the shear failure surface smoothly to the cap.

The elastic modulus is considered linear elastic by using the generalized Hooke's law. The start of plastic deformation is controlled by the cap yield surface and Drucker-Prager failure surface. The Drucker–Prager failure surface in p–t plane is given as follows:

$$F_s = t - p * tan\beta - d = 0 \tag{6}$$

where β and d are the soil's angle of friction and cohesion in the $p - t$ plane. p is the equivalent pressure stress obtaining from:

$$p = -\frac{1}{3} trace(\sigma) \tag{7}$$

where t is the deviatoric stress measure obtaining from:

$$t = \frac{q}{2}\left[1 + \frac{1}{K} - \left[1 - \frac{1}{K}\right]\left[\frac{r}{q}\right]^3\right] \tag{8}$$

where q is the Mises equivalent stress obtaining from:

$$q = \sqrt{\frac{3}{2}(S:S)} \tag{9}$$

where r is the third invariant of deviatoric stress obtaining from:

$$r = (\frac{9}{2} S.S:S)^{\frac{1}{3}} \tag{10}$$

where S is the stress deviator, defined as:

$$S = \sigma + pI \tag{11}$$

and K is a material parameter that may depend on temperature and other pre-defined fields to ensure convexity of the yield surface $0.778 \leq K \leq 1$.

The cap surface expands or shrinks (i.e., hardens or softens) based on the volumetric plastic strain magnitude. The expansion of the cap (i.e., hardening) occurs when the stress path reaches the cap and results in compaction. On the other hand, the shrinkage (i.e., softening) of the cap happens when the stress path reaches the Drucker-Prager shear failure surface and results in dilation. The following equations represent the cap and transition surfaces, respectively.

$$F_c = \sqrt{(P - P_a)^2 + (\frac{Rt}{1 + \alpha - \alpha/cos\beta})^2} - R(d + P_a tan\beta) = 0 \tag{12}$$

$$F_t = \sqrt{(P - P_a)^2 + [t - (1 - \frac{\alpha}{cos\beta})(d + P_a tan\beta)]^2} - \alpha(d + P_a tan\beta) = 0 \tag{13}$$

where R determines the shape of the cap, α is a small coefficient between 0.01 to 0.05 for a smooth transition surface between the shear failure surface and cap, and P_a determines the softening–hardening behavior based on the volumetric plastic strain magnitude.

The softening-hardening behavior is defined by a linear function relating the volumetric plastic strain $P_b = P_b(\varepsilon_{vol}^{pl})$ to the mean effective stress P_b; see Figure 25.

Figure 25. Typical cap hardening behavior

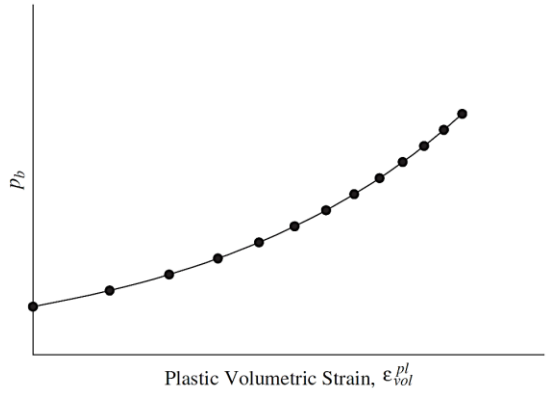

The function can be achieved from an isotropic consolidation test with several unloading-reloading cycles. Thus, P_a can be obtained from Equation 14:

$$P_a = \frac{P_b - Rd}{1 + R\ tan\beta} \tag{14}$$

The flow potential surface in this model in the *p*–*t* plane consists of two curves. The plastic flow for the cap is associated, meaning the flow potential is similar to the yield surface. The plastic flow for the Drucker–Prager yield surface and the transition surface is non-associated, which means the flow potential shape is different from the yield surface in the *p*–*t* plane; see Figure 26.

Figure 26. Flow potential of the modified cap model in the *p* -*t* plane

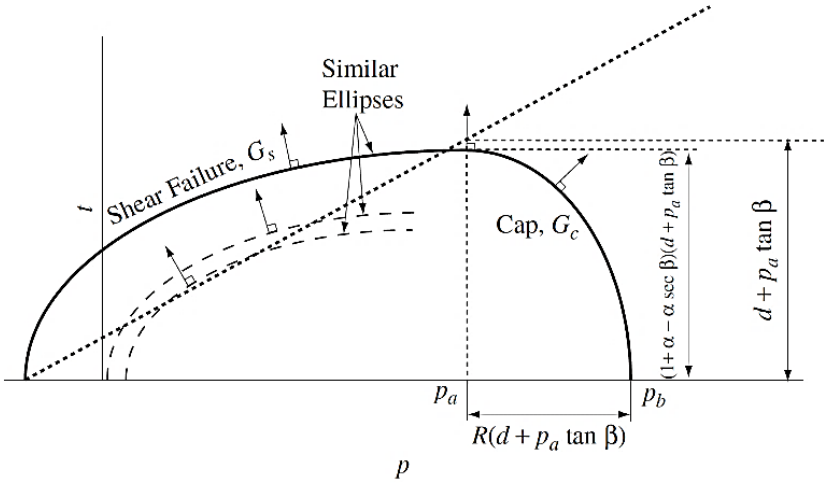

The associated flow potential surface in the cap region is elliptical and is given as Equation 15:

$$G_c = \sqrt{(P - P_a)^2 + (\frac{Rt}{1 + \alpha - \alpha/cos\beta})^2} \tag{15}$$

The non-associated flow potential surface in the Drucker‑Prager and transition regions is given as Equation 16:

$$G_c = \sqrt{[(P - P_a)\, tan\beta]^2 + (\frac{t}{1 + \alpha - \alpha/cos\beta})^2} \tag{16}$$

A series of consolidated undrained (CU) triaxial tests were conducted by Nazzal on large granular base material specimens with dimensions of 6×12 inches (diameter × height) [86]. The parameters of the modified Drucker-Prager with cap plasticity model were calibrated using the CU laboratory test results from Nazzal [86]. Table 3 depicts the calibrated constitutive model parameters.

Table 3. Properties of Drucker-Prager with cap plasticity model for base course material

Constants	Definitions	Variable	Value
Elasticity	Elastic Modulus (psi)	E	36000
	poissons ratio	ν	0.35
Cap Plasticity	Material Cohesion (psi)	d	7
	Angle of friction	β	66
	Cap eccentricity		0.015
	Initial yield surface position		0.005
	Transition surface radius		0.07
	Flow stress ratio		1

Figure 27 compares the results of CU triaxial test from the calibrated FE model and the laboratory test results, showing excellent agreement.

Figure 27. Comparison between the simulated triaxial test using the calibrated modified Drucker-Prager with cap plasticity model and the experimental triaxial test on crushed limestone

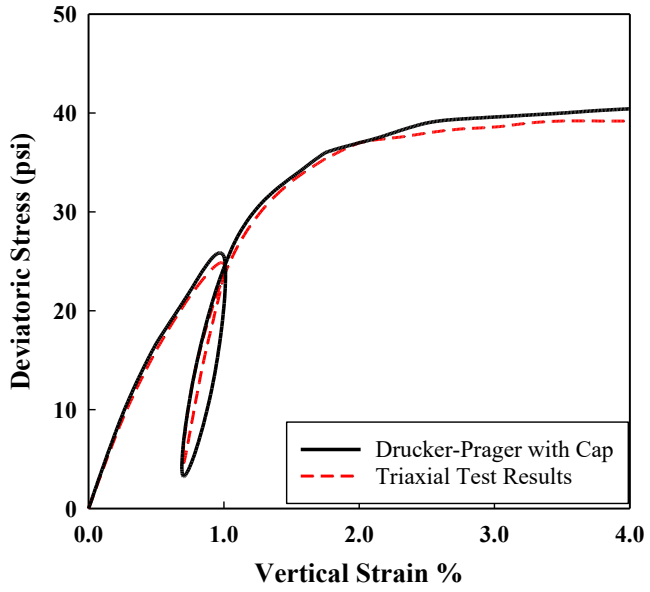

Subgrade Layer

The subgrade layer was modeled using the Modified Cam-Clay (MCC) model available in ABAQUS software package. This constitutive model is an elastoplastic model based on the critical state concept theory. The MCC yield surface in the p'–q plane is an ellipse that is controlled with the magnitude of pre-consolidation pressure, which is defined as:

$$\frac{q^2}{p'^2} + M^2\left(1 - \frac{p'_c}{p'}\right) = 0 \qquad (17)$$

The yield surface is presented in Figure 28; the intersection of yield surface with mean effective stress axis is the pre-consolidation pressure p'_c that controls the size of the yield surface and would change during unloading-reloading. The Critical State Line (CSL) with the slope of M intersects with the ellipse crown with mean effective stress equal to $p'_c/2$ at point A. When the stress state lies inside the ellipse, soil behavior is elastic and would be plastic after hitting the yield surface.

Figure 28. Yield surface of Modified Cam Clay (MCC) model

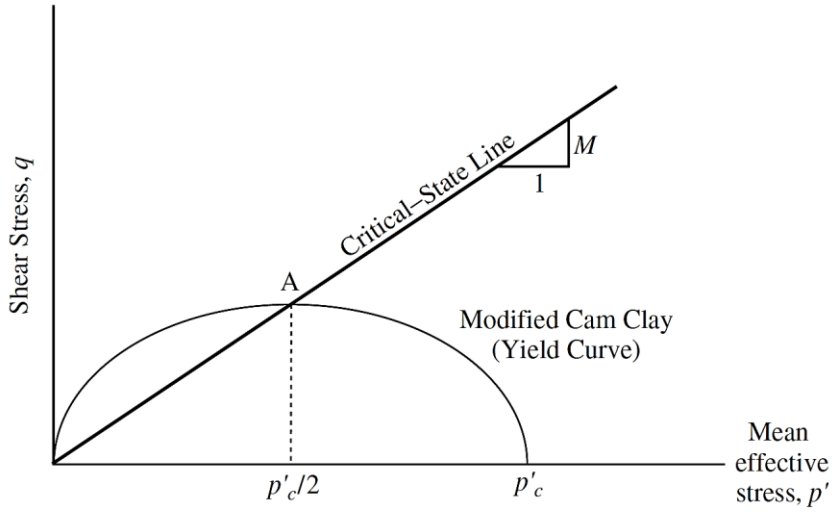

When a slightly over-consolidated (OCR = $p'_c/p'_0 < 2$) soil is subjected to drained loading, the stress path and yield surfaces during loading would look like Figure 29 (i.e, the stress path starts from point B with the present pressure of p'_0 and the pre-consolidation of p'_c). The initial size of the ellipse is controlled by the size p'_c; see Figure 29. During shearing, the stress path would be first inside the yield surface with the slope of 3 to 1 (i.e., vertical to horizontal) with purely elastic behavior. The compression of soil and hardening occurs when the stress path reaches the first yield surface at the right side of the intersection point with CSL. When the stress path touches the yield surface, the plastic strain occurs along with elastic strains. After the first touch to yield surface, hardening (i.e., expansion of yield surface) occurs until the stress path reaches to CSL line at point F. After reaching this point, the soil will continue to shear with constant volume until failure.

Figure 29. Cam Clay hardening behavior: (a) evolution of a yield surface during hardening; (b) stress–strain curve with strain hardening

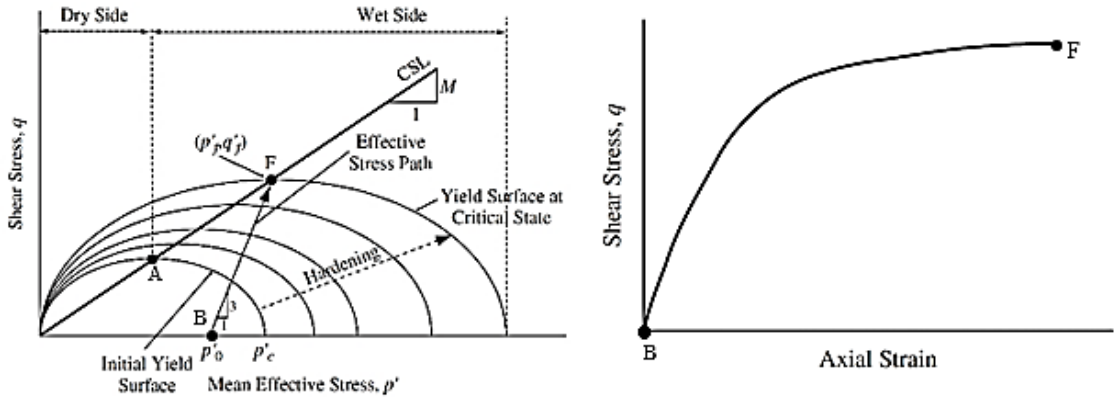

When an over-consolidated (OCR = p_c'/p_0' > 1) soil is subjected to drained loading, the stress path and yield surfaces during loading would look like Figure 30 (i.e., with the present pressure of p_0' and the pre-consolidation of p_c'). Again, during shearing, the stress path starts from point B and would be first inside the yield surface with the slope of 3 to 1 (i.e., vertical to horizontal) with purely elastic behavior. The dilation of soil and softening occurs when the stress path reaches the first yield surface at the left side of the intersection point with CSL at point C; see Figure 30. It is notable that the stress path traverses the CSL before the first touch without initiating failure in soil. When the stress path touches the yield surface at point C, the plastic strain occurs along with elastic strains. After the first touch to yield surface, softening (i.e., contraction of yield surface) occurs until the stress path reaches to CSL line at point F.

Figure 30. Cam Clay softening behavior: (a) evolution of a yield surface during softening; (b) stress–strain curve with strain softening

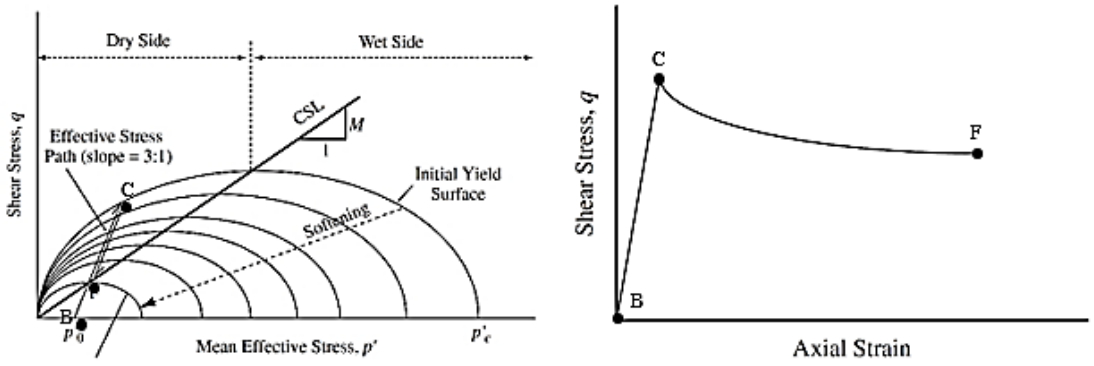

Different parameters were calibrated for the MCC constitutive model based on soil properties for subgrade material existing in Louisiana and calibrated with the experimental tests performed in previous studies at LTRC. Table 4 shows the MCC calibrated parameters for the weak subgrade.

Table 4. Properties of subgrade layers for MCC model

Stiffness	G (psi)	ν	M	λ	κ	e_0
Weak	1070	0.4	0.56	0.173	0.035	1.5
Medium stiff	2775	0.4	0.86	0.087	0.017	1.3
Stiff	4612	0.4	1.2	0.043	0.009	0.7

The value of over-consolidation ratio (OCR) at the top of subgrade was assumed to be equal to 3, which decreases with depth to one after 15 ft. The corresponding lateral stress coefficient (k_0) in the subgrade is derived from Equation 18 and the change with the depth is presented in Figure 31.

$$k_0 = (1 - sin\emptyset') * OCR^{sin\emptyset'} \quad (18)$$

Figure 31. Changes in OCR and K_0 in subgrade with depth

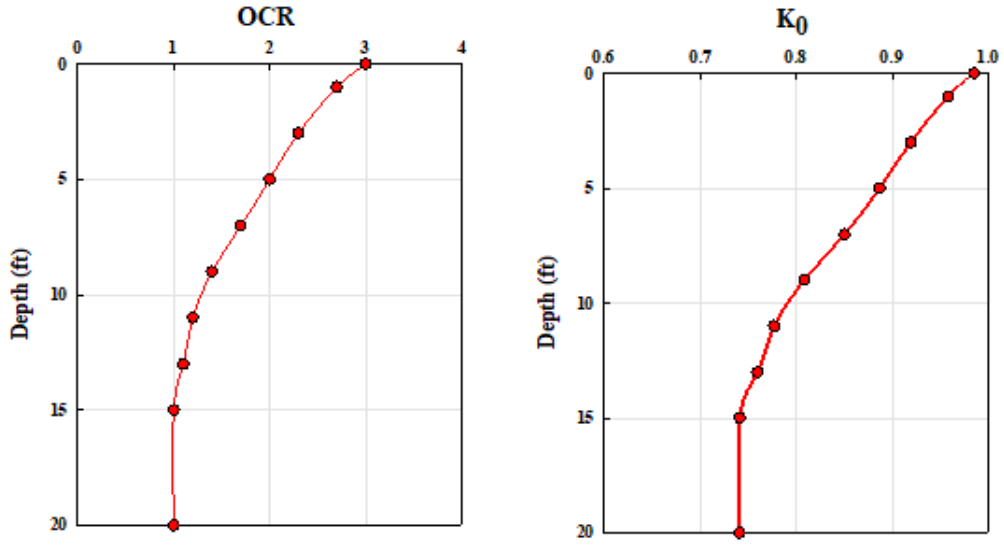

Geosynthetics

To evaluate the effects of geosynthetic type and stiffness on the benefits of reinforcing/stabilizing pavement structures, both geogrid and geotextile types with three different tensile stiffnesses were used to reinforce/stabilize the pavement at the interface between the base course and subgrade layer. The difference between the geogrid and geotextile in the FE numerical models was distinguished through the simulation of the geogrid/geotextile-geomaterial interface, as discussed in the following section.

Three different types of geosynthetics were tested at the bottom of the base course layer to assess the effects of geosynthetics as reinforcement. As mentioned previously, according to the machine and cross-machine stiffness of geosynthetics, an equivalent stiffness for geosynthetics was calculated and used in the FE simulations. This method is used to convert the orthotropic linear elastic behavior of geosynthetics to equivalent isotropic elastic properties for using in the 2-D axisymmetric simulations according to Equation 19:

$$E_{equivalent} = \frac{1 - 0.5a + a^2 + 2.5b^2}{\frac{1}{E_{xm}} + \frac{a^2}{E_m} - 2a\frac{v_{xm-m}}{E_{xm}} + \frac{b^2}{G_{xm-x}}} \quad (19)$$

where, a = 0.35;
b = 0.035;
E_{xm} is the cross-machine direction elastic modulus;
E_m is machine direction elastic modulus;
G is shear modulus; and
υ is Poisson's ratio

The equivalent isotropic elastic stiffnesses, $E_{equivalent}$, of the geosynthetics used in this study were derived from the geosynthetics' orthotropic linear elastic properties according to the machine and cross-machine directions. The values of $E_{equivalent}$ for the three different geosynthetic stiffness ranges (i.e., low, medium, and high) are shown in Table 5.

Table 5. Equivalent elastic modulus for low, medium, and high stiffness of geosynthetics

No.	Geogrid and Geotextile Stiffness	v	$E_{equivalent}$ (ksi)
1	Low	0.25	62.4
2	Medium	0.25	134.6
3	High	0.25	182.7

To consider the geosynthetic confinement effect on base aggregates, Gu et al. analyzed a series of experimental results on geosynthetic reinforced specimens and proposed a stress distribution scheme in which the additional confinement stress on the aggregates is properly accounted for; see Figure 32 [70].

Figure 32. Schematic drawing of geosynthetic confinement effect on aggregates **[70]**

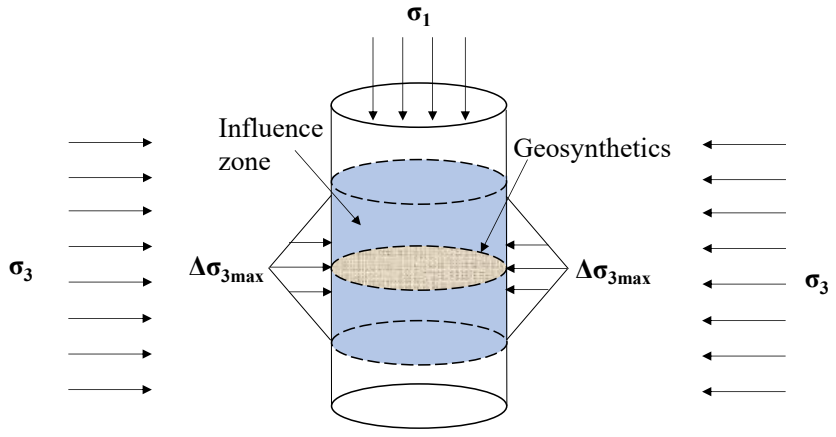

In this approach, it is suggested that in addition to the compaction-induced lateral stress σ_3, the geosynthetics generate an influence zone during vertical loading, providing additional confinement to the aggregates within the influence zone. This influence zone can be quantified as a 3 in. zone on both the top and bottom of the geosynthetic layer, with a maximum confining stress of $\Delta\sigma_{3max}$ at the center and zero $\Delta\sigma_3$ at the edges; see Figure 32. In this study, σ_3 is taken as 3 psi, and the $\Delta\sigma_{3max}$ values for different geosynthetics can be calculated using the following equation [70]:

$$\Delta\boldsymbol{\sigma_{3max}} = \left(\frac{\boldsymbol{2M}}{\boldsymbol{(1-V_g)\delta\alpha}} \cdot \left[\frac{(\sigma_3+\Delta\sigma_3\ \mathbf{max})}{\boldsymbol{E_H}} - \frac{\boldsymbol{V_{13}\,\sigma_1}}{\boldsymbol{E_V}} - \frac{\boldsymbol{V33\,(\sigma_3+\Delta\sigma_3\ max)}}{\boldsymbol{E_H}} + \mathbf{0.85}\boldsymbol{\varepsilon_0 e^{-(\frac{\rho}{N})^{\beta}}}\left(\sqrt{\boldsymbol{J_2}}\right)^{\boldsymbol{m}}\right)(\boldsymbol{\alpha I_1} + \boldsymbol{K}) \quad (20)$$

where, σ_3 is the initial confining pressure;
σ_1 is the axial stress applied to the specimen;
ν_{13} is the Poisson's ratio in x-z direction;
ν_{33} is the Poisson's ratio in z-z direction to characterize the effect of lateral stress on lateral strain;
E_V is the vertical modulus of the specimen;
E_H is the horizontal modulus of the specimen;
ν_g is the Poisson's ratio of the geosynthetic;
δ is the thickness of the influence zone (i.e., δ = 6 in.);
M is geosynthetic sheet stiffness;
$\Delta\sigma_3$ max is the maximum additional confining stress;
J_2 is the second invariant of the deviatoric stress tensor;
I_1 is the first invariant of stress tensor; and
ε_0, ρ, β, m, and n are permanent deformation properties of the unbound base course material.

The calculated $\Delta\sigma_{3max}$ values for the low, medium and high stiffness geosynthetics are presented in Table 6. The lateral confining stresses are added into the FE model through Fortran subroutines at the initial stress stage of analysis.

Table 6. Maximum lateral confining stress for geosynthetics of various stiffness

Geogrid Stiffness	$\Delta\sigma_{3max}$ (psi)	Geotextile Stiffness	$\Delta\sigma_{3max}$ (psi)
Low	4.2	Low	3.63
Medium	4.5	Medium	4.2
High	4.93	High	4.7

Interface Models between Geotextile/Geogrid and Geomaterials

The interface behavior between geosynthetics and soils was simulated using the Coulomb friction model available in ABAQUS; see Figure 33. No separation between the two adjacent materials is allowed. In this model, hard contact is used for normal interaction, while the tangential interaction is simulated using a frictional coefficient (μ) and elastic slip (E_{slip}) to describe the shearing behavior along with the geosynthetic-base aggregate interface. In this study, the values of friction coefficient $\mu = 0.85$ and elastic slip $E_{slip} = 0.04$ in. were used for the interface between geotextile and base course aggregate, and the values of $\mu = 0.75$ and $E_{slip} = 0.04$ in. are used for the interface between geotextile and subgrade. Similarly, for the interface between geogrid and base course aggregate friction, the values of $\mu = 1.475$ and $E_{slip} = 0.04$ in. were used, while for the interface between geogrid and subgrade friction, the coefficient of $\mu = 0.75$ and $E_{slip} = 0.04$ in. were used.

Figure 33. Coulomb friction model for the geogrid-pavement interface

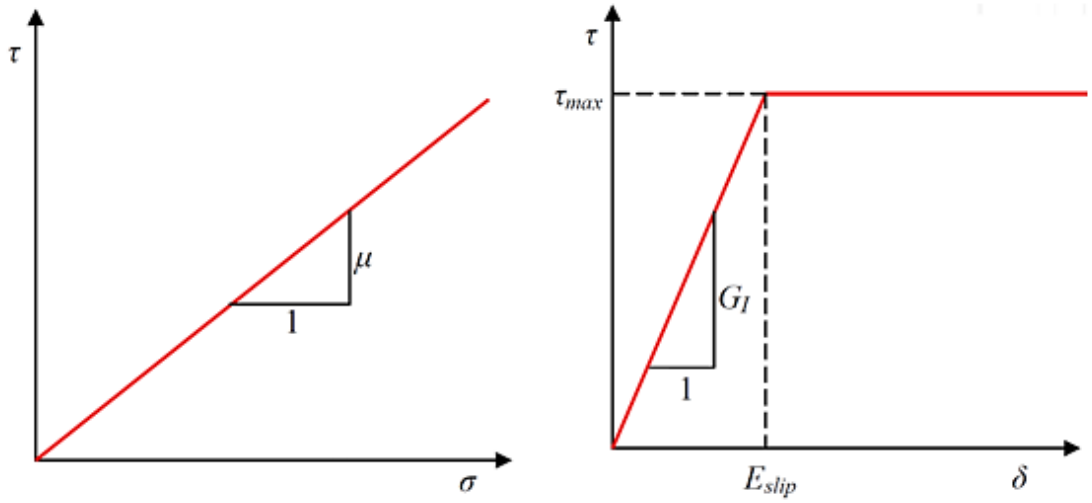

An important geometrical feature that differentiates geogrids from geotextiles is that geogrids are composed of apertures that can trap stones/aggregates within the aperture openings, hence leading to an interlocking effect with the aggregates. This interlocking effect can further enhance the performance of geogrid in reducing the pavement rutting. In this study, a new interface model was introduced to simulate the interlocking effect between the geogrid layer and the surrounding aggregates. In this model, the geogrid-aggregate interlocking is simulated by geometrically decomposing the geogrid layer into two sublayers, which bound a thin layer of interlocked aggregates; see Figure 34.

Figure 34 : Simulation of geogrid-aggregate interlocking effect

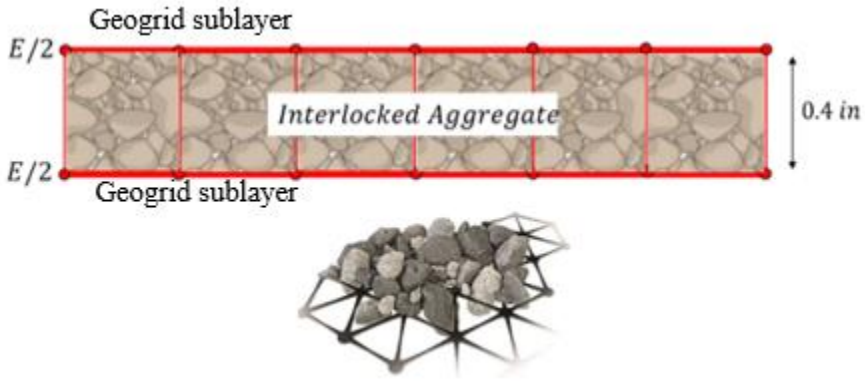

The tensile modulus for each sublayer of geogrid is reduced to half the stiffness properties of the geogrid (E/2). The thickness of this interlocked aggregate layer is assumed to be equal to 0.4 in. (or 10 mm), which is taken as half of the maximum aggregate size of crushed limestones ($D_{max}/2$). In this new modeling approach, the enhanced performance of geogrid due to the geogrid-aggregate interlocking mechanism can be properly simulated, which is shown later.

Mechanistic-Empirical (ME) Rutting Equations

For many years, several mechanistic-empirical (ME) pavement design methodologies have commonly linked permanent deformation to excessive vertical strains applied to the subgrade. The prevailing belief was that by designing the pavement effectively and maintaining the quality of the materials above the subgrade, rutting could be kept at acceptable levels by limiting the vertical strain on the subgrade. This approach closely aligned with the historical design philosophy for flexible pavements, which viewed structural design primarily as a means to reduce the shear stresses within the critical subgrade layer. However, as time passed and engineering knowledge and capabilities improved, it became increasingly evident to design engineers that the total permanent deformation resulted from the cumulative development of ruts across all layers of the pavement system. The rate or accumulation of plastic deformation is measured in the laboratory using repeated load permanent deformation triaxial tests for both HMA mixtures and unbound materials. The laboratory-derived relationship is then adjusted to match the rut depth measured on the roadway. In the ME approach, the total rutting is the sum of rutting of each sublayer. The rutting of HMA, base course, and subgrade layers are directly related to the resilient vertical strain within these layers. The equations correlate the resilient vertical strain (i.e., elastic deformation) to permanent deformation (i.e., rutting) for each layer as the following:

1. The rutting for the HMA layer can be evaluated using the following equations:

$$\Delta_{HMA} = \varepsilon_{p(HMA)} h_{HMA} = \beta_{1r} k_z \varepsilon_{r(HMA)} 10^{k_{1r}} N^{k_{2r}\beta_{2r}} T^{k_{3r}\beta_{3r}} h_{HMA} \quad (21)$$

where, Δ_{HMA} is the permanent rutting;
$\varepsilon_{p(HMA)}$ is the permanent plastic strain;
h_{HMA} is the layer thickness;
k_z = depth confinement factor;
$\varepsilon_{r(HMA)}$ = vertical resilient strain calculated by the structural response model at the mid-depth;
T = pavement temperature in $F°$;
N = number of load cycles:
k_{1r}, k_{2r}, k_{3r} = global field calibration coefficient (from the NCHRP 1-40D recalibration;
k_{1r} = –3.35412;
k_{2r} = 0.4791;
k_{3r} = 1.5606); and
β_{1r}, β_{2r}, β_{3r} = local calibration coefficient, these constants were all set to 1.0.

$$k_z = (C_1 + C_2 D) 328196^D \quad (22)$$

$$C_1 = -0.1039(h_{HMA})^2 + 2.4868 h_{HMA} - 17.342 \quad (23)$$

$$C_2 = 0.0172(h_{HMA})^2 - 1.7331 h_{HMA} + 27.428 \quad (24)$$

where D is the depth below the surface.

2. The rutting for base course and subgrade layer is evaluated using the following equation:

$$\Delta_{base/subgrade} = \beta_{s1} k_{s1} \varepsilon_v h_{soil} \left(\frac{\varepsilon_0}{\varepsilon_r}\right) e^{-\left(\frac{\rho}{N}\right)^{\beta}} \quad (25)$$

where, $\Delta_{base/subgrade}$ is the permanent rutting for base or subgrade;
β_{s1} is a calibration factor;
k_{s1} is a global field calibration coefficient;
ε_v is the average vertical resilient strain computed from the layer;
N is the number of load cycles; and
h_{soil} is the layer thickness of the base course or subgrade.

β, ρ and $\frac{\varepsilon_0}{\varepsilon_r}$ are material parameters derived from the following equations:

$$\log\beta = -0.61119 - 0.017638(W_C) \quad (26)$$

$$\rho = 10^9\left(\frac{C_0}{(1-(10^9)^\beta)}\right)^{\frac{1}{\beta}} \quad (27)$$

$$C_0 = Ln\left(\frac{a_1 M_r^{b_1}}{a_9 M_r^{b_9}}\right) \quad (28)$$

$$\frac{\varepsilon_0}{\varepsilon_r} = \frac{(e^{\rho^\beta} * a_1 M_r^{b_1} + e^{\left(\rho/10^9\right)^\beta} * a_9 M_r^{b_9})}{2} \quad (29)$$

where, W_C is the water content(%);
M_r is the resilient modulus of the unbound layer or sublayer (psi);
$a_{1,9}$ are regression constant; $a_1 = 0.15$ and $a_9 = 20$; and
$b_{1,9}$ are regression constant; $b_1 = 0$ and $b_9 = 0$.

Metrics of Reinforcement Benefits

The benefits of incorporating geosynthetic reinforcement into pavement construction projects are assessed by various researchers using a range of benefit metrics. These metrics are instrumental in quantifying the advantages of geosynthetics and help in decision-making processes related to pavement design and construction. Several of these benefit metrics are explained in this section.

Traffic Benefit Ratio (TBR)

The use of geosynthetic reinforcement usually results in increasing the service life of pavement structures by reducing permanent deformation due to vehicular loadings. The increased service life of pavement structures can be expressed in terms of Traffic Benefit Ratio (TBR), which is defined as the ratio between the required cycles of a reinforced section (N_R) to an unreinforced section (N_U) for a specific level of performance or reaching to a rutting target. The rutting target is typically chosen to be 0.5 in., 0.75 in., or 1.0 in. rut depth.

$$TBR = \frac{N_R}{N_U} \quad (30)$$

To derive the TBR value from Equation 30, the number of cycles to reach the rutting target is derived for the pavement section without reinforcement (N_U) and the pavement section with reinforcement (N_R) from the calibrated/extended curves of numerical modeling; see Figure 35.

Figure 35. Definition of Traffic Benefit Ratio (TBR)

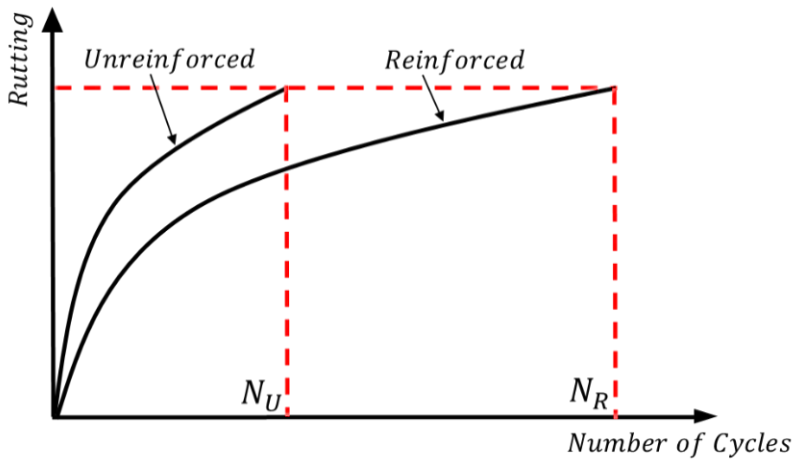

Effective Resilient Modulus ($M_{R\text{-}eff}$)

One way to integrate the advantages of geosynthetic reinforcement into Pavement ME Design is by adjusting the resilient modulus (M_R) of the base aggregate layer to account for the increased stiffness of base layer caused by the use of geosynthetics, which is known as the base reinforcement effect of geosynthetics; see Figure 36. Specifically, the M_R value can be transformed into M_{R-eff}, where $M_{R-eff} = (1 + \alpha)\, M_R$ that represents an improvement factor for the entire base thickness. However, it is assumed that the use of geosynthetics has no stabilizing effect on the subgrade layer, and as such, the subgrade resilient modulus of geosynthetic reinforced sections remains the same as that of the corresponding unreinforced condition.

Figure 36. M_{R-eff} for geosynthetic-reinforced base

In theory, the use of geosynthetics increases the resilient modulus of the base layer only within the influence zone of geosynthetics. This zone is typically assumed to extend 4 in. above and below the geosynthetic layer. The improvement factors for the base and subgrade within the influence zone (α_b and α_s) can be determined by back-calculating from the improvement factor for the entire base layer (α), using the equation below:

$$(1+\alpha)M_R = \frac{(1+\alpha_1)M_R \times 4 + M_R \times (D-4)}{D} \quad (31)$$

Equivalent Base Thickness (EBT)

The benefits of geosynthetic reinforcement can be integrated into the Pavement ME Design process by modifying the thickness of the base aggregate layer to reflect the additional equivalent thickness of geosynthetics. This adjustment accounts for the reinforcing effect of geosynthetics in the pavement structure. By doing so, the Pavement ME Design process accurately considers how geosynthetics enhance the pavement's structural performance; see Figure 37.

Figure 37. Equivalent base thickness (EBT) for geosynthetic-reinforced base

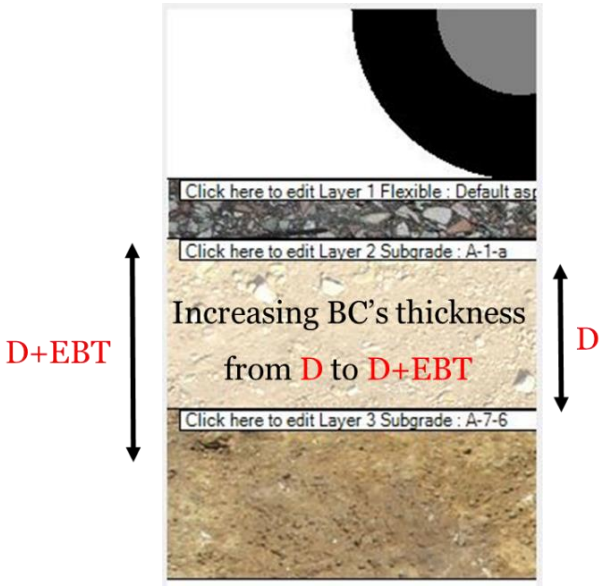

Reduction Coefficients (α_b or α_s)

Within the current framework of the MEPDG, the benefits of geosynthetics can also be incorporated by adjusting the permanent deformation model. The model for predicting permanent deformation in the unbound material layer and the subgrade are implemented in the ME Design as follows:

$$\Delta_{soil} = \beta_{s1} k_{s1} \varepsilon_v h_{soil} \left(\frac{\varepsilon_0}{\varepsilon_r}\right) e^{-\left(\frac{\rho}{N}\right)^{\beta}} \tag{32}$$

where,

Δ_{soil} is permanent deformation;

β_{s1} is a calibrating factor;

ε_v is the mid-depth and top vertical resilient strain for the base course and subgrade;

$\frac{\varepsilon_0}{\varepsilon_r}$, β and ρ are material parameter;

N is the number of loading cycles; and

h_{soil} is the layer thickness of the base course or subgrade.

By establishing calibrated rutting curves for both the unreinforced and geosynthetic reinforced cases within the base and subgrade layers, the process of deriving the modification/reduction coefficients α_b and α_s for the base and subgrade layers becomes

feasible. These coefficients are determined by dividing the rutting values observed in the geosynthetic reinforced layers by those in the unreinforced layers. This division operation encapsulates the effect of reinforcement on mitigating permanent deformation. Subsequently, the modification/reduction coefficients α_b and α_s are integrated into a new predictive equation for evaluating permanent deformation. This equation serves as a refined and more accurate tool for forecasting how the incorporation of reinforcement materials impacts the permanent deformation behavior of the base and subgrade layers within pavement structures.

$$\Delta_{soil} = (\alpha_b \; or \; \alpha_s) * \beta_{s1} k_{s1} \varepsilon_v h_{soil} (\frac{\varepsilon_0}{\varepsilon_r}) e^{-(\frac{\rho}{N})^{\beta}} \tag{33}$$

where α_b is the vertical strain modification/reduction factor for the base course layer and α_s is the permanent deformation modification/reduction factor for the subgrade layer, both controlled by geosynthetic tensile modulus, geosynthetic type, asphalt/base thicknesses, and subgrade stiffness.

Calculations of the Benefit Metrics

Calculations of MR-eff and EBT. The AASHTOWare pavement software is a suite of powerful tools and modules developed by the American Association of State Highway and Transportation Officials (AASHTO) to assist transportation agencies and professionals in the planning, design, management, and maintenance of pavement infrastructure. This comprehensive software package is a staple in the field of civil engineering and transportation, providing essential solutions for optimizing pavement performance and durability. AASHTOWare pavement software offers a wide array of functions, with modules that cater to various aspects of pavement engineering. These modules cover pavement design, analysis, and management, offering tools for predicting pavement distresses, assessing structural integrity, and optimizing maintenance strategies. Users can rely on these software tools to make informed decisions regarding pavement rehabilitation, materials selection, and cost-effective maintenance practices. One of the key strengths of AASHTOWare pavement software is its adherence to mechanistic-empirical (ME) pavement design principles. ME design considers the structural response of pavements under various loads and conditions, offering a more accurate and reliable approach than traditional empirical methods. The software leverages ME design principles to help engineers and agencies design pavements that can withstand the demands of modern transportation systems. AASHTOWare pavement software also assists in the evaluation of pavement performance over time. It can predict distresses such as rutting, cracking, and roughness, helping agencies proactively plan

maintenance and rehabilitation efforts to extend the pavement service life and reduce life-cycle costs. Additionally, the software facilitates the analysis of various pavement materials, including asphalt concrete and concrete, allowing engineers to select materials that meet specific project requirements and performance criteria.

The AASHTOWare version 2.6.0 program was used in this study to calculate the structural benefits of geosynthetic reinforced sections in terms of enhanced effective resilient modulus of the base and subgrade ($M_{R\text{-}eff}$) and equivalent base thickness (EBT). To evaluate the structural benefits of the different geosynthetic reinforced sections included in the FE parametric study in terms of $M_{R\text{-}eff}$ and EBT, the derived TBRs for the different geosynthetic reinforced sections were incorporated into the ME approach using AASHTOWare 2.6.0 software.

The values of $M_{R\text{-}eff}$ and EBT for the geosynthetic reinforced sections were then evaluated using the following stages; see Figure 38.

Figure 38. Different stages of structural benefits calculations

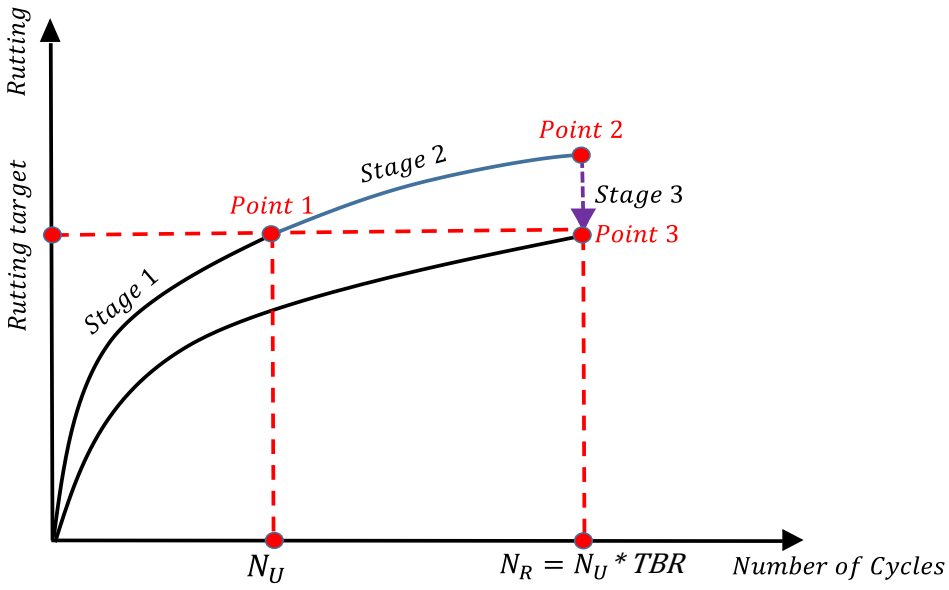

1. *Stage 1:* The N_U value that corresponds to the rutting target for the unreinforced pavement section is derived. Using the Louisiana calibrated design coefficients for each sublayer, the relevant pavement section for a selected TBR value is modeled in AASHTOWare at this stage. The model is then modified to change the average annual daily truck (AADT) number until the rutting curve achieves the desired rutting at Point 1.

The rutting corresponding to a selected TBR value (0.5, 0.75, or 1 in.) are taken as the rutting targets.

2. *Stage 2:* The rutting value for the unreinforced section that matches the N_R value is determined. By increasing the number of load cycles from N_U to N_R, the rutting curve from Stage 1 is extended in this step, reaching Point 2. The value of $AADT_R$ ($AADT_R$=$AADT_U$*TBR) is obtained by multiplying the derived AADT in Stage 1 ($AADT_U$) by the derived TBR from the FE modeling. The rutting value of the unreinforced section at Point 2 is higher than the rutting target of the reinforced section.
3. *Stage 3:* This stage aims at determining the $M_{R\text{-}eff}$ value for the selected TBR value and target rutting. The rutting curve of the unreinforced section is pushed down by increasing the M_R value of the base layer (i.e., the influenced zone of the base and subgrade layers) until it matches the rutting target level (i.e., each sublayer rutting value) of the reinforced section at N_R value at Point 3, which marks the conclusion of the new rutting curve in this stage.
4. *Stage 4:* In this stage, the base course layer's thickness, without changing the M_R, was incrementally increased to push down the rutting curve of the unreinforced section until it matched the rutting curve of the reinforced section at Point 3. The values of EBT, which refers to the increase in the base course thickness equivalent to geosynthetic reinforcement, are determined for the different geosynthetic-reinforced sections.

Calculations of Reduction Coefficients (α_s and α_b). In this section, the required calculation stages for reduction coefficients (α_b and α_s) are illustrated. The proposed method generated new calibration factors for the base layer (α_b) and subgrade (α_s), which can be used as input factors into the Pavement ME Design software to account for the benefits of geosynthetic reinforcement on the permanent deformation of the pavement structure. The parameters α_b and α_s are the permanent deformation reduction factor, controlled by the geosynthetic type and tensile modulus, asphalt and base layer thicknesses, and subgrade stiffness.

The current study followed a four-step process to determine the reduction factors (α_b and α_s) associated with the utilization of geosynthetic reinforcement in pavement construction. These steps involved the calibration of FE models and their integration with the transfer functions in the MEPDG. Subsequently, the long-term rutting performance of the pavement was estimated using the calibrated rutting equations. To calculate the reduction factors for geosynthetics, the rutting curve of the sublayers (i.e., base and subgrade) in the reinforced

pavement was compared with the rutting curves of the corresponding unreinforced pavement section. The following steps are required for the calculations:

1. During Step 1, a parametric investigation was carried out using 2-D axisymmetric quasi-static FE models. These models were specifically developed to replicate the behavior of geosynthetic reinforced pavements subjected to repeated loading for 100 cycles. Through the analysis, the rutting curve throughout the loading cycles and the resilient vertical strain of each sublayer were obtained for the base and subgrade layers for every individual model.
2. During Step 2, the rutting equations of the MEPDG were calibrated by aligning them with the rutting curves of each sublayer and the resilient vertical strains obtained in Step 1. The calibration process aimed to closely match the observed rutting curves by adjusting the rutting equations. This adjustment was carried out by minimizing the sum of squared errors, ensuring the closest fit between the calibrated equations and the actual rutting behavior.
3. During Step 3, the rutting curves that were calibrated for each sublayer are extended to reach the target total rutting of 1 in. for the pavement. This extrapolation process allows for the development of long-term rutting curves that illustrate the relationship between rutting and the number of loading cycles.
4. During Step 4, the reduction factors for the base and subgrade layers (α_b and α_s) were determined by contrasting the elongated rutting curves of the reinforced pavement section with the rutting curves of the corresponding unreinforced pavement section. The reduction factor is computed to establish a correlation between the two sets of curves, indicating the impact of geosynthetic reinforcement in diminishing rutting in the base and subgrade layers.

Computational Prediction Models

Within this study, a diverse set of six regression models and machine learning (ML) algorithms were harnessed for the development of predictive models based on the outcomes derived from the FE dataset. These models encompass Multiple Linear Regression (MLR), Multivariate Exponential Model (MER), Support Vector Machine (SVM), Decision Tree (DT), Random Forest (RF), and Gradient Boosting (GB). Google Colab serves as the platform for constructing these regression models and employing advanced ML techniques to discern the relationships among various variables within the collected dataset obtained from the parametric study.

Multiple Linear Regression (MLR)

Multiple Linear Regression (MLR) analysis is used to simulate the relationship between the explanatory (i.e., independent) and response (i.e., dependent) variables. Stepwise regression is the process of building a regression model iteratively, step by step, and involves choosing independent variables to be included in the final model. After each iteration, the potential explanatory factors are successively added or removed, and the statistical significance is tested. Equation 34 provides the general formula for multiple linear regression:

$$y = \beta_0 + \beta_1 x_1 + \beta_2 x_2 + \beta_3 x_3 + \cdots + \beta_n x_n \tag{34}$$

where,
y is the dependent variable;
x_i are independent variables; and
β_i are regression coefficients.

Multivariate Exponential Regression (MER)

Multivariate Exponential Regression (MER) is a powerful statistical modeling technique used to analyze relationships between multiple independent variables and a dependent variable when the underlying data exhibits exponential growth or decay patterns. In this approach, the response variable is modeled as a function of multiple predictors, each with its own coefficient, and the model assumes that the response variable follows an exponential distribution.

The general formulation for MER can be expressed as:

$$y = a * \exp\left(b_1 x_1 + b_2 x_2 + b_3 x_3 + \cdots + b_n x_n\right) \tag{35}$$

In this equation, a represents the scale parameter that determines the overall magnitude of the exponential growth or decay, while b_1 to b_n are the coefficients associated with each independent variable x_1 to x_n. These coefficients quantify the impact of each predictor on the exponential behavior of the dependent variable$y$. MER allows for a comprehensive analysis of complex relationships between multiple variables and is particularly useful in fields where exponential growth or decay phenomena are commonly observed and need to be studied in a multivariate context.

Support Vector Machine (SVM)

Support Vector Machine (SVM) regression is a powerful ML technique used for modeling and predicting continuous numeric outcomes. Unlike traditional linear regression, SVM Regression seeks to find a hyperplane that best fits the data while simultaneously minimizing prediction errors. What sets SVM Regression apart is its ability to handle complex, non-linear relationships using kernel functions. By transforming the feature space into a higher-dimensional one, SVM can capture intricate patterns that might be missed by linear models. SVM Regression is particularly adept at handling datasets with a small number of outliers or noisy data points, as it focuses on maximizing the margin of separation between data points and the regression hyperplane. Its versatility and robustness make it a valuable tool for various regression tasks, ranging from finance to healthcare, in which modeling the relationship between variables with precision is essential.

Decision Tree (DT)

Decision tree regression is an ML technique used for modeling and predicting numeric (i.e., continuous) target variables. It builds a tree-like structure of decisions and outcomes, where each internal node represents a feature or attribute, and each leaf node represents a predicted numeric value; see Figure 39. This model is constructed by recursively splitting data based on the selected features to minimize the variance of the target variable within each leaf node. It is a versatile algorithm that can capture complex relationships in data.

Figure 39. Schematic view of Decision Tree

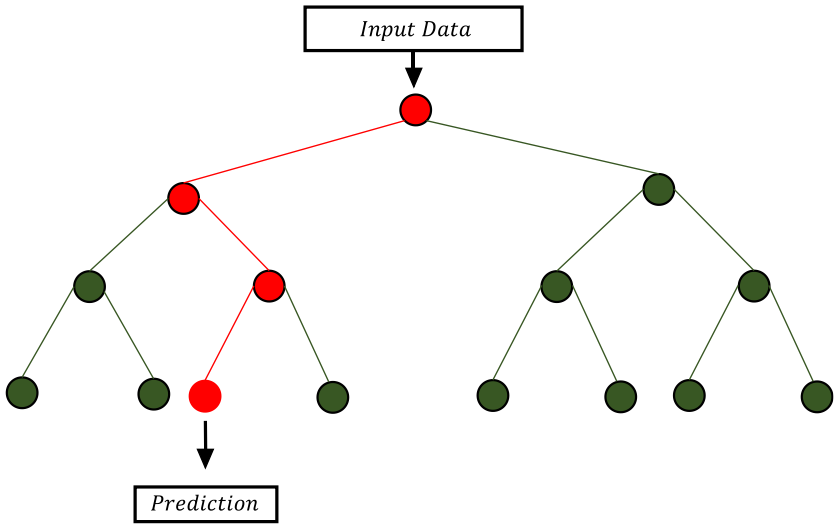

Random Forest (RF)

The ensemble learning method combines predictions from various ML algorithms to provide more accurate predictions than those from a single model. Bootstrapping involves randomly selecting subsets of a dataset over a predetermined number of repetitions and variables. These results are then averaged to provide a more potent outcome. The bootstrapping Random Forest approach uses ensemble learning techniques with the decision tree framework to generate numerous randomly selected decision trees from the data and average the results to get a new result that frequently produces accurate predictions or classifications. The structure of a common RF algorithm is shown in Figure 40, which researchers have used to manage complex non-linear behavior between predictors and responses. A group of weak DTs can generate better outcomes because the number of predictors and DTs used in the model determines how accurate the predictions will be. The primary advantage of the RF algorithm is that it forbids overfitting. Its disadvantages include being less resistant to outliers and less predictive than methods such as least square regression.

Figure 40. Schematic illustration of RF algorithm

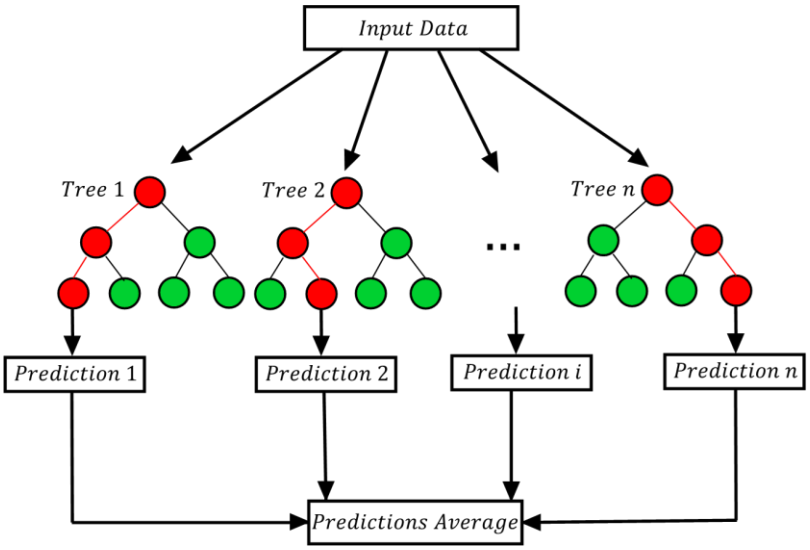

Gradient Boosting (GB)

Gradient Boosting regression is a powerful ML technique renowned for its remarkable predictive ability in regression tasks. This ensemble learning method works by combining the strengths of multiple decision trees, sequentially refining each tree's predictions to minimize the model's prediction errors. Gradient Boosting Regression excels in capturing complex relationships within data, handling both linear and non-linear patterns with remarkable precision. By iteratively optimizing the model's predictions in response to previous errors, it provides a robust mechanism for mitigating overfitting and achieving high predictive accuracy. The flexibility of gradient boosting, as well as its ability to handle missing data and outliers, makes it an invaluable tool for an array of applications in which accurate predictions are paramount. These applications range from finance to healthcare. With its proven track record for delivering precise and reliable regression models, Gradient Boosting Regression remains a favored choice among data scientists and ML practitioners.

Finite Element (FE) Parametric Study

The effects of the different variables/parameters on the performance of geosynthetic reinforced pavement sections were evaluated based on the pavement's response to repeated loading. To do so, FE models were first developed for each case using ABAQUS software. To create these models, the thickness of HMA was assumed to be 3.5, 6.5, and 10 in., which

corresponds to the thickness of low, medium, and high volume traffic roads in Louisiana, respectively. To further investigate the contribution of each variable/parameter, an extensive FE parametric study was performed on different subgrade strengths/stiffnesses, different base thicknesses, two types of geosynthetics, and different geosynthetic tensile moduli. This involved analyzing the pavement's responses to repeated loading under different conditions to determine the effect of each parameter on the performance of geosynthetic reinforced pavement structure. Table 7 shows that the researchers selected three different stiffnesses for the subgrade, four different thicknesses for the base coarse aggregate, and three different stiffnesses for the geosynthetics, including two different types of geotextiles and geogrids. Additionally, the researchers assumed that the geosynthetic layer is located at the base-subgrade interface in this study.

Table 7. Parametric study

Subgrade Strength	Base thickness (in.)	HMA thickness (in.)	Geosynthetic location	Geosynthetic stiffness	Geosynthetic Type
Weak Medium stiff Stiff	8	3.5 6.5 10	Base/sub Interface	Low Medium High	Geogrid Geotextile
	10		Base/sub Interface		
	12		Base/sub Interface		
	14		Base/sub Interface		

Discussion of Results

Introduction

In this section, the findings and insights obtained from two pivotal components of this study, the Finite Element Models (FEM) Results and AASHTOWare Results, are presented. These comprehensive analyses are regarded as the backbone of this research, as they facilitate a detailed understanding of the effects of different variables and parameters onto the benefits of geosynthetic reinforcement on flexible pavements.

In the following subsection, the outcomes of the developed FE models, which indicate the behaviors and responses of pavement structures under various loading scenarios, are showcased. Through these models, the resilient vertical strain and rutting characteristics across the different pavement sublayers, coupled with geosynthetic reinforcement, are explored. In this subsection, valuable insights into the long-term performance of geosynthetic reinforced pavements are offered, ultimately contributing to quantifying the benefits in terms of the Traffic Benefit Ratio (TBR).

Moving to the next subsection, the results yielded by the AASHTOWare analysis are examined. In this subsection, the values of TBR obtained from the previous subsection are utilized as inputs in the AASHTOWare software. Consequently, the values of EBT and M_{Reff}, which are recognized as structural benefits of geosynthetics in flexible pavement structures, are derived and subjected to comparison. This comprehensive analysis enables the assessment of the substantial advantages conferred by the utilization of geosynthetics on pavement structures, offering insights into their contributions to long-term performance.

Results of Finite Element (FE) Models

This subsection contains the results of the comprehensive parametric study that was performed utilizing the developed FE analysis of different geosynthetic reinforced pavement sections. The advantage conferred upon flexible pavements through the incorporation of geosynthetic reinforcement is illustrated through a comparative analysis, in which the results from geosynthetic reinforced pavement sections are compared to those of their equivalent unreinforced sections.

Stresses and Strains

The confining effect of lateral stresses induced by geosynthetic reinforcement can reduce the lateral deformation and the associated vertical deformation [40]. Figure 41 presents the change in lateral strain profiles with depth for different scenarios obtained at the peak of loading. Figure 41a shows the lateral strain profiles for the case of a 10 in. base thickness pavement section for the unreinforced case and for the cases with one layer of medium stiffness geogrid or geotextile reinforcement, obtained at the wheel center, 6 in. from the center, and 12 in. from the center. The figure clearly demonstrates that using one layer of geogrid or geotextile at the base-subgrade interface can significantly decrease the lateral strain in both the base and subgrade layers. This reduction is most significant below the wheel center, which is expected. Additionally, the figures show that geogrid reinforcement has greater effect than geotextile reinforcement of the same stiffness in terms of reducing the lateral strain due to the interlocking mechanism between geogroid apertures and the aggregate base particles. Figure 41b presents three subfigures of lateral strain profiles for the case of geotextile-reinforced pavements with a 12 in. base thickness and different geotextile stiffnesses. The figure shows that increasing geotextile stiffness can reduce the lateral strains in the subgrade layer [87].

Figure 41. Lateral strain profiles for: (a) unreinforced and reinforced pavements for 10 in. base course at different locations for medium stiffness geogrid and geotextile; (b) geotextile reinforced pavements of 12 in. base course with different geotextile stiffnesses

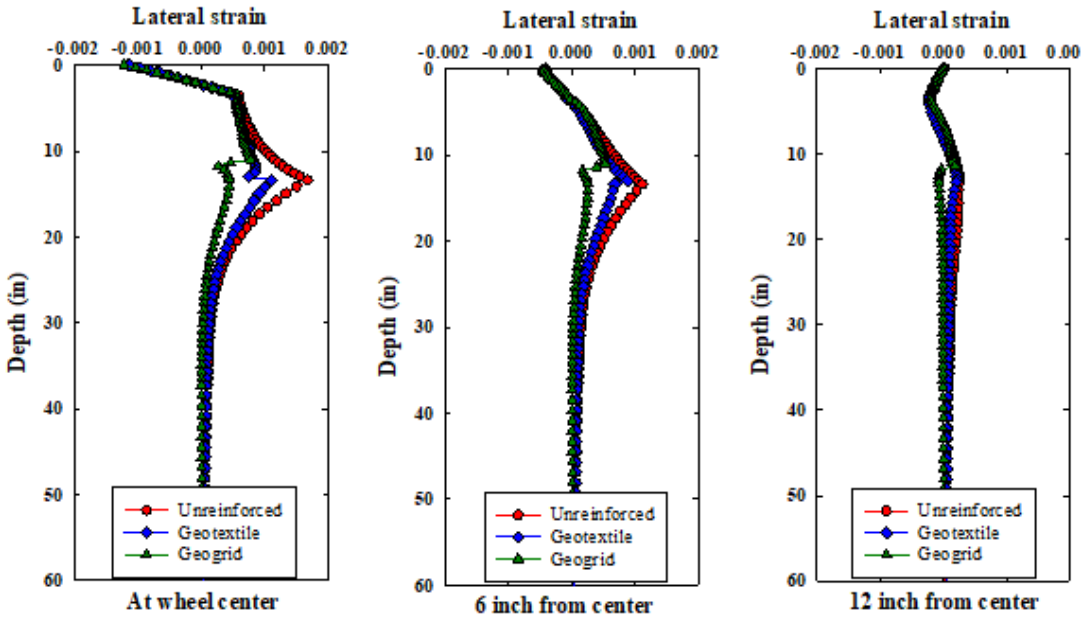

(a)

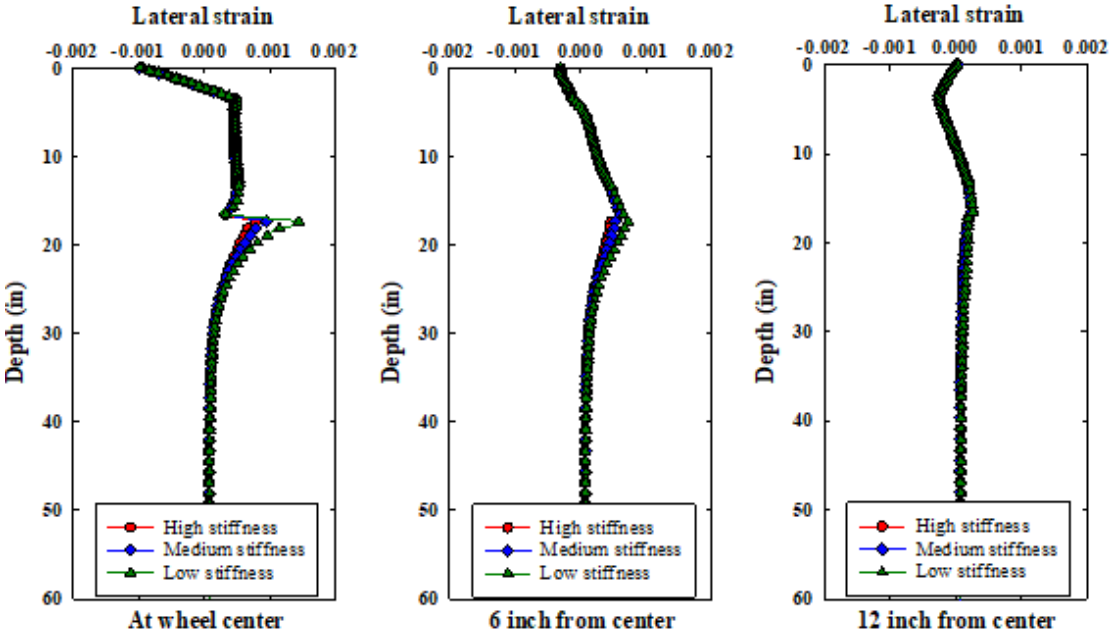

(b)

The induced vertical strains on top of subgrade layers are directly associated with the permanent vertical deformation at the pavement surface. The distributions of vertical strains obtained at the top of the subgrade layer for unreinforced and geosynthetic reinforced pavement sections are presented in Figure 42. Figure 42a depicts the comparison of vertical strain distribution obtained for the unreinforced pavement with 10 in. base thickness and those reinforced with one layer of medium stiffness geogrid or geotextile. The figure clearly illustrates that using one layer of geogrid or geotextile at the base-subgrade interface can significantly decrease the vertical strain, which is reflected in reducing the surface rutting of the geosynthetic reinforced pavement sections. Similar to the lateral strain behavior, the geogrid layer provides stronger support from interlocking mechanism, hence resulting in smaller vertical strains than the geotextile layer. Figure 42b presents the effect of geotextile stiffness on the distribution of vertical strains on top of the subgrade layer for the geotextile reinforced pavement section with 12 in. base thickness. The figure demonstrates that increasing geotextile stiffness will result in decreasing the vertical strains at the top of the subgrade layer. Figure 42c depicts the effect of geogrid reinforcement on the distribution of vertical strains on top of the subgrade layer for 12 in. base thickness for one-layer geogrid stiffnesses and double-layers of medium stiffness geogrids.

Similar to geotextile reinforcement, the figure reveals the effect of increasing the geogrid stiffness on decreasing the vertical strain on top of the subgrade layer. The figure clearly demonstrates the advantage of using double geogrid reinforcement layers, one placed at the base-subgrade interface and another placed at the middle of the base layer, on further decreasing the vertical strains at the top of the subgrade layer. This will significantly enhance the performance and benefits of double geogrid reinforced pavements, as will be described later in the TBR values.

Figure 42. Comparison of vertical strain distributions obtained at top of subgrade layer for: (a) different types of medium stiffness geosynthetics with 10 in. base thickness; (b) geotextile reinforced pavements with 12 in. base thickness and different geotextile stiffnesses; (c) geogrid reinforced pavements with 12 in. base thickness and different geogrid stiffnesses for single and double layers

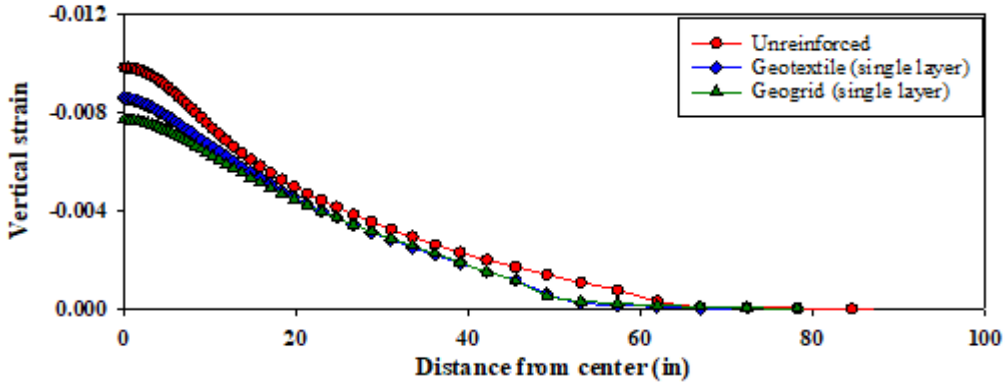

(a)

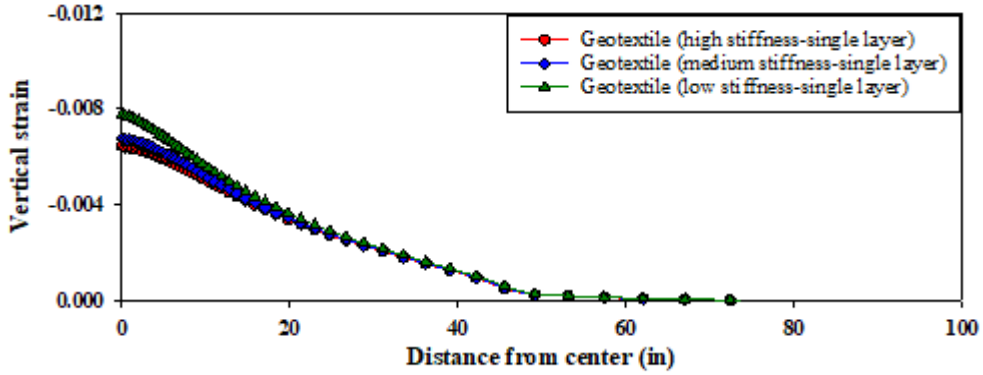

(b)

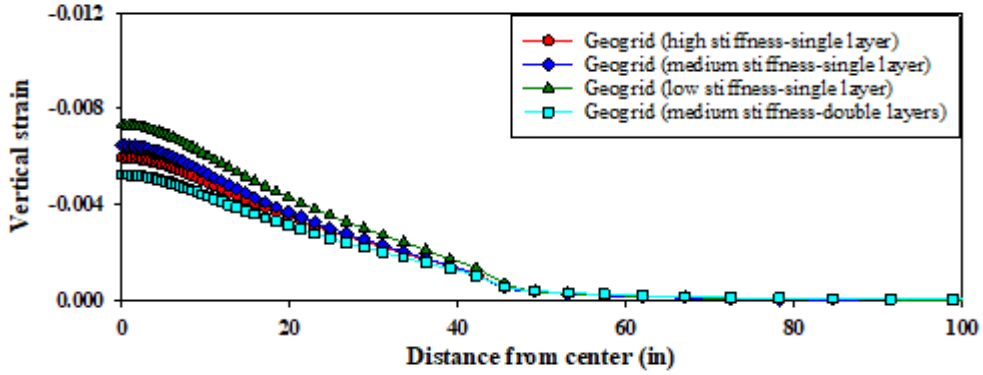

(c)

The reduction of rutting in geosynthetic reinforced pavements can also be attributed to the reduction of shear strains at the top of the subgrade layer [16] [88]. Figure 43 plots the distribution of shear strains at the top of the subgrade layer for unreinforced and geosynthetic reinforced pavements. The benefits of using geosynthetics on reducing the shear strains are very clear. Figure 43a demonstrates a significant decrease in shear strain on the top of the subgrade layer when one layer of medium stiffness geosynthetic is used. For example, the maximum shear strain for the unreinforced section with 10 in. base thickness is 0.35%, while the maximum shear strain for the geogrid reinforced section is only 0.15%. Hence, the reduction is approximately 57%. A similar large reduction in shear strain can be observed in Figure 43b, where the effect of geotextile stiffness is examined.

Figure 43. Comparison of shear strain profile at the top of the subgrade layer between: (a) different types of medium stiffness geosynthetics for 10 in. base thickness; (b) geotextile reinforced pavements with 12 in. base thickness and different geotextile stiffnesses

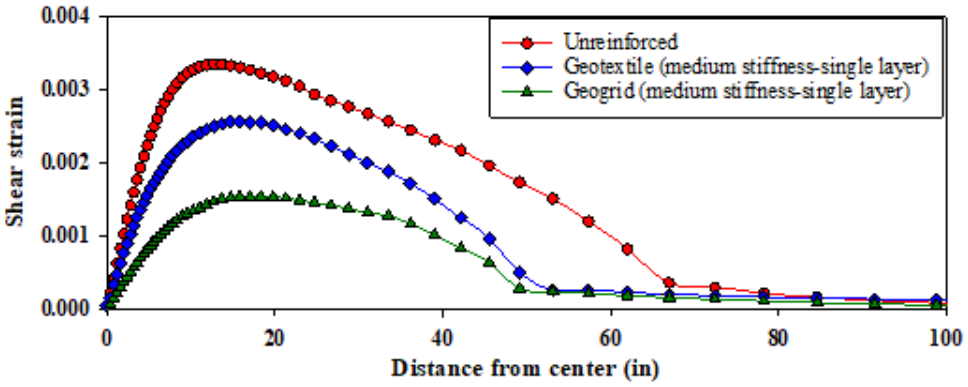

(a)

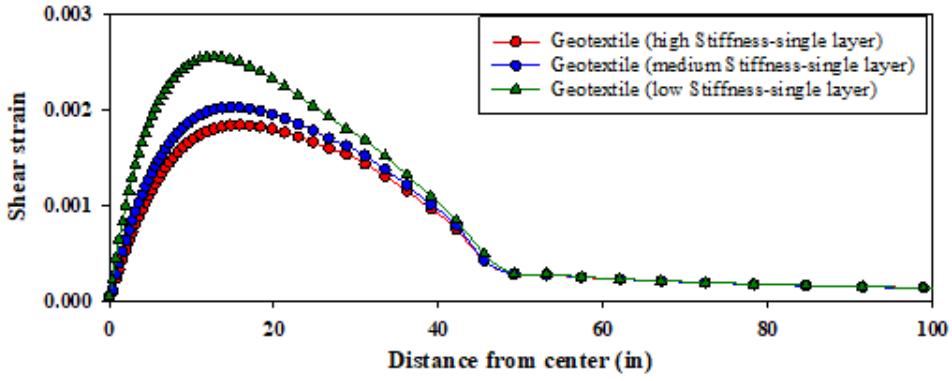

(b)

Permanent Deformation

As stated earlier, FE analyses were conducted for 100 load cycles. The permanent deformation (i.e., rutting) results for the different pavement sections were used to calibrate each pavement sublayer's ME rutting equation parameters to extend the rutting curves for long-term cycles. Figure 44 presents comparison examples between the FE results for the first 100 load cycles and the ME predictions using the calibrated rutting equations for the geotextile reinforced sections with different base thicknesses, which demonstrates good agreement between the two approaches. It can be seen that the total rutting at 100 cycles increases as the base thickness decreases.

Figure 44. Comparison of rutting between FE analysis and calibrated ME equations for: (a) 8 in.; (b) 10 in.; (c) 12 in.; (d) 14 in. base thickness with medium stiffness geotextile reinforcement

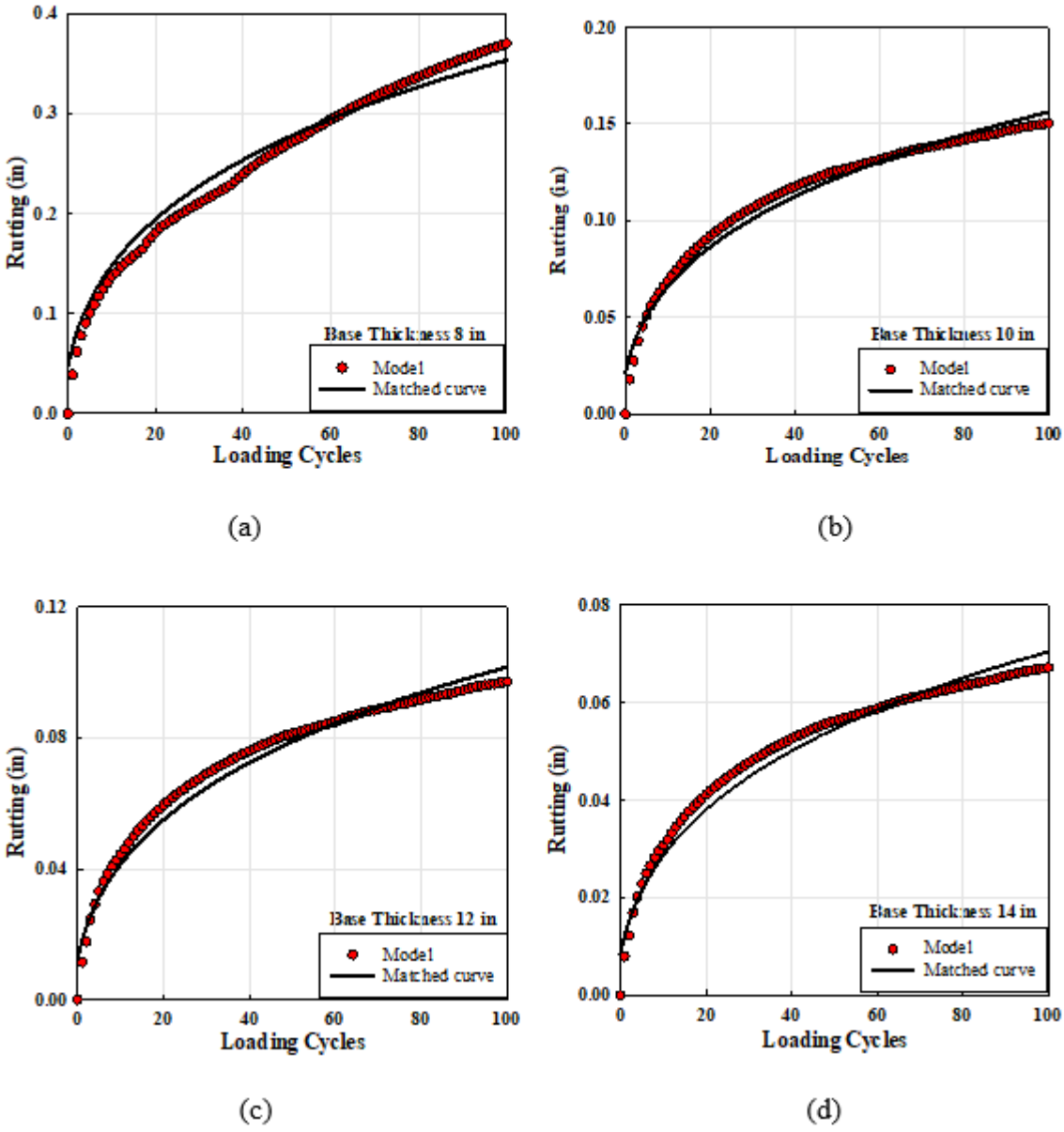

By using the calibrated ME equations, the long-term benefits of the different geosynthetic reinforced pavement sections can be easily evaluated. Figure 45 presents examples of the rut curves obtained for the unreinforced and geogrid/geotextile reinforced pavement section for the case of 12 in. base thickness and using medium stiffness geosynthetics. The first 100-cycle rutting curves are shown in Figure 45a, and the long-term ME rutting curves are shown in Figure 45b. As can be seen, the long-term benefits of using geosynthetics, both geogrids and geotextiles, in reducing rutting is significant. A more detailed discussion related to this topic is presented in the following section.

Figure 45 : Comparison between: (a) 100 cycles ME calibrated rut curves section; (b) long-term rutting curves for unreinforced and geogrid/geotextile reinforced pavements for the case of 12 in. base thickness and medium stiffness geosynthetics

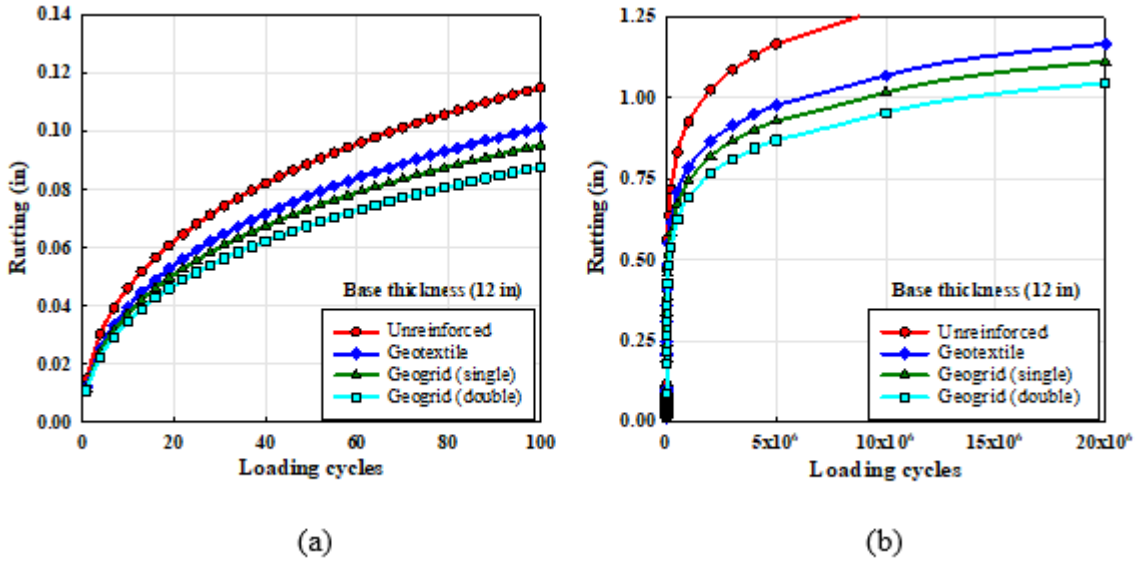

The influence of each sublayer on the ultimate rutting of the pavement structure undergoes alterations when the pavement structure parameters are changed. In the case of low volume roads with a 3.5 in. asphalt thickness, the subgrade layer is the predominant contributor to surface rutting, which accounts for approximately 60%, followed by the base layer at approximately 30% and the asphalt layer at roughly 10%.

For medium volume roads, as the number of required equivalent axle loads (ESALs) to attain a rutting target increases, the significance of the asphalt layer's contribution to the final rutting of the pavement structure rises. In scenarios with a 6.5 inch asphalt thickness, the primary contributor in surface rutting remains the subgrade layer, which accounts for

approximately 55%, followed by the base layer at approximately 20% and the asphalt layer at approximately 25%.

Similarly, for high volume roads, the contribution of the asphalt layer to the final rutting of pavement structure increases compared to the other sublayers. In high volume road situations with a 10 in. asphalt thickness, the foremost contributor to rutting is the asphalt layer, accounting for approximately 50% of the final rutting, followed by the subgrade at approximately 40% and the base layer at roughly 10%.

Figure 46 compares the rutting curves for base course (BC) and subgrade layers of unreinforced sections and sections reinforced with a single layer of geogrid or geotextile. Figure 46a illustrates the contribution of one geogrid reinforced layer on the BC and subgrade rutting, and Figure 46b illustrates the contribution of one layer of geotextile on the BC and subgrade rutting for 12 in. base pavement sections.

Figure 46. Comparison between the rutting curves of pavement sublayers for the unreinforced and reinforced sections: (a) one geogrid reinforced layer; (b) one geotextile reinforced layer for the case of 12 in. base thickness and medium stiffness geosynthetics

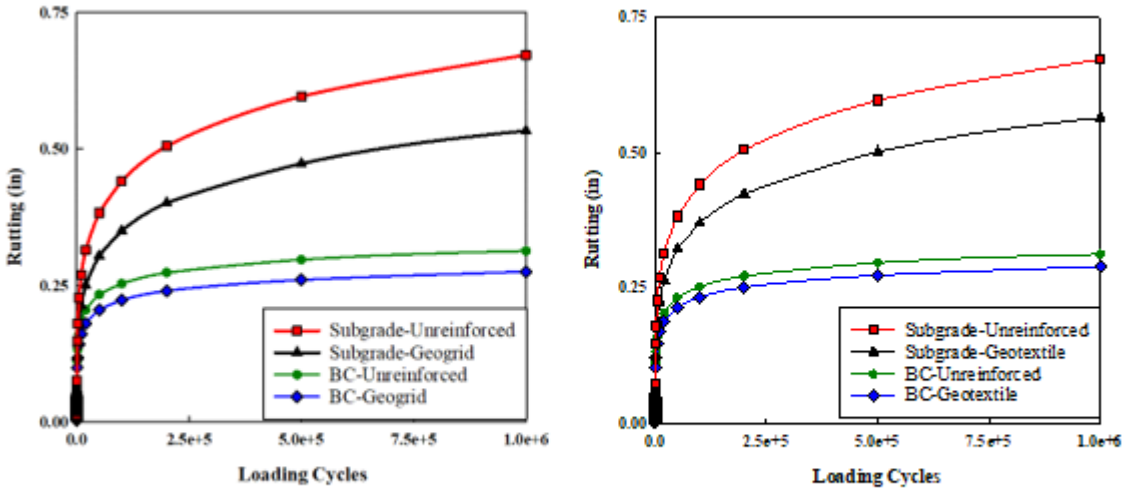

Verification of Finite Element Models

In this section, the verification and validation of the proposed FE-ME methodology is carried out by utilizing the outcomes of cyclic plate load tests (CPLT) and accelerated wheel loading tests (ALT) that were conducted on full-scale geosynthetic reinforced test lane sections. These test lane sections were originally constructed as part of a prior study at the Pavement Research Facility (PRF) site, as detailed in the work of Abu-Farsakh et al. [14]. At the PRF site, a total of six test lane sections were meticulously constructed, each measuring 80 ft. in length and 13 ft. in width, all situated atop a weak subgrade soil characterized by a CBR value of approximately 1.5.

To verify the FE-ME results, we have specifically selected three test sections, denoted as Sections 3, 4, and 6. Section 3, featuring an 18 in. base aggregate thickness, was fortified with a single layer of geogrid reinforcement positioned at the base-subgrade interface. Section 4, on the other hand, remains unreinforced but boasts an 18 in. base thickness. Lastly, Section 6, with a 10 in. base aggregate thickness, underwent reinforcement with a high strength geotextile layer, strategically placed at the base-subgrade interface. Across all sections, a 3 in. HMA surface course was meticulously constructed.

To verify/validate our FE results, researchers calibrated and extrapolated the simulated FE rutting curves for Sections 3, 4, and 6 over a span of 100 load cycles, using the ME rutting equations. These extended FE rutting curves were subsequently compared with the actual rut results obtained from the experimental field tests. As portrayed in Figure 47a-c, which depict the comparison of rutting curves between the FE-ME results and the experimental tests results for Sections 3, 4 and 6, a commendable level of agreement becomes evident. These figures underscore the alignment of the FE-ME outcomes with the results of the cyclic plate load tests and accelerated wheel loading tests, reaffirming the accuracy and reliability of the proposed methodology.

Figure 47. Comparison between FE extrapolated rutting curve obtained from FE-ME method with the laboratory CPLTs and field ALTs for: (a) 18 in. base geogrid reinforced section; (b) 10 in. base geotextile reinforced section; (c) 18 in. base unreinforced section

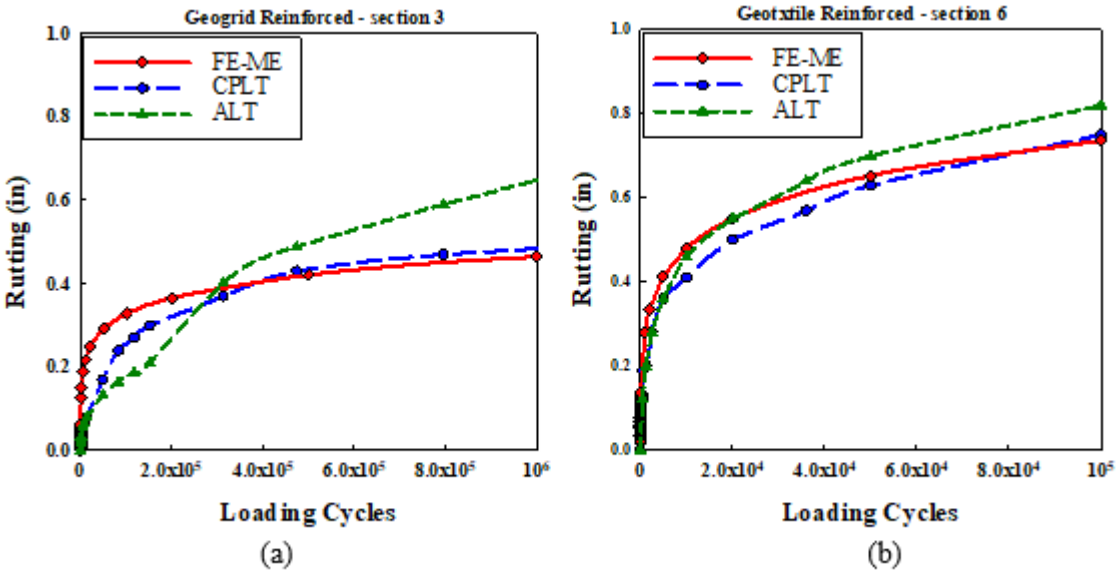

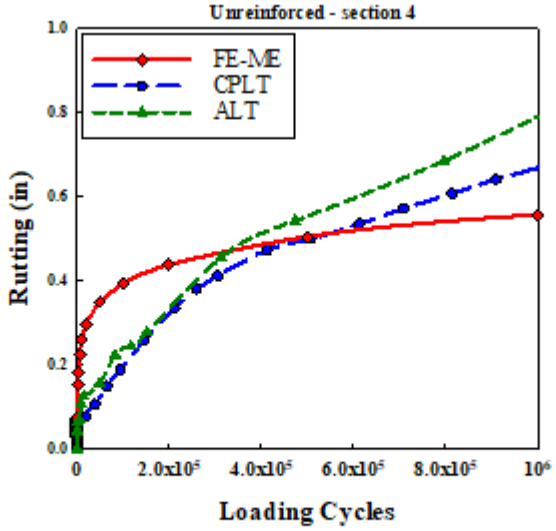

(c)

Evaluation of Traffic Benefit Ratio (TBR)

One approach to quantifying the benefits of using geosynthetic reinforcement in flexible pavement structures is by evaluating the TBR. The TBR value represents the increased ratio of the pavement's service life due to the inclusion of geosynthetics for a selected level of performance or rutting target. The TBR values were derived for three different levels of performance, corresponding to rut depths of 0.5, 0.75, and 1 in., from the FE-ME rutting curves obtained for the different reinforced sections using the procedure explained earlier.

All of the TBR values obtained from the generated FE-ME rut curves for the different geosynthetic-reinforced pavement sections are presented in tables and figures in Appendix A. The results clearly demonstrated that the TBR values increased when increasing the rutting target for all cases; see Figure 48. The differences in TBRs for low volume roads (i.e., asphalt thickness of 3.5 in.) for different rutting targets are usually higher for geogrid reinforced cases compared to geotextile reinforced cases, with the maximum difference of up to 96% at 10 in. base thickness on the weak subgrade soil. The maximum differences of TBR values for medium volume roads (i.e., asphalt thickness of 6.5 in.) and high volume roads (i.e., asphalt thickness of 10 in.) for the different rutting targets are lower and primarily occur for 8 in. base thickness. The maximum differences for medium and high volume roads are 64% and 58%, respectively.

The thickness of the base course layer also shows significant effect on the TBR values. The TBR values for all cases of low volume roads (i.e., asphalt thickness of 3.5 in.) reach a maximum (i.e., optimal) value at 10 in. base thickness. Reaching a peak value for TBR due to changing the base thickness was also reported by other researchers [11] [89]. Apparently, the benefits of using geosynthetics to reinforce pavements show an optimal TBR value for a base course thickness of 10 in. For medium volume roads (i.e., asphalt thickness of 6.5 in.) and high volume roads (i.e., asphalt thickness of 10 in.), the TBR values significantly decrease when increasing the base thickness; see Figure 49.

Figure 48. TBR variations with base thickness for pavements reinforced with a single layer of high stiffness geosynthetic for (a) low volume and (b) medium volume roads on weak subgrade

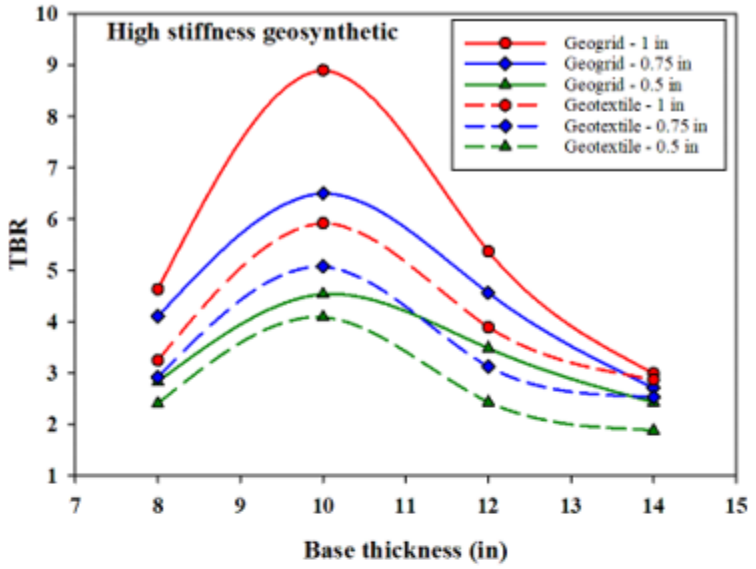

(a)

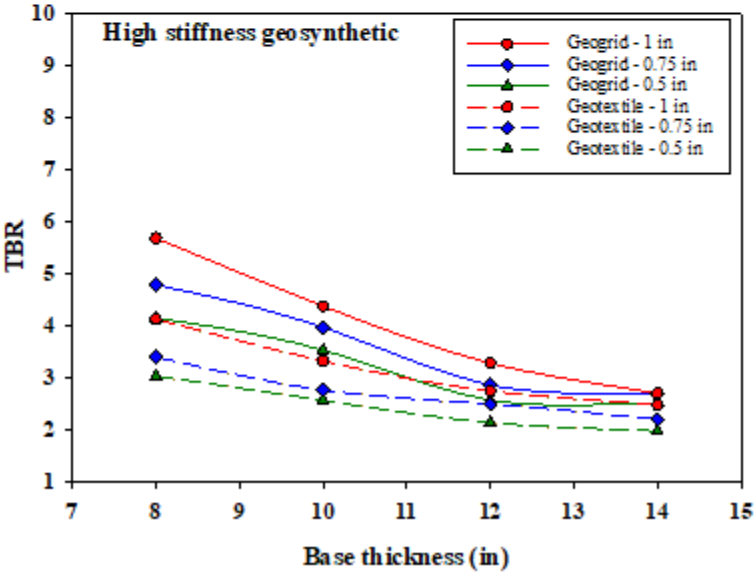

(b)

Figure 49. TBR variations with base thickness for pavements reinforced with a single layer of medium stiffness geosynthetic for (a) low volume and (b) high volume roads on medium-stiff subgrade

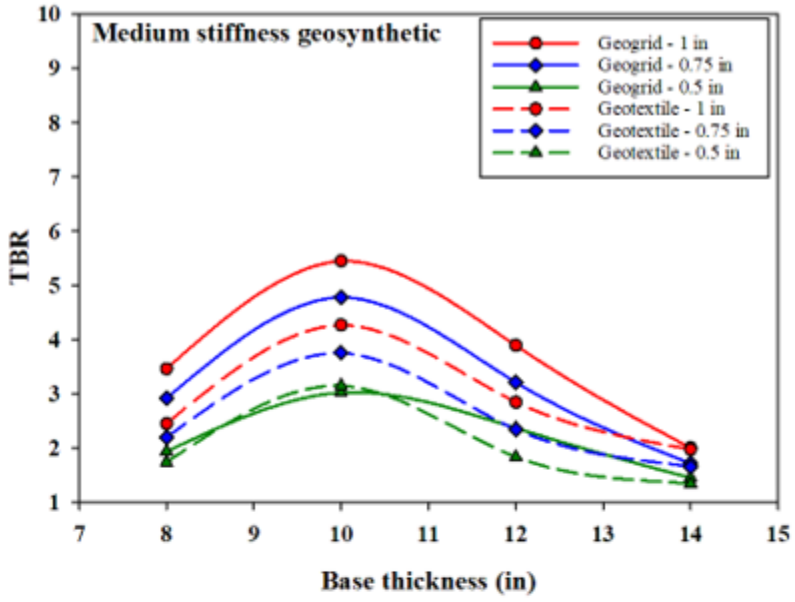

(a)

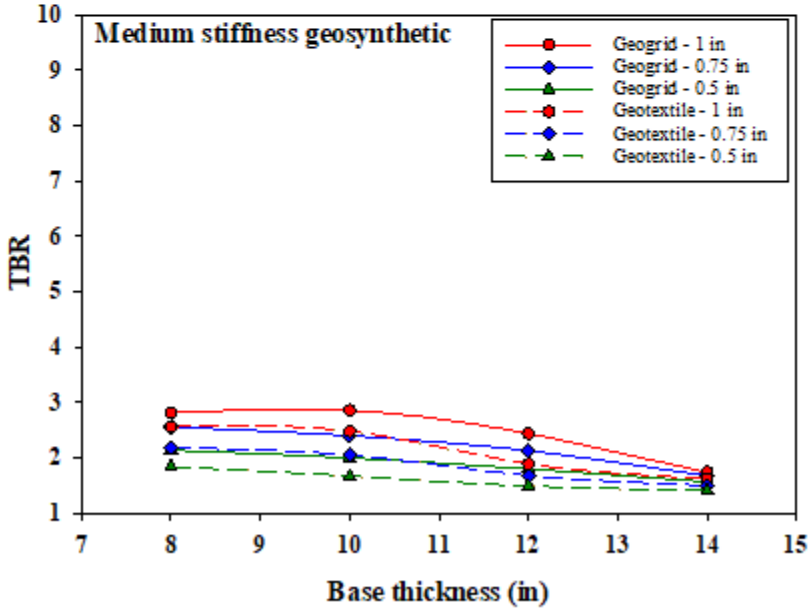

(b)

For all cases, the type of geosynthetic (i.e., geogrids versus geotextiles) has an important effect on the benefits evaluated by TBR, and the differences between TBR values are the highest for weak subgrades compared to other subgrade stiffnesses. The comparison between the TBR values for geogrid and geotextile reinforced pavement sections shows that geogrids have up to 40% higher TBR values than the geotextiles. The higher TBR values for geogrids can be attributed to the interlocking mechanism between the geogrid apertures and base aggregate particles that were modeled in this study, which resulted in consistent rutting behavior with the accelerated field test sections [14].

The effect of geosynthetic tensile stiffness was also evaluated for all geosynthetic reinforced pavement sections. For the geogrid reinforced cases for low volume roads, the TBR values for the low geogrid stiffness range from 1.35 to 5.3, and for the high geogrid stiffness, it ranges from 1.74 to 8.9. The changes in geogrid stiffness from low to high for geogrid reinforced cases result in an increase in TRB value of up to 68%. However, for the geotextile reinforced cases, the TBR values for the low geotextile stiffness cases range from 1.25 to 3.75, and for the high geotextile stiffness cases, it ranges from 1.58 to 5.92. The changes in geotextile stiffness from low to high for geotextile-reinforced cases result in up to a 54% increase in TBR value; Figure 50.

In the context of geogrid reinforced scenarios on medium volume roads, the TBR values for cases with low geogrid stiffness vary between 1.46 and 3.36, while for high geogrid stiffness scenarios, they range from 1.73 to 5.69. Transitioning from low to high stiffness levels in geogrid reinforced scenarios yields a notable increase in TBR values, with improvements of up to 69%. Conversely, in geotextile reinforced scenarios, TBR values for low geotextile stiffness cases span from 1.44 to 3.26, and for high geotextile stiffness cases, they span from 1.61 to 4.13. The shift from low to high geotextile stiffness in these scenarios leads to a maximum 27% enhancement in TBR values.

For high volume roads with geogrid reinforcement, the TBR values for the low geogrid stiffness cases fall within the range of 1.19 to 3.07, while for high geogrid stiffness cases, they extend from 1.41 to 4.55. The transition from low to high geogrid stiffness results in a TBR value increase of up to 48%. However, in geotextile reinforced situations on high volume roads, the TBR values for low geotextile stiffness cases span from 1.16 to 2.99, and for high geotextile stiffness cases, they range from 1.3 to 3.84. Shifting from low to high geotextile stiffness in these scenarios leads to a maximum 28% improvement in TBR values.

Figure 50. TBR variations with base thickness for pavements reinforced with a single layer of (a) high stiffness and (b) low stiffness geosynthetic for medium volume roads on medium-stiff subgrade

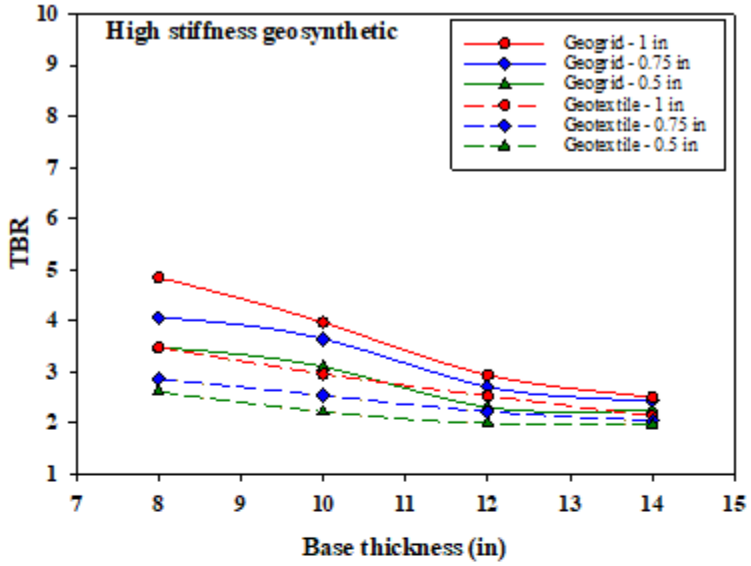

(a)

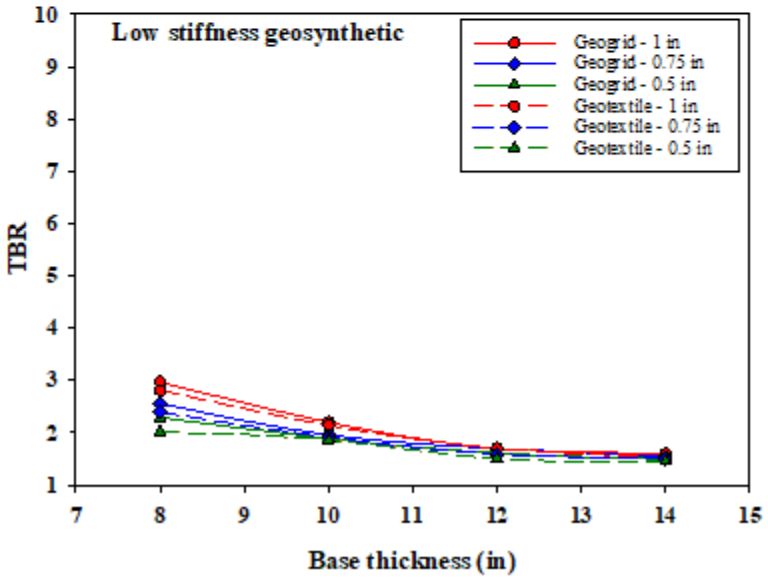

(b)

Results of AASHTOWare Analyses

Effective Resilient Modulus ($M_{R\text{-}eff}$) Increase

One approach to incorporate the benefits of geosynthetic reinforcement into the ME design of flexible pavements is to assume that for design purposes, all of the geosynthetic benefits go into reinforcing the base course layer only. In this method, the resilient modulus of the whole base layer thickness will be increased from M_R to $M_{R\text{-}eff}$, such that the rutting curve of the unreinforced section (i.e., with $M_{R\text{-}eff}$) is pushed down to match the rutting target of the corresponding geosynthetic reinforced pavement section. In this approach, the properties of other sublayers will be kept the same as those of the reinforced section.

The calculated TBR values obtained from FE analyses are used as inputs in the AASHTOWare to derive the corresponding $M_{R\text{-}eff}$ values for the base course layer. As a result, the variation in $M_{R\text{-}eff}$ values follows the same pattern as the TBR values that show a peak value at 10 in. base thickness for low volume roads. Additionally, the maximum $M_{R\text{-}eff}$ values occur for 8 in. base thickness for medium and high volume roads.

The derived $M_{R\text{-}eff}$ values are usually higher for higher rutting targets. The results of AASHTOWare analyses show that the effective base modulus ($M_{R\text{-}eff}$) can be increased up to 192% for the geosynthetic reinforced pavement sections at 0.75 in. rutting for low volume roads. The maximum $M_{R\text{-}eff}$ increase for medium and high volume roads at 0.75 in. rutting are 171% and 125%, respectively. Additionally, the results show that the value of $M_{R\text{-}eff}$ decreases when increasing the subgrade strength/stiffness, increases when increasing the geosynthetic tensile modulus, and increases when decreasing the base thickness. In all cases, $M_{R\text{-}eff}$ values are higher for geogrid reinforced pavement sections than for geotextile reinforced pavement sections. All the values of $M_{R\text{-}eff}$ obtained from the FE-ME analyses are presented as tables in Appendix B.

The derived $M_{R\text{-}eff}$ values show that the subgrade strength/stiffness has a significant impact on the results, as reflected in the TBR values. For geotextile reinforced pavement sections and 0.75 in. rutting target for low volume roads, the maximum increase in $M_{R\text{-}eff}$ (i.e., corresponding to base thickness of 10 in.) for high tensile stiffness geotextile ranges from 171% to 52% as the subgrade stiffness changes from weak to stiff; see Figure 51. However, the values of maximum $M_{R\text{-}eff}$ change from 130% to 48% for medium tensile stiffness geotextile and from 106% to 31% for low tensile stiffness cases. For the geogrid reinforced pavement sections, the results show similar patterns. For high tensile geogrid and 0.75 in. rutting target, the maximum increase in $M_{R\text{-}eff}$ is 192% for weak subgrade and 67% for stiff

subgrade. However, for the medium and low tensile stiffness and 0.75 in. rutting target for low volume roads, the maximum increase in $M_{R\text{-}eff}$ values changes from 179% to 61%, and from 126% to 42%, respectively.

Figure 51. Changes in $M_{R\text{-}eff}$ of pavement reinforced with high tensile stiffness geotextile for different subgrade stiffnesses on low volume roads

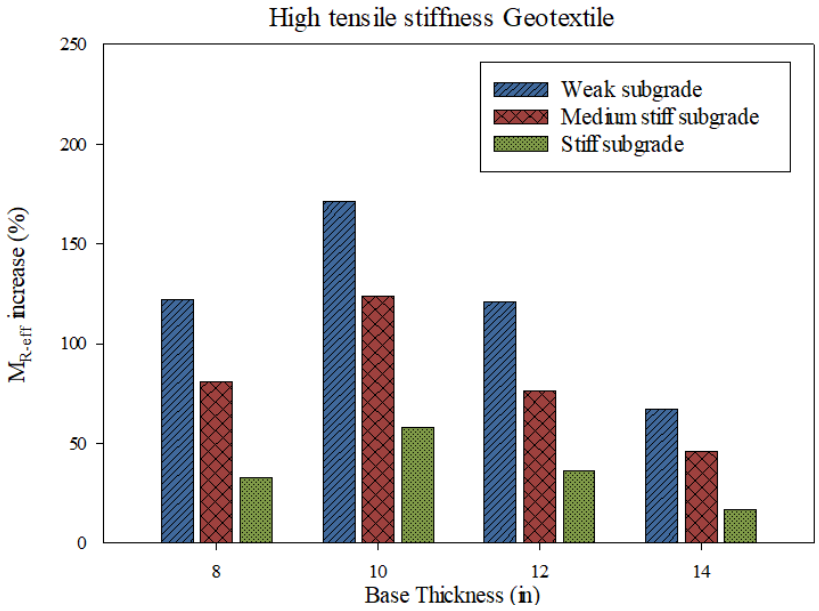

The comparison between the geogrid and geotextile reinforced cases shows that the sections reinforced with geogrids always have higher $M_{R\text{-}eff}$ values than those reinforced with geotextiles. The maximum $M_{R\text{-}eff}$ value at 0.75 in. rutting target for pavements on a weak subgrade using high tensile stiffness geosynthetics increases from 171% to 192% by changing the geosynthetic type from geotextile to geogrid for low volume roads; see Figure 52. Additionally, for the same pavement section with medium and low tensile stiffness geosynthetics, the maximum value of $M_{R\text{-}eff}$ increases from 130% to 179% and from 106% to 126% by changing the geosynthetic type from geotextile to geogrid, respectively.

For the pavement sections on medium stiff subgrade soil and 0.75 in. rutting target, the maximum value of $M_{R\text{-}eff}$ also increases by changing the geosynthetic type from geotextile to geogrid. For low volume roads, these changes range from 127% to 173% for high tensile stiffness geosynthetics, from 116% to 158% for medium tensile stiffness geosynthetics, and from 70% to 104% for low stiffness geosynthetics.

Figure 52. Changes in $M_{R\text{-}eff}$ for pavement sections reinforced with high tensile modulus of geogrids and geotextiles on weak subgrades on low volume roads

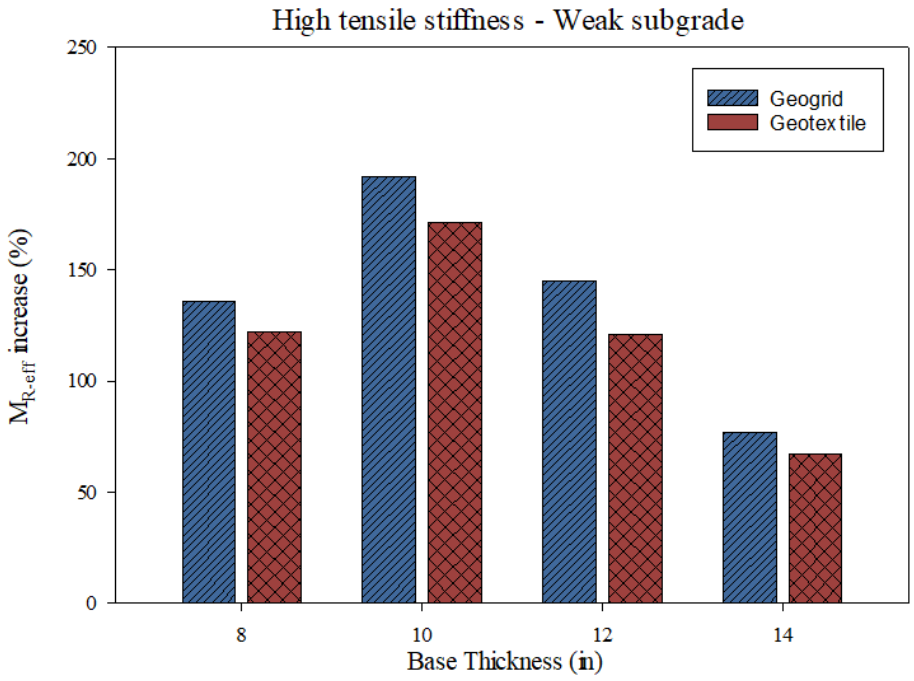

The change in $M_{R\text{-}eff}$ values due to a change in geosynthetic type for pavements on stiff subgrade also follows similar trends. The maximum increase in $M_{R\text{-}eff}$ values by changing the geosynthetic type from geotextile to geogrid for low volume roads ranges from 52% to 67% for high tensile stiffness geosynthetics, from 48% to 61% for medium tensile stiffness geosynthetics, and from 31% to 42% for low stiffness geosynthetics.

The effect of the geosynthetic tensile modulus on $M_{R\text{-}eff}$ is evaluated in this section. For the geotextile reinforced cases, the change in geotextile tensile modulus from low to high at 0.75 in. rutting for pavements on weak subgrade results in increasing the maximum $M_{R\text{-}eff}$ value from 106% to 171%; see Figure 53. For the same pavement sections on medium stiff and stiff subgrades, the maximum value of $M_{R\text{-}eff}$ increases from 70% to 127% and from 31% to 52%, by changing the geotextile tensile modulus from low to high, respectively. However, for the geogrid reinforced pavement cases, the change in geogrid tensile modulus from low to high at 0.75 in. rutting for pavements on weak subgrade results in increasing the maximum $M_{R\text{-}eff}$ value from 126% to 192%. For the same pavement sections on medium stiff and stiff subgrades, the value of $M_{R\text{-}eff}$ increases from 104% to 173% and from 42% to 67% by changing the geogrid tensile modulus from low to high, respectively.

Figure 53. Changes in $M_{R\text{-}eff}$ increase of pavement reinforced with geotextile on weak subgrade for different geosynthetic stiffnesses on low volume roads

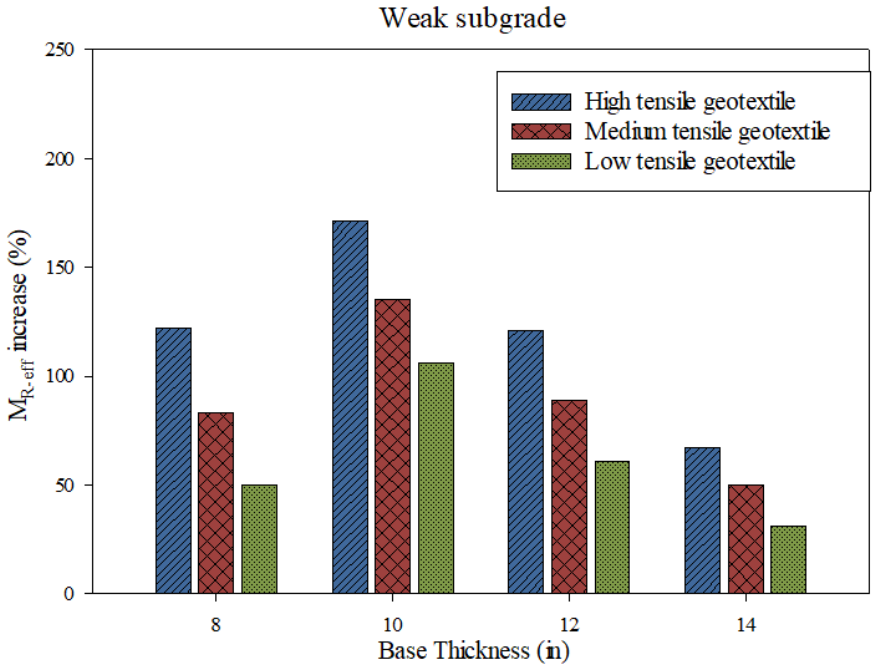

Equivalent Base Thickness (EBT)

Another approach to quantifying the structural benefits of geosynthetic reinforcement in flexible pavements is by evaluating the equivalent base thickness (EBT), which refers to the increase in base course thickness that is equivalent to geosynthetic reinforcement. In this method, the number of loadings, in terms of ESALs, of the reinforced section (i.e., service life) without changing the resilient modulus of base layer (M_R) is assumed to be equal to that of the corresponding unreinforced section. The structural benefits of geosynthetics are presented in terms of equivalent base thickness (EBT), which is defined as the thickness added to the base thickness for the unreinforced section of the same service life as the reinforced section. The values for all EBT derived in this study for low, medium, and high volume traffic roads are provided in tables in Appendix C. Note that the values of EBT presented in these tables were selected to ensure that the base aggregate layer thickness for the geosynthetic reinforced sections is at least 6 in. The remaining benefits for some pavement sections will be transferred to extend the service life of the pavement.

The subgrade stiffness has an important effect on the derived EBT values. For geogrid reinforcement on low volume roads, the EBT for geogrids with high tensile stiffness cases at 0.75 in. rutting varies from 6.7 in. at 12 in. base thickness for a weak subgrade to 3.4 in. at 8

in. base thickness for a stiff subgrade; see Figure 54. By altering the subgrade stiffness from weak to stiff, the EBT values exhibit a change from 6.7 in. to 5.4 in. for a 12 in. base thickness and high stiffness geogrid. For geotextile reinforcement, the results show similar trends in EBT. For high tensile geotextiles, the EBT values at 0.75 in. rutting varies from 6.1 in. at 12 in. base thickness for a weak subgrade soil to 2.8 in. at 8 in. base thickness for a stiff subgrade. For geotextile reinforcement, by altering the subgrade stiffness from weak to stiff, the EBT values show a change from 6.1 in. to 4.6 in. for a 12 in. base thickness and high stiffness geotextile.

Figure 54. Changes in EBT of pavement reinforced with high tensile stiffness geogrid for different subgrade conditions and different base thicknesses

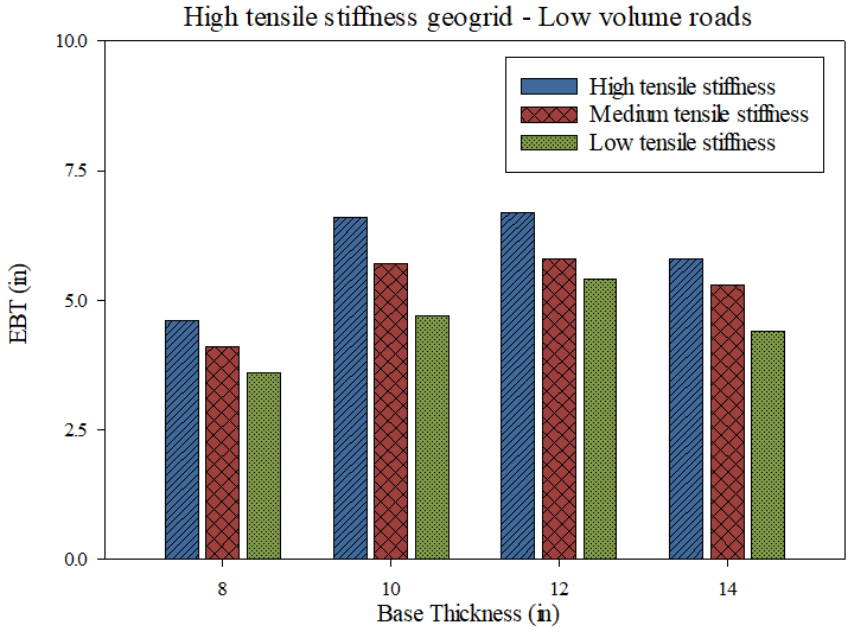

The comparison of EBT values between the geogrid and geotextile reinforcements shows that the geogrids have higher EBT values than geotextiles. The value of EBT at 0.75 in. rutting for pavements on a weak subgrade for high tensile stiffness geogrid varies from 6.7 in. to 3.4 in., while for geotextile reinforcement, it varies from 6.1 in. to 2.8 in. for different base thicknesses, showing up to a 20% decrease in EBT values; see Figure 55. For the 12 in. base thickness, the EBT value at 0.75 in. EBT changed from 6.7 in. for geogrid to 6.1 in. for geotextile, approximately a 10% decrease.

Figure 55. Changes in EBT of pavement reinforced with high tensile stiffness geogrids and geotextiles on a weak subgrade for different base thicknesses

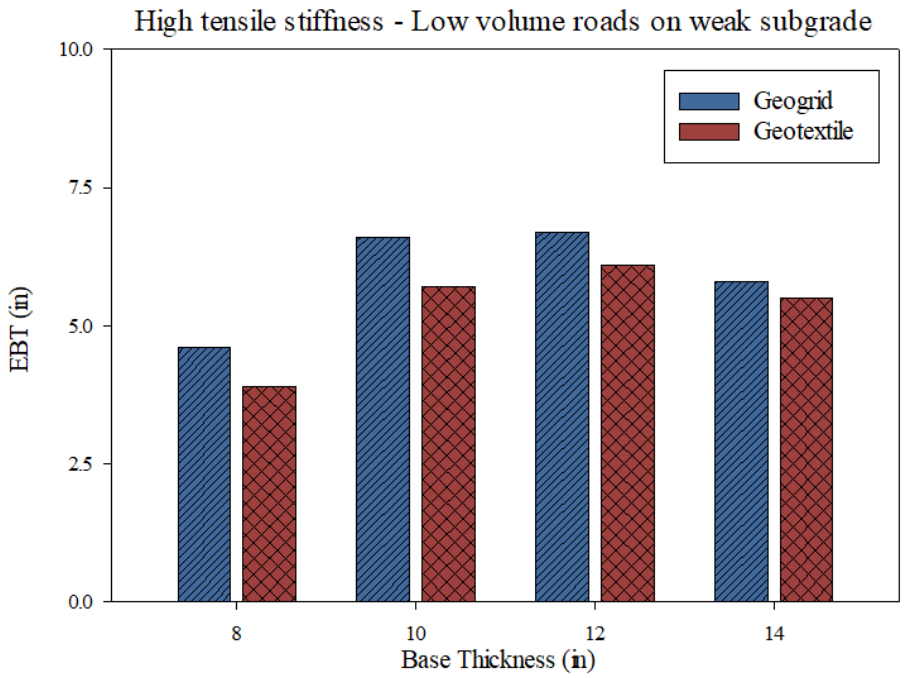

The results of this study demonstrated the importance of the geosynthetic tensile modulus on the EBT value. For geogrid reinforced cases, the EBT values at 0.75 in. rutting for different tensile modulus cases, varies from 6.7 in. to 3.7 in. for a weak subgrade and different base thicknesses, and it varies from 6.1 in. to 3.1 in. for a stiff subgrade and different base thicknesses. The value of EBT at 0.75 in. rutting for pavements on weak subgrade and 12 in. base thickness changes from 6.7 in. to 5.6 in. for low volume roads by changing the geogrid stiffness from high to low, showing an approximate 20% decrease in EBT value; see Figure 56. Meanwhile, the derived EBT values for the geotextile reinforced cases show the same trend as geogrid reinforcement. The EBT values for the geotextile tensile modulus cases for the same condition varies from 6.1 in. to 3.1 in. for different base thicknesses, while it varies from 4.6 in. to 2.5 in. for stiff subgrade and different base thicknesses. The EBT value at 0.75 in. rutting for pavements on a weak subgrade and 12 in. base thickness for low volume roads changes from 6.1 in. to 5.1 in. by changing the geogrid stiffness from high to low, showing an approximate 23% decrease in EBT value.

Figure 56. Changes in EBT of pavement reinforced with geotextile on a weak subgrade for different geosynthetic stiffnesses

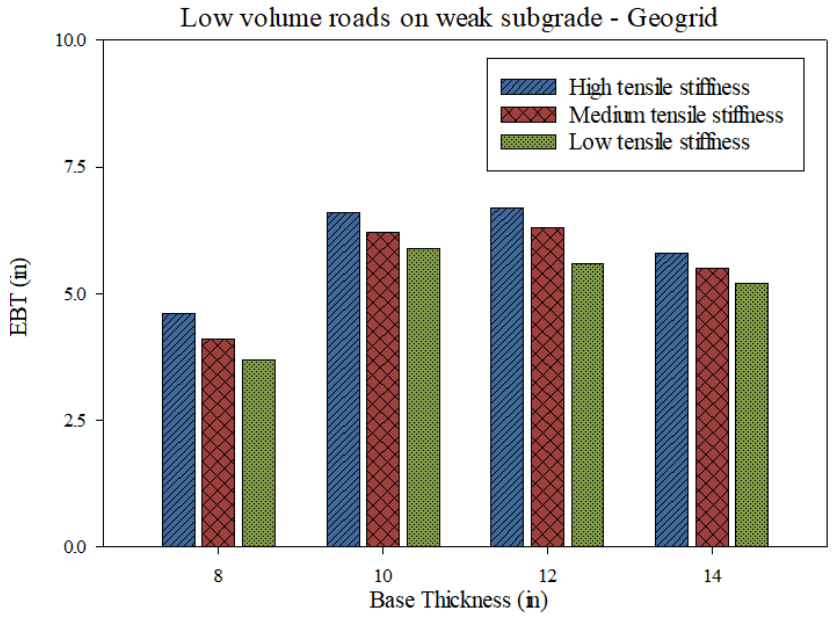

The results of this study also show the effect of road traffic volume (i.e., change in AC thickness) on the EBT values. For geogrid reinforced pavements, the EBT values for sections on a medium stiff subgrade and a medium geogrid tensile modulus vary from 5.5 in. to 2.8 in. for different base thicknesses. The value of EBT at 0.75 in. rutting for the 12 in. base thickness changes from 5.5 in. to 3.4 in. by changing the road traffic volume from low (i.e., 3.5 in. AC thickness) to high (i.e., 10 in. AC thickness), showing an approximate 62% decrease in EBT value; see Figure 57. Additionally, the derived EBT values for the geotextile-reinforced pavements show the same trend as geogrid reinforcement by changing the road traffic volume. The EBT values for sections on a medium stiff subgrade and a medium geotextile tensile modulus vary from 4.8 in. to 2.4 in. for different base thicknesses. The EBT value at 0.75 in. rutting for the sections on a medium stiff subgrade and a medium geotextile tensile modulus for 12 in. base thickness change from 4.8 in. to 2.8 in. by changing the road traffic volume from low to high, showing an approximate 71% decrease.

Figure 57. Changes in EBT of pavement reinforced with geotextile on a weak subgrade for different volume roads

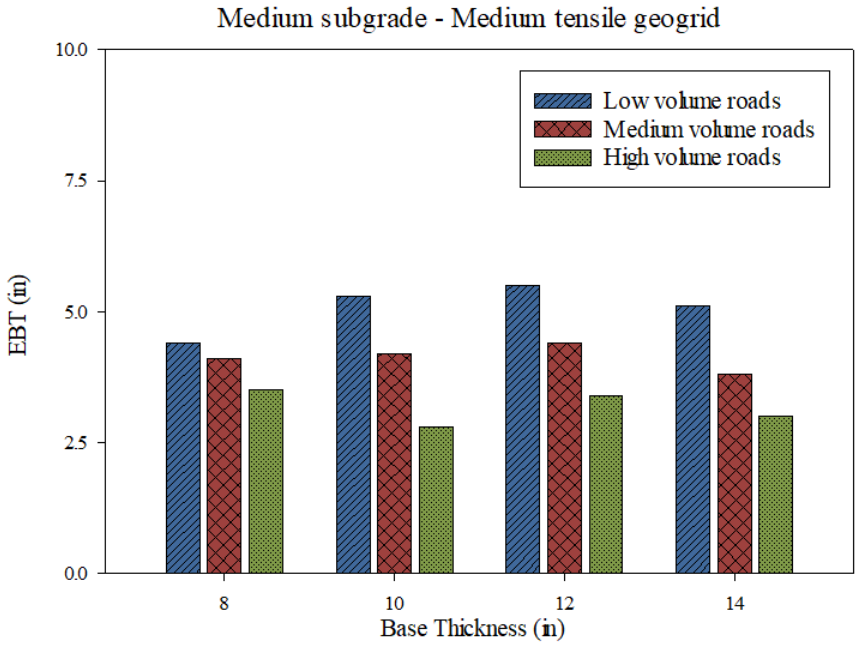

Rutting Reduction Coefficients (α_b or α_s)

In this section, the outcomes derived from the performed FE comprehensive study encompassing multiple cases of pavement structures reinforced/stabilized by geosynthetic were used to evaluate the rutting reduction factors, denoted as α_b and α_s. These are crucial components in modified rutting Equation 36 for both the base course (α_b) and subgrade (α_s) layers in a geosynthetic reinforced pavement design. The results (α_b and α_s) obtained from all geosynthetic reinforced pavement sections are presented in Appendix D as tables and graphs.

$$\Delta_{base/subgrade} = \left(\frac{\alpha_b}{\alpha_s}\right).\beta_{s1}.k_{s1}.\varepsilon_v h_{soil}.\left(\frac{\varepsilon_0}{\varepsilon_r}\right)e^{-\left(\frac{\rho}{N}\right)^{\beta}} \quad (36)$$

The results show that the values of base reduction factor α_b for different pavement sections are approximately 6% higher on average than the values for subgrade reduction factor α_s for the same section, implying that the benefits (i.e., higher reduction in rutting) are higher for the subgrade than the base. This difference highlights the greater advantages of using geosynthetics to stabilize the subgrade, as indicated by the lower α_s values. The range of

values for α_b for the base layer was found to span from 0.84 to 0.98, indicating the variability observed within different pavement sections. However, the reduction factor of α_s for the subgrade layer exhibited a range of values spanning from 0.72 to 0.95 across the various sections under consideration.

By increasing the thickness of the base course layer, a consistent trend emerges, wherein the values for α_b and α_s show an increase (i.e., a decrease in geosynthetic benefits) with the increase of base thickness. This outcome can be attributed to the reduction in induced stress levels caused by wheel loading on top of the subgrade layer, as well as the lower average stress experienced by the base course layer. Further, an inverse relationship is observed when the stiffness of geosynthetics is heightened. In this case, the values for α_b and α_s decrease (i.e., the benefits of geosynthetic increase) with the increase of geosynthetic stiffness. This pattern can be attributed to the ability of geosynthetics with higher stiffness to absorb a greater amount of stress induced within the pavement structure. Transitioning from low to medium geosynthetic stiffness, and subsequently from medium to high stiffness, results in a decrease of approximately 1% and 2% in the values for α_b and α_s, respectively; see Figure 58.

The results also indicate that geogrids exhibit an average of 3% lower α_b and α_s values compared to geotextiles, thus providing greater benefits. This discrepancy is due to the interlocking mechanism between the geogrid aperture and the base aggregate particles; see Figure 59.

The results show that increasing the stiffness of the subgrade layer leads to an increase in the values for α_b and α_s (i.e., a decrease in the benefits of geosynthetics). Transitioning from low to medium subgrade stiffness results in an average decrease of 1% and 4% in the values for α_b and α_s, respectively. Likewise, transitioning from medium to high subgrade stiffness leads to a decrease of approximately 1% and 2% in the values for α_b and α_s, respectively; see Figure 60.

When employing geosynthetics to reinforce flexible pavements in low volume traffic roads (i.e., those with lower asphalt thickness), the resulting α_b and α_s values are lower compared to medium and high volume traffic roads that have higher asphalt thicknesses, indicating higher geosynthetic benefits. The lower values of α_b and α_s in low volume roads can be attributed to the higher level of induced stresses at the base/subgrade interface, resulting in greater mobilization and stress absorption by the geosynthetic layer. Specifically, the values of α_b and α_s for low volume traffic roads are 2% higher than those for medium volume

traffic roads, while the values for medium volume traffic roads are 3% and 4% lower than those for high volume traffic roads; see Figure 61.

Figure 58. Values of α_b and α_s for geogrid reinforced medium traffic volume road on a weak subgrade for: (a) subgrade α_s; (b) base α_b

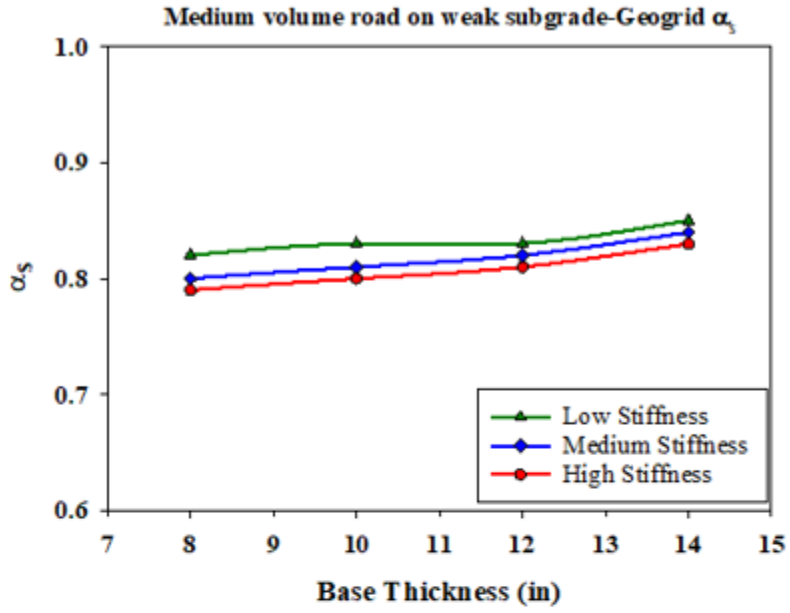

(a)

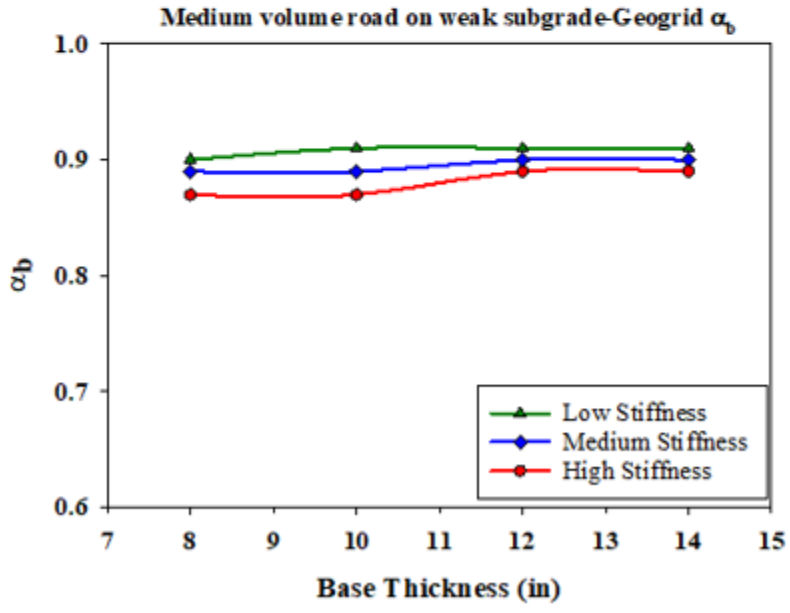

(b)

Figure 59. Values of α_s for medium traffic volume road on a weak subgrade: (a) geogrid; (b) geotextile

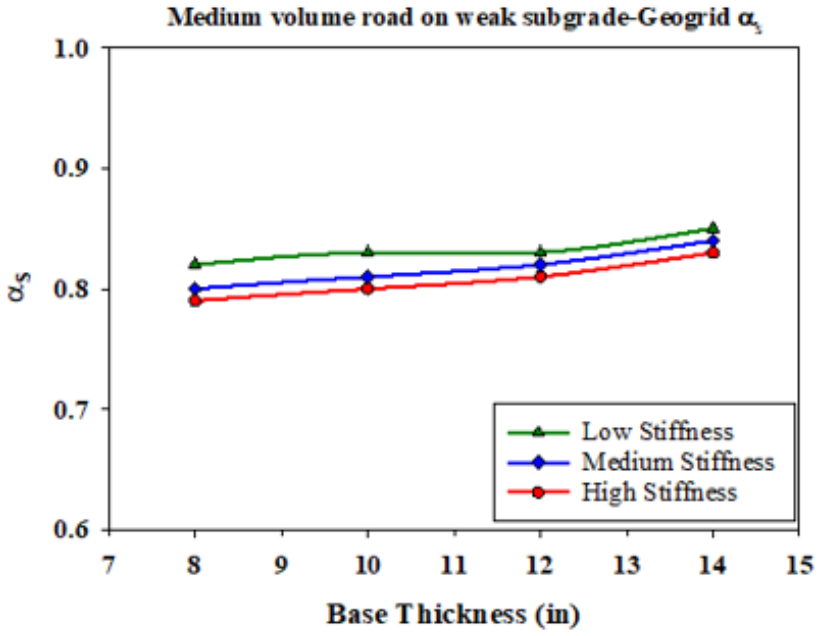

(a)

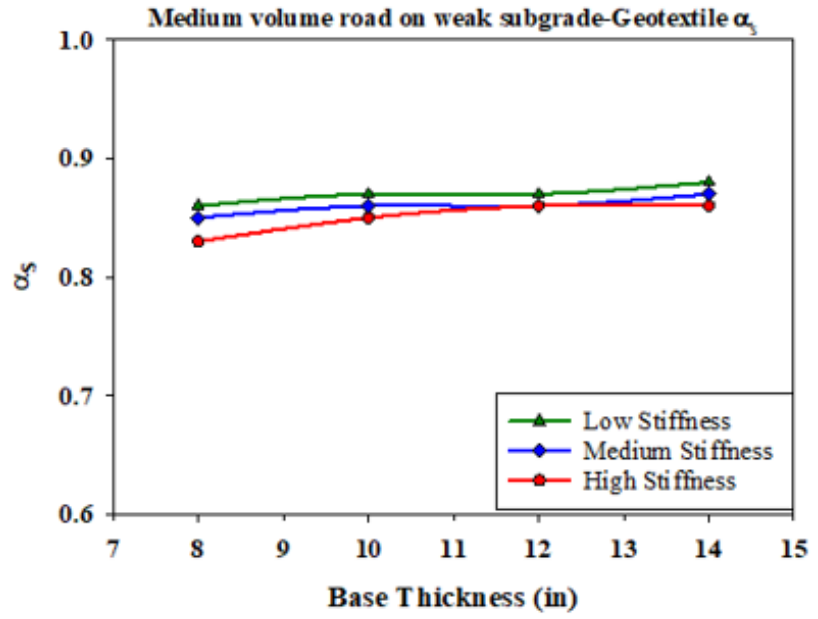

(b)

Figure 60. Values of α_s and α_b for geogrid reinforced medium traffic volume road on: (a) and (c) weak subgrade; (b) and (d) stiff subgrade

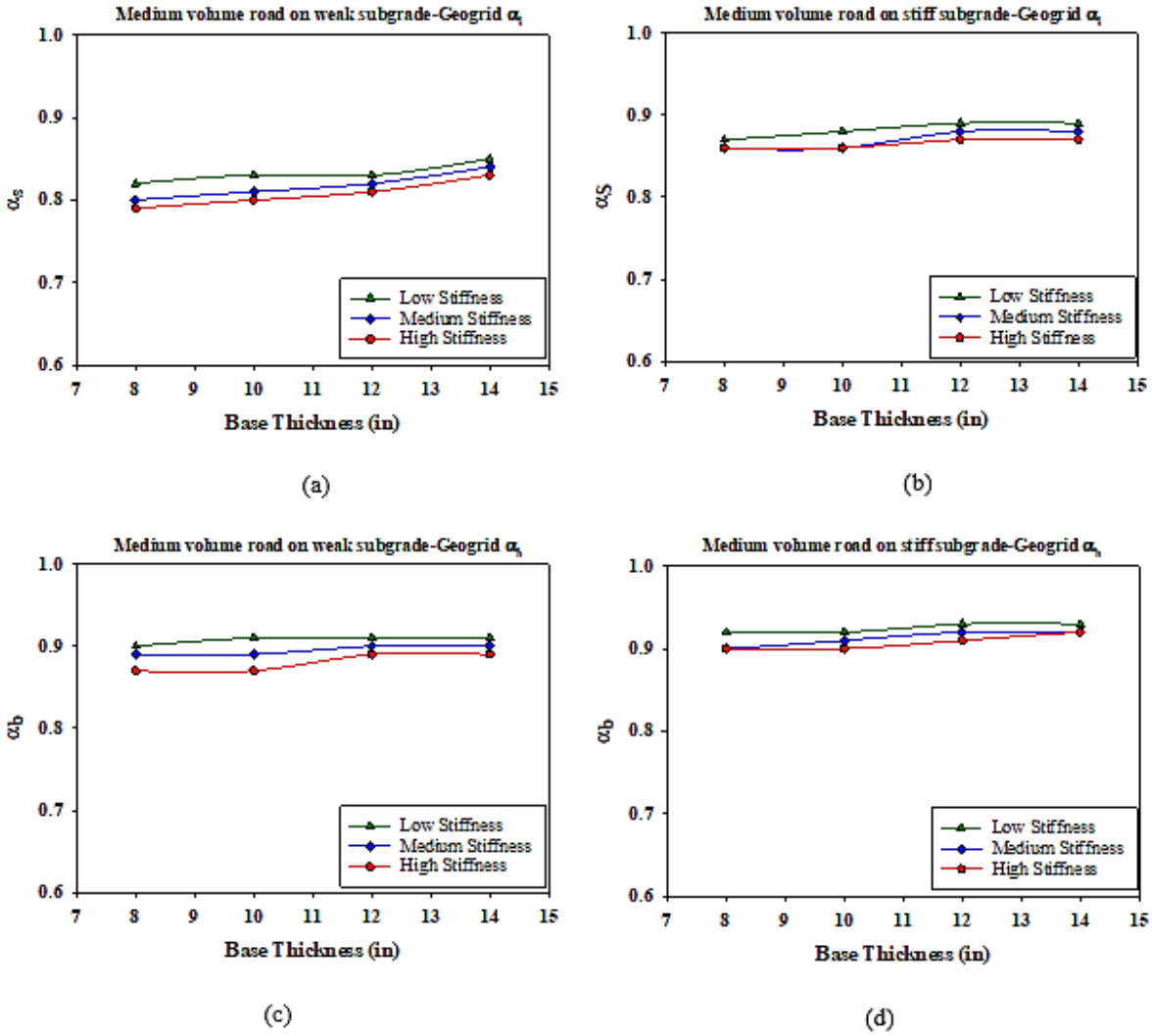

Figure 61. Values of α_s and α_b for geogrid reinforced pavement on a weak subgrade for: (a) and (c) low traffic volume road; (b) and (d) high traffic volume road

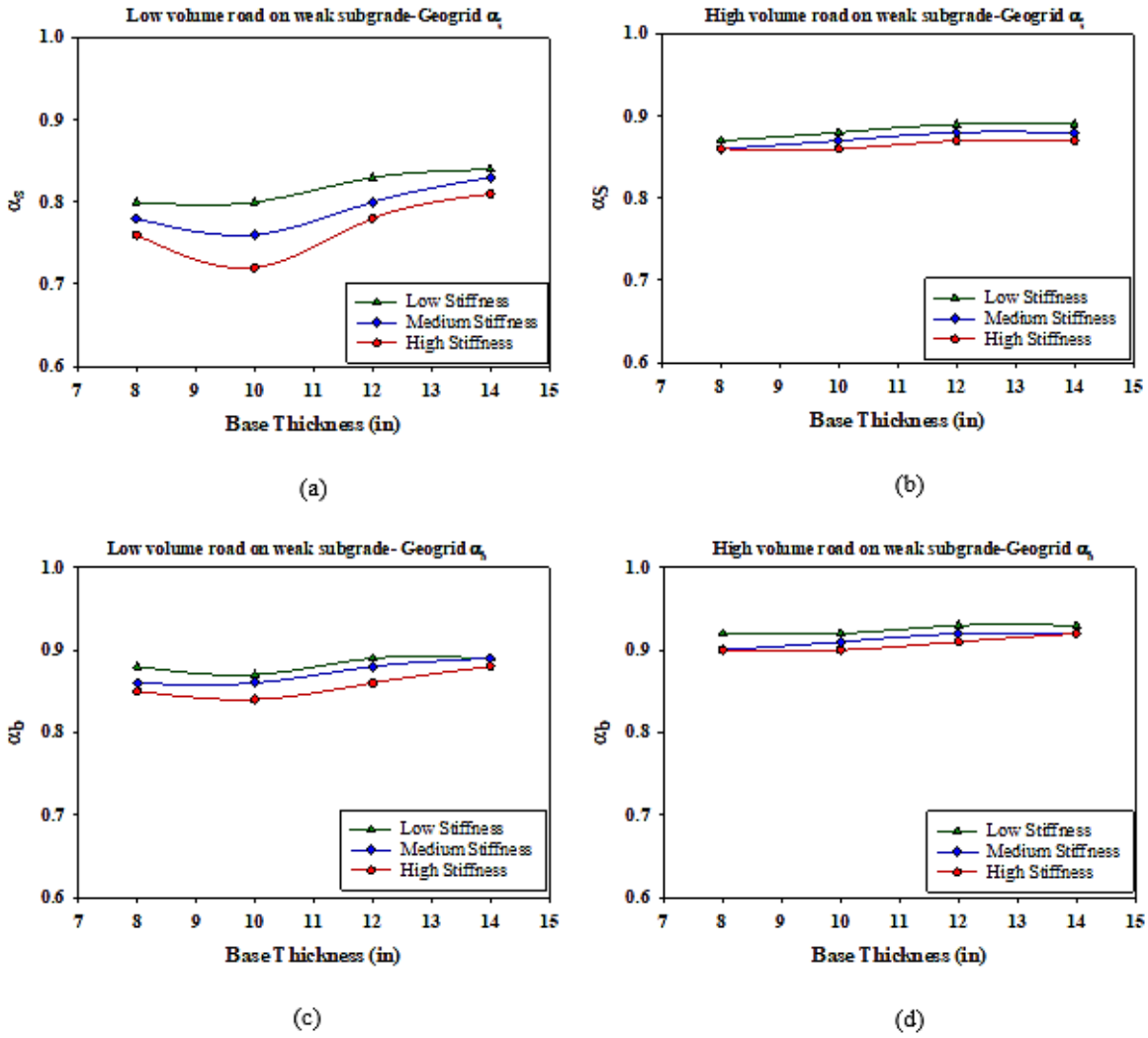

Development of Prediction Models

Introduction

Computational prediction models have revolutionized the way we approach complex problems in various fields, ranging from engineering to finance, climate change, and artificial intelligence. These models use advanced mathematical algorithms, statistical methods, and machine learning (ML) techniques to analyze and predict the behavior of complex systems, processes, and phenomena. Computational prediction models can offer useful insights and assist in making well-informed decisions that can result in better outcomes by modeling real-world events and forecasting the effects of various variables and inputs.

One of the primary benefits of computational prediction models is their ability to process large volumes of data and identify patterns, trends, and relationships that would be difficult, if not impossible, to detect through manual analysis. This makes them particularly useful in many fields, including geotechnical engineering. The use of computational prediction models is anticipated to grow increasingly popular as computing power and data availability continue to rise, completely altering how researchers tackle difficult issues and reach conclusions.

In this study, Google Colab was utilized to develop regression models and employ ML techniques to establish correlations between the different variables and parameters in the collected dataset from the FE parametric study. Google Colab, short for Google Colaboratory, is a cloud-based platform that has become a valuable resource for data scientists, researchers, and developers. It offers a free and easily accessible environment for creating, sharing, and running Python codes, particularly for ML and advanced data analysis tasks. What sets Google Colab apart is its integration with Google Drive, allowing users to store and access notebooks seamlessly. With pre-installed libraries and access to powerful Graphics Processing Unit (GPU) and Tensor Processing Unit (TPU) resources, it enables users to perform resource-intensive computations and train ML models without the need for high end hardware. Overall, Google Colab has access to high performance computing resources and has become an indispensable tool in the toolkit of many data professionals.

Datasets Introduction and Pre-Processing

The datasets utilized to develop prediction models in this study are described and explored in this section. All datasets are generated using the results obtained from the FE-ME proposed

method in the previous chapters and presented as tables in Appendices A to D. The datasets include various independent variables that influence the dependent variable. Each independent variable underwent a procedure known as feature scaling or feature normalization. Feature scaling, specifically between 0 and 1, is a data pre-processing technique in ML that rescales the values of a feature or variable to a range between 0 and 1. This normalization ensures that all values fall within a uniform and standardized interval, making it easier for ML algorithms to process the data effectively.

Several prediction models were developed in this study to quantify the benefits of geosynthetic reinforcement of flexible pavement structure in terms of TBR, $M_{R\text{-}eff}$, EBT, and rutting reduction coefficients, α_b and α_s. Six types of regression and ML models were developed to estimate the values for each of the stated geosynthetic benefits from sets of independent variables.

For the TBR, $M_{R\text{-}eff,}$ and EBT models, the datasets include seven independent variables and one dependent variable. To eliminate scale factors, all independent variables are scaled between 0 and 1. The independent variables are:

- Asphalt thickness, which is scaled between 0 and 1 based on the maximum thickness of asphalt layer in this study, which is 10 in. The scaled asphalt thickness values for the low, medium, and high traffic volume roads are 0.35, 0.65, and 1, respectively.
- Base thickness, which is scaled between 0 and 1 based on the maximum thickness of base layer in this study, which is 14 in. The scaled asphalt thickness values for the 8, 10, 12, and 14 in. thicknesses are 0.5714, 0.7142, 0.8571, and 1, respectively.
- Geosynthetic stiffness, which is scaled between 0 and 1 based on the maximum geosynthetic stiffness in this study, which is 182.7 ksi. The scaled asphalt thickness values for the 62.4, 134.6, and 182.7 ksi stiffnesses are 0.3415, 0.7367, and 1, respectively.
- Subgrade stiffness, which is scaled between 0 and 1 based on the maximum subgrade stiffness in this study, which is 4612 psi. The scaled asphalt thickness values for the 1070, 2775, and 4612 psi stiffnesses are 0.2320, 0.6017, and 1, respectively.
- Rutting target, which is already between 0 and 1 (0.5, 0.75, and 1 in.).
- Geogrid, which is 1 in the case of geogrid reinforcement; otherwise it is equal to 0.
- Geotextile, which is 1 in the case of geotextile reinforcement; otherwise it is equal to 0.

For the α_b and α_s prediction models, the independent variables are the same, with the exception of the rutting target. α_b and α_s are being derived as a proportion of rutting curves, so they are independent of rutting targets.

The number of dataset instances for TBR, $M_{R\text{-}eff,}$ and EBT models is 648, and for α_b and α_s it is 216. To ensure the reliability of the prediction models, the datasets underwent a shuffling process, followed by a random split into two subsets: one dedicated to testing, comprising 20% of the data, and the other to training, encompassing 80% of the dataset. This division was expertly executed through the utilization of the train_test_split function from the sklearn_model_selection module in Python.

Datasets Correlation

The correlation and visualization of datasets are essential components of the data analysis process. Valuable insights into the underlying patterns and trends can be gained by examining relationships and dependencies among various data points. Visualization plays a key role in this process, as it permits complex data to be represented in a comprehensible manner. The manner in which different variables interact with each other can be visually assessed through charts, graphs, and plots. The identification of outliers, clusters, and trends that may not be immediately apparent in raw data is facilitated by these visual representations.

Figure 62 presents the visually informative depiction in the form of a color-coded correlation graph for TBR that eloquently illustrates the intricate interconnections among the various attributes contained within the dataset. This graphical representation serves as a powerful tool for delving into the complex web of relationships that exist between the individual independent variables, offering a nuanced understanding of how they influence one another. All color-coded correlation graphs of TBR, $M_{R\text{-}eff}$, EBT, α_b and α_s datasets are presented in Appendix E.

The color-coded correlations plot among different attributes in TBR dataset shows significant information about the dataset. Initially, it is evident that the correlation between independent attributes is 0, except for the relationship between geogrid and geotextile, which is -1, signifying that when geogrid is present, geotextile is absent, and vice versa. The figure shows the relation between TBR and independent variables. According to the correlation values, the maximum absolute correlation is observed between subgrade stiffness and TBR, with a value of 0.44, followed by base thickness and rutting target with values of 0.37 and 0.3, respectively.

Figure 62. Colored correlation graph between attributes for TBR dataset

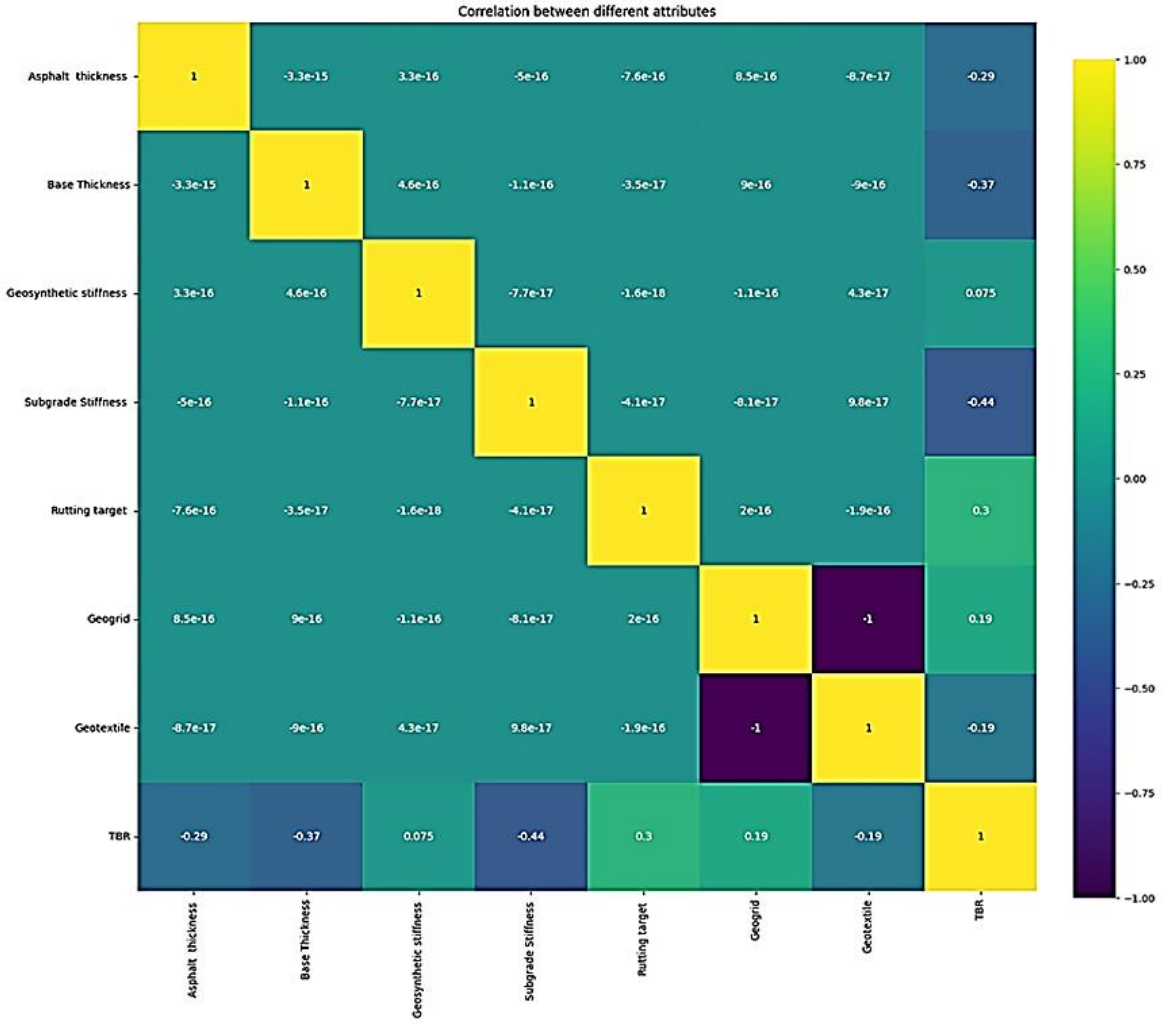

Evaluation Accuracy

The effectiveness of regression and ML models depends on the evaluation method, which can aid in the discovery of the best algorithm for use. Each dataset in this study underwent k-fold cross-validation for evaluation and validation. In this study, the performance of the utilized model was assessed using the coefficient of determination (R^2), Root Mean Square Error (RMSE), and Mean Absolute Error (MAE), in accordance with the literature. The following equations describe these parameters:

$$R^2 = \frac{\sum(\hat{y}_i - \bar{y})^2}{\sum(y_i - \bar{y})^2} \tag{37}$$

$$RMSE = \sqrt{\frac{\sum(\hat{y}_i - \bar{y})^2}{n}} \tag{38}$$

$$MAE = \frac{1}{n}\sum|\hat{y}_i - \bar{y}| \tag{39}$$

where,
n is the number of data;
$\hat{y}$ is the prediction value;
$\bar{y}$ is the mean of all values; and
y_i is the actual value, respectively.

Tuning of Hyperparameters

The majority of ML algorithms have a collection of parameters that express higher-level model features, which influence many elements of the algorithm's behavior. These variables are referred to as hyperparameters. Prior to starting the learning process, hyperparameters need to be fixed. By adjusting these hyperparameters, the model's performance and its capacity to forecast accurate estimates when used with new inputs (i.e., unseen or future data) can be enhanced. Approaches such as grid search and random search are frequently used to alter hyperparameters. These methods take several hyperparameter combinations into account iteratively to optimize the model's performance. Unlike random search, which only considers a small number of combinations, grid search considers every conceivable combination.

For each ML technique employed in this study, a grid search was first conducted to identify the optimal hyperparameters. This grid search was executed on the training sets using a five-fold cross-validation process. Subsequently, the determined set of hyperparameters was applied to predict the unseen data within the testing set for each respective model. For the Decision Tree algorithm, the optimal hyperparameters for each geosynthetic benefit are presented in Table 8. The tuned hyperparameters for all models and benefits are presented as Tables F-1 to F-4 in Appendix F.

Table 8: Tuned hyperparameters for the Decision Tree (DT) algorithm

	max_depth	max_features	min_samples_leaf	min_samples_split
TBR	None	auto	2	2
$M_{R\text{-}eff}$	None	auto	1	2
EBT	10	auto	1	2
α_b	30	auto	1	2
α_s	30	auto	1	2

Evaluation Models

As stated earlier, TBR, $M_{R\text{-}eff}$, and EBT values are influenced by different variables, such as base thickness, geosynthetic type, geosynthetic stiffness, subgrade stiffness, and rutting target. The calculated coefficients for Multiple Linear Regression (MLR) and Multivariate Exponential Regression (MER) are presented in Appendix G in Table G-1 and Table G-2.

The performance metrics of various prediction models, including Multiple Linear Regression (MLR), Multivariate Exponential Regression (MER), Decision Tree (DT), Random Forest (RF), Support Vector Machine (SVM), and Gradient Boosting (GB), were assessed in terms of their ability to predict the geosynthetic benefits in terms of Traffic Benefit Ratio (TBR); see Table 9. In terms of R^2, which measures the goodness of fit, the DT model achieved a perfect score of 1 on the training data, indicating an ideal fit, while the GB model closely followed with an R^2 of 0.998. On the test data, RF and GB outperformed the other ML models with R^2 values of 0.844 and 0.974, respectively, signifying their strong predictive capabilities. When considering RMSE, a lower value indicates better model performance. Using this method, the DT recorded an RMSE of 0 on the training data, which could be an indication of overfitting. By contrast, RF had the lowest RMSE of 0.204 on the test data, showcasing its superior predictive accuracy. The MAE values, which measure the average absolute differences between predicted and actual values, showed that the GB model exhibited the lowest MAE of 0.112 on the test data, emphasizing its ability to provide precise predictions.

Table 9. Performance metrics of different TBR prediction models

			Prediction Model					
			MLR	**MER**	**DT**	**RF**	**SVM**	**GB**
Performance Metrics of TBR	R^2	Train	0.550	0.589	1	0.977	0.797	0.998
		Test	0.508	0.569	0.603	0.844	0.688	0.974
	RMSE	Train	0.363	0.331	0	0.018	0.163	0.001
		Test	0.648	0.567	0.523	0.204	0.410	0.033
	MAE	Train	0.409	0.380	0	0.083	0.213	0.023
		Test	0.482	0.448	0.434	0.257	0.306	0.112

In terms of R^2, the GB model achieved the highest value of 0.974 on the testing set; see Figure 63. This was closely followed by RF with an R^2 of 0.844, indicating its strong predictive capabilities. In terms of RMSE, the RF model exhibited the lowest value of 0.204 on the testing set, emphasizing its superior predictive accuracy. The MAE values demonstrated that the GB model has the lowest value of 0.112 on the testing set, showcasing its ability to provide precise predictions.

Figure 63. Predicted and actual values of TBR using trained GB model on testing set

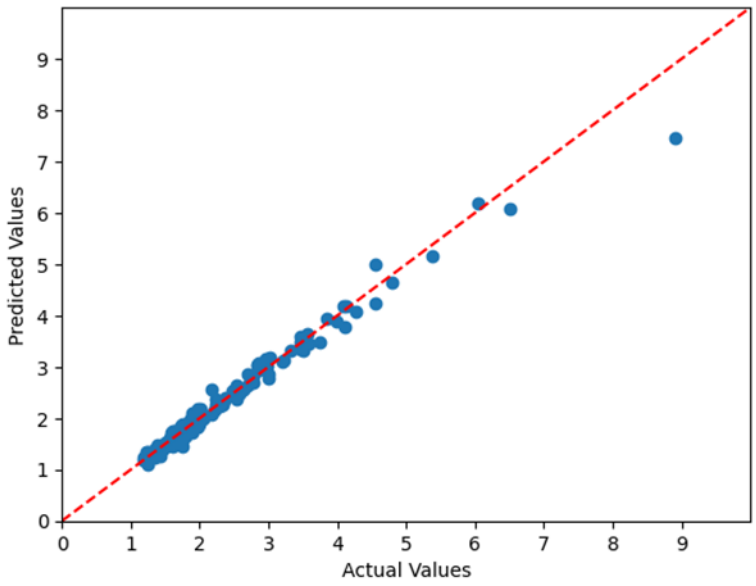

The performance metrics of various prediction models, including MLR, MER, DT, RF, SVM, and GB, were assessed in terms of their ability to predict the geosynthetic benefits in terms of the effective resilient modulus ($M_{R\text{-}eff}$) of the base layer; see Table 10. In the training set, the DT and GB achieved perfect R^2 values of 1.0 and 0.993, respectively, indicating a strong fit to the training data. The RF also performed well with an R^2 of 0.985. When assessing the RMSE and MAE criteria, the DT exhibited the lowest values among all ML models in the

training set, highlighting its ability to provide accurate predictions with minimal errors. The negative R^2 values observed in the MER model indicate its poor performance, failing to explain the variance in the data effectively.

Table 10. Performance metrics of different $M_{R\text{-}eff}$ prediction models

			Prediction Model					
			MLR	**MER**	**DT**	**RF**	**SVM**	**GB**
Performance Metrics of $M_{R\text{-}eff}$	R^2	Train	0.699	-1.454	1	0.985	0.839	0.993
		Test	0.723	-1.530	0.863	0.905	0.814	0.971
	RMSE	Train	894.7	7301.4	0	42.6	477.9	18.6
		Test	769.0	7041.1	379.2	262.5	517.1	79.3
	MAE	Train	21.6	65.7	0	4.0	12.1	3.2
		Test	21.4	65.2	12.4	10.8	13.8	6.3

On the testing set, the GB model maintained high accuracy with an R^2 of 0.971, further emphasizing its predictive capabilities, followed by RF model with an R^2 of 0.905, indicating its robust generalization to unseen data; see Figure 64. In conclusion, while DT and GB models excelled on the training set, the GB and RF demonstrated superior generalization to the testing set, making them strong candidates for predicting $M_{R\text{-}eff}$.

Figure 64. Predicted and actual values of $M_{R\text{-}eff}$ using trained GB model on testing set

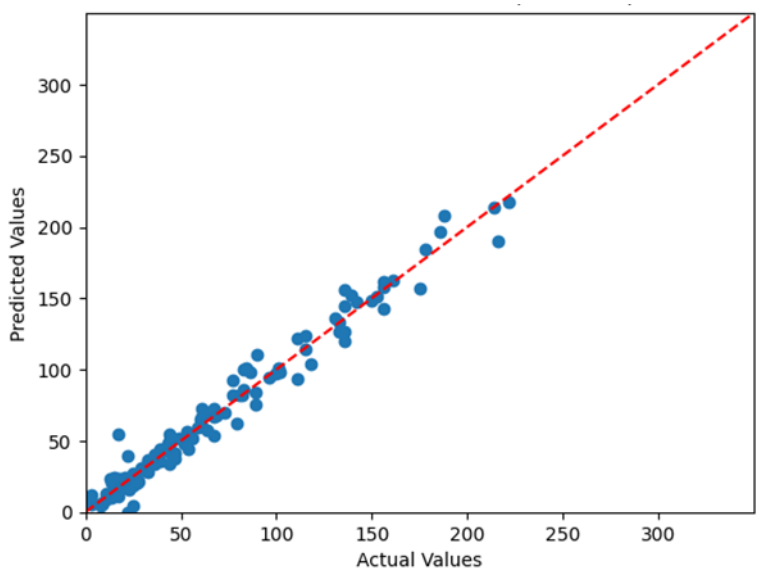

The performance metrics of various prediction models (e.g., MLR, MER, DT, RF, SVM, and GB) were assessed in terms of their ability to predict effective base thickness (EBT); see Table 11. The performance of various prediction models was evaluated on the training dataset for predicting the geosynthetic benefits in terms of Equivalent Base Thickness (EBT). Among the different ML models, the DT model achieved a perfect R^2 of 1.0, indicating an excellent fit to the training data. This was followed closely by the GB model with an R^2 of 0.993. The MLR model also showed good performance with an R^2 of 0.708. However, the MER model had a negative R^2, suggesting that it performed poorly on the training data.

Table 11. Performance metrics of different EBT prediction models

			Prediction Model					
			MLR	**MER**	**DT**	**RF**	**SVM**	**GB**
Performance Metrics of EBT	R^2	Train	0.708	-5.320	1	0.989	0.839	0.993
		Test	0.665	-4.329	0.879	0.915	0.810	0.975
	RMSE	Train	1.160	25.153	0	0.041	0.636	0.026
		Test	1.788	28.497	0.645	0.452	1.013	0.132
	MAE	Train	0.826	4.601	0	0.150	0.657	0.122
		Test	0.985	4.811	0.586	0.439	0.764	0.271

For the testing dataset, a similar pattern emerges with some variations. The GB model outperforms the other ML models with R^2 of 0.975; see Figure 65. This is followed by the RF, which demonstrated its robustness on unseen data with an R^2 of 0.915. The DT model continued to perform well, maintaining an R^2 of 0.879. However, it is noted that the MER model, which struggled on the training data, also performed poorly on the testing set with a negative R^2 of -4.329, indicating a significant discrepancy between predicted and actual values. Overall, the models' performance on the testing set largely echoed their performance on the training data, with the GB and RF models being the top performers and the MER showing a substantial need for improvement.

Figure 65. Predicted and actual values of EBT using trained GB model on testing set

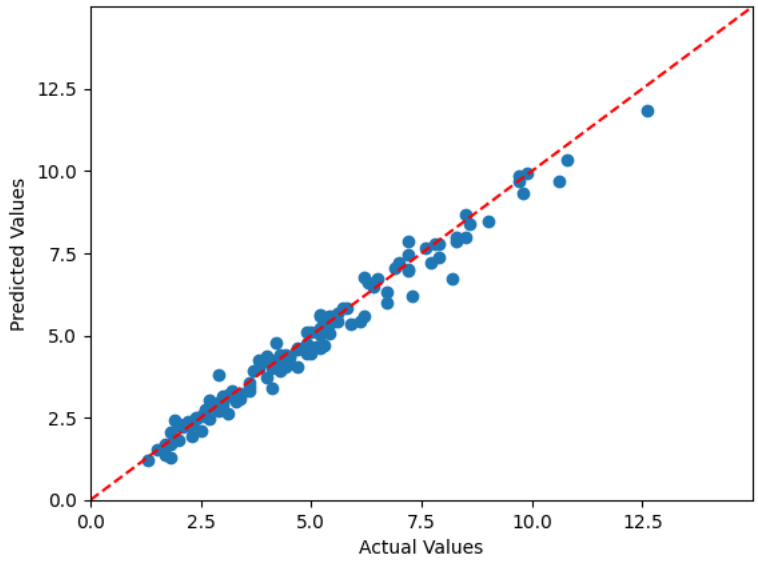

The performance metrics of various prediction models (e.g., MLR, MER, DT, RF, SVM, and GB) were assessed in terms of their ability to predict the rutting reduction coefficient for base (α_b); see Table 12. The results for training set for predicting α_b using various prediction models reveal remarkable performance. The DT and GB models demonstrated exceptional predictive power, achieving perfect R^2 values of 1.0 and 0.99, respectively. This suggests that both ML models fit the training data almost perfectly. The MLR and SVM models also displayed strong performance with R^2 values of 0.946 and 0.956, respectively. The MLR and SVM models exhibited minimal errors, with negligible MSE and MAE values.

Table 12. Performance metrics of different α_b prediction models

			Prediction Model					
			MLR	**MER**	**DT**	**RF**	**SVM**	**GB**
Performance Metrics of α_b	R^2	Train	0.946	0.946	1	0.994	0.956	0.990
		Test	0.946	0.947	0.933	0.963	0.944	0.975
	RMSE	Train	0	0	0	0	0	0
		Test	0	0	0	0	0	0.002
	MAE	Train	0.005	0.005	0	0.001	0.005	0
		Test	0.004	0.004	0.004	0.003	0.005	0.003

When assessing the models' performance on the testing set, consistent trends emerge with slight variations. The GB and RF models maintained their impressive performance, securing R^2 values of 0.975 and 0.963, respectively; see Figure 66. These models exhibited remarkable generalizations to unseen data. The SVM model demonstrated stability with an

R^2 of 0.944, while the MER model also maintained a high R^2 of 0.947. Despite slight increases in MSE and MAE for most models on the testing set, the overall performance remained impressive, highlighting the models' ability to generalize well.

Figure 66. Predicted and actual values of α_b using trained GB model on testing set

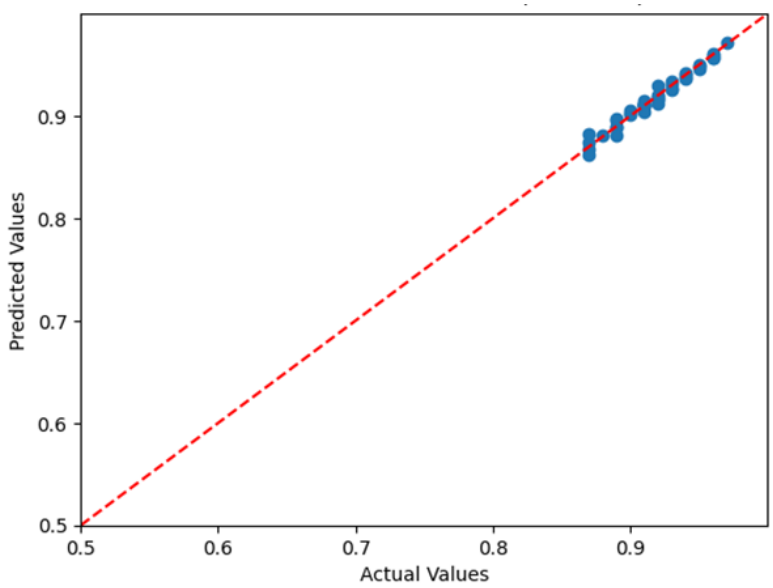

The performance metrics of various prediction models (e.g., MLR, MER, DT, RF, SVM, and GB) were assessed in terms of their ability to predict the rutting reduction coefficient for subgrade (α_s); see Table 13. The results show that the DT and GB models showcased remarkable predictive capabilities, achieving near-perfect R^2 values of 1.0 and 0.998, respectively. This indicates an exceptional fit to the training data by both ML models. Meanwhile, the RF and SVM models displayed robust performance, boasting R^2 values of 0.991 and 0.966, respectively. These models exhibited minimal errors, as evidenced by their negligible RMSE and MAE values.

Table 13. Performance metrics of different α_s prediction models

			Prediction Model					
			MLR	**MER**	**DT**	**RF**	**SVM**	**GB**
Performance Metrics of α_s	R^2	Train	0.741	0.883	1	0.991	0.966	0.998
		Test	0.878	0.880	0.920	0.952	0.920	0.963
	RMSE	Train	0	0	0	0	0	0
		Test	0	0	0	0.002	0	0
	MAE	Train	0.010	0.010	0	0	0.006	0.001
		Test	0.009	0.009	0.007	0.005	0.008	0.005

When evaluating the models' performance on the testing set, researchers observed consistent trends with slight variations. The GB and RF models sustained their impressive performance, achieving R^2 values of 0.963 and 0.952, respectively, indicating remarkable generalization capabilities to previously unseen data; see Figure 67. The SVM and DT models exhibited stability with an R^2 of 0.922, while the MER model also maintained a high R^2 of 0.88.

Figure 67. Predicted and actual values of α_s using trained GB model on testing set

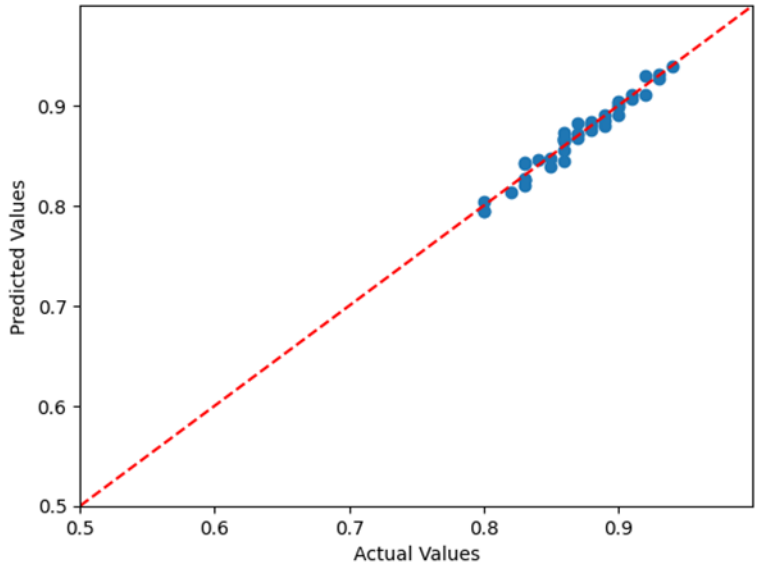

Comparison of Prediction Models

The comparison of R^2 values across six distinct regression and ML prediction models, both on the training and testing datasets, provides valuable insights into their respective performance; see Table 14.

Analyzing the training datasets across the various benefit indices reveals distinct model behaviors. In most cases, the DT ML model demonstrates exceptional training performance, achieving perfect R^2 values, indicating an outstanding fit to the data. However, the MER regression model occasionally struggles, with some benefit indices resulting in negative R^2 values during training, indicating potential limitations of the model in capturing underlying patterns. On the other hand, the GB ML model consistently excels across all benefit indices, with R^2 values close to 1.0, highlighting its strong predictive power. The SVM ML model and MLR regression model also exhibit robust training performance, consistently maintaining high R^2 values, indicating their effectiveness in modeling complex relationships.

Analyzing the testing datasets across the different benefit indices sheds light on the models' generalization abilities. The GB ML model consistently outperforms the other ML models, securing high R^2 values close to 1.0, demonstrating its superior predictive power and adaptability to unseen data. The implementation procedure of the GB model for any desired combination of input variables is explained in Appendix J. Following closely behind GB is the RF model, which also displays strong performance with consistently high R^2 values across various benefit indices, indicating its capacity to generalize effectively. The DT ML model, while achieving excellent training performance, shows some variability in testing results, highlighting the need for careful consideration when deploying it in predictive applications. The SVM ML model maintains its stability, with consistently high R^2 values during testing, showcasing its reliability in handling diverse datasets. These findings emphasize the importance of selecting the most suitable prediction model for specific benefit indices and the potential impact on result quality.

Table 14. R^2 of the performed prediction models

			R^2					
			MLR	**MER**	**DT**	**RF**	**SVM**	**GB**
Benefit index	TBR	Train	0.550	0.589	1	0.977	0.797	0.998
		Test	0.508	0.569	0.603	0.844	0.688	0.974
	$M_{R\text{-}eff}$	Train	0.699	-1.454	1	0.985	0.839	0.993
		Test	0.723	-1.530	0.863	0.905	0.814	0.971
	EBT	Train	0.708	-5.320	1	0.989	0.839	0.993
		Test	0.665	-4.329	0.879	0.915	0.810	0.975
	α_b	Train	0.946	0.946	1	0.994	0.956	0.990
		Test	0.946	0.947	0.933	0.963	0.944	0.975
	α_s	Train	0.741	0.883	1	0.991	0.966	0.998
		Test	0.878	0.880	0.920	0.952	0.920	0.963

Feature Importance Analysis

Feature importance analyses of the different variables contributing to the benefits of geosynthetic reinforcement in flexible pavement (i.e., AC thickness, base thickness, geosynthetic stiffness, subgrade stiffness, rutting target, and geosynthetic type) reveals valuable insights into the predictors that significantly influence the benefit prediction. The results of feature importance analysis for the different benefit indices of the Random Forest (RF) model are presented in Table 15.

Table 15. Feature importance for different variables from RF model

		Feature Importance						
		AC thickness	**Base thickness**	**Geosynthetic stiffness**	**Subgrade stiffness**	**Rutting target**	**Geogrid**	**Geotextile**
Benefit index	TBR	0.1569	0.2900	0.1184	0.2296	0.1334	0.0346	0.0372
	$M_{R\text{-}eff}$	0.0736	0.2097	0.2753	0.2565	0.1192	0.0335	0.0321
	EBT	0.2096	0.1579	0.3361	0.1655	0.0781	0.0265	0.0263
	α_b	0.6368	0.0610	0.0770	0.1428	-	0.0405	0.0419
	α_s	0.5426	0.0801	0.0633	0.1927	-	0.0612	0.0601

An analysis of feature importance reveals distinct patterns of feature contributions across different benefit indices, which are presented in Appendix H as graphs H-1 to H-5. In the case of the TBR benefit index, the base thickness emerges as the most influential feature, with a relatively high importance score of 0.29, followed by subgrade stiffness (0.23) and AC thickness (0.16). Geotextile stiffness (0.12) and geogrid stiffness (0.13) also exhibit moderate importance, underlining their roles in influencing the geosynthetic benefits as determined by the TBR. Meanwhile, geosynthetic type (geogrid or geotextile) and rutting target show relatively lower importance scores, suggesting their limited impact on the TBR predicted values; see Figure 68.

Shifting to the effective base thickness ($M_{R\text{-}eff}$) benefit index, the geosynthetic stiffness takes the lead in importance with a score of 0.28, closely followed by subgrade stiffness (0.26) and base thickness (0.21). The AC thickness (0.07), geogrid (0.03), and geotextile (0.03) display relatively lower importance, indicating their reduced influence on $M_{R\text{-}eff}$ predictions. For the EBT benefit index, geosynthetic stiffness (0.34) emerges as the most crucial feature, followed by AC thickness (0.21) and subgrade stiffness (0.17). The base thickness (0.16), rutting target (0.08), and geotextile (0.03) have relatively lower importance, signifying their limited contributions to EBT predictions. Remarkably, the α_b and α_s benefit indices show distinct feature importance profiles. In both cases, the AC thickness dominates as the most influential feature, with importance scores of 0.64 and 0.54, respectively, emphasizing its critical role in predicting these indices. Other features exhibit considerably lower importance scores, indicating their reduced impact or absence in the models for these specific benefit indices.

Figure 68. Feature importance graph of TBR from RF model

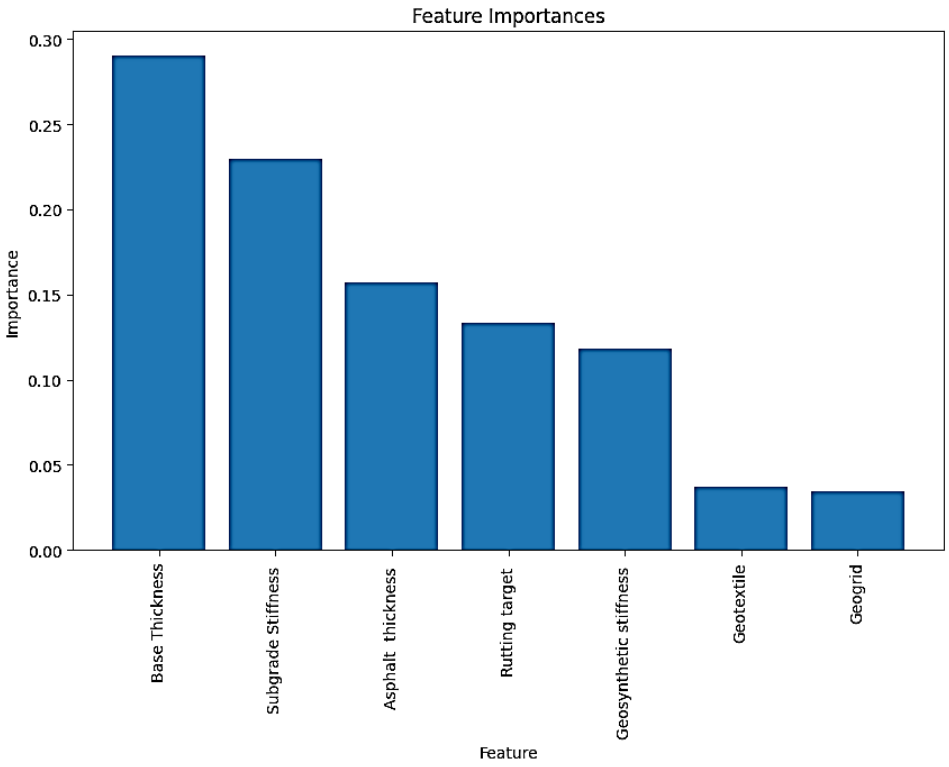

Developing Multiple Linear Regression (MLR) with Interactions

To enhance the predictive capabilities of the Multiple Linear Regression (MLR) model and investigate the potential interactions among independent variables concerning geosynthetics benefit indices and modification coefficients, researchers created various datasets that encompass all of the possible combinations of these independent variables.

For benefit indices of the TBR, $M_{R\text{-}eff,}$ and EBT models, the datasets include 28 independent variables and all their possible interactions, as well as one dependent variable. The scaled independent variables of asphalt thickness, base thickness, geosynthetic stiffness, subgrade stiffness, rutting target, geogrid presence and geotextile presence are defined as x_1 to x_7 in the regression models. The general equation for the MLR with interactions is given as follows:

$$y = \beta_0 + \beta_1 x_1 + \beta_2 x_2 + \beta_3 x_3 + \beta_4 x_4 + \beta_5 x_5 + \beta_6 x_6 + \beta_7 x_7 + \beta_8 x_1 x_2 + \beta_9 x_1 x_3$$
$$+\beta_{10} x_1 x_4 + \beta_{11} x_1 x_5 + \beta_{12} x_1 x_6 + \beta_{13} x_1 x_7 + \beta_{14} x_2 x_3 + \beta_{15} x_2 x_4 + \beta_{16} x_2 x_5$$
$$+\beta_{17} x_2 x_6 + \beta_{18} x_2 x_7 + \beta_{19} x_3 x_4 + \beta_{20} x_3 x_5 + \beta_{21} x_3 x_6 + \beta_{22} x_3 x_7 + \beta_{23} x_4 x_5$$
$$+\beta_{24} x_4 x_6 + \beta_{25} x_4 x_7 + \beta_{26} x_5 x_6 + \beta_{27} x_5 x_7 + \beta_{28} x_6 x_7 \quad (40)$$

For modifying the coefficients of the α_b and α_s models, the datasets include 21 independent variables and all of their possible interactions, as well as one dependent variable. The scaled independent variables of asphalt thickness, base thickness, geosynthetic stiffness, subgrade stiffness, geogrid presence, and geotextile presence are defined as x_1 to x_6 in regression models.

The overall model significance test measures the model's effectiveness by determining whether there is a linear relationship between the dependent and independent variables. To ensure the selection of statistically significant variables from the general model, a stepwise variable selection process with a 95% confidence level, known as the F statistic test, was carried out on the general model. The optimal approach is to use the Analysis of Variance (ANOVA). In this model, backward selection is employed to choose the features. The backward selection is a stepwise feature selection method used in statistical modeling and machine learning. It begins with all available features and iteratively removes the least significant ones based on predetermined criteria, such as p-values or cross-validation performance. Its primary benefits include simplifying the models, minimizing overfitting, and enhancing their interpretability.

The values of the coefficients in regression models were then derived as presented in Appendix I as Tables I-1 and I-2. The performance metrics of MLR with interaction models were assessed in terms of their ability to predict the geosynthetic benefit indices (i.e., TBR, $M_{R\text{-}eff}$, EBT) and their modifying coefficients; see Table 16.

Table 16. Performance metrics of MLR with interaction model for benefit indices and modifying coefficients

		MLR with Interactions				
		TBR	**$M_{R\text{-}eff}$**	**EBT**	**α_b**	**α_s**
R^2	Train	0.683	0.806	0.744	0.956	0.927
	Test	0.659	0.814	0.700	0.945	0.899
RMSE	Train	0.255	574.37	1.018	0	0
	Test	0.449	515.56	1.603	0	0
MAE	Train	0.334	15.38	0.781	0.005	0.008
	Test	0.395	15.69	0.942	0.005	0.008

The results indicate the performance of a Multiple Linear Regression (MLR) model with interactions across the various evaluation metrics. The R^2 values for both training and testing datasets show that the model explains a substantial portion of the variance in the target variable. Notably, the $M_{R\text{-}eff}$ and α_b variables exhibit high R^2 values, suggesting strong predictive power. However, the model might be slightly overfitting, as the R^2 for the training dataset is slightly higher than the testing dataset. Looking at the Root Mean Squared Error (RMSE), it is evident that the models perform relatively well on the training dataset, with low RMSE values for TBR, $M_{R\text{-}eff}$, and EBT. However, the RMSE values are noticeably higher on the testing dataset, suggesting that the model's predictions might have higher errors when applied to new data. The Mean Absolute Error (MAE) values show a similar trend, with low values on the training dataset but higher values on the testing dataset, indicating some level of prediction error when the model is generalized to new data.

Introducing interactions into the Multiple Linear Regression model has noticeably improved its performance, as indicated by higher R^2 values across all variables for both the training and testing datasets; see Table 17. The MLR with interaction models demonstrates a better ability to explain the variance in the target variable compared to MLR without interaction models, particularly for $M_{R\text{-}eff}$ and α_b. This suggests that considering the interaction among independent variables offers a more precise depiction of the fundamental relationships in the data, leading to a more efficient predictive model. However, it is essential to further assess the models' performance using additional evaluation metrics and guard against potential overfitting to ensure the generalization of these findings to new, unseen data.

Table 17: Comparing R^2 of MLR model for datasets without and with interactions

		MLR				
		TBR	**$M_{R\text{-}eff}$**	**EBT**	**α_b**	**α_s**
Without interactions R^2	Train	0.550	0.699	0.708	0.946	0.741
	Test	0.508	0.723	0.665	0.946	0.878
With interaction R^2	Train	0.683	0.806	0.744	0.956	0.927
	Test	0.659	0.814	0.700	0.945	0.899

Conclusions

This research study utilized finite element (FE) numerical modeling to investigate and quantify the benefits of incorporating geosynthetics to reinforce/stabilize flexible pavements. The primary objective of the study aligns with the Mechanistic-Empirical Pavement Design Guide (MEPDG) framework, which aims to establish a basis for incorporating geosynthetic reinforcement into standard pavement design methodologies.

Several FE models were developed to simulate the performance of geosynthetic reinforced flexible pavements for different sections corresponding to low, medium, and high volume roads with different thicknesses and different subgrade conditions. A comprehensive FE parametric analysis was conducted to assess the effects of different variables and parameters contributing to the benefits of employing geosynthetics in flexible pavements. These variables include thickness of asphalt layer, thickness of base course layer, subgrade strength/stiffness, geosynthetic type, and geosynthetic stiffness. The FE simulations involved applying 100 loading cycles, with the resulting permanent deformation (PD) data used to fine-tune and calibrate the ME rutting equation parameters for each pavement layer. The extrapolation of PD curves using the ME calibrated rutting parameters enabled the determination of pavement service life. The FE-ME methodology was rigorously validated using the results from cyclic plate load tests (CPLT) on in-box test sections and accelerated wheel loading tests (ALT) on full scale geosynthetic reinforced test lane sections. The comparison between the PD curves obtained for unreinforced and geosynthetic reinforced pavement sections enabled the calculation of geosynthetic benefits in terms of Traffic Benefit Ratios (TBR) at different rutting targets. The TBR values were utilized as input parameters in the AASHTOWare software to determine other quantified benefits such as the Effective Resilient Modulus ($M_{R\text{-}eff}$) and the Equivalent Base Thickness (EBT). By determining the ratio between the calibrated rutting curves for the base and subgrade layers between unreinforced and geosynthetic reinforced sections, the rutting reduction coefficients of α_b and α_s were derived. These can be directly applied in ME rutting equations for use in designing geosynthetic reinforced flexible pavements.

To estimate and quantify the benefits of incorporating geosynthetic reinforcement in flexible pavements in terms of the TBR, $M_{R\text{-}eff}$, EBT, α_b and α_s key parameters, a set of predictive models were developed. These models included both regression and machine learning (ML) approaches, encompassing Multiple Linear Regression (MLR), Multivariate Exponential Regression (MER), Decision Tree (DT), Random Forest (RF), Support Vector Machine

(SVM), and Gradient Boosting (GB). The predictive accuracy of these models was rigorously assessed using metrics such as the coefficient of determination (R^2), Root Mean Square Error (RMSE) and Mean Absolute Error (MAE). The results demonstrated the remarkable accuracy of the RF and GB predictive models in quantifying the benefits of using geosynthetics in pavement structures, encompassing TBR, $M_{R\text{-}eff}$, EBT, α_b and α_s for designing geosynthetic reinforced pavements.

Based on the findings of this study, the following conclusions can be drawn:

- The developed 2-D axisymmetric FE models were able to effectively simulate the performance of geosynthetic reinforced flexible pavements of different sections for low, medium, and high volume roads, of different base thicknesses and different subgrade conditions, under cyclic (i.e, vehicular) traffic loads.
- The proposed FE interlocking model was able to accurately simulate the interlocking behavior between the geogrid apertures and the base aggregate particles, in addition to interface friction, to distinguish geogrid reinforcement from geotextile reinforcement in geosynthetic reinforced flexible pavements. The results of FE analyses demonstrated the superior benefits of using geogrids in reducing rutting compared to geotextile cases, which is attributed to their effective interlocking with the base aggregates.
- The inclusion of a single geosynthetic (e.g., geogrid or geotextile) layer at the base-subgrade interface will significantly enhance the pavement's performance by providing lateral restrain, confinement effect, and reducing shear stresses, hence reducing the permanent surface deformation (i.e., rutting) of the different geosynthetic reinforced pavement sections.
- The results of this study highlighted the effect of different variables and parameters on the performance and benefits of the geosynthetic reinforcement/stabilization of flexible pavements, which include the thickness of base course layer, subgrade strength/stiffness, geosynthetic stiffness, geosynthetic type, and road traffic volume (i.e., different thicknesses of asphalt layer). The results clearly demonstrated that the geosynthetic benefits in terms of TBR, $M_{R\text{-}eff}$, and EBT increase with decreasing the base thickness, with decreasing subgrade strength/stiffness, with increasing geosynthetic tensile stiffness, and with decreasing the road traffic volume (i.e., thinner asphalt layer). Geogrid reinforced pavement sections performed better than geotextile reinforced pavement sections due to interlocking behavior.

- For low volume traffic roads with 3.5 in. asphalt thickness, the optimal values of TBR, $M_{R\text{-}eff}$, and EBT were obtained at a 10 in. base thickness. However, in medium and high volume traffic roads, the benefits of geosynthetic reinforcement (TBR, $M_{R\text{-}eff}$, and EBT) decreased when increasing the thickness of base layer.
- The selected performance level in terms of rutting targets significantly influences the TBR, $M_{R\text{-}eff}$, and EBT values, which tend to increase when increasing the rutting target for all geogrid/geotextile reinforced pavement sections.
- The geosynthetic benefits evaluated in terms of Traffic Benefit Ratio (TBR) showed that the TBR values can reach up to 8.9 for low volume traffic road sections reinforced with high tensile stiffness geogrid and up to 5.92 for low volume roads using high tensile stiffness geotextile. The TBR values for medium volume traffic roads can reach up to 5.69 for sections reinforced with high tensile stiffness geogrid and up to 4.31 for sections reinforced with high tensile stiffness geotextile. However, for high volume traffic roads, the values of TBR can reach up to 4.55 for sections reinforced with high tensile stiffness geogrid and up to 3.84 for sections reinforced with high tensile stiffness geotextile.
- The geosynthetic benefits evaluated in terms of Effective Resilient Modulus ($M_{R\text{-}eff}$) showed that the derived $M_{R\text{-}eff}$ at 0.75 in. rutting target can increase up to 239% for low volume traffic road sections reinforced with high tensile stiffness geogrid. The maximum $M_{R\text{-}eff}$ increase for medium and high volume traffic roads for sections reinforced with high tensile stiffness geogrid are 222% and 156%, respectively. The derived $M_{R\text{-}eff}$ values for low volume road sections reinforced with high tensile stiffness geotextile can increase up to 222%. For sections reinforced with high tensile stiffness geotextile, the highest $MR\text{-}_{eff}$ increase for medium and high volume traffic roads are 169% and 106%, respectively.
- The geosynthetic benefits evaluated in terms of Equivalent Base Thickness (EBT) showed that the values of EBT at 0.75 in. rutting target can reach up to 6.7 in. for low volume road sections reinforced with high tensile geogrid and up to 6.1 in. for high tensile geotextile. The corresponding maximum EBT values for medium volume roads are 5.4 in. for sections reinforced with high tensile geogrid and 5.0 in. for sections reinforced with high tensile geotextile. For high volume roads, the maximum EBT values are 4.7 in. for sections reinforced with high tensile geogrid and 4.1 in. for sections reinforced with high tensile geotextile.
- The values of rutting reduction coefficient for the base layer (α_b) range from 0.84 to 0.98, indicating the variability observed within the different geosynthetic reinforced

pavement sections. Meanwhile, the rutting reduction coefficient for the subgrade layer (α_s) ranges from 0.72 to 0.95 across the different geosynthetic reinforced pavement sections. The average rutting reduction coefficient for the base layer (α_b) was approximately 6% higher than that of the subgrade layer (α_s), indicating greater benefits for the subgrade layer.

- Several regression and ML predictive models were developed to evaluate the geosynthetic benefits in terms of TBR, $M_{R\text{-}eff}$, and EBT. The results of evaluation showed that Multiple Linear Regression (MLR) with Interactions model and the Random Forest (RF) and Gradient Boosting (GB) ML models, can effectively predict the benefit indices of the geosynthetic reinforced pavements.

Recommendations

This study aimed to quantify the benefits of using geosynthetics to reinforce/stabilize flexible pavements in terms of Traffic Benefit Ratio (TBR), Effective Resilient Modulus ($M_{R\text{-}eff}$), and Equivalent Base Thickness (EBT), and to evaluate the effect of different variables and parameters contributing to the performance of geosynthetic reinforced pavement structures. Several regression and machine learning (ML) models were developed to quantify the benefits using the normalized variables as inputs in the models. Based on the findings of this research study, the following recommendations are offered to DOTD engineers:

- It is recommended that DOTD pavement design engineers consider reinforcing/stabilizing flexible pavements, especially in conditions where it is difficult to stabilize or treat weak subgrade soils with cement or lime; for widening highways; in construction of highway exits/entrances built over weak to medium subgrade soils; and to create working platforms for constructing pavements and embankments over weak soils. The benefits of geosynthetic reinforcement are more evident in pavement sections with thin base thickness (≤ 12 in.), high geosynthetic stiffness, low subgrade stiffness (M_R < 4500 psi or CBR < 3), and/or a thin asphalt layer (i.e., low volume traffic roads).
- To achieve the long-term benefits of using geosynthetic reinforcement/stabilization in flexible pavement design, it is recommended to use the TBR values presented in the tables and figures in Appendix A for different pavement sections and three traffic volume roads, along with the TBR prediction models, to estimate the extended service life of geosynthetic reinforced/stabilized flexible pavements.
- It is recommended that DOTD pavement design engineers use the values of the Effective Resilient Modulus ($M_{R\text{-}eff}$) of the base layer presented in tables in Appendix B for different pavement sections and three traffic volume roads, and/or the $M_{R\text{-}eff}$ values from the prediction models in the AASHTOWare software for designing geosynthetic reinforced/stabilized flexible pavements.
- DOTD pavement design can use geosynthetic reinforcement/stabilization for the benefit of reducing the pavement structure thickness. Table 18 provides the recommended Equivalent Base Thickness (EBT) values obtained at 0.5 in. rut depth for the three different traffic volume roads. The EBT is not the reduced base thickness of a reinforced section ($D_{rein\text{-}base}$); it is the amount of stone savings. The reduced base thickness for the geosynthetic reinforced flexible pavements ($D_{rein\text{-}base}$) is calculated by subtracting the EBT from the unreinforced base thickness as ($D_{rein\text{-}base} = D_{unrein\text{-}base}$ - EBT); see Figure 69.

The reduced base thickness ($D_{rein-base}$) should not be less than 6 in. to mobilize the geosynthetic base material reinforcement/stabilization mechanism.

Table 18. Recommended EBT values for low, medium and high volume roads

Type	Gesynth. Stiffness	Base thickness (in.) (D_{base})	Low volume roads			Medium volume roads			High volume roads		
			Weak subgrade	Medium stiff subgrade	Stiff subgrade	Weak subgrade	Medium stiff subgrade	Stiff subgrade	Weak subgrade	Medium stiff subgrade	Stiff subgrade
Geogrid	High tensile stiffness	10	4	4	3.5	4	4	3.5	3.5	3	2.5
		12	5	4.5	4	4.5	4.5	3.5	4	3.5	3
		14	4.5	4	3.5	4	3.5	3	3.5	3	2.5
	Medium tensile stiffness	10	4	3.5	3	4	3.5	3.5	3.5	3	2.5
		12	4.5	4	3.5	4	3.5	3.5	3.5	3	3
		14	4	4	3.5	3.5	3	2.5	3.5	2.5	2.5
	Low tensile stiffness	10	4	3.5	2.5	3.5	3	2.5	3	2	1.5
		12	4.5	4	3.5	3.5	3	3	3	2.5	2
		14	4	3.5	3	3	2.5	2.5	2.5	2	2
Geotextile	High tensile stiffness	10	4	3.5	3	4	3.5	3	3	3	2.5
		12	4.5	4	3.5	4	4	3	3.5	3	2.5
		14	4	3.5	3	3.5	3	2.5	3	2.5	2
	Medium tensile stiffness	10	4	3.5	2.5	3.5	3	2.5	3	2	2
		12	4.5	4	3.5	3.5	3	2.5	3	2.5	2.5
		14	4	3.5	3	3	2.5	2.5	3	2.5	2
	Low tensile stiffness	10	3.5	3	2.5	3	2.5	2	2.5	2	1.5
		12	4	3.5	3	3	3	2.5	2	2	2
		14	3.5	3	2	2.5	2.5	2	2	2	2

Note on minimum thickness: Reduced base thickness should not be less than 6 in.

Figure 69. Unreinforced pavement sections versus reinforced pavement sections with EBT

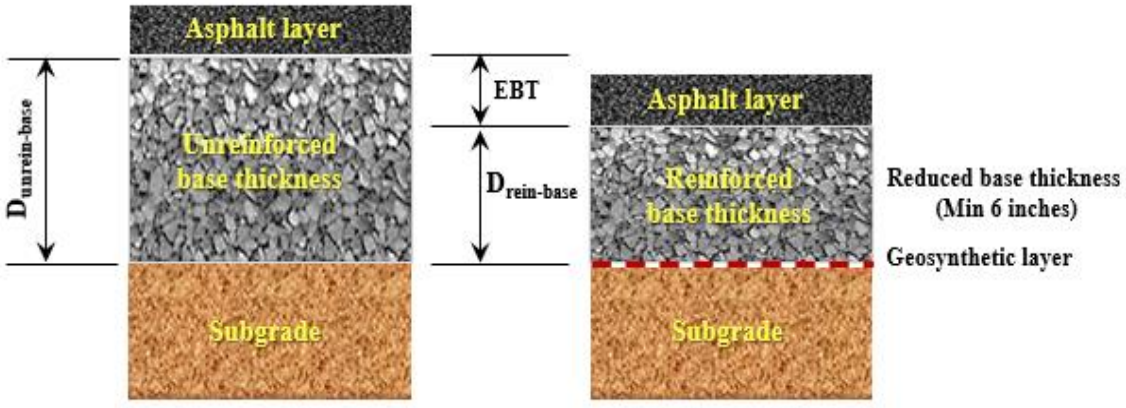

- DOTD pavement design engineers should consider using the rutting reduction coefficients for base and subgrade (α_b or α_s) presented in Appendix D to calculate the rutting performance of geosynthetic reinforced/stabilized pavements using the MEPDG permanent deformation (i.e., rutting) equations.
- It is recommended that DOTD engineers consider constructing several geosynthetic reinforced field test sections in parallel to sections treated/stabilized with lime or cement for long-term performance comparison, as well as to verify/validate the findings and the predictive computational models developed in this study.
- It is recommended that DOTD engineers consider incorporating the effect of dynamic traffic loading and vibrations on the material properties and pavement response over the lifespan of pavements in a future study. This could involve developing advanced constitutive models that account for the evolution of material properties such as stiffness and strength under dynamic loading conditions, leading to a more realistic evaluation of the performance of geosynthetic reinforced pavements.

Acronyms, Abbreviations, and Symbols

Term	Description
AADT	Average annual daily traffic number
$AADT_R$	Average annual daily traffic number for reinforced section
$AADT_U$	Average annual daily traffic number for unreinforced section
AASHTO	American Association of State Highway and Transportation Officials
AC	Asphalt concrete
ANOVA	Analysis of Variance
ALF	Accelerated Load Facility
APT	Accelerated pavement testing
ASCE	American Society of Civil Engineers
BCR	Base Course Reduction
cm	centimeter(s)
CBR	California bearing ratio
CPLT	Cyclic plate load test
CSL	Critical State Line
CU	Consolidated undrained
D	Depth
d	Soil's angle of cohesion in $p-t$ plane
D_{max}	Maximum aggregate size
DOTD	Louisiana Department of Transportation and Development
DT	Decision Tree
E	Equivalent isotropic elastic modulus
EBT	Equivalent Base Thickness
E_m	Machine direction elastic modulus
ESAL	Equivalent single axle load
E_{slip}	Elastic slip
E_{xm}	Cross-machine direction elastic modulus
FE	Finite Element
FEM	Finite Element Model

Term	Description
FHWA	Federal Highway Administration
ft	foot (feet)
G	Shear modulus
GB	Gradient Boosting
G_0	Instantaneous shear modulus
GPa	Gigapascal
GPU	Graphics Processing Unit
G(t)	Relaxation shear modulus
h_{HMA}	Thickness of HMA layer
HMA	Hot mix asphalt
h_{soil}	Layer thickness of base or subgrade
in.	inch(es)
IRI	International Roughness Index
kN	Kilonewton
kPa	Kilopascal
K_0	Instantaneous bulk modulus
k_0	Lateral stress coefficient
k_{1r}, k_{2r}, k_{3r}	Global field calibration rutting coefficients for HMA
k_{s1}	Global field calibration rutting coefficient for base and subgrade
ksi	Kips per square inch
K(t)	Relaxation bulk modulus
k_z	Depth confinement factor
LTPP	Long-term pavement performance
LTRC	Louisiana Transportation Research Center
LVDT	Linear variable differential transformer
M	Geosynthetic sheet stiffness
m	meter(s)
mm	millimeter(s)
MAE	Mean Absolute Error

Term	Description
MCC	Modified Cam-Clay
ME	Mechanistic Empirical
MPa	Megapascal
MEPDG	Mechanistic-Empirical Pavement Design Guide
MER	Multivariate Exponential Regression
ML	Machine learning
MLR	Multiple Linear Regression
MDT	Montana Department of Transportation
M_R	Resilient modulus
$M_{R\text{-}eff}$	Effective Resilient Modulus
MSE	Mean Square Error
N	Number of load cycles
NCHRP	National Cooperative Highway Research Program
N_R	Number of cycles of reinforced section
N_U	Number of cycles of unreinforced section
OCR	Over-consolidation ratio
p	Equivalent pressure stress
P_b	Mean effective stress
p_c'	Pre-consolidation
PCI	Pavement Condition Index
PD	Permanent deformation
p_0'	Present pressure
PRF	Pavement Research Facility
psi	Pound(s) per square inch
q	Mises equivalent stress
r	Third invariant of deviatoric stress
R^2	Coefficient of determination
RAP	Reclaimed asphalt pavement
RCA	Recycled concrete aggregate

Term	Description
RF	Random Forest
RMSE	Root Mean Squared Error
S	Stress deviator
SN	Structural number
SVM	Support Vector Machine
T	Time
t	Deviatoric stress
TBR	Traffic Benefit Ratio
TPU	Tensor Processing Unit
WIM	Weigh-in-motion
W_C	Water content (%)
2-D	Two-dimensional
3-D	Three-dimensional
α	Coefficient
α_b	Rutting reduction coefficient for base
α_s	Rutting reduction coefficient for subgrade
α*	Calibration coefficient
β	Soil's angle of friction in $p-t$ plane
β_{1r}, β_{2r}, β_{3r}	Local calibration rutting coefficients for HMA layer
β_{s1}	Rutting calibration factor for base or subgrade
$\varepsilon_{p(HMA)}$	Permanent plastic strain for HMA
ε_v	Average vertical resilient strain
$\emptyset'$	Effective friction angle
μ	Interface frictional coefficient
υ	Poisson's ratio
σ_1	Axial pressure
σ_3	Confining pressure

References

[1] American Society of Civil Engineers, "Failure to Act: Current Investment Trends in Our Surface Transportation Infrastructure: Preliminary Findings," 2020. [Online]. Available: https://www.ebp.global/us-en/projects/failure-act-current-investment-trends-our-surface-transportation-infrastructure-2020.

[2] Federal Highway Administration, "Status of the Nation's Highways, Bridges, and Transit Conditions and Performance Report to Congress," Government Printing Office, Washington, D.C., 2017.

[3] United States Congress, "Public Spending on Transportation and Water Infrastructure," United States Congress, Washington, D.C., 2015.

[4] M. Abu-Farsakh and M. Nazzal, "Report No. FHWA/LA.04/450: Evaluation of the Base/Subgrade Soil Under Repeated Loading: Phase 1–Laboratory Testing and Numerical Modeling of Geogrid Reinforced Bases in Flexible Pavement," Louisiana Transportation Research Center, Baton Rouge, LA, 2009.

[5] S. Perkins, "Report No. FHWA/MT-99-00/8138: Geosynthetic Reinforcement of Flexible Pavements: Laboratory Based Pavement Test Sections," Montana Department of Transportation, Bozeman, MT, 1999.

[6] I. Al-Qadi, S. Dessouky, J. Kwon and E. Tutumluer, "Geogrid in Flexible Pavements: Validated Mechanics," *Transportation Research Record,* vol. 2045, p. 102–109, 2008.

[7] R. Luo, F. Gu, X. Luo, R. Lytton, E. Hajj, R. E. S. Siddharthan, M. Piratheepan and S. Pournoman, "NCHRP Report 01-50: Quantifying the Influence of Geosynthetics on Pavement Performance," National Academy of Science, Washington D.C., 2017.

[8] E. Tutumluer, M. Kang and I. Qamhia, "Geosynthetic Stabilization of Road Pavements, Railroads, and Airfields," *Transportation Geotechnics,* vol. 50, p. 101321, 2025.

[9] American Association of State Highways and Transportation Officials, "AASHTO," 1993.

[10] F. Montanelli, A. Zhao and P. Rimoldi, "Geosynthetic-Reinforced Pavement System: Testing and Design," in *Proceedings of Geosynthetics 1997*, Long Beach, CA, 1997.

[11] S. Perkins and M. Edens, "A Design Model for Geosynthetic-Reinforced Pavements," *International Journal of Pavement Engineering,* vol. 4, no. 1, p. 37–50, 2003.

[12] S. Perkins and E. Cuelho, "Report No. FHWA/MT-21-003/9564-602: Large-Scale Laboratory Testing of Geosynthetics in Roadway Applications," Montana Department of Transportation, Bozeman, MT, 2021.

[13] J. Gu, Finite Element Analysis to Evaluate Geogrid Base Reinforcement in Flexible Pavement, Baton Rouge, LA: Louisiana State University, 2011.

[14] M. Abu-Farsakh, Q. Chen and S. Hanandeh, "Report No. FHWA/LA.18/603: Accelerated Load Testing of Geosynthetic Base Reinforced/Stabilized Unpaved and Pavement Test Sections," Louisiana Transportation Reserach Center, Baton Rouge, LA, 2019.

[15] J. Zornberg, "Geosynthetic-Reinforced Pavement Systems," in *Fifth European Geosynthetics Conference, EuroGeo5*, Valencia, Spain, 2012.

[16] R. Berg, B. Christopher and S. Perkins, "Geosynthetic Reinforcement of the Aggregate Base/Subbase Courses of Flexible Pavement Structures," *GMA White Paper II,* no. Geosynthetic Materials Association, 2000.

[17] M. Ashby and D. Jones, Engineering Materials 1: An Introduction to the Properties and Applications, Pergamon, 1980.

[18] J. Christison and K. Anderson, "The Response of Asphalt Pavements to Low Temperature Climatic Environments," in *Proceedings of the Third International Conference on the Structural Design of Asphalt Pavements*, London, England, 1972.

[19] N. Reck, "Mechanistic-Empirical Design of Geogrid-Reinforced Paved Flexible Pavements," in *Proceedings of Jubilee Symposium on Polymer Grid Reinforcement, Institute of Civil Engineers*, London, England, 2009.

[20] ARA, Inc., "Guide for Mechanistic-Empirical Design of New and Rehabilitated Pavement Structures," ERES Consultants Division, 2004.

[21] R. Kerkhoven and G. Dormon, "Some Considerations on the California Bearing Ratio Method for the Design of Flexible Pavements," Shell Petroleum Company, 1953.

[22] R. Saal and P. Pell, "Fatigue of Bituminous Road Mixes," *Highway Research Board,* vol. 171, no. 1, pp. 61-71, 1960.

[23] G. Dormon and C. Metcalf, "Design Curves for Flexible Pavements Based on Layered System Theory," *Highway Research Record,* vol. 71, p. 69–84, 1964.

[24] Federal Highway Administration, "Traffic Monitoring Guide," U.S. Department of Transportation, Washington, D.C., 2001.

[25] M. Witczak, "NCHRP Report 547: Simple Performance Tests: Summary of Recommended Methods and Database," Transportation Research Board, Washington, D.C., 2005.

[26] S. Bhatia and J. Smith, "Geotextile Characterization and Pore-Size Distribution: Part II, A Review of Test Methods and Results," *Geosynthetics International,* vol. 3, no. 2, p. 155–180, 1996.

[27] J. Giroud, C. Ah-Line and R. Bonaparte, "Design of Unpaved Roads and Trafficked Areas with Geogrids," *Polymer Grid Reinforcement,* p. 116–127, 1984.

[28] S. Maxwell, "Effectiveness of Geosynthetics in Stabilizing Soft Subgrades," Wisconsin Highway Research Program, 2005.

[29] T. Haliburton, J. Lawmaster and V. McGuffey, "Use of Engineering Fabrics in Transportation Related Applications," Federal Highway Administration, DTFH61- 80-C-00094, Washington, D.C., 1981.

[30] R. Holtz, B. Christopher and R. Berg, "Geosynthetic Design and Construction Guidelines," Federal Highway Administration, Washington, D.C., 1998.

[31] M. Wimalasena, "Evaluate the Performance of Geosynthetic Reinforced Subgrades Under Monotonic Loading," Queensland University of Technology, Brisbane, Australia, 2022.

[32] F. Moghaddas-Nejad and J. Small, "Effects of Geogrid Reinforcement in Model Track Tests on Pavements," *Journal of Transportation Engineering,* vol. 122, no. 6, pp. 468-474, 1996.

[33] S. Perkins, M. Ismeik, M. L. Fogelsong, Y. Wang and E. V. Cuelho, "Geosynthetic-Reinforced Pavements: Overview and Preliminary Results," in *Sixth International Conference on Geosynthetics*, Atlanta, GA, 1998.

[34] R. Haas, J. Wall and R. Carroll, "Geogrid Reinforcement of Granular Bases in Flexible Pavements," *Transportation Research Record,* vol. 1188, pp. 19-27, 1988.

[35] S. Perkins, "Mechanical Response of Geosynthetic-Reinforced Flexible Pavements," *Geosynthetics International,* vol. 6, no. 5, p. 347–382, 1999.

[36] M. Abu-Farsakh and Q. Chen, "Evaluation of Geogrid Base Reinforcement in Flexible Pavement Using Cyclic Plate Load Testing," *International Journal of Pavement Engineering,* vol. 12, no. 3, p. 275–288, 2011.

[37] A. Halim, R. Haas and W. Chang, "Geogrid Reinforcement of Asphalt Pavements and Verification of Elastic Layer Theory," *Transportation Research Record,* vol. 949, pp. 55-85, 1983.

[38] R. Carroll, J. Walls and R. Haas, "Granular Base Reinforcement of Flexible Pavements Using Geogrids," in *Proceedings of Geosynthetics*, St Paul, MN, 1987.

[39] I. Al-Qadi, T. Brandon, R. Valentine, B. Lacina and T. Smith, "Laboratory Evaluation of Geosynthetic-Reinforced Pavement Sections," *Transportation Research Record,* vol. 21, no. 2, pp. 25-31, 1994.

[40] S. Perkins, B. Christopher and C. Eli, "Report No. DTFH61-01-X-00068: Development of Design Methods for Geosynthetic Reinforced Flexible Pavements," U.S. Department of Transportation, Federal Highway Administration, Washington D.C., 2004.

[41] J. Leng, T. Ju and M. Gabr, "Characteristics of Geogrid-Reinforced Aggregate Under Cyclic Load," *Transportation Research Record,* vol. 1786, p. 29–35, 2002.

[42] F. Moghaddas-Nejad and J. Small, "Resilient and Permanent Characteristics of Reinforced Granular Materials by Repeated Load Triaxial Tests," *ASTM Geotechnical Testing Journal,* vol. 26, no. 2, pp. 152-166, 2003.

[43] Q. Chen, M. Abu-Farsakh and M. Tao, "Laboratory Evaluation of Geogrid Base Reinforcement and Corresponding Instrumentation Program," *Geotechnical Testing Journal,* vol. 32, no. 6, pp. 516-525, 2009.

[44] Y. Qian, J. Han, S. Pokharel and R. Parsons, "Stress Analysis on Triangular-Aperture Geogrid-Reinforced Bases Over Weak Subgrade Under Cyclic Loading," *Transportation Research Record,* vol. 2204, no. 1, pp. 83-91, 2011.

[45] N. Ghafoori and M. Sharbaf, "Report No. 327-12-803: Use of Geogrid for Strengthening and Reducing the Roadway Structural Sections," Nevada Department of Transportation, Carson City, NV, 2016.

[46] A. Nazeri, R. Ziaie-Moayed and H. Ghiasinejad, "Evaluating the Efficiency of a Composite Geosynthetic Reinforcement in Container Yard Pavements Via Laboratory Plate Load Test," *International Journal of Pavement Engineering,* vol. 23, no. 5, 2022.

[47] S. Marelli, P. Recalcati, A. Crippa and E. Cuelho, "Performance Evaluation of Three-Dimensional Geogrid for Base Stabilization in Pavement Applications," in *Geosynthetics: Leading the Way to a Resilient Planet*, London, UK, CRC Press, 2023, pp. 1267-1273.

[48] M. Divakar, B. Gottumukkala, S. Swarna, P. Prasad and G. Arunkumar, "Performance Evaluation of Geosynthetic-Reinforced Marginal Material as Base Layer Over Weak Subgrade," *International Journal of Pavement Engineering,* vol. 25, no. 1, 2024.

[49] C. Jayalath, K. Wimalasena and C. Gallage, "Small-Scale Cyclic Loading Test to Investigate the Rutting Performance of Geogrid-Reinforced Unpaved Pavements," *International Journal of Pavement Research and Technology,* vol. 17, p. 615–635, 2024.

[50] S. Srivastava and U. Balunaini, "Performance of Geogrid and Geotextile-Reinforced Low to Moderately Expansive Subgrades," *Geosynthetics International,* pp. 1-15, 2025.

[51] M. Badiger, K. Mamatha and S. Dinesh, "Laboratory Study on the Performance Evaluation of RCA Reinforced with Geosynthetics for GSB Layer Application in Low Volume Roads," *Sustainable Materials and Technologies,* vol. 44, 2025.

[52] A. Cancelli and F. Montanelli, "In-Ground Test for Geosynthetic-Reinforced Flexible Paved Roads," in *Proceedings of the Conference Geosynthetics 1999*, Roseville, MN, 1999.

[53] J. Tingle and S. Webster, "Corps of Engineers Design of Geosynthetic-Reinforced Unpaved Roads," *Transportation Research Record,* vol. 1849, p. 193–201, 2003.

[54] S. Aran, "Base Reinforcement with Biaxial Geogrid: Long-Term Performance," *Transportation Research Board,* vol. 1975, no. 1, p. 115–123, 2006.

[55] C. Helstrom, D. Humphrey and S. Hayden, "Geogrid Reinforced Pavement Structure in a Cold Region," in *Proceedings of the 13th International Conference on Cold Regions Engineering*, Orono, ME, 2007.

[56] E. Duncan-Williams and N. Attoh-Okine, "Effect of Geogrid in Granular Base Strength: An Experimental Investigation," *Journal of Construction and Building Materials,* vol. 22, p. 2180–2184, 2008.

[57] K. Henry, J. Clapp, W. Davids, D. Humphrey and L. Barna, "Structural Improvements of Flexible Pavements Using Geosynthetics for Base Course Reinforcement," Federal Highway Administration, McLean, VA, 2009.

[58] B. Cox, J. McCartney, C. Wood and B. Curry, "Performance Evaluation of Full-Scale Geosynthetic-Reinforced Flexible Pavements Using Field Cyclic Plate Load Tests," in *Transportation Research Board*, Washington, D.C., 2010.

[59] J. McCartney, B. Cox, C. Wood and B. Curry, "Evaluation of Geosynthetic-Reinforced Flexible Pavements Using Static Plate Load Tests," in *9th International Conference on Geosynthetics - Geosynthetics: Advanced Solutions for a Challenging World*, Guarujá, Brazil, 2010.

[60] I. Al-Qadi, S. Desouky, E. Utumluer and J. Kwon, "Geogrid Mechanism in Low-Volume Flexible Pavements: Accelerated Testing of Full-Scale Heavily Instrumented Pavement Sections," *International Journal of Pavement Engineering,* vol. 12, no. 2, p. 121–135, 2011.

[61] S. Jersey, J. Tingle, G. Norwood, J. Kwon and M. Wayne, "Full-Scale Evaluation of Geogrid-Reinforced Thin Flexible Pavements," *Transportation Research Record,* vol. 2310, p. 61–71, 2012.

[62] J. Greene, A. Nazef, B. Choubane and D. Horhota, "Long-Term Evaluation of Geosynthetic Reinforcement of Flexible Pavements Constructed Over Thick Organic Soil Deposits," *Transportation Research Record,* vol. 2462, no. 1, p. 89–97, 2014.

[63] T. Imjai, K. Pilakoutas and M. Guadagnini, "Performance of Geosynthetic-Reinforced Flexible Pavements in Full-Scale Field Trials," *Geotextiles and Geomembranes,* vol. 47, no. 2, p. 217–229, 2019.

[64] M. Singh, A. Trivedi and S. Shukla, "Evaluation of Geosynthetic Reinforcement in Unpaved Road Using Moving Wheel Load Test," *Geotextiles and Geomembranes,* vol. 50, no. 4, 2022.

[65] A. Shahkolahi, C. Gallage, D. Lacy and J. Klompmaker, "Full-Scale Field Study on Performance of Geogrid-Stabilized Pavement on Soft and Expansive Subgrade," in *Proceedings of the 14th Australia and New Zealand Conference on Geomechanics*, Port Melbourne, Victoria, Australia, 2023.

[66] J. Leng and M. Gabr, "Numerical Analysis of Stress–Deformation Response in Reinforced Unpaved Road Sections," *Geosynthetics International,* vol. 12, no. 2, pp. 111-119, 2005.

[67] J. Kwon, E. Tutumluer and M. Kim, "Development of a Mechanistic Model for Geosynthetic-Reinforced Flexible Pavements," *Geosynthetics International,* vol. 12, no. 6, p. 310–320, 2005.

[68] S. Perkins, B. Christopher, E. Cuelho, G. Eiksund, C. Schwartz and G. Svanø, "A Mechanistic–Empirical Model for Base-Reinforced Flexible Pavements," *International Journal of Pavement Engineering,* vol. 10, no. 2, pp. 101-114, 2009.

[69] M. Kim and J. Lee, "Effects of Geogrid Reinforcement in Low Volume Flexible Pavement," *Journal of Civil Engineering and Management,* vol. 19, no. 1, pp. S14-S22, 2013.

[70] F. Gu, X. Luo, R. Luo, E. Hajj and R. Lytton, "A Mechanistic-Empirical Approach to Quantify the Influence of Geogrid on the Performance of Flexible Pavement Structures," *Transportation Geotechnics,* vol. 13, pp. 69-80, 2017.

[71] S. Zhi, W. Wing, W. Gun, L. Hui and T. Bo, "Evaluation of Fatigue Crack Behavior in Asphalt Concrete Pavements with Different Polymer Modifiers," *Construction and Building Materials,* vol. 27, no. 1, pp. 117-125, 2012.

[72] Y. Sun, C. Du, H. Gong, Y. Li and J. Chen, "Effect of Temperature Field on Damage Initiation in Asphalt Pavement: A Microstructure-Based Multiscale Finite Element Method," *Mechanics of Materials,* vol. 144, p. 103367, 2020.

[73] R. Barksdale, S. Brown and F. Chan, "NCHRP Report No. 315: Potential Benefits of Geosynthetics in Flexible Pavement Systems," Transportation Research Board, Washington, D.C., 1989.

[74] G. Wathugala, B. Huang and S. Pal, "Numerical Simulation of Geosynthetic-Reinforced Flexible Pavements," *Transportation Research Record,* vol. 1534, no. 1, p. 58–65, 1996.

[75] S. W. Perkins, "Report No. FHWA/MT-01-002/99160-1A: Mechanistic-Empirical Modeling and Design Model Development of Geosynthetic Reinforced Flexible Pavements," Montana Department of Transportation, Helena, MT, 2001.

[76] Y. Dafalias and L. Herrmann, "Bounding Surface Plasticity II: Application to Isotropic Cohesive Soils," *Journal of Engineering Mechanics,* vol. 112, no. 12, p. 1263–1291, 1986.

[77] J. Leng and M. Gabr, "Numerical Analysis of Stress–Deformation Response in Reinforced Unpaved Road Sections," *Geosynthetics International,* vol. 12, no. 2, p. 111–119, 2005.

[78] I. Howard and K. Warren, "Finite Element Modeling Approach for Flexible Pavements with Geosynthetics," in *GeoCongress 2006: Geotechnical Engineering in the Information Technology Age*, Atlanta, GA, 2006.

[79] B. Saad, H. Mitri and H. Poorooshasb, "Three-Dimensional Dynamic Analysis of Flexible Conventional Pavement Foundation," *Journal of Transportation Engineering,* vol. 131, no. 6, p. 460–469, 2005.

[80] S. Perkins, B. Christopher, E. Cuelho, G. Eiksund, C. Schwartz and G. Svanø, "A Mechanistic–Empirical Model for Base-Reinforced Flexible Pavements," *International Journal of Pavement Engineering,* vol. 10, no. 2, p. 101–114, 2009.

[81] I. Al-Qadi, J. Kwon and E. Tutumluer, "Validated Mechanistic Model for Geogrid Base Reinforced Flexible Pavements," *Journal of Transportation Engineering,* vol. 135, no. 12, pp. 915-926, 2009.

[82] H. Taherkhani and M. Jalali, "Determination of the Visco-Elastic Properties of Asphaltic Mixtures for Finite Element Modeling In ABAQUS," *Roads,* vol. 24, no. 89, p. 219–236, 2016.

[83] Z. Yin, K. Ndiema, R. Lekalpure and C. Kiptum, "Numerical Study of Geotextile-Reinforced Flexible Pavement Overlying Low-Strength Subgrade," *Applied Science,* vol. 12, no. 20, p. 10325, 2022.

[84] S. Chhetri and P. Deb, "Finite Element Analysis of Geogrid-Incorporated Flexible Pavement with Soft Subgrade," *Applied Science,* vol. 14, no. 13, p. 5798, 2024.

[85] S. Kim, M. Won and B. McCullough, "Dynamic Stress Response of Concrete Pavements to Moving Tandem-Axle Loads," *Transportation Research Record,* vol. 1809, no. 1, p. 32–41, 2002.

[86] M. Nazzal, Laboratory Characterization and Numerical Modeling of Geogrid Reinforced Bases in Flexible Pavements, Baton Rouge, LA: Louisiana State University, 2007.

[87] M. Zadehmohamad, N. Luo, M. Abu-Farsakh and G. Voyiadjis, "Evaluating Long-Term Benefits of Geosynthetics in Flexible Pavements Built Over Weak Subgrades by Finite Element and Mechanistic-Empirical Analyses," *Geotextiles and Geomembranes,* vol. 50, no. 3, pp. 455-469, 2022.

[88] S. Perkins, "Report No. DTFH61-01-X-00068: Evaluation of Geosynthetic Reinforced Flexible Pavement Systems Using Two Pavement Test Facilities," U.S. Department of Transportation, Federal Highway Administration, Washington, D.C., 2002.

[89] J. Collin, T. Kinney and X. Fu, "Full Scale Highway Load Test of Flexible Pavement Systems with Geogrid-Reinforced Base Courses," *Geosynthetics International,* vol. 3, no. 4, pp. 537-549, 1996.

Appendix A

Values of Traffic Benefit Ratio (TBR)

The TBR values for all cases are presented in the following tables and figures.

Table 19. TBR values for low volume roads (asphalt thickness of 3.5 in.)

Type	Gesy. Stiffness	Base Thickness (in.)	TBR								
			Weak subgrade			Medium stiff subgrade			Stiff subgrade		
			0.5 in.	0.75 in.	1 in.	0.5 in.	0.75 in.	1 in.	0.5 in.	0.75 in.	1 in.
Geogrid	High tensile stiffness	8	2.30	2.88	3.38	1.75	2.05	2.57	1.24	1.32	1.55
		10	3.55	4.73	5.30	2.70	3.35	4.03	1.63	2.18	2.44
		12	2.73	3.51	4.12	2.12	2.57	3.13	1.34	1.61	1.90
		14	1.59	1.88	2.10	1.33	1.56	1.62	1.25	1.45	1.58
	Medium tensile stiffness	8	2.55	3.84	4.55	1.94	2.92	3.46	1.75	1.98	2.09
		10	3.98	6.05	7.80	3.02	4.78	5.45	1.83	2.78	3.59
		12	3.12	4.05	5.12	2.37	3.21	3.89	1.44	1.86	2.36
		14	1.91	2.26	2.64	1.45	1.72	2.00	1.34	1.45	1.58
	Low tensile stiffness	8	2.83	4.10	4.63	2.15	3.12	3.52	1.82	2.01	2.53
		10	4.54	6.50	8.90	3.45	4.94	5.90	2.09	2.99	3.96
		12	3.48	4.56	5.37	2.64	3.47	4.08	1.60	2.10	2.47
		14	2.43	2.71	2.99	1.85	2.06	2.27	1.34	1.45	1.58
Geotextile	High tensile stiffness	8	1.85	2.01	2.37	1.46	1.59	1.87	1.43	1.64	1.73
		10	2.86	3.23	3.85	2.26	2.55	3.04	1.56	1.78	2.01
		12	1.98	2.32	2.96	1.56	1.83	2.34	1.40	1.56	1.85
		14	1.53	1.78	2.12	1.21	1.41	1.67	1.35	1.45	1.74
	Medium tensile stiffness	8	2.20	2.78	3.10	1.74	2.20	2.45	1.55	1.83	1.95
		10	3.99	4.75	5.40	3.15	3.75	4.27	2.00	2.38	2.70
		12	2.32	2.96	3.60	1.83	2.34	2.84	1.52	1.98	2.12
		14	1.70	2.10	2.50	1.34	1.66	1.98	1.35	1.45	1.74
	Low tensile stiffness	8	2.41	2.92	3.25	1.90	2.31	2.57	1.73	1.89	1.93
		10	4.09	5.08	5.92	3.23	3.90	4.45	2.05	2.54	2.96
		12	2.43	3.12	3.89	1.92	2.85	3.12	1.78	1.92	2.33
		14	1.88	2.53	2.87	1.49	2.00	2.27	1.35	1.45	1.74

Table 20. TBR values for medium volume roads (asphalt thickness of 6.5 in.)

Type	Gesy. Stiffness	Base Thickness (in.)	TBR								
			Weak subgrade			Medium stiff subgrade			Stiff subgrade		
			0.5 in.	0.75 in.	1 in.	0.5 in.	0.75 in.	1 in.	0.5 in.	0.75 in.	1 in.
Geogrid	High tensile stiffness	8	4.15	4.79	5.69	3.47	4.06	4.84	2.00	2.33	2.82
		10	3.53	3.97	4.38	3.09	3.64	3.96	1.97	2.16	2.48
		12	2.57	2.86	3.28	2.30	2.70	2.93	1.73	1.76	1.90
		14	2.52	2.69	2.70	2.24	2.42	2.50	1.65	1.66	1.66
	Medium tensile stiffness	8	3.51	4.26	5.19	3.00	3.75	4.31	1.82	2.20	2.78
		10	2.66	3.57	4.03	2.37	3.23	3.76	1.76	1.99	2.40
		12	1.94	2.33	2.69	1.86	2.13	2.50	1.64	1.77	2.24
		14	1.78	1.94	1.95	1.64	1.81	1.86	1.49	1.70	1.71
	Low tensile stiffness	8	2.72	3.00	3.36	2.29	2.56	2.97	1.70	1.96	1.99
		10	1.98	2.10	2.22	1.89	1.96	2.20	1.48	1.88	1.87
		12	1.79	1.83	1.79	1.61	1.70	1.70	1.50	1.67	1.70
		14	1.52	1.61	1.64	1.49	1.54	1.60	1.46	1.49	1.53
Geotextile	High tensile stiffness	8	3.03	3.40	4.13	2.60	2.85	3.47	1.87	2.22	2.51
		10	2.56	2.76	3.32	2.21	2.53	2.95	1.88	2.15	2.42
		12	2.13	2.49	2.74	1.98	2.21	2.52	1.66	1.70	1.97
		14	1.97	2.20	2.48	1.96	2.04	2.13	1.61	1.64	1.65
	Medium tensile stiffness	8	2.47	2.83	3.60	1.95	2.43	3.01	1.81	2.06	2.35
		10	2.01	2.95	3.31	1.82	2.33	2.81	1.74	1.89	2.23
		12	1.80	1.97	2.39	1.62	1.87	2.20	1.61	1.73	2.06
		14	1.74	1.79	1.87	1.62	1.66	1.76	1.60	1.66	1.70
	Low tensile stiffness	8	2.38	2.81	3.26	2.01	2.39	2.81	1.63	1.74	1.88
		10	1.97	2.01	2.17	1.86	1.91	2.14	1.45	1.50	1.76
		12	1.74	1.77	1.82	1.50	1.59	1.70	1.44	1.52	1.59
		14	1.51	1.51	1.54	1.46	1.50	1.52	1.44	1.47	1.49

Table 21. TBR values for high volume roads (asphalt thickness of 10 in.)

Type	Gesy. Stiffness	Base Thickness (in.)	TBR								
			Weak subgrade			Medium stiff subgrade			Stiff subgrade		
			0.5 in.	0.75 in.	1 in.	0.5 in.	0.75 in.	1 in.	0.5 in.	0.75 in.	1 in.
Geogrid	High tensile stiffness	8	2.98	3.63	4.55	2.24	2.69	3.30	1.70	1.87	2.10
		10	2.77	3.23	3.64	2.12	2.55	2.99	1.57	1.73	2.00
		12	1.98	2.30	2.70	1.89	2.28	2.66	1.50	1.69	1.81
		14	2.00	2.18	2.20	1.78	1.98	2.11	1.41	1.61	1.74
	Medium tensile stiffness	8	2.64	3.40	4.34	2.14	2.56	2.81	1.60	1.74	1.94
		10	2.09	2.87	3.35	2.00	2.40	2.86	1.46	1.75	1.89
		12	1.98	2.24	2.52	1.80	2.13	2.44	1.41	1.64	1.85
		14	1.62	1.80	1.90	1.57	1.68	1.74	1.34	1.51	1.64
	Low tensile stiffness	8	2.50	2.79	3.36	2.02	2.26	2.70	1.63	1.80	2.00
		10	1.76	1.88	2.20	1.67	1.77	1.98	1.42	1.64	1.85
		12	1.57	1.61	1.78	1.38	1.56	1.67	1.32	1.42	1.45
		14	1.23	1.46	1.56	1.21	1.26	1.38	1.19	1.22	1.24
Geotextile	High tensile stiffness	8	2.73	3.11	3.84	2.09	2.54	3.09	1.54	1.74	1.85
		10	2.27	2.47	3.03	1.93	2.26	2.80	1.44	1.65	1.83
		12	1.82	2.19	2.45	1.77	2.06	2.47	1.37	1.57	1.75
		14	1.67	1.90	2.18	1.57	1.74	1.84	1.30	1.50	1.60
	Medium tensile stiffness	8	2.35	2.55	3.33	1.84	2.18	2.56	1.51	1.66	1.86
		10	1.73	2.20	2.54	1.67	2.05	2.48	1.44	1.64	1.82
		12	1.51	1.71	2.11	1.49	1.68	1.89	1.36	1.59	1.79
		14	1.45	1.58	1.72	1.41	1.50	1.62	1.29	1.44	1.58
	Low tensile stiffness	8	2.32	2.54	2.99	1.88	2.15	2.59	1.55	1.67	1.89
		10	1.69	1.74	1.90	1.56	1.64	1.85	1.35	1.60	1.79
		12	1.46	1.52	1.73	1.36	1.49	1.55	1.27	1.40	1.43
		14	1.19	1.39	1.52	1.17	1.21	1.24	1.16	1.19	1.21

Figure 70. TBR variations with base thickness for pavements reinforced with a high stiffness single layer of geosynthetic on weak subgrade for low volume roads

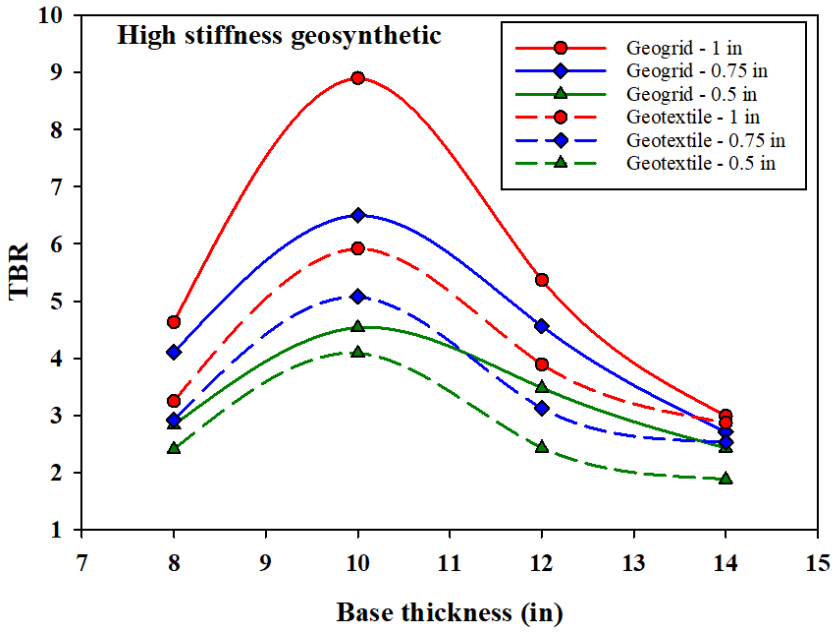

Figure 71. TBR variations with base thickness for pavements reinforced with a medium stiffness single layer of geosynthetic on weak subgrade for low volume roads

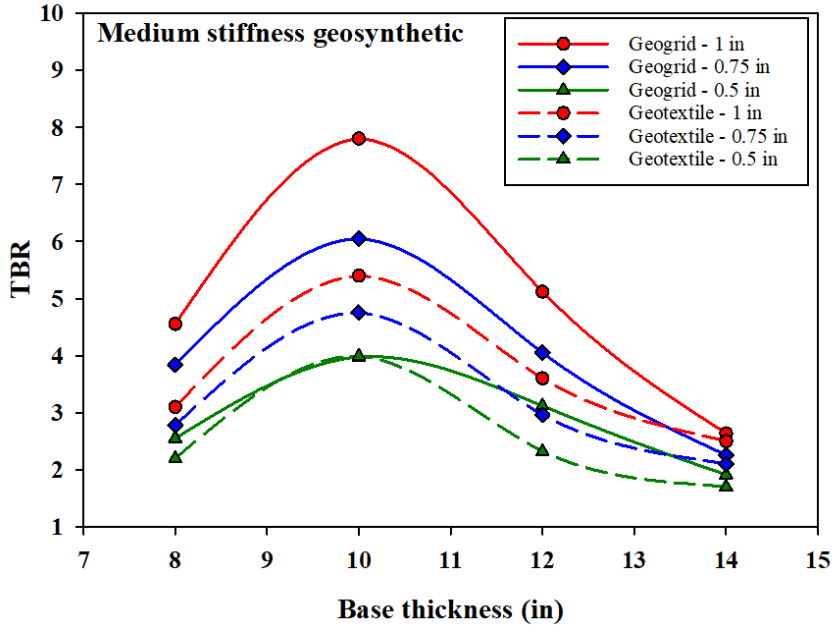

Figure 72. TBR variations with base thickness for pavements reinforced with a low stiffness single layer of geosynthetic on weak subgrade for low volume roads

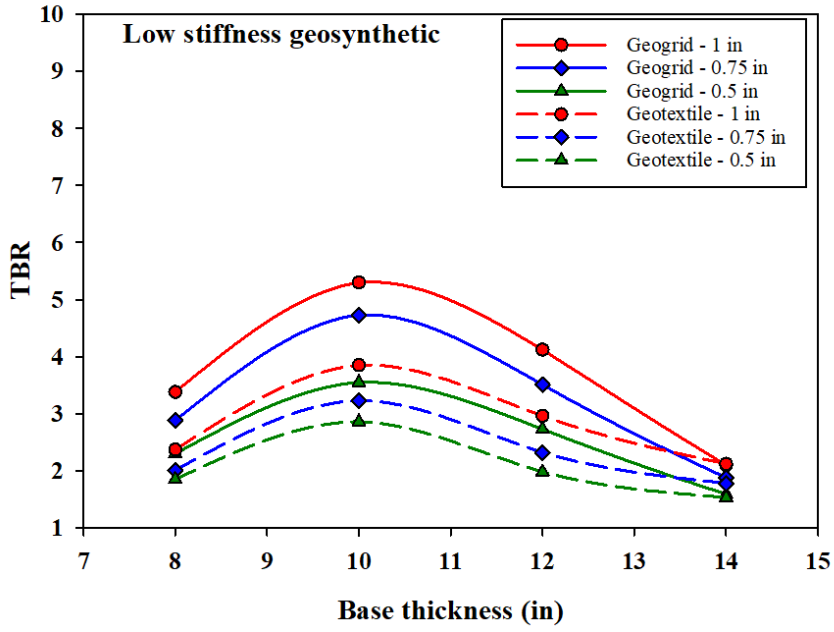

Figure 73. TBR variations with base thickness for pavements reinforced with a high stiffness single layer of geosynthetic on medium-stiff subgrade for low volume roads

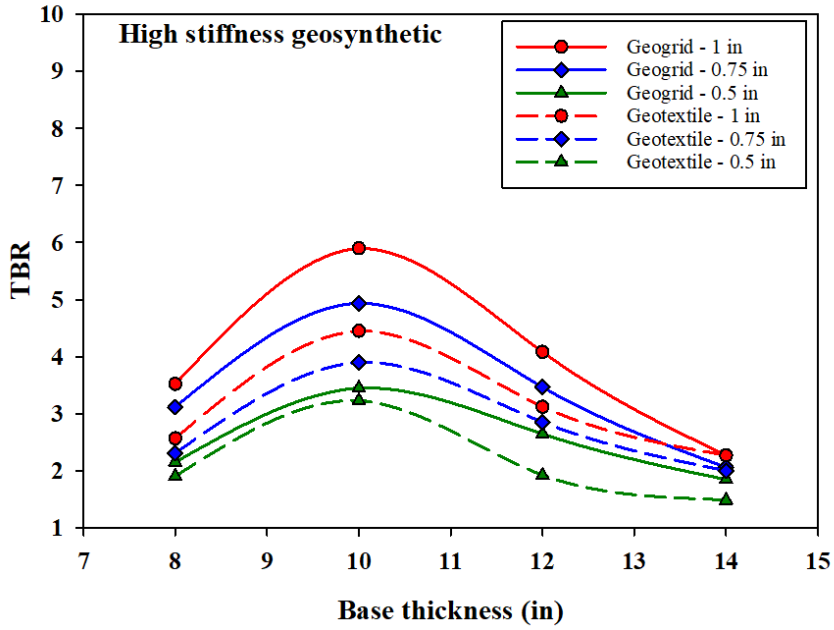

Figure 74. TBR variations with base thickness for pavements reinforced with a medium stiffness single layer of geosynthetic on medium-stiff subgrade for low volume roads

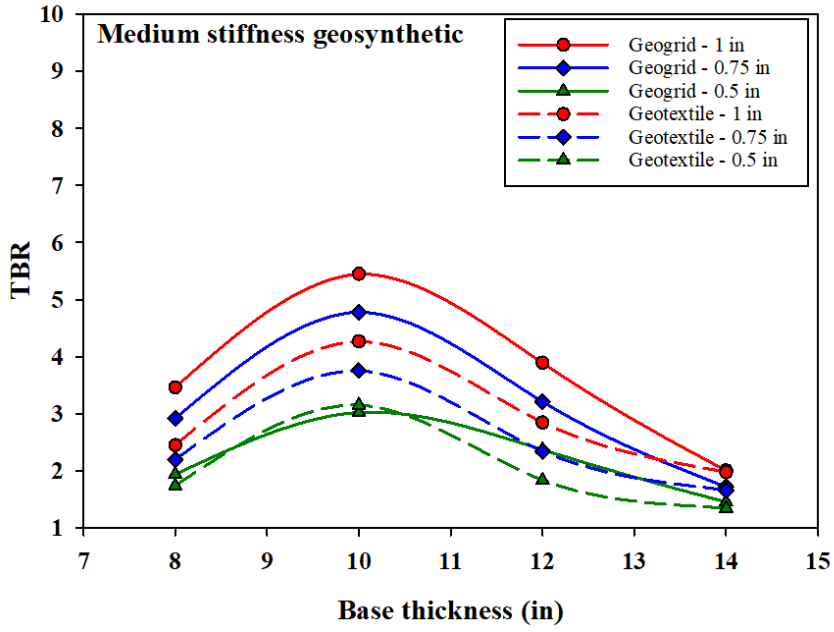

Figure 75. TBR variations with base thickness for pavements reinforced with a low stiffness single layer of geosynthetic on medium-stiff subgrade for low volume roads

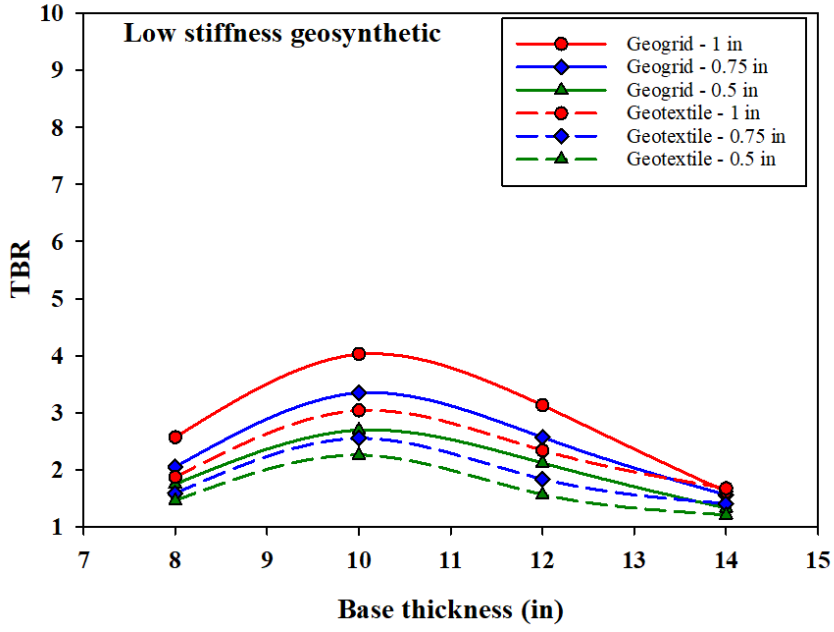

Figure 76. TBR variations with base thickness for pavements reinforced with a high stiffness single layer of geosynthetic on stiff subgrade for low volume roads

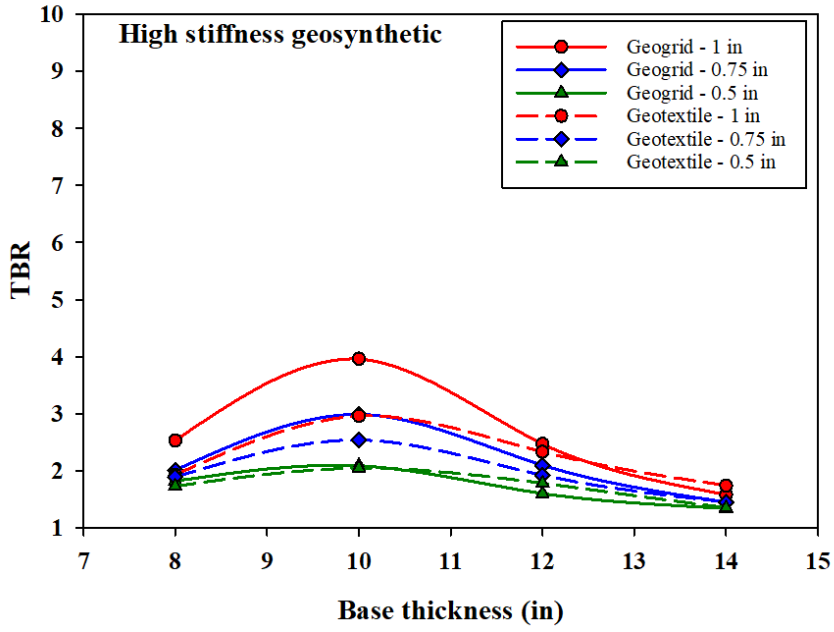

Figure 77. TBR variations with base thickness for pavements reinforced with a medium stiffness single layer of geosynthetic on stiff subgrade for low volume roads

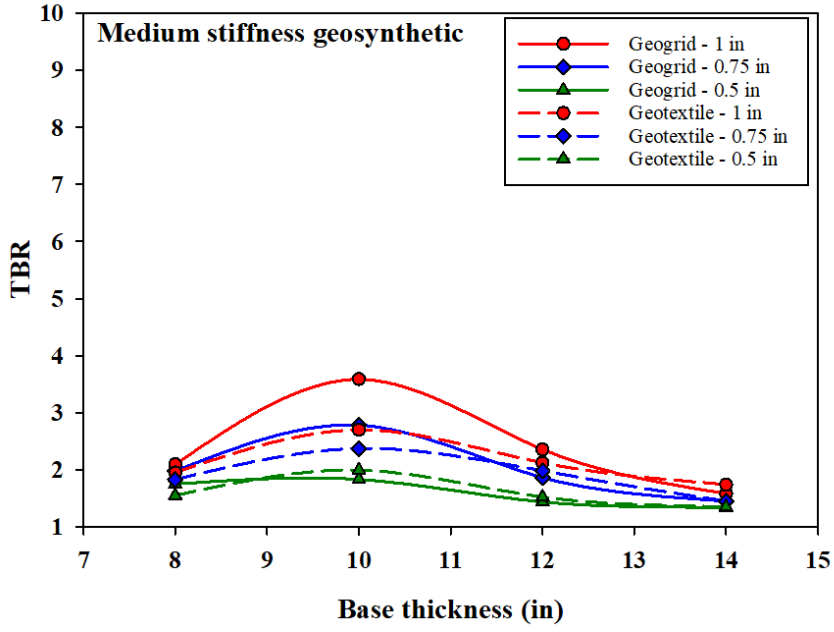

Figure 78. TBR variations with base thickness for pavements reinforced with a low stiffness single layer of geosynthetic on stiff subgrade for low volume roads

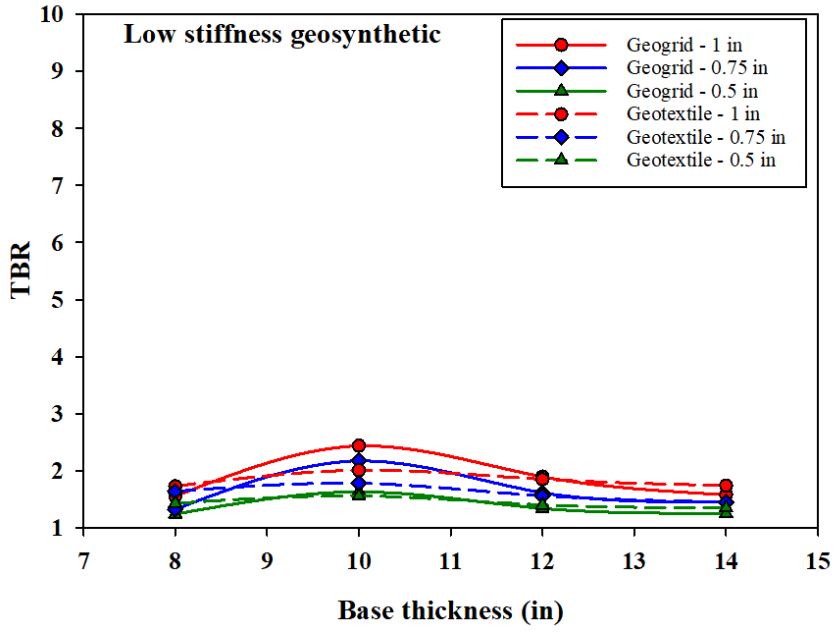

Figure 79. TBR variations with base thickness for pavements reinforced with a high stiffness single layer of geosynthetic on weak subgrade for medium volume roads

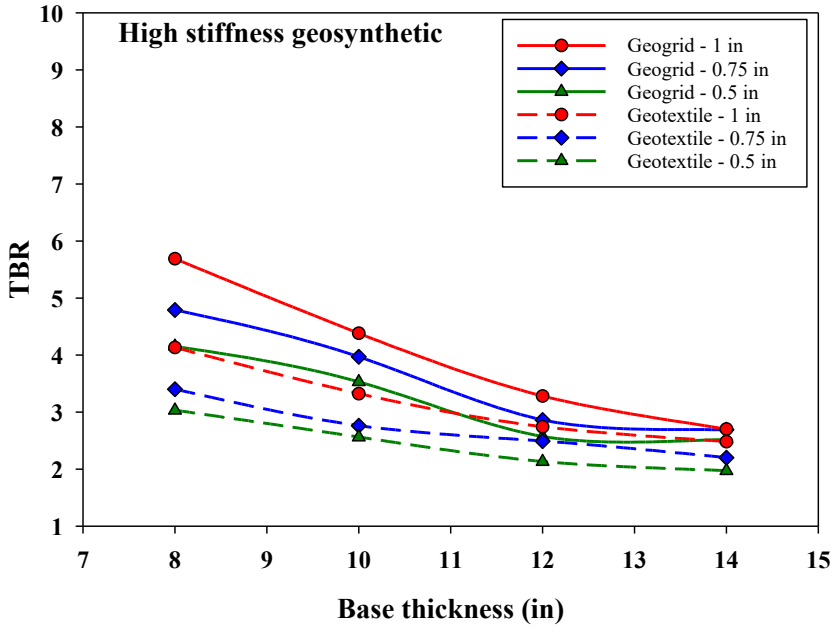

Figure 80. TBR variations with base thickness for pavements reinforced with a medium stiffness single layer of geosynthetic on weak subgrade for medium roads

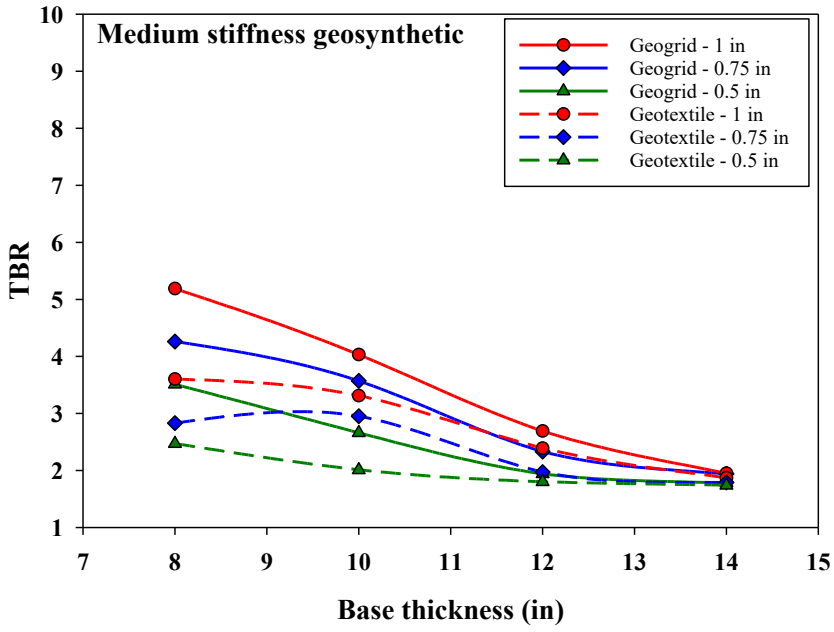

Figure 81. TBR variations with base thickness for pavements reinforced with a low stiffness single layer of geosynthetic on weak subgrade for medium volume roads

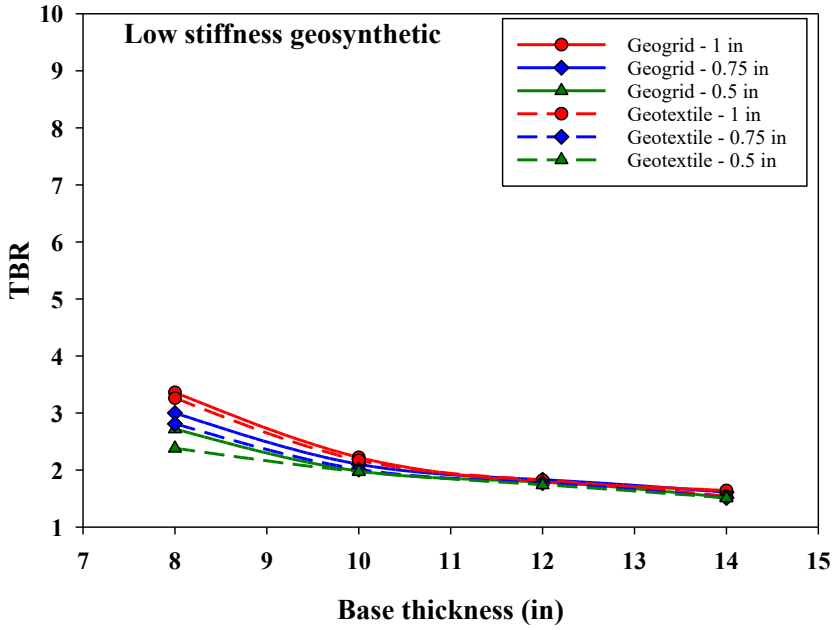

Figure 82. TBR variations with base thickness for pavements reinforced with a high stiffness single layer of geosynthetic on medium-stiff subgrade for medium volume roads

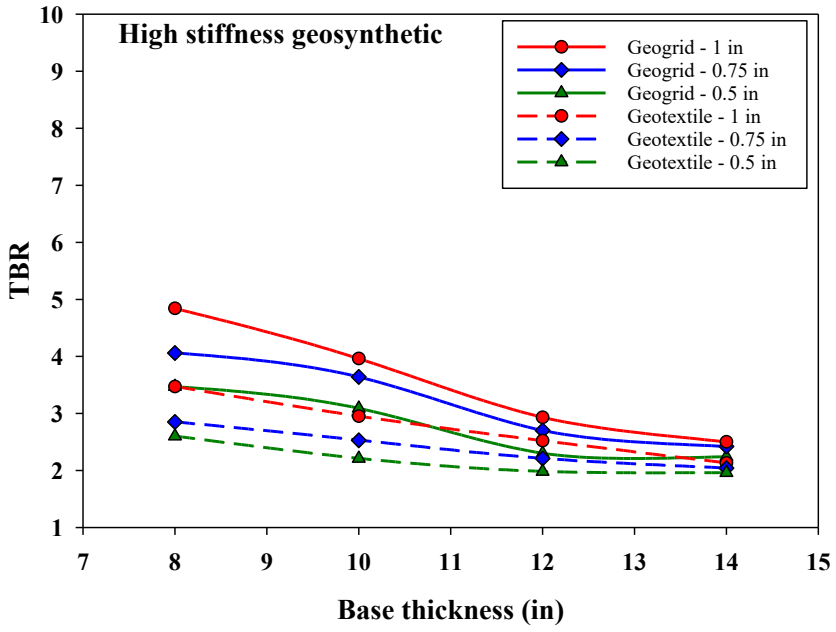

Figure 83. TBR variations with base thickness for pavements reinforced with a medium stiffness single layer of geosynthetic on medium-stiff subgrade for medium volume roads

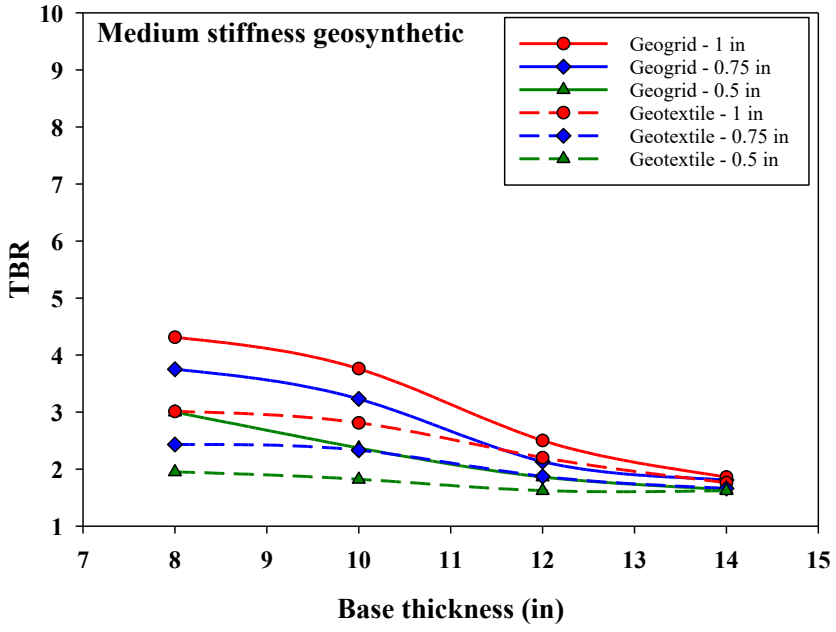

Figure 84. TBR variations with base thickness for pavements reinforced with a low stiffness single layer of geosynthetic on medium-stiff subgrade for medium volume roads

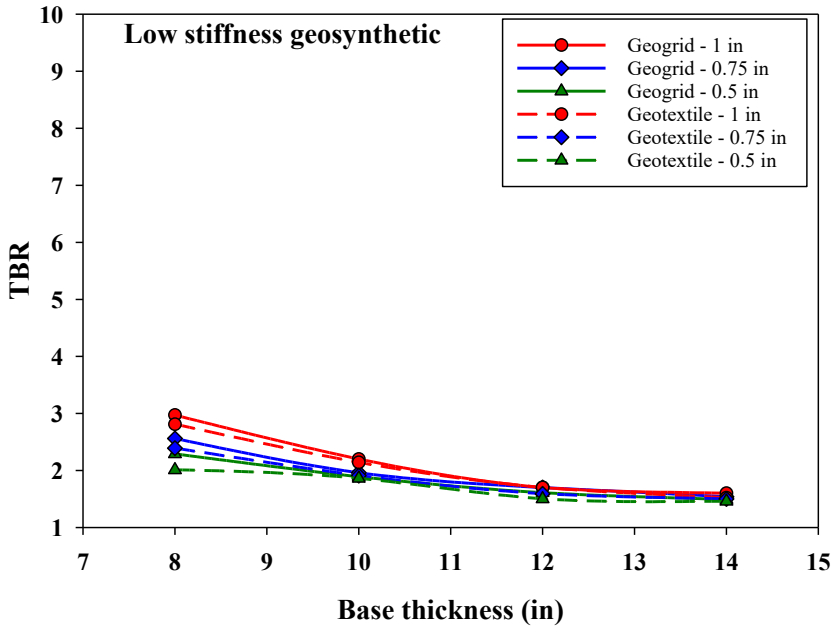

Figure 85. TBR variations with base thickness for pavements reinforced with a high stiffness single layer of geosynthetic on stiff subgrade for medium volume roads

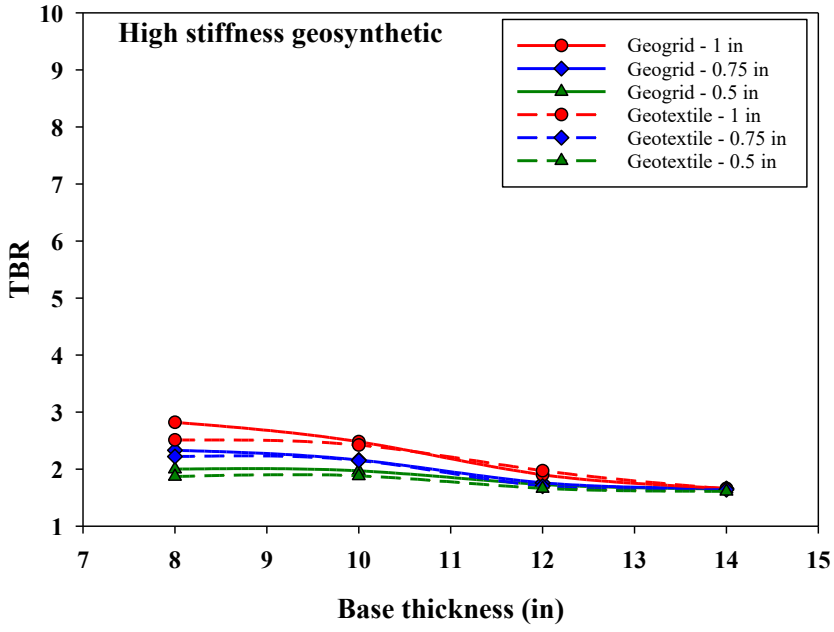

Figure 86. TBR variations with base thickness for pavements reinforced with a medium stiffness single layer of geosynthetic on stiff subgrade for medium volume roads

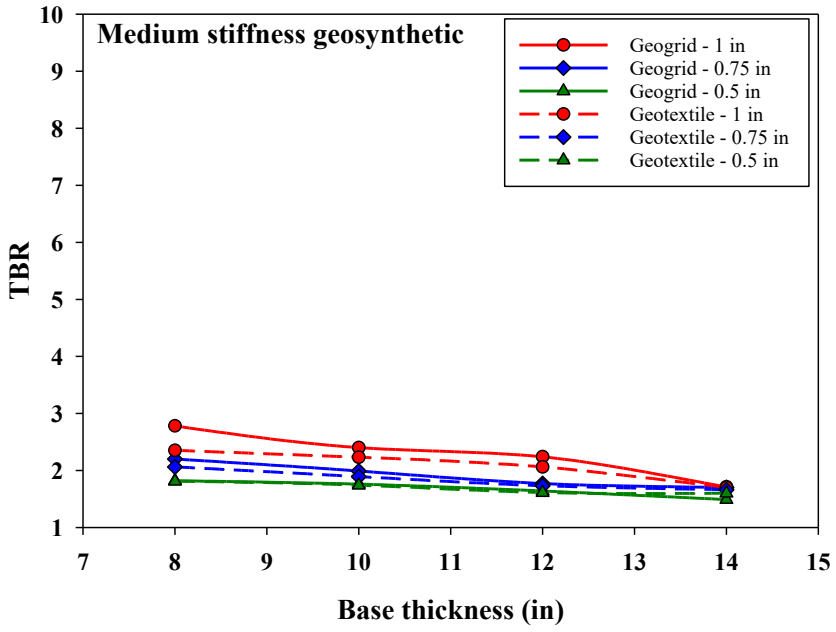

Figure 87. TBR variations with base thickness for pavements reinforced with a low stiffness single layer of geosynthetic on stiff subgrade for low medium volume roads

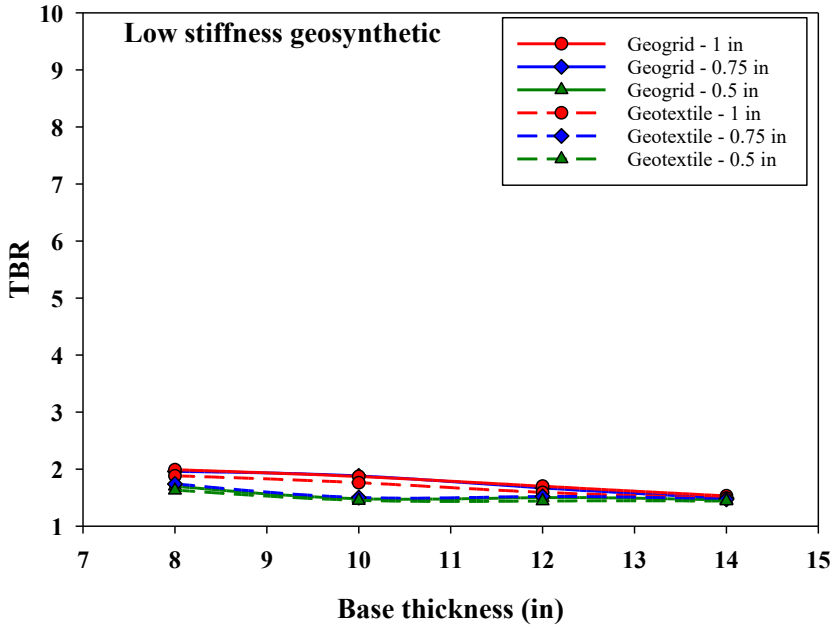

Figure 88. TBR variations with base thickness for pavements reinforced with a high stiffness single layer of geosynthetic on weak subgrade for high volume roads

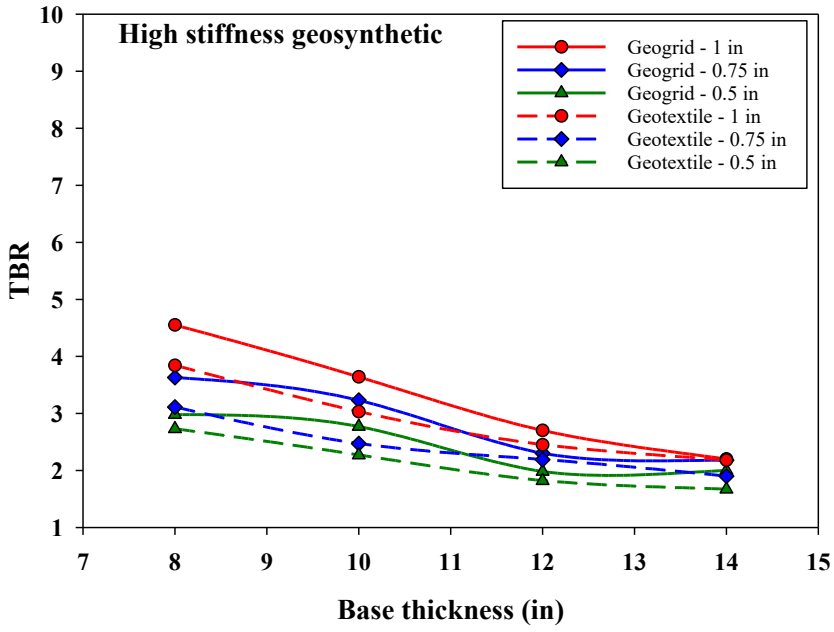

Figure 89. TBR variations with base thickness for pavements reinforced with a medium stiffness single layer of geosynthetic on weak subgrade for high volume roads

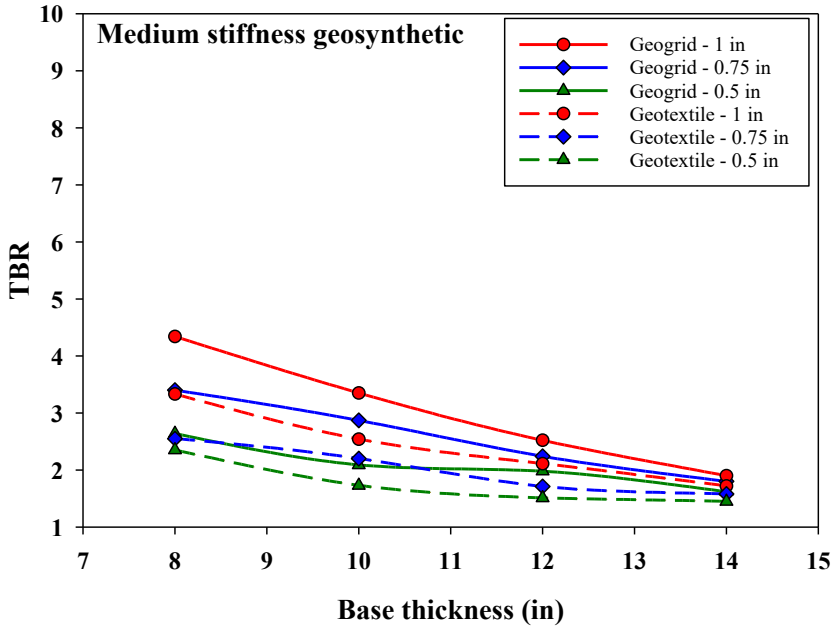

Figure 90. TBR variations with base thickness for pavements reinforced with a low stiffness single layer of geosynthetic on weak subgrade for high volume roads

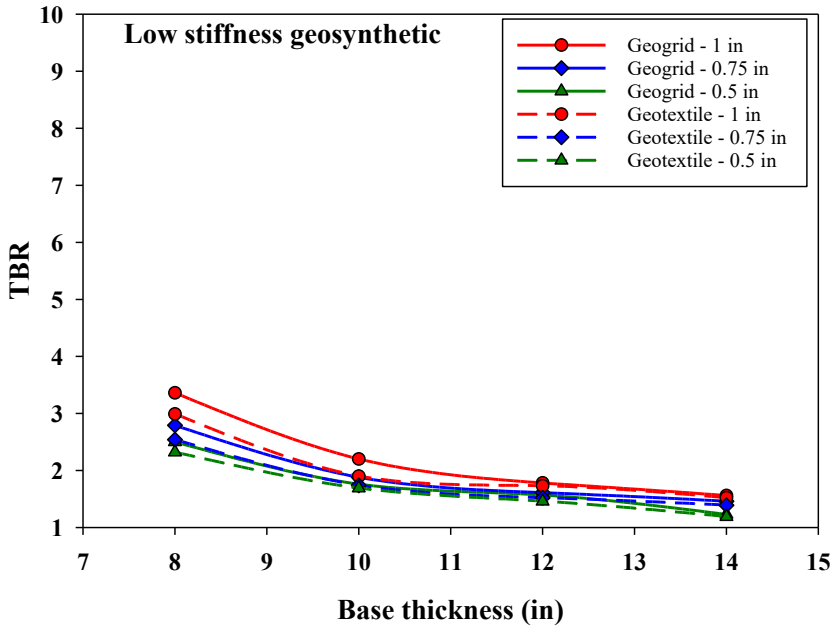

Figure 91. TBR variations with base thickness for pavements reinforced with a high stiffness single layer of geosynthetic on medium-stiff subgrade for high volume roads

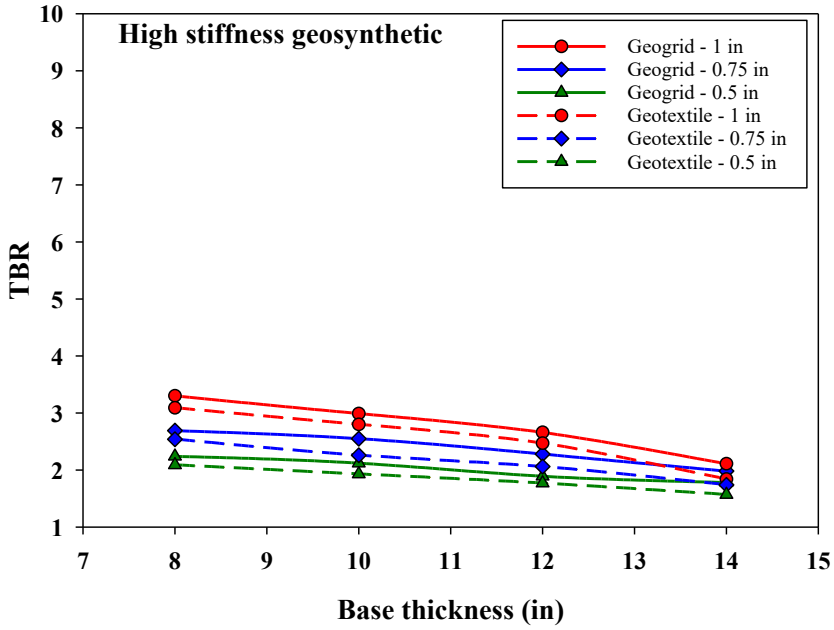

Figure 92. TBR variations with base thickness for pavements reinforced with a medium stiffness single layer of geosynthetic on medium-stiff subgrade for high volume roads

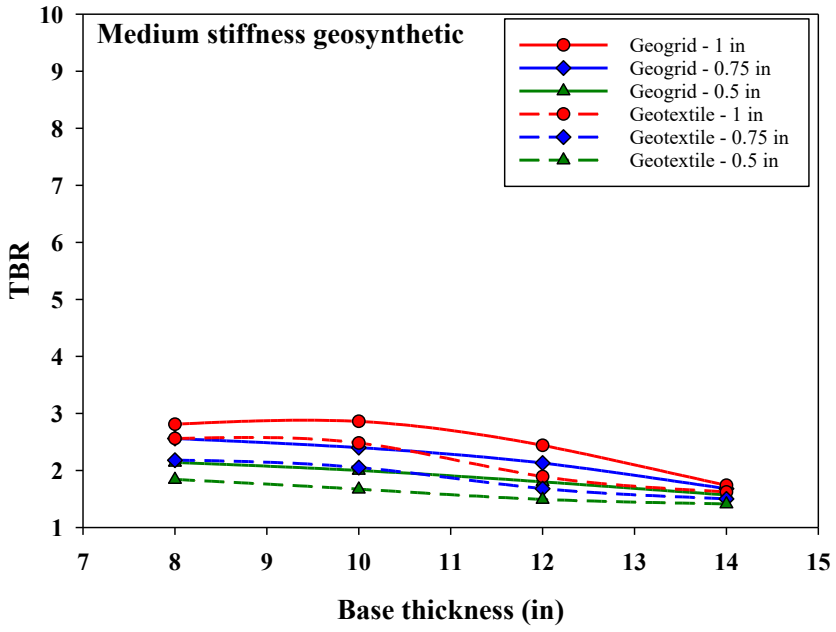

Figure 93. TBR variations with base thickness for pavements reinforced with a low stiffness single layer of geosynthetic on medium-stiff subgrade for high volume roads

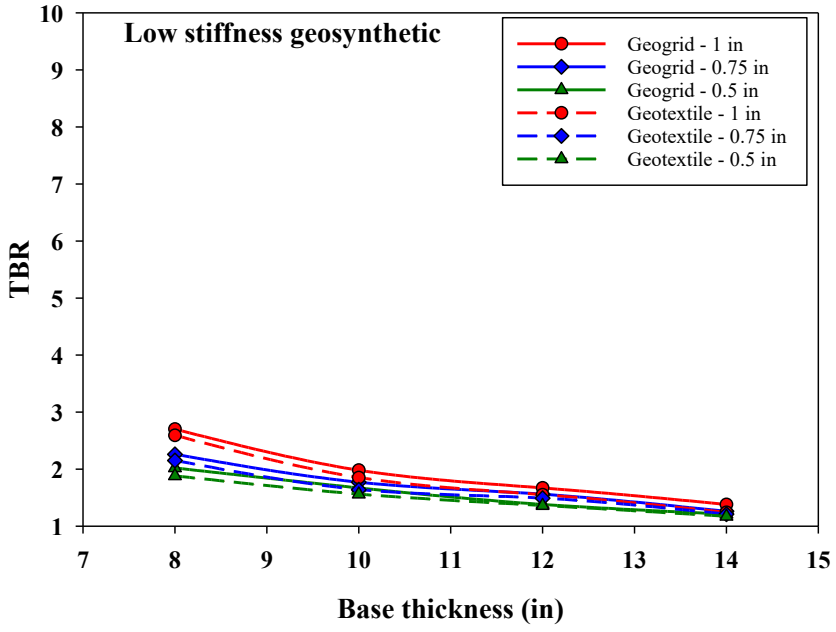

Figure 94. TBR variations with base thickness for pavements reinforced with a high stiffness single layer of geosynthetic on stiff subgrade for high volume roads

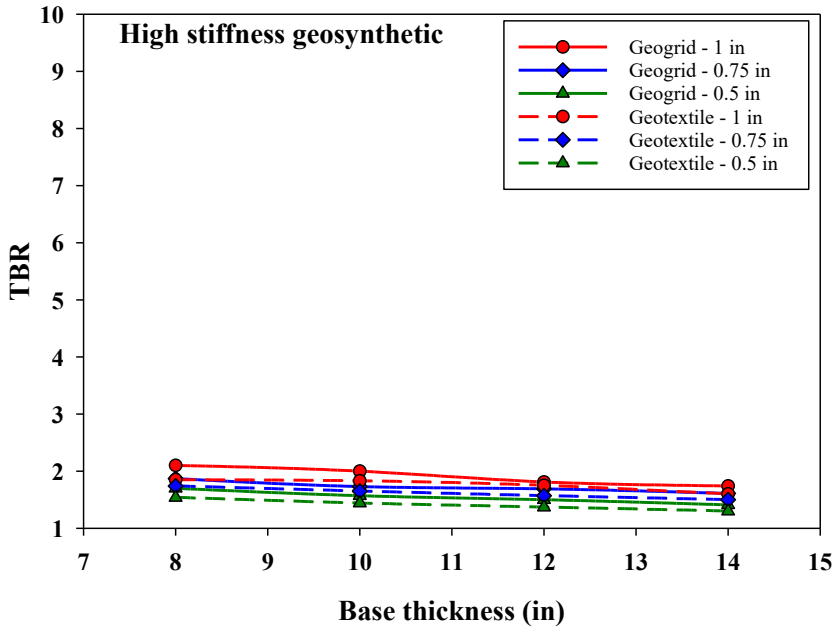

Figure 95. TBR variations with base thickness for pavements reinforced with a medium stiffness single layer of geosynthetic on stiff subgrade for high volume roads

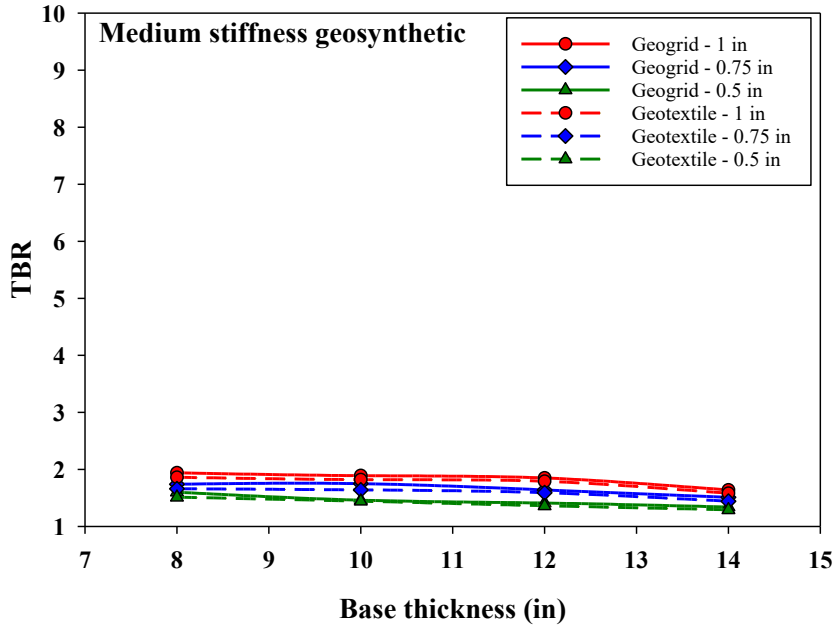

Figure 96. TBR variations with base thickness for pavements reinforced with a low stiffness single layer of geosynthetic on stiff subgrade for high volume roads

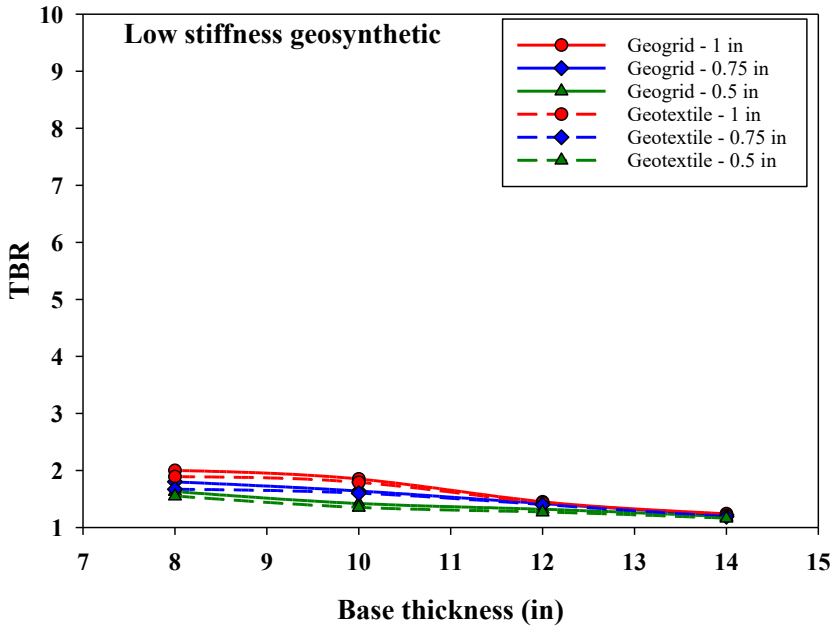

Appendix B

Increase in Effective Resilient Modulus ($M_{R\text{-}eff}$) Values

The percentage increase in effective resilient modulus ($M_{R\text{-}eff}$) values for all cases are presented in the following tables.

Table 22. Increase in $M_{R\text{-}eff}$ values for low volume roads (asphalt thickness of 3.5 in.)

Type	Gesy. Stiffness	Base Thickness (in.)	Increase in $M_{R\text{-}eff}$ %								
			Weak subgrade			Medium stiff subgrade			Stiff subgrade		
			0.5 in.	0.75 in.	1 in.	0.5 in.	0.75 in.	1 in.	0.5 in.	0.75 in.	1 in.
Geogrid	High tensile stiffness	8	94	136	155	81	122	138	29	44	65
		10	126	192	227	114	173	207	38	67	100
		12	103	145	173	82	132	153	32	47	67
		14	67	77	100	58	70	87	21	27	36
	Medium tensile stiffness	8	77	122	140	65	104	122	24	42	47
		10	109	179	228	95	158	196	33	61	80
		12	93	124	163	76	109	138	28	39	57
		14	44	70	83	35	57	69	15	22	28
	Low tensile stiffness	8	57	89	105	48	67	88	17	27	35
		10	85	126	143	73	104	119	25	42	50
		12	72	111	133	55	87	103	21	34	41
		14	28	42	61	22	35	48	9	19	25
Geotextile	High tensile stiffness	8	77	122	136	58	87	93	24	35	47
		10	105	171	218	93	127	145	32	52	74
		12	91	121	148	64	94	97	26	33	47
		14	46	67	83	42	49	66	17	19	27
	Medium tensile stiffness	8	62	87	94	50	73	83	17	32	37
		10	98	130	143	75	116	127	27	48	58
		12	65	89	117	55	77	97	21	31	44
		14	31	50	61	22	42	52	12	17	22
	Low tensile stiffness	8	44	62	72	34	42	52	13	18	21
		10	69	106	123	54	70	89	21	31	36
		12	55	75	92	38	53	64	17	22	28
		14	22	33	48	17	24	31	8	14	20

Table 23. Increase in $M_{R\text{-}eff}$ values for medium volume roads (asphalt thickness of 6.5 in.)

Type	Gesy. Stiffness	Base Thickness (in.)	Increase in $M_{R\text{-}eff}$ %								
			Weak subgrade			Medium stiff subgrade			Stiff subgrade		
			0.5 in.	0.75 in.	1 in.	0.5 in.	0.75 in.	1 in.	0.5 in.	0.75 in.	1 in.
Geogrid	High tensile stiffness	8	115	171	206	106	164	194	34	62	91
		10	105	150	195	84	125	170	30	58	81
		12	85	119	126	75	95	116	22	38	49
		14	68	82	92	58	74	84	13	20	26
	Medium tensile stiffness	8	106	170	184	92	133	164	32	46	62
		10	94	131	176	74	104	118	28	42	52
		12	65	82	107	55	73	84	11	36	56
		14	34	67	79	31	56	62	10	15	22
	Low tensile stiffness	8	62	90	113	53	74	95	22	26	36
		10	66	71	80	33	59	69	19	25	35
		12	51	62	66	36	48	56	9	22	29
		14	20	36	48	12	30	32	8	18	23
Geotextile	High tensile stiffness	8	92	148	185	76	115	129	31	54	75
		10	86	124	150	69	98	110	26	40	55
		12	78	104	110	54	73	77	18	21	34
		14	40	65	72	18	41	62	10	15	23
	Medium tensile stiffness	8	68	102	110	55	75	99	21	37	52
		10	67	84	107	50	66	84	18	32	46
		12	43	59	76	29	43	53	11	29	41
		14	29	39	46	12	33	41	9	15	17
	Low tensile stiffness	8	59	69	95	47	50	74	14	17	21
		10	57	62	66	43	45	60	13	15	20
		12	45	51	59	20	21	38	10	14	20
		14	20	29	41	12	21	29	7	13	19

Table 24. Increase in $M_{R\text{-}eff}$ values for high volume roads (asphalt thickness of 10 in.)

Type	Gesy. Stiffness	Base Thickness (in.)	Increase in $M_{R\text{-}eff}$ %								
			Weak subgrade			Medium stiff subgrade			Stiff subgrade		
			0.5 in.	0.75 in.	1 in.	0.5 in.	0.75 in.	1 in.	0.5 in.	0.75 in.	1 in.
Geogrid	High tensile stiffness	8	90	125	175	76	136	178	34	49	66
		10	88	120	163	72	111	142	28	43	63
		12	77	100	118	65	82	92	17	38	45
		14	58	67	76	43	54	62	8	14	22
	Medium tensile stiffness	8	87	115	136	80	103	124	23	37	45
		10	80	95	133	62	84	93	21	36	42
		12	60	72	86	54	63	80	10	35	40
		14	33	62	73	27	52	60	9	13	21
	Low tensile stiffness	8	56	63	67	42	47	63	19	24	31
		10	50	53	63	29	46	51	13	20	28
		12	31	39	48	23	33	36	7	17	21
		14	12	23	33	8	18	18	6	12	17
Geotextile	High tensile stiffness	8	85	119	173	61	94	111	24	39	55
		10	79	103	142	59	85	100	21	28	40
		12	73	90	102	38	72	74	11	18	32
		14	36	54	66	14	39	52	7	14	18
	Medium tensile stiffness	8	64	78	103	52	64	80	18	31	40
		10	59	72	85	47	61	72	15	25	37
		12	36	51	68	27	38	44	9	26	35
		14	25	34	41	11	24	36	7	13	16
	Low tensile stiffness	8	53	59	79	34	34	61	12	14	19
		10	46	47	51	27	30	47	11	12	17
		12	33	38	48	16	17	30	9	11	14
		14	13	22	35	8	16	20	7	10	17

Appendix C

Recommended Values of Equivalent Base Thickness (EBT)

The EBT values for all cases are presented in the following tables.

Table 25. Recommended EBT values for low volume roads (asphalt thickness of 3.5 in.)

Type	Gesy. Stiffness	Base Thickness (in.)	EBT (in.)								
			Weak subgrade			Medium stiff subgrade			Stiff subgrade		
			0.5 in.	0.75 in.	1 in.	0.5 in.	0.75 in.	1 in.	0.5 in.	0.75 in.	1 in.
Geogrid	High tensile stiffness	8	2*	2*	2*	2*	2*	2*	2*	2*	2*
		10	4*	4*	4*	4*	4*	4*	4*	4*	4*
		12	5.6	6*	6*	5.1	5.8	6*	4.7	5.4	6
		14	4.7	5.8	6.7	4.4	5.3	6.2	4.1	4.4	5.1
	Medium tensile stiffness	8	2*	2*	2*	2*	2*	2*	2*	2*	2*
		10	4*	4*	4*	4*	4*	4*	4	4*	4*
		12	5.4	6*	6*	4.3	5.5	6*	4.4	5.1	5.8
		14	4.4	5.5	6.4	3.7	5.1	5.9	3.8	4.5	4.9
	Low tensile stiffness	8	2*	2*	2*	2*	2*	2*	1.4	2*	2*
		10	4.7	5.9	7.2	4.2	4.5	5.1	2.8	3.7	4.5
		12	5	5.6	6*	3.9	4.8	5.3	4	4.7	5.2
		14	4	5.2	5.6	4	4.7	5.4	2.3	2.9	3.6
Geotextile	High tensile stiffness	8	2*	2*	2*	2*	2*	2*	2*	2*	2*
		10	4*	4*	4*	4	4*	4*	3.3	3.8	4*
		12	5.5	6*	6*	4.5	5.1	5.3	4	4.6	4.8
		14	4.7	5.5	5.9	4.1	4.8	5.1	2.7	3.2	4
	Medium tensile stiffness	8	2*	2*	2*	2*	2*	2*	2*	2*	2*
		10	4*	4*	4*	3.8	4*	4*	2.5	3.1	3.2
		12	5.1	5.8	6*	4.3	4.8	5.2	3.9	4.5	4.9
		14	4.2	4.6	5	3.7	4	4.3	2.8	3.2	3.9
	Low tensile stiffness	8	2*	2*	2*	2*	2*	2*	2*	2*	2*
		10	4*	4*	4*	3.4	3.7	4*	3	3.2	4
		12	4.8	5.1	5.6	3.9	4.2	4.9	3.3	3.4	4.2
		14	3.6	4.2	4.8	3.3	3.7	4.2	2.3	3.1	3.7

*EBT values to ensure that the base layer thickness of the geosynthetic-reinforced pavements is at least 6 in.

Table 26. Recommended EBT values for medium volume roads (asphalt thickness of 6.5 in.)

Type	Gesy. Stiffness	Base Thickness (in.)	EBT (in.)								
			Weak subgrade			Medium stiff subgrade			Stiff subgrade		
			0.5 in.	0.75 in.	1 in.	0.5 in.	0.75 in.	1 in.	0.5 in.	0.75 in.	1 in.
Geogrid	High tensile stiffness	8	2*	2*	2*	2*	2*	2*	2*	2*	2*
		10	4*	4*	4*	4*	4*	4*	3.9	4*	4*
		12	4.7	5.1	5.5	4.5	4.9	5.2	3.4	3.8	3.9
		14	4.5	4.7	4.8	3.8	4.2	4.7	3.4	3.6	3.4
	Medium tensile stiffness	8	2*	2*	2*	2*	2*	2*	2*	2*	2*
		10	4*	4*	4*	3.9	4*	4*	3.9	4	4*
		12	4	4.3	4.7	3.6	4.4	4.2	3.5	3.7	3.8
		14	3.2	3.8	4.2	2.7	3.8	3.9	2.7	2.8	3.2
	Low tensile stiffness	8	2*	2*	2*	2*	2*	2*	2*	2*	2*
		10	3.2	3.8	4*	3	3.4	3.9	2.6	3.2	3.7
		12	3.9	4.3	4.4	3.1	3.4	3.6	3	3.2	3.5
		14	3.1	3.3	3.8	2.6	2.9	3.4	2.5	2.9	3.3
Geotextile	High tensile stiffness	8	2*	2*	2*	2*	2*	2*	2*	2*	2*
		10	4*	4*	4*	3.6	4	4*	3.9	4*	4
		12	3.9	4.3	4.6	4.1	4.4	4.8	3.3	3.6	3.8
		14	3.3	3.9	4.4	2.9	3.2	3.3	2.3	2.8	2.9
	Medium tensile stiffness	8	2*	2*	2*	2*	2*	2*	2*	2*	2*
		10	3.8	4	4*	3.2	3.7	3.9	2.7	3.1	3.2
		12	3.4	3.8	4.2	3.4	3.7	4	2.7	3.1	3.4
		14	3	3.4	3.6	2.6	3	3.2	3	3.5	4.1
	Low tensile stiffness	8	2*	2*	2*	2*	2*	2*	2*	2*	2*
		10	3.4	3.5	3.8	2.6	2.9	3.1	2	2.3	3.5
		12	3	3.2	3.4	3	3.3	3.5	2.7	3.1	3.2
		14	2.5	2.6	2.9	2.4	2.6	2.8	2	2.5	2.8

*EBT values to ensure that the base layer thickness of the geosynthetic-reinforced pavements is at least 6 in.

Table 27. Recommended EBT values for high volume roads (asphalt thickness of 10 in.)

Type	Gesy. Stiffness	Base Thickness (in.)	EBT (in.)								
			Weak subgrade			Medium stiff subgrade			Stiff subgrade		
			0.5 in.	0.75 in.	1 in.	0.5 in.	0.75 in.	1 in.	0.5 in.	0.75 in.	1 in.
Geogrid	High tensile stiffness	8	2*	2*	2*	2*	2*	2*	2*	2*	2*
		10	3.8	4*	4*	3.2	3.6	4*	2.9	3.6	4*
		12	4.3	4.8	4.9	3.7	4.1	4.4	3.5	3.9	3.9
		14	3.8	4	4.2	3	3.4	3.6	3	3.1	3.3
	Medium tensile stiffness	8	2*	2*	2*	2*	2*	2*	2*	2*	2*
		10	2.7	2.8	3	2.6	2.8	3.1	2.5	2.5	3.3
		12	3.2	3.3	3.6	3.2	3.4	3.7	3.2	3.3	3.5
		14	3.8	4.7	4.8	2.7	3	3.8	2.8	3.1	3.3
	Low tensile stiffness	8	2*	2*	2*	2*	2*	2*	2*	2*	2*
		10	2.6	2.9	3.2	2.4	2.7	2.9	2.1	2.4	2.7
		12	2.7	3.1	3.4	2.6	2.8	3.2	2.4	2.6	2.8
		14	2.3	2.8	3.2	2.2	2.5	2.9	2.2	2.1	2.5
Geotextile	High tensile stiffness	8	2*	2*	2*	2*	2*	2*	2*	2*	2*
		10	3.6	3.7	4*	3.5	3.7	4	2.9	3.2	3.9
		12	3.3	3.6	3.7	2.8	3.2	3.5	3.3	3.5	3.9
		14	2.7	3.2	3.7	2.5	2.8	3.4	2.6	3	3.5
	Medium tensile stiffness	8	2*	2*	2*	2*	2*	2*	1.5	1.8	2*
		10	2.4	2.6	2.8	2.1	2.4	2.7	2.1	2.2	2.5
		12	2.8	3.1	3.4	2.7	2.8	2.9	2.8	3.1	3.3
		14	3.7	4	4.4	3.1	3.3	3.6	2.4	2.7	3
	Low tensile stiffness	8	2*	2*	2*	2*	2*	2*	1.8	2*	2*
		10	2.3	2.7	2.9	2.4	2.7	2.9	2.5	2.7	3.1
		12	2.2	2.5	2.7	2.1	2.4	2.6	2.4	2.6	2.9
		14	1.9	2.3	2.6	2	2.2	2.4	2.3	1.9	2.5

*EBT values to ensure that the base layer thickness of the geosynthetic-reinforced pavements is at least 6 in.

Appendix D

Values of Reduction Coefficients (α_b or α_s)

The rutting reduction coefficients for base and subgrade (α_b or α_s) values for all cases are presented in the following tables and figures.

Table 28. Values of rutting reduction coefficients for base (α_b)

Type	Gesy. Stiffness	Base Thickness (in.)	α_b								
			Weak subgrade			Medium stiff subgrade			Stiff subgrade		
			Low volume roads	Medium volume roads	High volume roads	Low volume roads	Medium volume roads	High volume roads	Low volume roads	Medium volume roads	High volume roads
Geogrid	High tensile stiffness	8	0.85	0.87	0.9	0.86	0.89	0.9	0.88	0.9	0.92
		10	0.84	0.87	0.9	0.86	0.89	0.91	0.87	0.91	0.92
		12	0.86	0.89	0.91	0.88	0.9	0.92	0.89	0.91	0.93
		14	0.88	0.89	0.92	0.89	0.9	0.92	0.89	0.91	0.93
	Medium tensile stiffness	8	0.86	0.89	0.92	0.87	0.9	0.93	0.87	0.91	0.94
		10	0.86	0.9	0.92	0.87	0.91	0.93	0.87	0.91	0.94
		12	0.87	0.91	0.93	0.88	0.92	0.94	0.89	0.92	0.95
		14	0.87	0.91	0.93	0.89	0.92	0.94	0.9	0.92	0.95
	Low tensile stiffness	8	0.86	0.9	0.93	0.87	0.9	0.94	0.87	0.92	0.95
		10	0.87	0.9	0.94	0.88	0.91	0.95	0.88	0.92	0.96
		12	0.88	0.91	0.95	0.88	0.92	0.96	0.89	0.93	0.97
		14	0.88	0.92	0.95	0.89	0.92	0.96	0.9	0.93	0.97
Geotextile	High tensile stiffness	8	0.86	0.89	0.92	0.87	0.9	0.93	0.88	0.91	0.94
		10	0.86	0.9	0.92	0.88	0.91	0.93	0.89	0.91	0.94
		12	0.87	0.9	0.93	0.88	0.91	0.94	0.89	0.92	0.95
		14	0.88	0.91	0.93	0.89	0.92	0.94	0.9	0.92	0.95
	Medium tensile stiffness	8	0.88	0.9	0.94	0.89	0.91	0.95	0.9	0.92	0.96
		10	0.88	0.9	0.94	0.89	0.91	0.95	0.9	0.92	0.96
		12	0.9	0.91	0.95	0.9	0.92	0.96	0.91	0.93	0.97
		14	0.9	0.91	0.95	0.9	0.92	0.96	0.91	0.92	0.97
	Low tensile stiffness	8	0.89	0.91	0.95	0.91	0.92	0.96	0.92	0.93	0.97
		10	0.89	0.91	0.95	0.91	0.92	0.96	0.92	0.93	0.97
		12	0.9	0.92	0.96	0.92	0.93	0.97	0.93	0.94	0.98
		14	0.91	0.92	0.96	0.92	0.93	0.97	0.93	0.94	0.98

Table 29. Values of rutting reduction coefficients for subgrade (α_s)

Type	Gesy. Stiffness	Base Thickness (in.)	α_s								
			Weak subgrade			Medium stiff subgrade			Stiff subgrade		
			Low volume roads	Medium volume roads	High volume roads	Low volume roads	Medium volume roads	High volume roads	Low volume roads	Medium volume roads	High volume roads
Geogrid	High tensile stiffness	8	0.76	0.79	0.86	0.78	0.8	0.86	0.8	0.82	0.87
		10	0.72	0.8	0.86	0.76	0.81	0.87	0.8	0.83	0.88
		12	0.78	0.81	0.87	0.8	0.82	0.88	0.83	0.83	0.89
		14	0.81	0.83	0.87	0.83	0.84	0.88	0.84	0.85	0.89
	Medium tensile stiffness	8	0.79	0.81	0.88	0.8	0.82	0.88	0.82	0.83	0.89
		10	0.76	0.82	0.88	0.78	0.83	0.89	0.82	0.84	0.89
		12	0.81	0.84	0.89	0.83	0.85	0.9	0.85	0.86	0.9
		14	0.83	0.86	0.9	0.85	0.86	0.91	0.86	0.86	0.91
	Low tensile stiffness	8	0.84	0.86	0.89	0.86	0.86	0.89	0.86	0.87	0.9
		10	0.83	0.86	0.89	0.86	0.86	0.9	0.86	0.88	0.9
		12	0.85	0.87	0.9	0.86	0.88	0.91	0.87	0.89	0.91
		14	0.86	0.87	0.91	0.86	0.88	0.92	0.88	0.89	0.92
Geotextile	High tensile stiffness	8	0.81	0.83	0.89	0.83	0.85	0.9	0.85	0.86	0.91
		10	0.77	0.85	0.89	0.8	0.86	0.9	0.83	0.87	0.91
		12	0.8	0.86	0.9	0.82	0.86	0.91	0.84	0.87	0.92
		14	0.82	0.86	0.91	0.83	0.87	0.92	0.85	0.88	0.93
	Medium tensile stiffness	8	0.83	0.84	0.91	0.85	0.86	0.92	0.86	0.86	0.92
		10	0.82	0.86	0.91	0.84	0.87	0.92	0.86	0.88	0.93
		12	0.83	0.86	0.92	0.85	0.87	0.92	0.86	0.88	0.93
		14	0.86	0.87	0.92	0.86	0.88	0.92	0.87	0.88	0.94
	Low tensile stiffness	8	0.86	0.86	0.92	0.87	0.86	0.93	0.88	0.88	0.94
		10	0.85	0.86	0.92	0.86	0.87	0.93	0.86	0.88	0.94
		12	0.86	0.87	0.93	0.87	0.88	0.94	0.88	0.89	0.95
		14	0.87	0.88	0.93	0.88	0.88	0.94	0.9	0.89	0.95

Figure 97. Values of rutting reduction coefficients for base and subgrade (α_b and α_s) for geogrid reinforced pavement with low traffic volume on weak subgrade

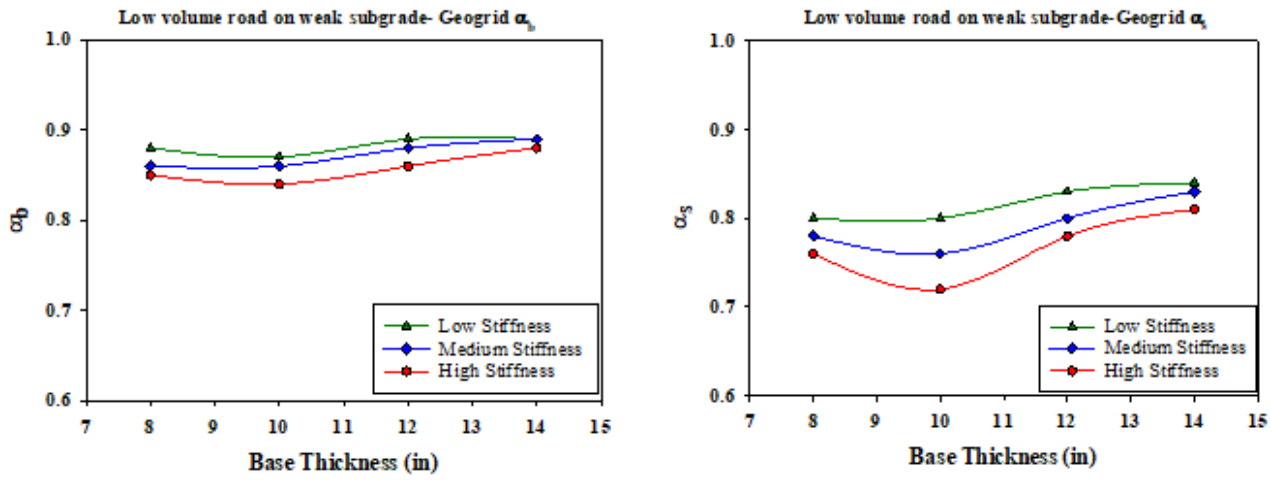

Figure 98. Values of rutting reduction coefficients for base and subgrade (α_b and α_s) for geogrid reinforced pavement with high traffic volume on medium stiff subgrade

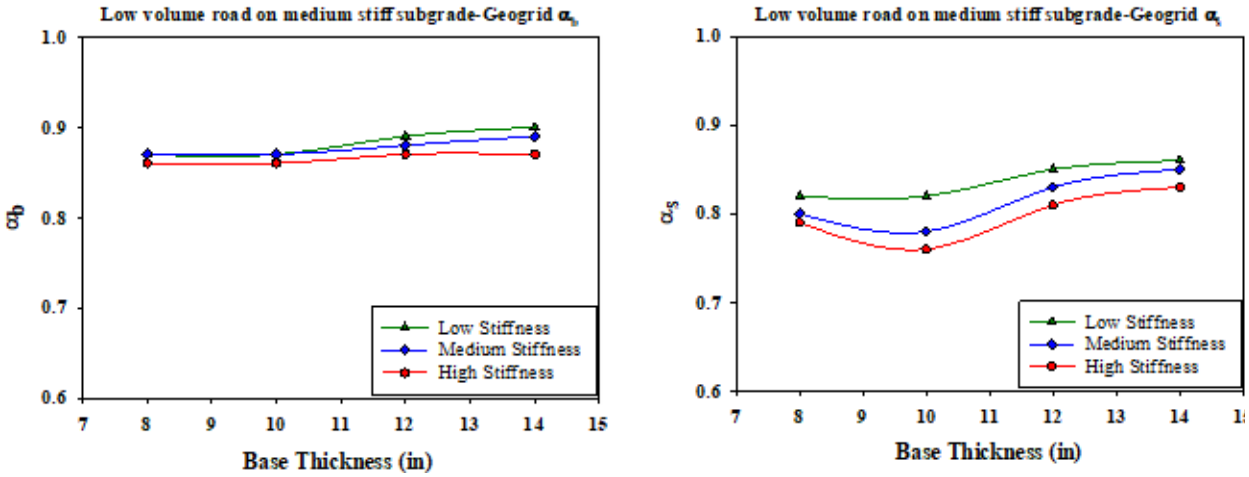

Figure 99. Values of rutting reduction coefficients for base and subgrade (α_b and α_s) for geogrid reinforced pavement with high traffic volume on stiff subgrade

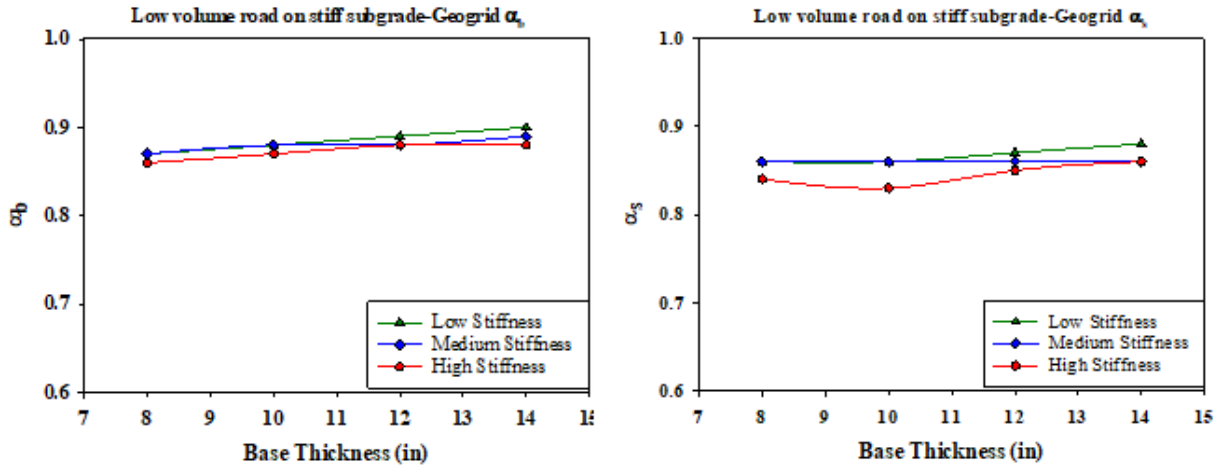

Figure 100. Values of rutting reduction coefficients for base and subgrade (α_b and α_s) for geogrid reinforced pavement with medium traffic volume on weak subgrade

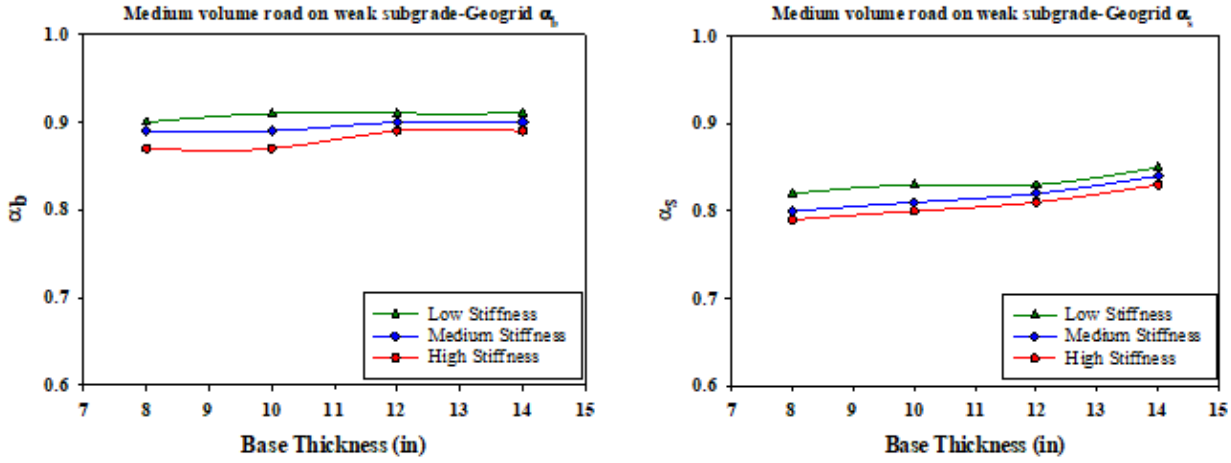

Figure 101. Values of rutting reduction coefficients for base and subgrade (α_b and α_s) for geogrid reinforced pavement with medium traffic volume on medium stiff subgrade

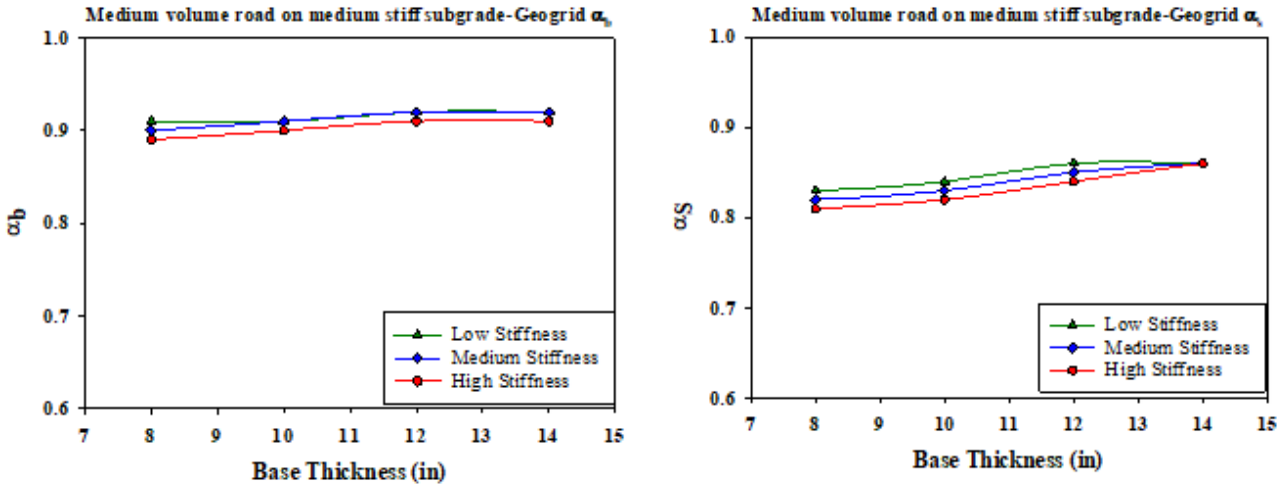

Figure 102. Values of rutting reduction coefficients for base and subgrade (α_b and α_s) for geogrid reinforced pavement with medium traffic volume on stiff subgrade

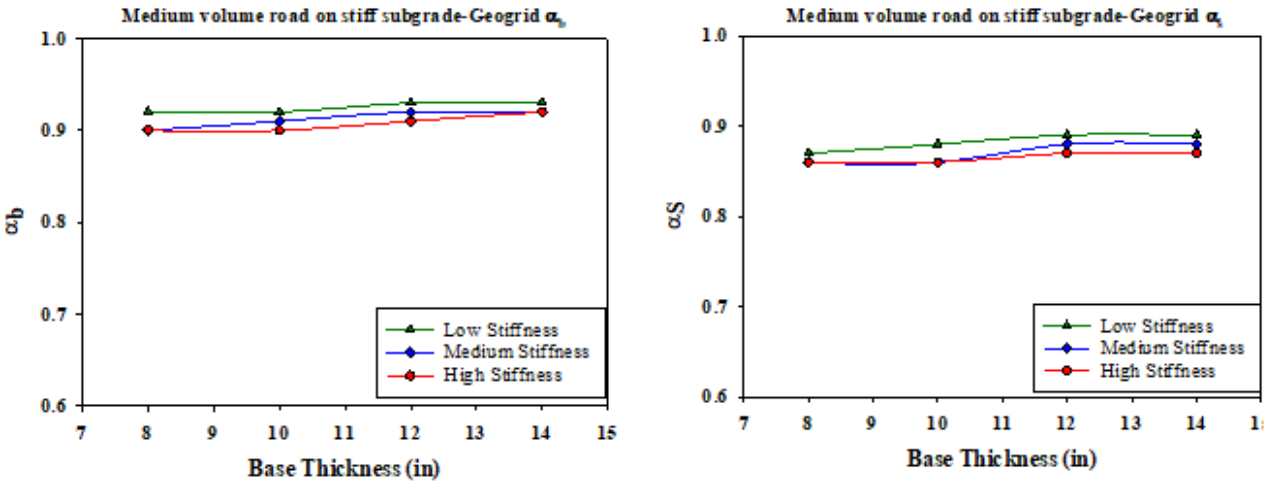

Figure 103. Values of rutting reduction coefficients for base and subgrade (α_b and α_s) for geogrid reinforced pavement with high traffic volume on weak subgrade

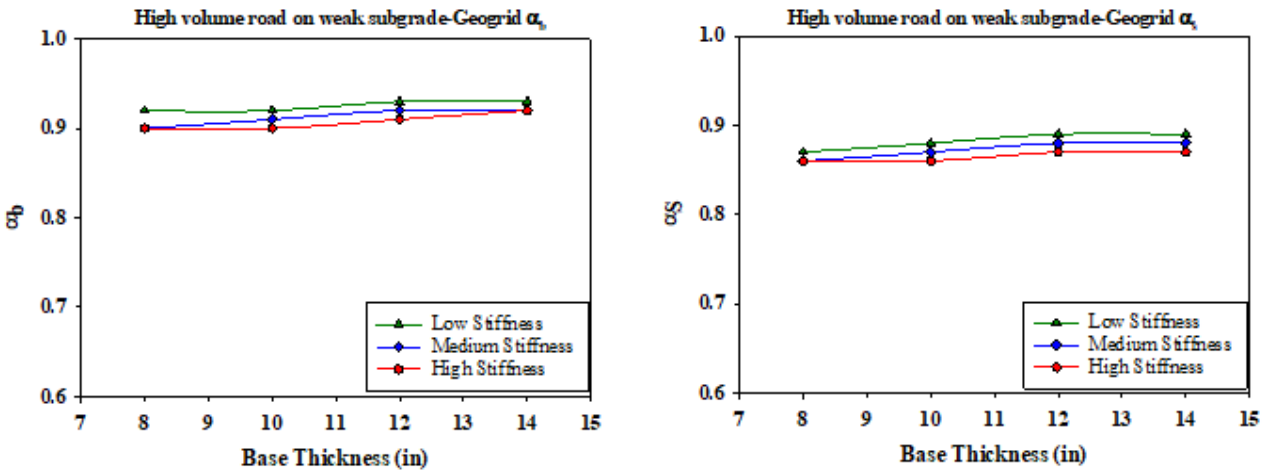

Figure 104. Values of rutting reduction coefficients for base and subgrade (α_b and α_s) for geogrid reinforced pavement with high traffic volume on medium stiff subgrade

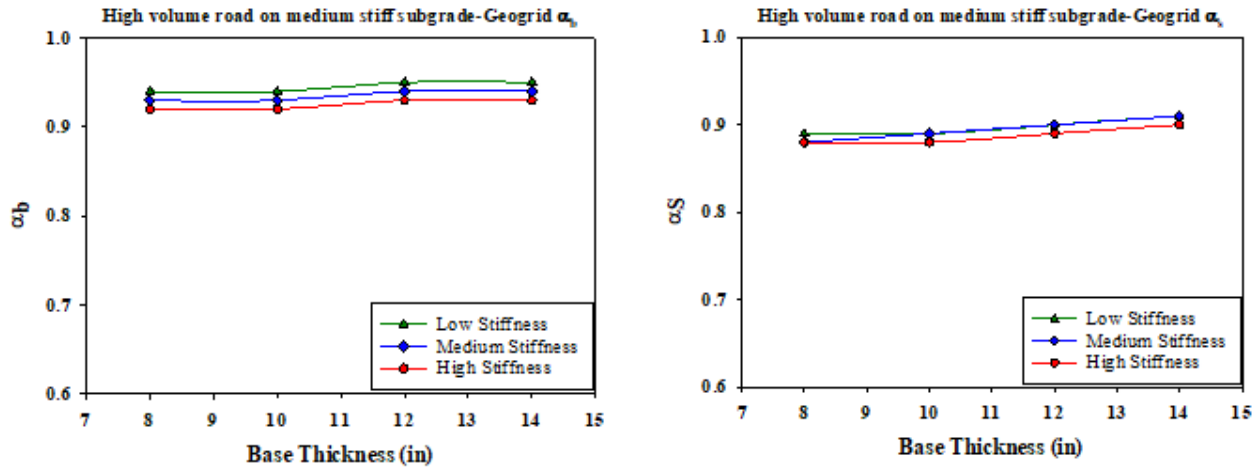

Figure 105. Values of rutting reduction coefficients for base and subgrade (α_b and α_s) for geogrid reinforced pavement with high traffic volume on stiff subgrade

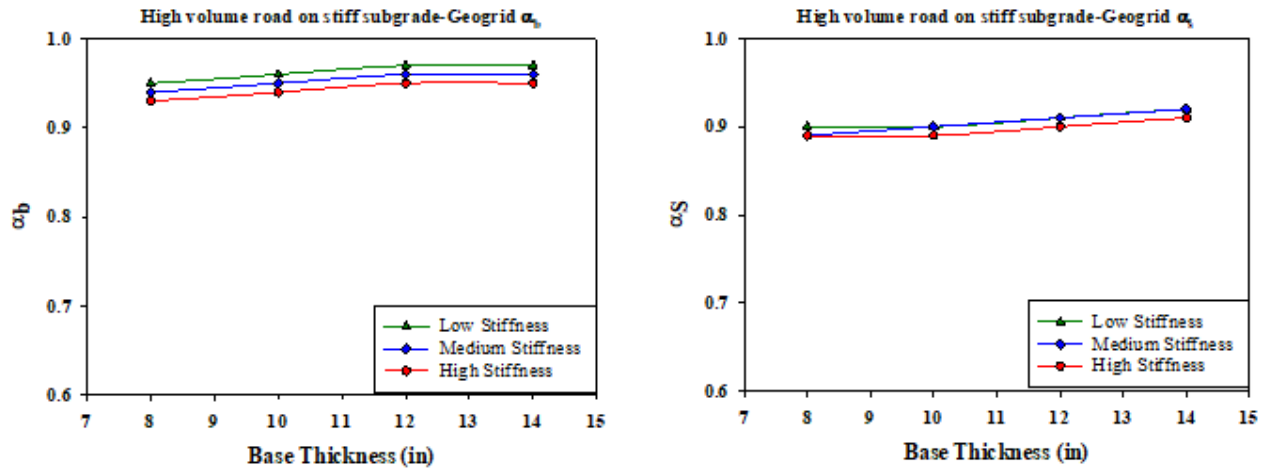

Figure 106. Values of rutting reduction coefficients for base and subgrade (α_b and α_s) for geotextile reinforced pavement with low traffic volume on weak subgrade

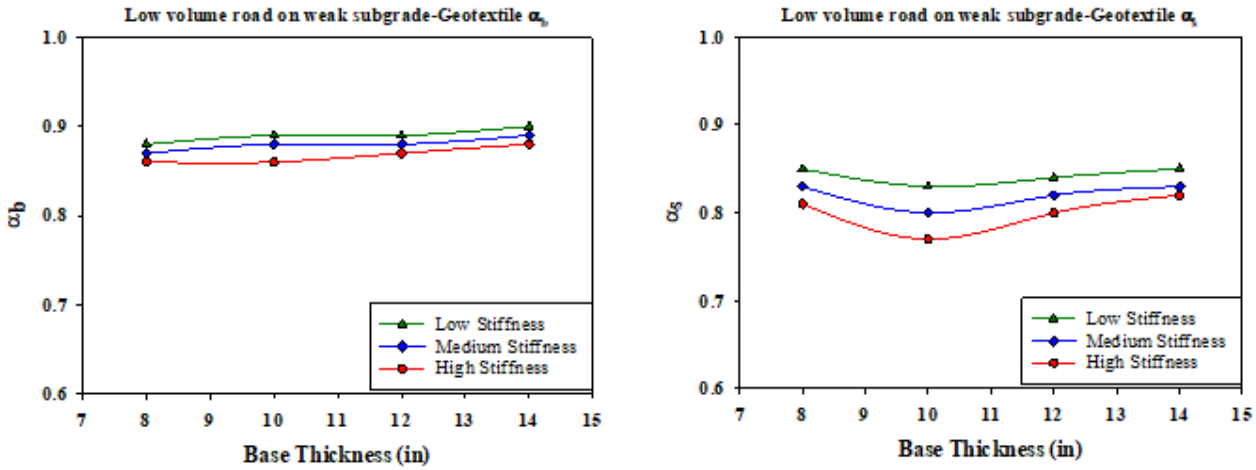

Figure 107. Values of rutting reduction coefficients for base and subgrade (α_b and α_s) for geotextile reinforced pavement with low traffic volume on medium stiff subgrade

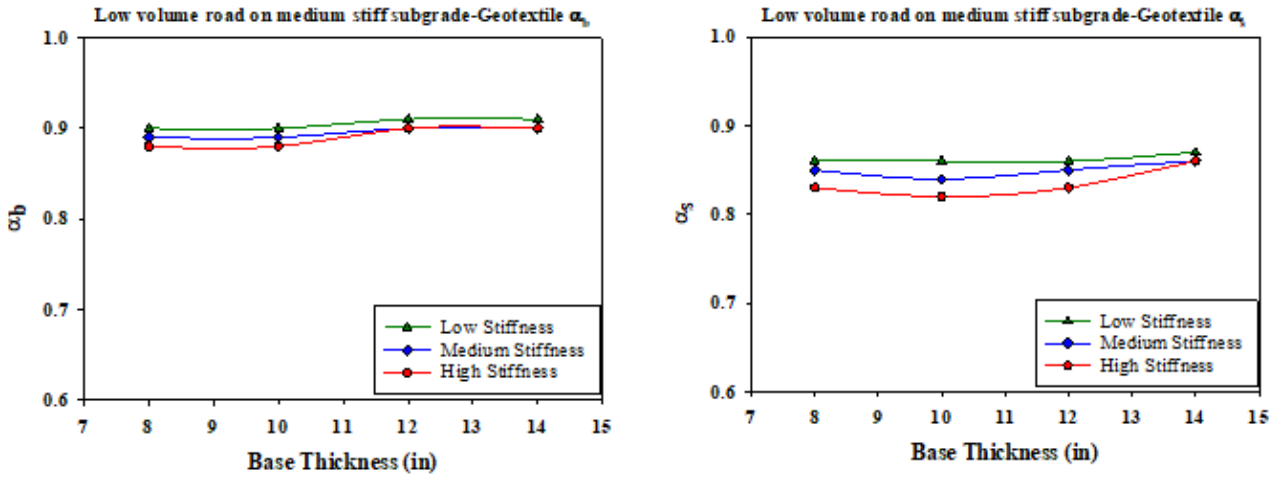

Figure 108. Values of rutting reduction coefficients for base and subgrade (α_b and α_s) for geotextile reinforced pavement with low traffic volume on stiff subgrade

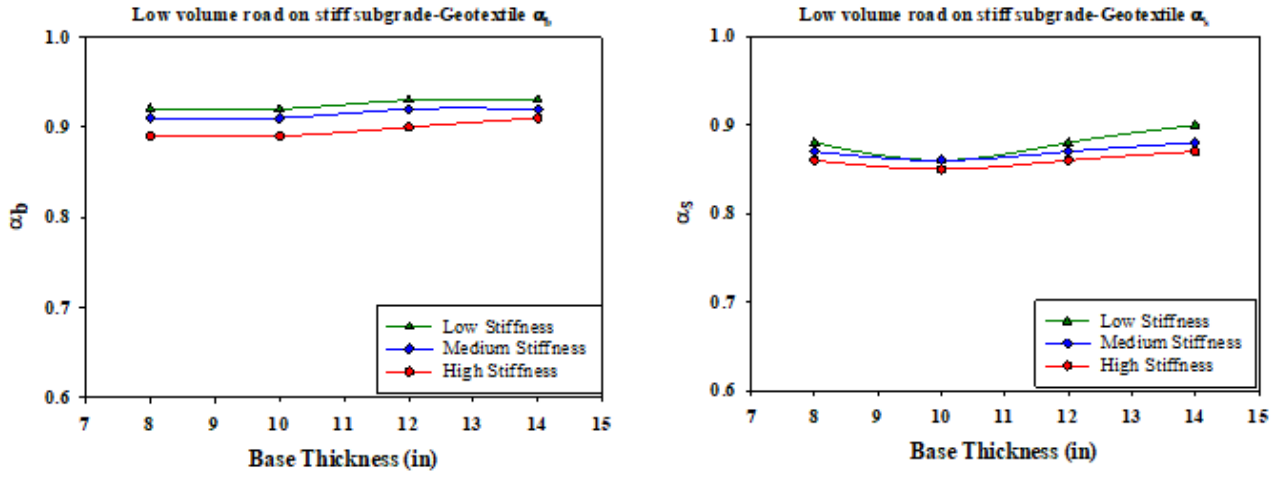

Figure 109. Values of rutting reduction coefficients for base and subgrade (α_b and α_s) for geotextile reinforced pavement with medium traffic volume on weak subgrade

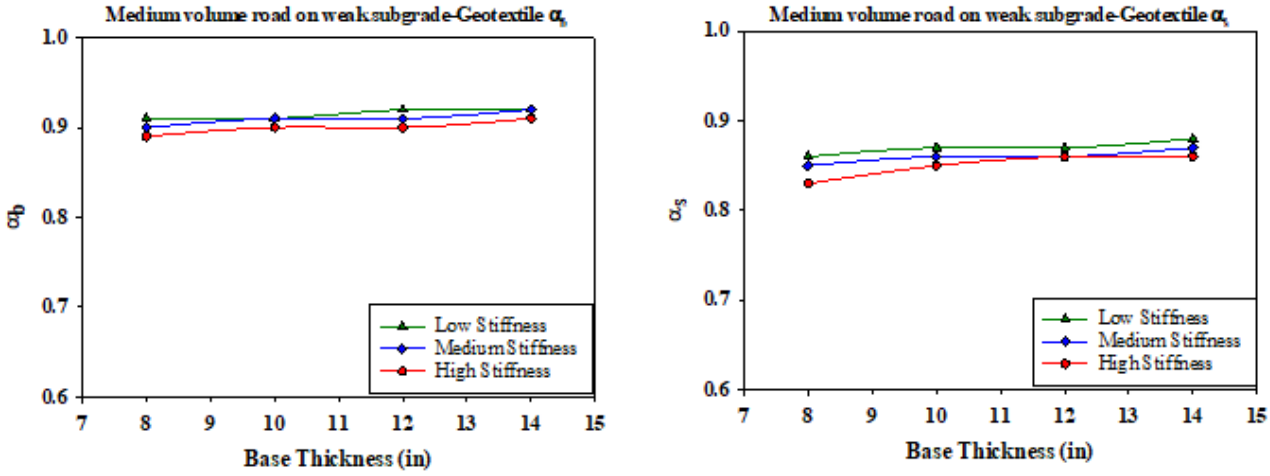

Figure 110. Values of rutting reduction coefficients for base and subgrade (α_b and α_s) for geotextile reinforced pavement with medium traffic volume on medium stiff subgrade

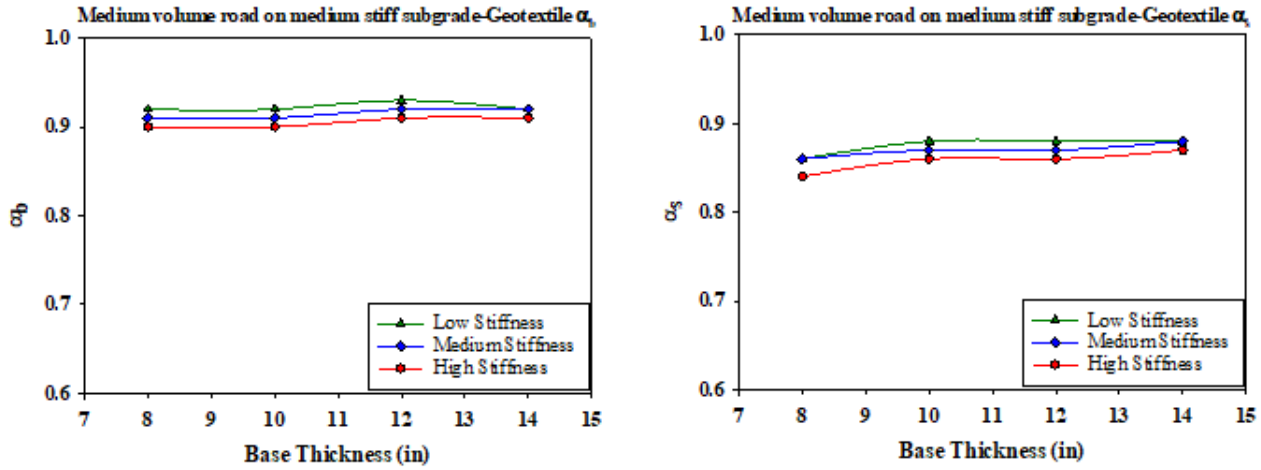

Figure 111. Values of rutting reduction coefficients for base and subgrade (α_b and α_s) for geotextile reinforced pavement with medium traffic volume on stiff subgrade

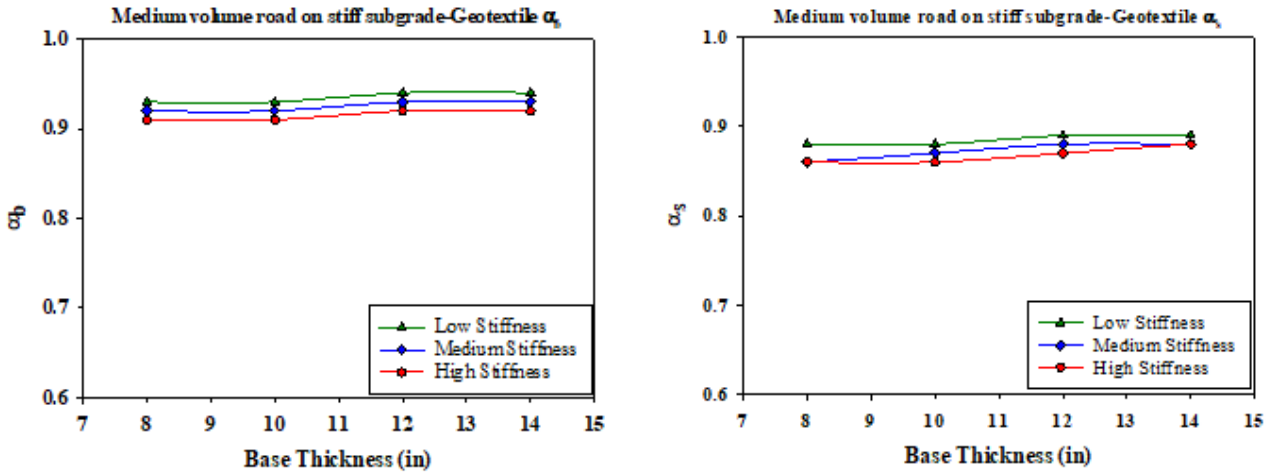

Figure 112. Values of rutting reduction coefficients for base and subgrade (α_b and α_s) for geotextile reinforced pavement with high traffic volume on weak subgrade

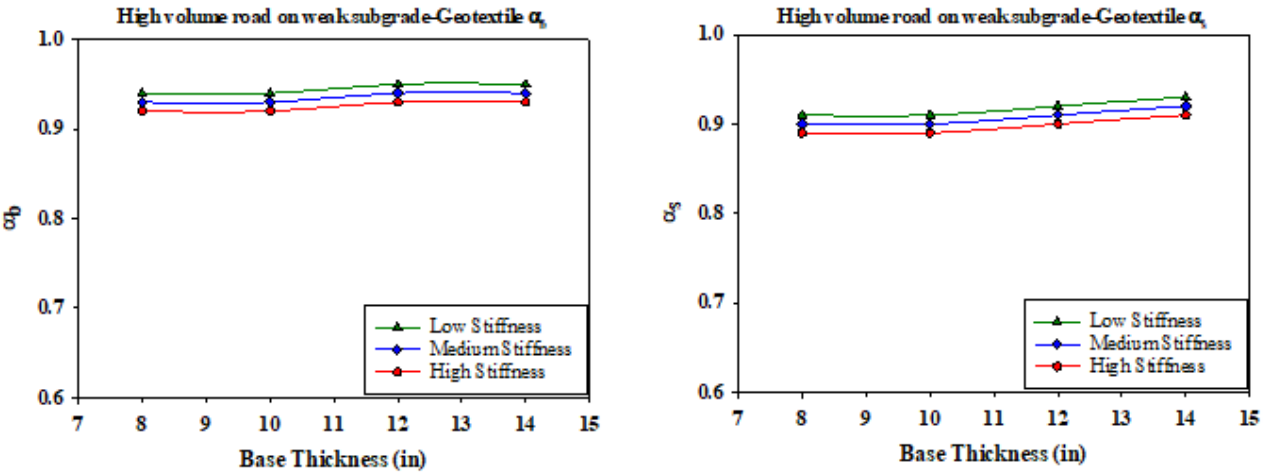

Figure 113. Values of rutting reduction coefficients for base and subgrade (α_b and α_s) for geotextile reinforced pavement with high traffic volume on medium stiff subgrade

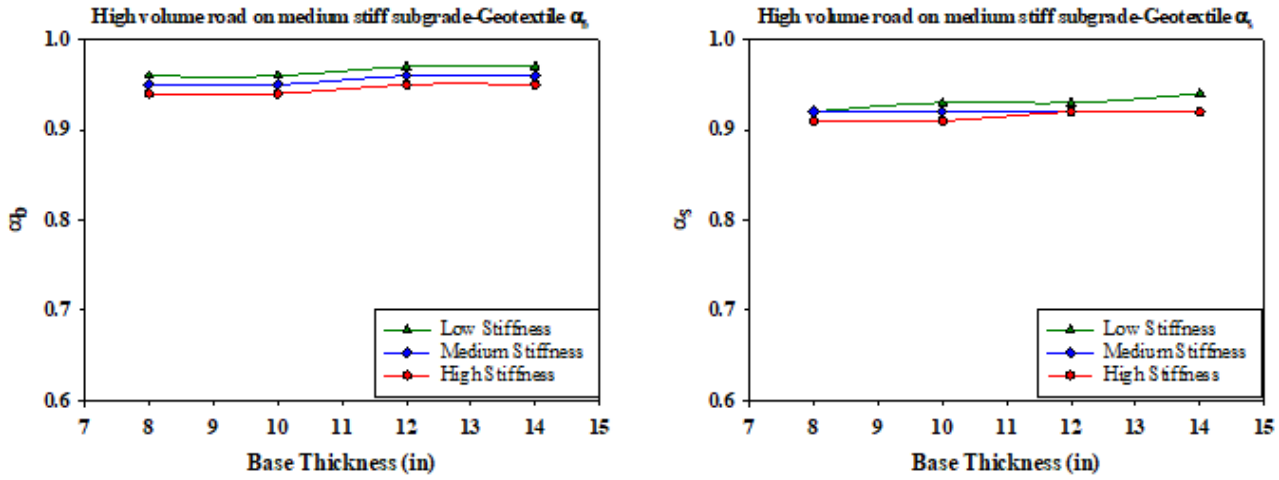

Figure 114. Values of rutting reduction coefficients for base and subgrade (α_b and α_s) for geotextile reinforced pavement with high traffic volume on stiff subgrade

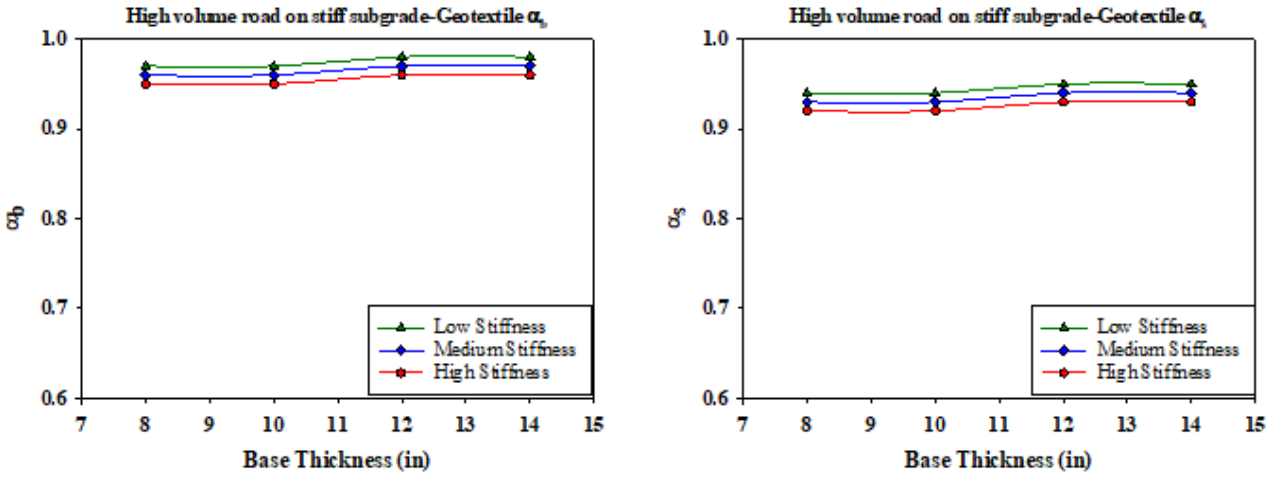

Appendix E

Color-Coded Correlation Graphs Between Attributes and Benefits

Figure 115. Colored correlation graph between attributes for TBR dataset

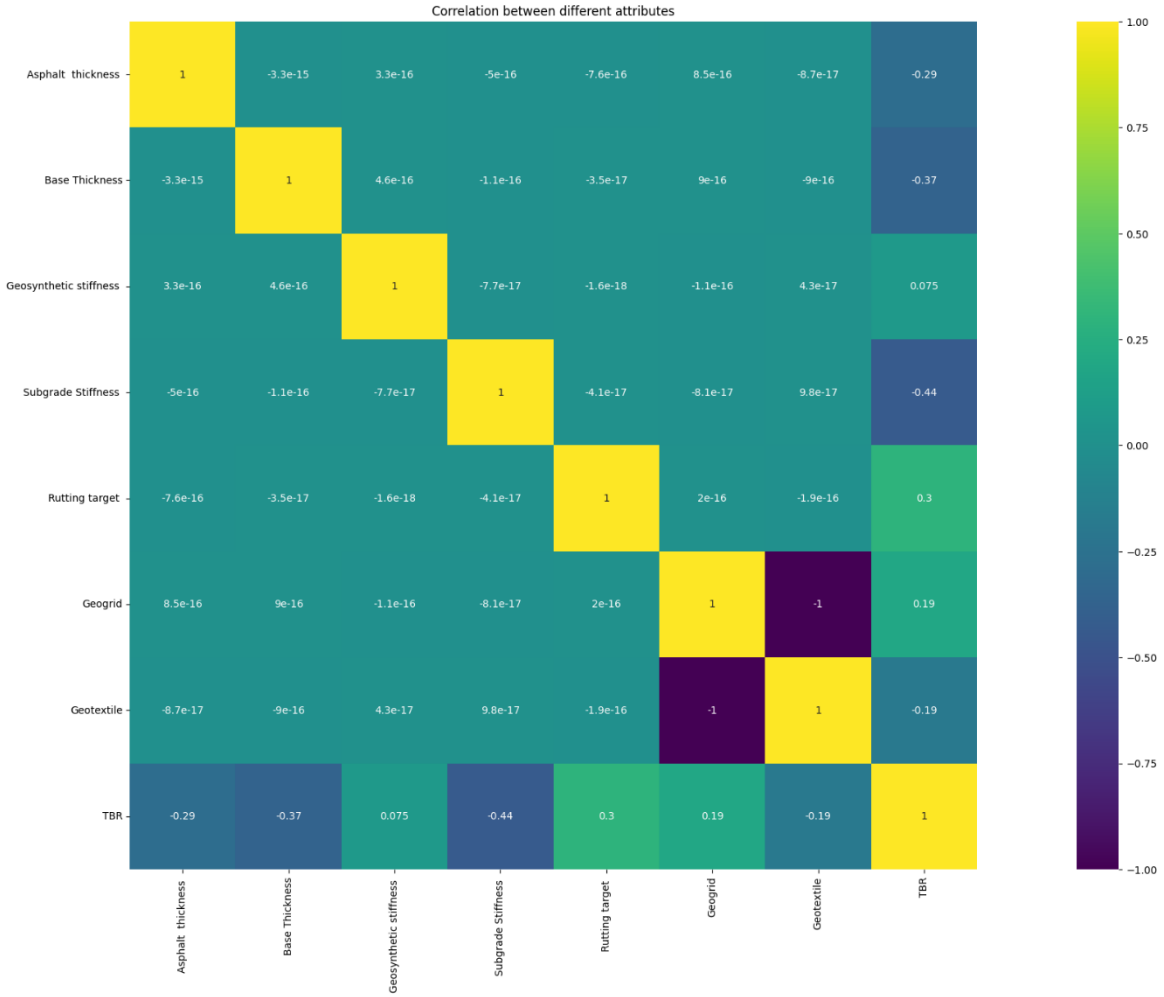

Figure 116. Colored correlation graph between attributes for $M_{R\text{-}eff}$ dataset

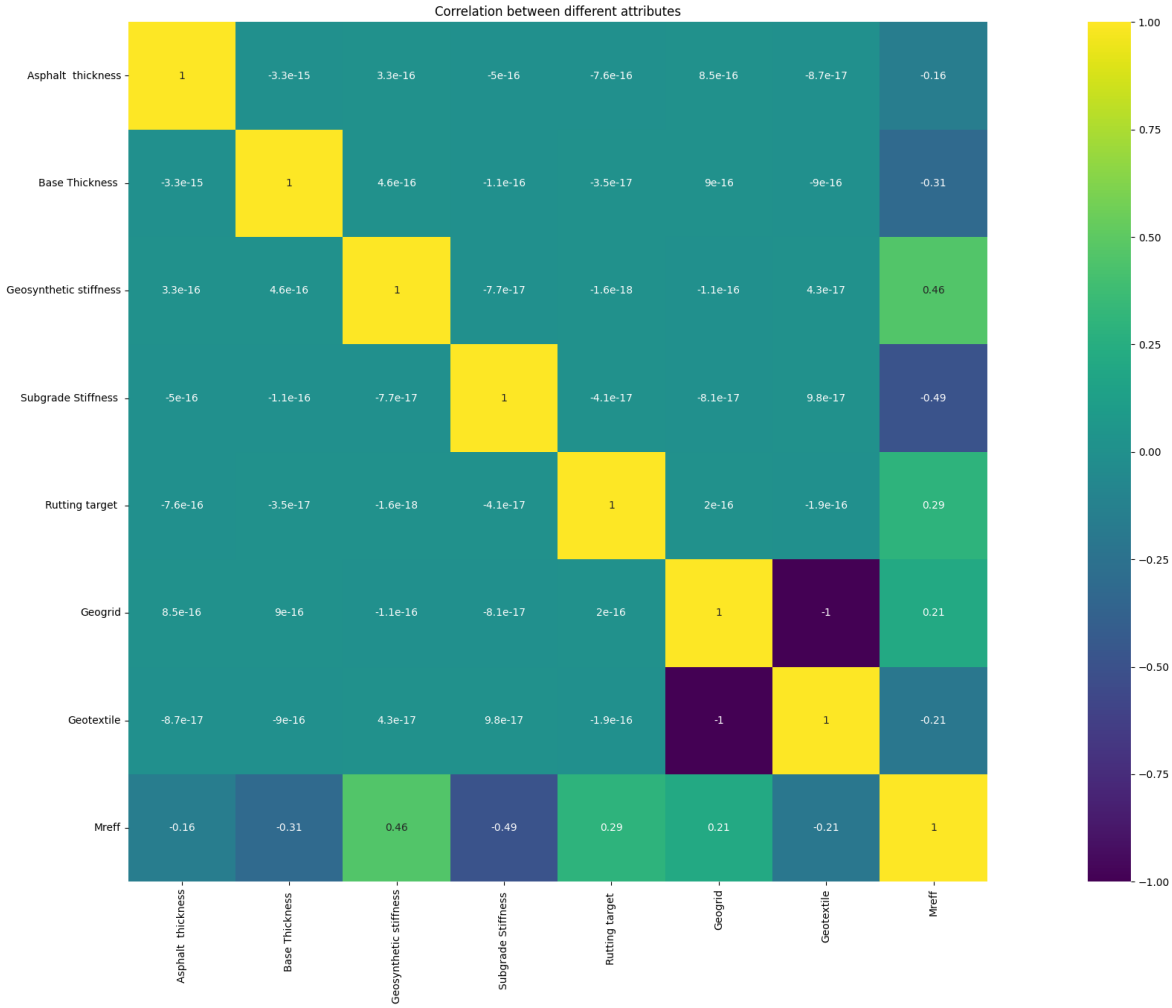

Figure 117. Colored correlation graph between attributes for EBT dataset

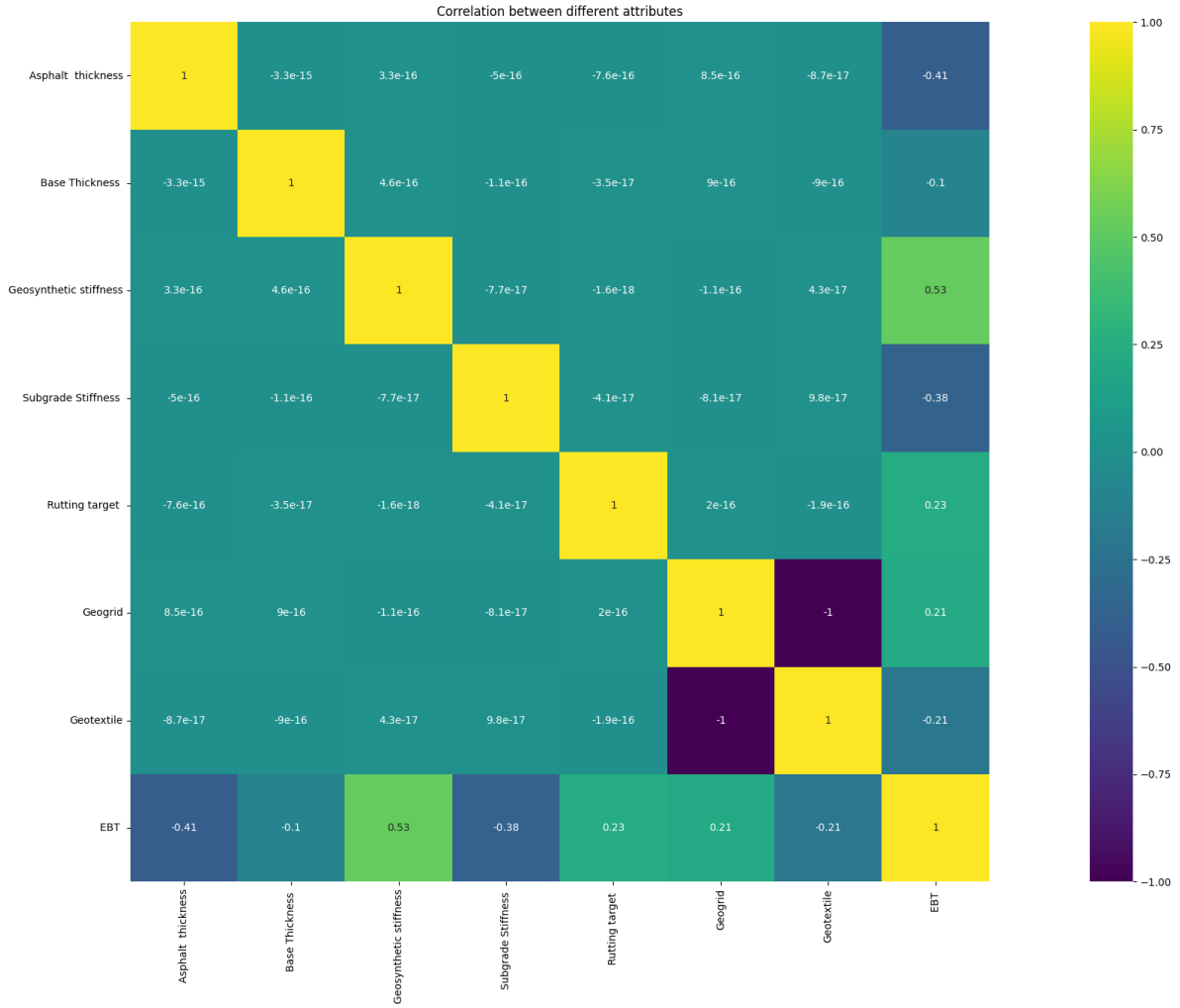

Figure 118. Colored correlation graph between attributes for rutting reduction coefficient for base (α_b) dataset

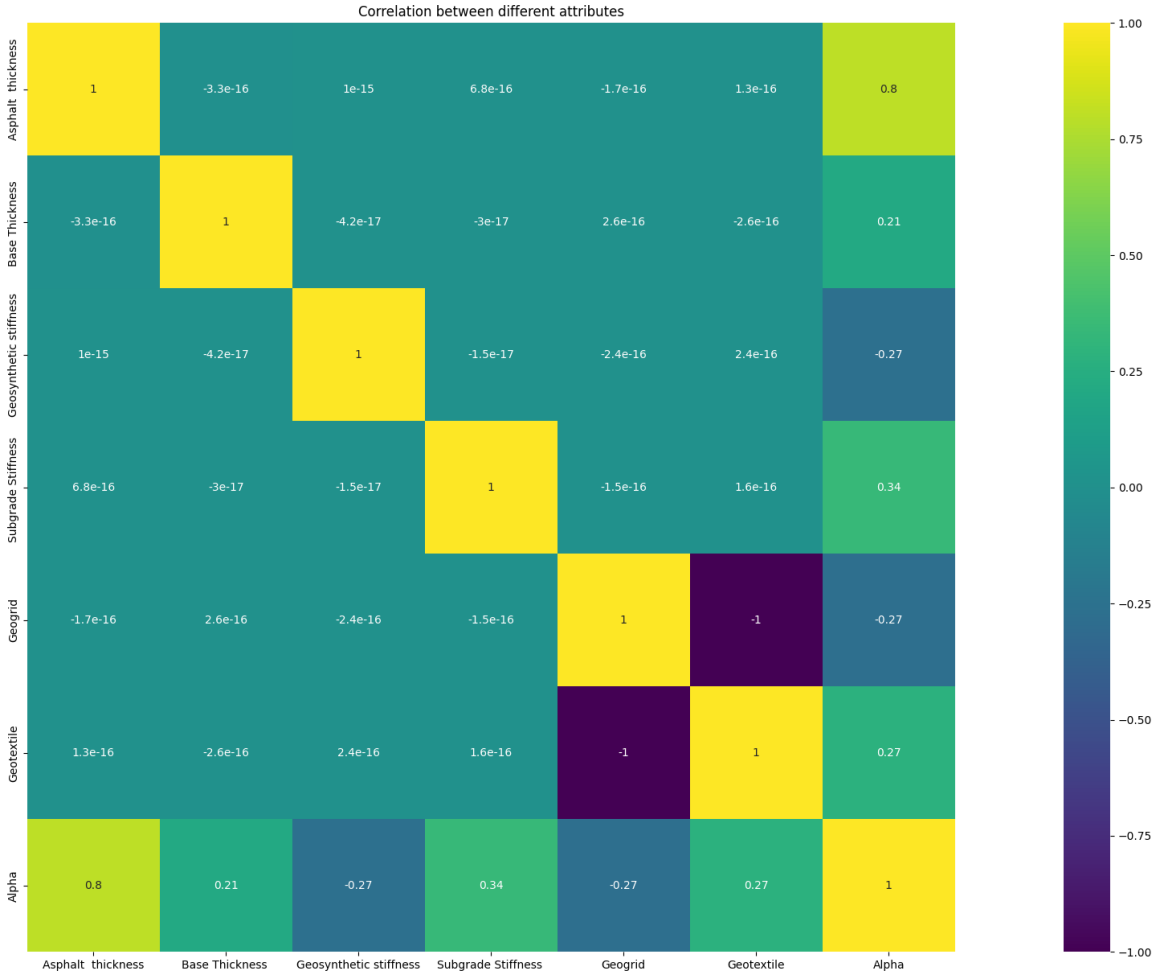

Figure 119. Colored correlation graph between attributes for rutting reduction coefficient for subgrade (α_s) dataset

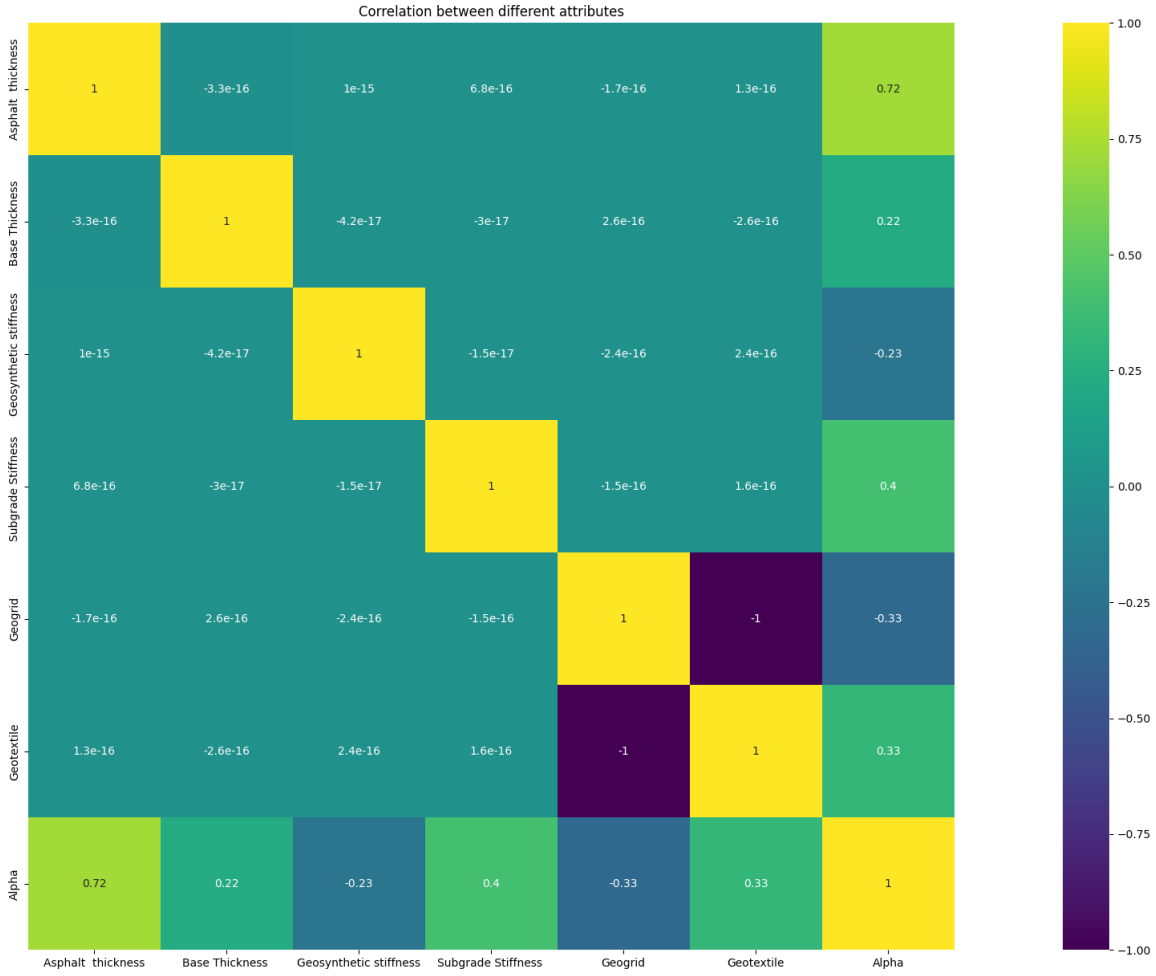

Appendix F

Tuned Hyperparameters for Different Algorithms and Benefits

Table 30. Tuned hyperparameters for Decision Tree (DT) algorithm

	max_depth	max_features	min_samples_leaf	min_samples_split
TBR	None	auto	2	2
$M_{R\text{-}eff}$	None	auto	1	2
EBT	10	auto	1	2
α_b	30	auto	1	2
α_s	30	auto	1	2

Table 31. Tuned hyperparameters for Random Forest (RF) algorithm

	max_depth	max_features	min_samples_leaf	min_samples_split	n_estimators
TBR	10	auto	1	2	100
$M_{R\text{-}eff}$	10	auto	1	2	200
EBT	None	auto	1	2	300
α_b	None	auto	1	2	300
α_s	None	auto	1	2	100

Table 32. Tuned hyperparameters for Support Vector Machine (SVM) algorithm

	C	epsilon	kernel
TBR	10	0.1	rbf
$M_{R\text{-}eff}$	10	0.01	poly
EBT	10	1	poly
α_b	0.1	0.01	poly
α_s	10	0.01	rbf

Table 33. Tuned hyperparameters for Gradient Boosting (GB) algorithm

	learning_rate	max_depth	n_estimators
TBR	0.2	5	300
$M_{R\text{-}eff}$	0.2	4	300
EBT	0.2	4	300
α_b	0.2	3	100
α_s	0.1	4	300

Appendix G

Derived MLR and MER Regression Coefficients

Multiple Linear Regression (MLR) and Multivariable Exponential Regression (MER) are performed to establish regression models for TBR, $M_{R\text{-}eff}$, EBT, $\alpha_b$and α_s that can aid in the derivation of anticipated values based on system variables. The general formula for MLR models is given below:

$$y = \beta_0 + \beta_1 x_1 + \beta_2 x_2 + \beta_3 x_3 + \beta_4 x_4 + \beta_5 x_5 + \beta_6 x_6 + \beta_7 x_7$$

For MER models, the general formula is:

$$y = a * \exp(b_1 x_1 + b_2 x_2 + b_3 x_3 + b_4 x_4 + b_5 x_5 + b_6 x_6 + b_7 x_7)$$

For MLR models β_i and for MER models a and b_i are regression coefficients.

For both models, x_i are scaled independent variables as following:

x_1 is scaled asphalt thickness , x_2 is scaled base thickness, x_3 is scaled geosynthetic stiffness, x_4 is scaled subgrade stiffness, x_5 is rutting target, x_6 is geogrid presence, x_7 is geotextile presence

Table 34. Derived MLR regression coefficients

	β_0	β_1	β_2	β_3	β_4	β_5	β_6	β_7
TBR	4.129	-0.918	-2.174	0.312	-1.259	1.358	0.153	-0.153
$M_{R\text{-}eff}$	103.4	-33.25	-107.45	92.38	-83.65	74.29	11.22	-11.22
EBT	4.554	-2.995	-1.265	4.055	-2.400	2.251	0.381	-0.381
α_b	0.824	0.088	0.038	-0.028	0.031	-	-0.008	0.008
α_s	0.741	0.110	0.052	-0.036	0.055	-	-0.013	0.013

Table 35. Derived MER regression coefficients

	a	b_1	b_2	b_3	b_4	b_5	b_6	b_7
TBR	4.523	-0.408	-0.940	0.115	-0.595	0.640	0.157	-0.157
$M_{R\text{-}eff}$	-	-	-	-	-	-	-	-
EBT	-	-	-	-	-	-	-	-
α_b	1.085	0.096	0.042	-0.031	0.035	-	-0.279	-0.261
α_s	2.314	0.127	0.059	-0.041	0.062	-	-1.142	-1.110

Appendix H

Feature Importance Graphs for Different Indices from RF Model

Figure 120. Feature importance graph of TBR from RF model

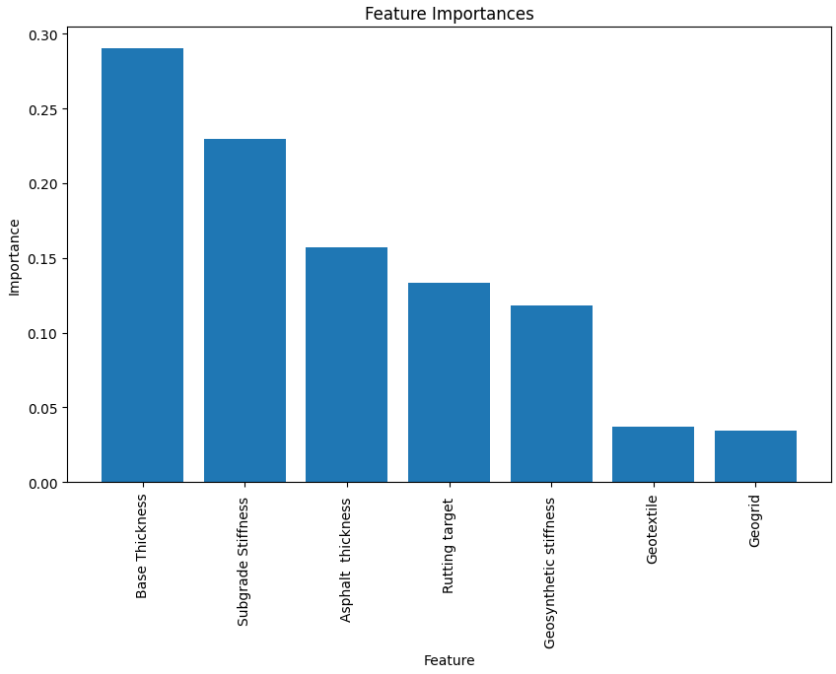

Figure 121. Feature importance graph of $M_{R\text{-}eff}$ from RF model

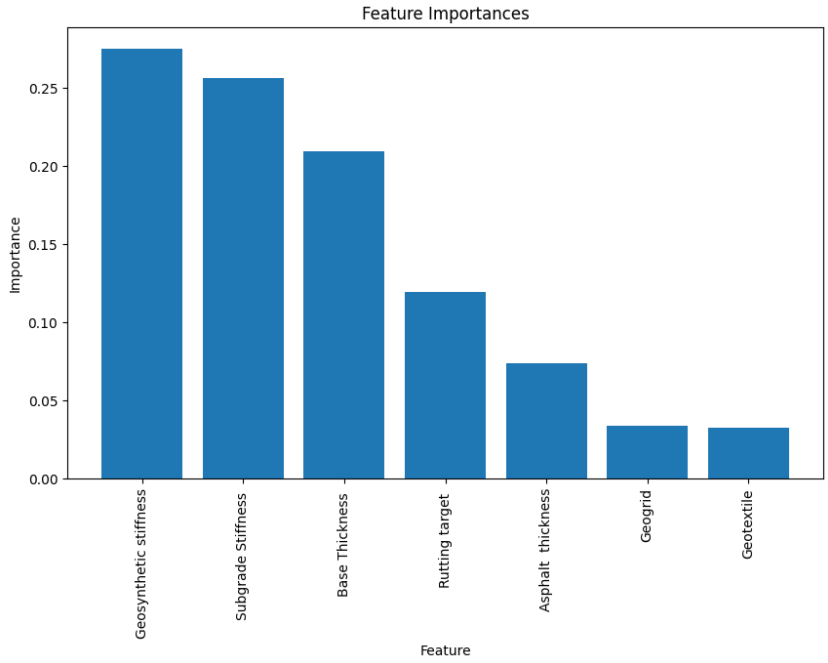

Figure 122. Feature importance graph of EBT from RF model

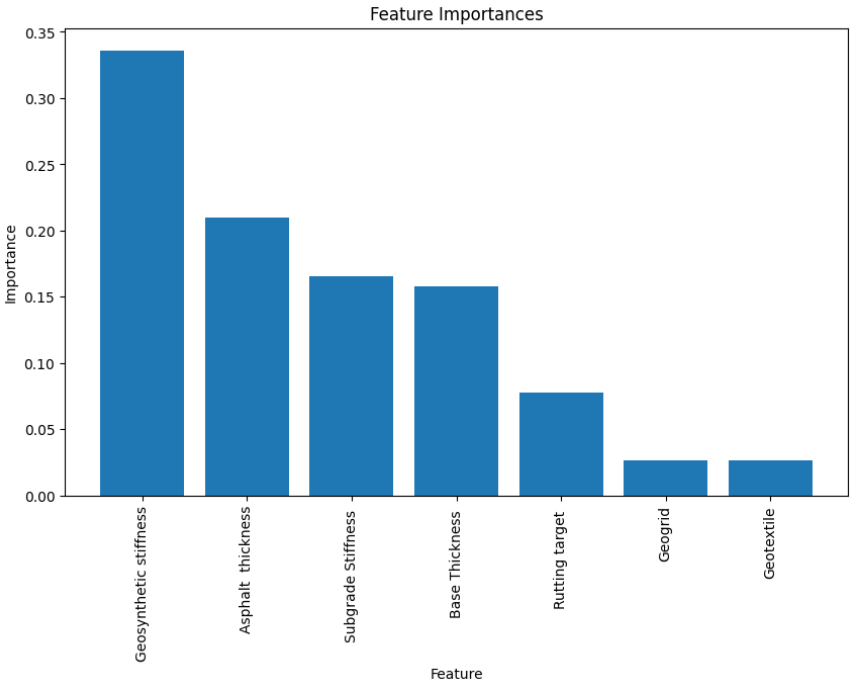

Figure 123. Feature importance graph of rutting reduction coefficient for base (α_b) from RF model

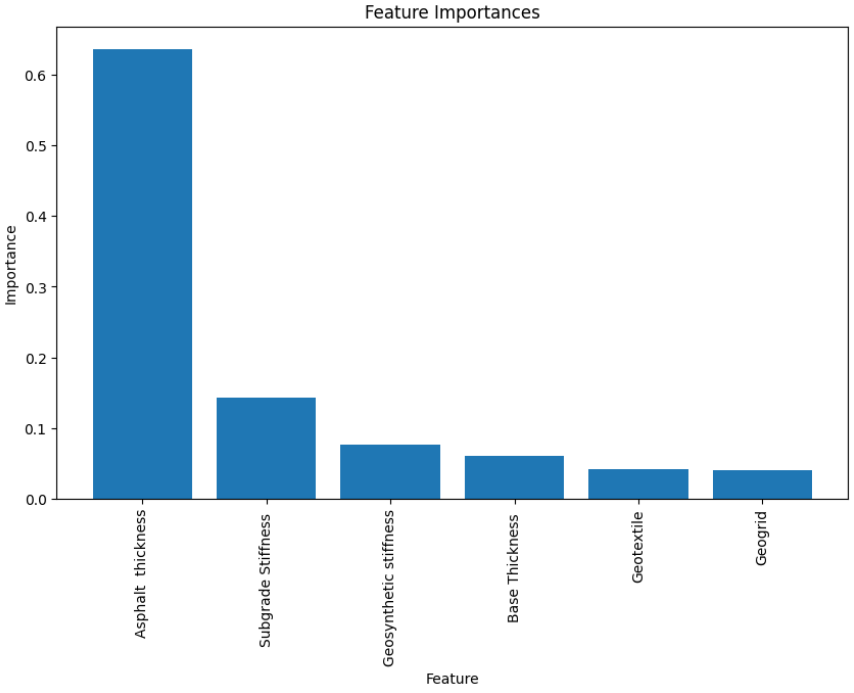

Figure 124. Feature importance graph of rutting reduction coefficient for subgrade (α_s) from RF model

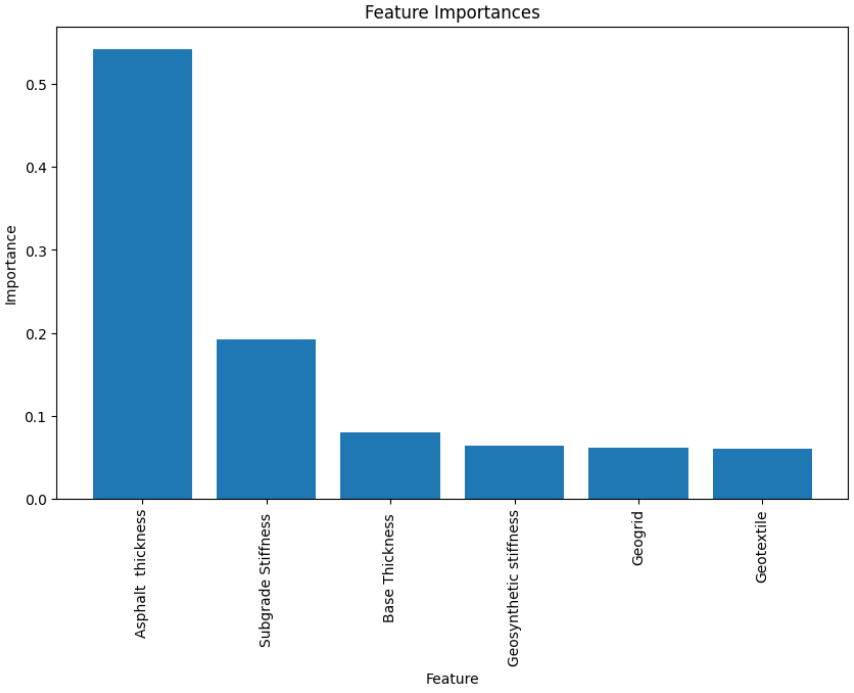

Appendix I

MLR with Interaction Models Derived Coefficients

Table 36. Derived MLR regression coefficients with interactions for benefit indices

Variable	Coefficients	Derived values for regression coefficients		
		TBR	$M_{R\text{-}eff}$	EBT
	β_0	4.3885	-27.32	6.2373
x_1	β_1	-1.6714	0	-2.6053
x_2	β_2	-1.7664	0	-2.5359
x_3	β_3	-0.8576	129.09	2.0620
x_4	β_4	-2.1557	-61.04	-2.9310
x_5	β_5	3.3467	110.95	1.9699
x_6	β_6	0.5754	38.10	-0.1029
x_7	β_7	-0.5754	0	0.1029
x_1 x_2	β_8	0	0	0
x_1 x_3	β_9	2.6644	0	2.1482
x_1 x_4	β_{10}	1.3936	47.03	2.3662
x_1 x_5	β_{11}	-1.4903	-66.92	-2.6645
x_1 x_6	β_{12}	- 0.9895	-19.42	-1.4841
x_1 x_7	β_{13}	-0.6818	0	-1.1212
x_2 x_3	β_{14}	0	-136.64	0
x_2 x_4	β_{15}	3.0667	132.98	2.0254
x_2 x_5	β_{16}	-2.4387	-100.36	0
x_2 x_6	β_{17}	-0.9531	-38.04	0
x_2 x_7	β_{18}	0	0	0
x_3 x_4	β_{19}	-0.6934	-117.12	-1.7118
x_3 x_5	β_{20}	0	104.26	1.5807
x_3 x_6	β_{21}	0	77.60	0.8548
x_3 x_7	β_{22}	-0.3672	51.49	0
x_4 x_5	β_{23}	-1.1971	-63.04	0
x_4 x_6	β_{24}	1.3662	-40.16	-1.1857
x_4 x_7	β_{25}	-0.7895	-20.88	-1.7452
x_5 x_6	β_{26}	1.8223	69.21	1.1795
x_5 x_7	β_{27}	1.5243	41.73	0.7903
x_6 x_7	β_{28}	0	0	0

Table 37. Derived MLR regression coefficients with interactions for modifying coefficients

Variable	Coefficients	Derived values for regression coefficients	
		α_b	α_s
	β_0	0.8337	0.7476
x_1	β_1	0.0488	0.0800
x_2	β_2	0.0324	0.0340
x_3	β_3	-0.0191	-0.0531
x_4	β_4	0.0115	0.0493
x_5	β_5	-0.0148	-0.0321
x_6	β_6	0.0148	0.0321
x_1 x_2	β_7	0	0
x_1 x_3	β_8	0	0.0417
x_1 x_4	β_9	0	-0.0625
x_1 x_5	β_{10}	0.0243	0.0352
x_1 x_6	β_{11}	0.0276	0.0447
x_2 x_3	β_{12}	0	0
x_2 x_4	β_{13}	0	0
x_2 x_5	β_{14}	0.0211	0.0373
x_2 x_6	β_{15}	0	0
x_3 x_4	β_{16}	0	0.0302
x_3 x_5	β_{17}	0.0140	-0.0276
x_3 x_6	β_{18}	-0.0072	-0.0255
x_4 x_5	β_{19}	-0.0119	0.0366
x_4 x_6	β_{20}	0.0089	0.0126
x_5 x_6	β_{21}	0	0